Modelling the interface in concrete-to-concrete connections between precast girders and cast-in-situ top layers

Justyna Urszula Botor



Modelling the interface in concrete-to-concrete connections between precast girders and cast-in-situ top layers

by

Justyna Urszula Botor

to obtain the degree of Master of Science
at the Delft University of Technology,
to be defended publicly on Thursday, March 30, 2022, at 10:00 AM.

Student number: 5396301

Thesis committee: Prof. Dr. ir. M.A.N Hendriks TU Delft, Chair

Prof. Dr. ir. J. G. Rots
TU Delft
Dr. ir. Y. Yang
TU Delft
Ir. N. W. Kostense
TU Delft



Acknowledgments

This thesis signifies the end of my time at TU Delft. The journey was not without its challenges, but it was undeniably the most developing and memorable adventure that I got to experience so far. I am deeply thankful that TU Delft gave me the opportunity to grow in such a motivating environment. Throughout the duration of my Master, I was lucky to know and meet numerous inspiring, open and kind people who left a mark on this experience and who I would like to acknowledge.

Firstly I would like to thank my thesis committee, for the guidance as well as for the knowledge and inspiration that I could gain. I would like to express my deepest gratitude to Max Hendriks, the chair of my committee, for the positive encouragement throughout the process and for always finding the time to help me with smaller and bigger issues. I would like to extend my sincere thanks to Yuguang Yang, for asking the questions, which I might not have asked myself, but which undoubtedly improved my work as I got to see things from a different perspective. I would also like to express my thanks to Jan Rots, for actively sharing ideas during progress meetings on how the work could be enhanced or what steps should I take. Many thanks to my daily supervisor, Niels Kostense, for sharing his insights on the subject and primarily his experience in finite element modelling.

I would also like to acknowledge Florentia Kavoura, who has been a great mentor and who provided me with the opportunity to be a Student Assistant. I am also thankful to Mohammed Ibrahim for taking the time to engage in discussions on concrete and structural matters.

Huge thanks should go to my TU Delft friends, without whom this experience would have been far more challenging. I appreciate all the coffee breaks, the late-night studying, the bike rides and many more. I would also like to thank my friends from Poland for making sure that I know they miss me. Karol, I really appreciate your support, thank you for helping me to focus on the bright side and most importantly, for encouraging me to take this big step of moving and studying abroad.

Last but not least I would like to thank my parents. Without your support, on every possible levels, I would not be able to undertake this journey and I would not have experienced all those great things in the past two and a half years. I truly cannot express how grateful I am. *Mamo, tato, bardzo wam dziękuję.*

I am sad that such a significant chapter of my life is closing. Nevertheless, I am happy and proud that I got to this point.

Justyna Urszula Botor Delft, March 2023

Summary

A significant part of composite concrete viaducts was built in the 50s and 60s. This has led to an increasing need for the reassessment of the precast concrete beam bridges in the Netherlands. Many of those bridges are nowadays subjected to higher traffic loads and consequently, have a certain risk of not complying with the currently used design codes. As a result, there is a demand for the development of nonlinear finite element solution strategies, which would increase the reliability of the numerical methods in safety assessment. In this research, special consideration is given to the precast, prestressed beam bridges which were made continuous by applying cast-in-situ cross beams and a top layer above the supports. In such structures, the hogging bending moment introduces more complex stress conditions in the concrete parts and more specific at the interface between precast girders and the top slab, compared to simply supported beam bridges.

Thus, one of the key aspects of the structural performance of composite bridges is the interfacial behaviour. The focus of this research is to study the stress conditions in the vicinity and at the interface and explore methods of numerical modelling of the interface in concrete-to-concrete connections between precast beams and top layers to initiate the development of modelling strategies for this type of interfaces.

The literature review was focused on prefabricated beam bridges, the current state of knowledge on concrete-to-concrete interfaces, along with design recommendations and past experimental and numerical research. Moreover, available interface element types, material models and modelling guidelines were explored. Since DIANA FEA is used within the course of this research, the study of the available models was limited to the ones provided by this software. It was noted that the Linear Elasticity model is the simplest way of interface modelling, therefore it was utilised in the initial stage of the research. More advanced models, Coulomb Friction and Combined Cracking-Shearing-Crushing, were considered worth investigating owing to accounting for coupling between normal and tangential behaviour. The Nonlinear Elasticity material model was also recognized due to the introduction of nonlinear effects, yet being relatively simple to assemble.

The initial phase of the research was a linear, phased analysis of the continuous, composite, concrete girder. Three models were tested within this part of the research - the model without interface elements, and two with linear elastic interface elements, one having high, penalty stiffness and the other having lower, more realistic value of shear stiffness. It was verified that the models without and with penalty stiffness interface performed almost equally. The decrease in stiffness and the deterioration of the composite action caused by this, resulted in an increase of stresses in the precast element. By the support, the extreme tension raised by a factor of 1.21 and under the point of load application the compressive stresses in the beams' web elevated by 2.26. Based on the linear analysis, no significant tensile stresses perpendicular to the interface were detected. According to the analysis of interfacial stresses interaction and assumed failure envelopes, at four chosen points - above the support, at midspan of the main span, at the local shear extreme and under the point of load application - it was observed that the point above the support is not at risk of failure, whereas the point in the midspan might be. It was concluded that the combination of stresses is relevant not only because of a possible

decrease in capacity due to tension but also increase under compression. As a result, models accounting for coupling between normal and shear tractions and relative displacements are worth investigating. It was also observed, that cracking in concrete elements by the support is expected, hence nonlinear analysis is required.

The component-level experiments found in the literature [1] were analysed in the following section to be able to perform verification study of Coulomb Friction (CF) and Combined Cracking-Shearing-Crushing (CCSC) interface material models. Based on single element FE tests it was concluded that both material models proved to be well-suited for capturing the shear-normal stresses coupling. With the same input parameters, but higher normal pressure, the shear capacity increased, representing well the reference data. The CCSC interface material model's ability to capture both cohesion and friction softening, was also verified with the single element models. Moreover, tension softening based on mode I fracture energy can be accounted for in that material model, as well as the fracture energy's and dilatancy's dependency on confining stress. However, those parameters were not verified, due to, among others, limited experimental data. Element assembly with the CCSC material model for the interface, circular beam bond-slip reinforcement and nonlinear material properties of concrete, was used to analyse the specimens with rebars crossing the interface. This approach, was assumed to represent the force transfer mechanisms to the highest extent, since cohesion and friction, generated by both external pressure and reinforcing bars, along with their softening, as well as dowel action, can theoretically be represented by such model. It was observed that this type of strategy resulted in convergence issues, and due to large number of input parameters it is quite complex to analyse or further calibrate. However, the approach seemed promising since the peak loads were underestimated by only 7-15% with respect to the mean, experimentally obtained values.

In the final Chapter the Combined Cracking-Shearing-Crushing (CCSC) interface material model, with bond-slip beam reinforcements was applied in the nonlinear analysis of the previously analysed composite girder. As an alternative, the model with the Nonlinear Elasticity(NE) interface material model was also constructed, based on the analogous input parameters, to be able to compare the modelling methods. In total four models were analysed, since two sets of input, one based on Eurocode 2 [2] and the other on best guess stemming from literature findings, were studied. What was found to be promising is that the global behaviour, assessed on the basis of crack patterns, of the beams with corresponding input, was quite similar for the analyses with the CCSC and the NE material models. With the applied numerical setup, it was not possible to obtain the total load-displacement path of the composite beams using the CCSC material model for the interface, since the models diverged. The NE material model performed more stable and allowed for the analyses to continue, which is its main advantage. Another benefit is the ease of assembly, in comparison with the CCSC model. Nevertheless, it was demonstrated that the NE might provide overestimated results due to not considering the interaction of tractions. It was highlighted that the models' validation with experiments is needed to recommend one of the models or either of the input sets. It was recommended to simplify the approach with the CCSC material model, by for instance, simplifying the numerical setup of interface reinforcement. Moreover, according to the literature findings the scatter of cohesion and friction coefficients, as well as other input parameters, is still quite large, thus experimental research in the form of push-off tests focused on those, particular interfaces is recommended.

Contents

1	Inti	odu	ction	1
	1.1	Bac	kground	1
	1.2	Pro	blem statement	2
	1.3	The	esis objective	2
	1.3	.1	General objective	2
	1.3	.2	Research questions	3
	1.4	Met	thodology and thesis outline	3
2	Lite	eratu	re review	4
	2.1	Pre	fabricated beam bridges	4
	2.1	.1	History	4
	2.1	.2	Production and assembly	5
	2.2	Cor	ncrete-to-concrete interface	6
	2.2	.1	Knowledge development	7
	2.2	.2	Analytical formulas for concrete-to-concrete interface	9
	2.2	.3	Shear transfer mechanisms	11
	2.2	.4	Previous experimental research	14
	2.3	Cor	nputational modelling of the interfaces	16
	2.3	.1	Finite element modelling	16
	2.3	.2	Interface element types in DIANA FEA	17
	2.3	.3	Interface material models available in DIANA FEA	18
	2.3	.4	Previous numerical research	20
	2.4	Cor	ncluding remarks	22
3	Cor	npos	site beam structural behaviour – Linear Analysis	24
	3.1	Tes	t specimen	24
	3.1	.1	Geometric and material properties	24
	3.1	.2	Phases of construction	25
	3.2	Ana	alytical calculations for validation purposes	26
	3.2	.1	Ordinary differential equations	27
	3.2	.2	Stress distribution in the composite beam	27
	3.3	Inte	erface capacity according to design codes	29
	3.3	.1	NEN-EN 1992-1-1:2005	29
	3.3	.2	NEN-EN 1992-1-1 draft version	29
	3.3	.3	Fib Model Code 2010	30
	3.4	Fin	ite element analysis	31

	3.4.1	Numerical setup	31
	3.4.2	Geometry and structural element types	32
	3.4.3	Material models	34
	3.4.4	Boundary and loading conditions	36
	3.4.5	Mesh	37
	3.4.6	Analysis characteristics	38
	3.5 Co	mparison of the results of the analytical and numerical calculations	38
	3.5.1	Longitudinal stresses	38
	3.5.2	Shear stresses	39
	3.6 Co	mparison of the results obtained from the finite element analyses	40
	3.6.1	Longitudinal stresses	40
	3.6.2	Shear stresses	41
	3.6.3	Normal tractions at the interface	41
	3.6.4	Relative displacement in normal direction at the interface	42
	3.6.5	Shear tractions at the interface	42
	3.6.6	Relative displacement in tangential direction at the interface	42
	3.6.7	Development of stresses at the selected points at the interface	43
	3.7 Di	scussion	45
	3.8 Co	nclusions	47
4	Verifica	ation study on models on a component level - Nonlinear Analysis	48
	4.1 Ex	perimental reference - modified push-off test	48
	4.1.1	Experimental setup and properties of the specimens	48
	4.1.2	Experimental results	49
	4.1.3	Choice motivation	51
	4.2 Nu	merical model – single element test	52
	4.2.1	Numerical setup	52
	4.2.2	Geometry and structural element types	53
	4.2.3	Material models	53
	4.2.4	Boundary and loading conditions	56
	4.2.5	Mesh	57
	4.2.6	Analysis characteristics	57
	4.2.7	Results	58
	4.3 Nu	merical model – element assembly	64
	4.3.1	Numerical setup	64
	4.3.2	Geometry and structural element types	64
	4.3.3	Material models	65
	4.3.4	Boundary and loading conditions	67

	4.3	.5	Mesh	68
	4.3	.6	Analysis characteristics	68
	4.3	.7	Results	68
4	4.4	Dis	cussion	70
4	4.5	Cor	nclusions	73
5	Co	mpos	site beam structural behaviour – Nonlinear Analysis	75
ļ	5.1	Tes	t specimen	75
!	5.2	Nuı	merical model	76
	5.2	.1	Numerical setup	76
	5.2	.2	Geometry and structural element types	76
	5.2	.3	Material models	77
	5.2	.4	Boundary and loading conditions	84
	5.2	.5	Mesh	84
	5.2	.6	Analysis characteristics	84
ļ	5.3	Res	sults	86
	5.3	.1	Crack pattern	87
	5.3	.2	Shear tractions at the interface	88
	5.3	.3	Normal tractions at the interface	89
	5.3	.4	Shear relative displacements	90
	5.3	.5	Normal relative displacements	91
	5.3	.6	Development of stresses in selected points	92
ļ	5.4	Dis	cussion	93
ļ	5.5	Cor	nclusions	95
6	Con	nclus	sions and recommendations	97
(6.1	Cor	nclusions	97
(6.2	Rec	commendations	99
Bil	bliog	aphy	y	100
An	nex A	A		105
An	nex l	В		107
An	nex (C		109
An	nex l	D		120
An	nex]	F [50	1	125

Introduction

1.1 Background

The growing need for reassessment of the bridges within the Dutch Highway system has increasingly been Rijkswaterstaat's subject of interest [3]. The motivation behind this, among others, is the fact that bridges, many of which were built over 60 years ago, are subjected to higher traffic loads than they were designed for [4]. Special attention goes out to the prestressed concrete beam bridges, as these types of structures constitute a significant part of Dutch road bridges [5]. A part of those structures was made continuous by casting an in situ top layer of concrete and cross beams above the supports [5]. On one hand, it enables the creation of more economical structures, but on the other, it results in more complex structural behaviour.

According to the available codes and design guidelines, which were also evolving in the past years, some bridges of this topology are at risk of not complying with the requirements [3]. In such a situation the question arises, whether it is possible to better understand the structural behaviour of these bridges and demonstrate that the resistance is sufficient. In accordance with [3], one of the crucial aspects that should be investigated is the influence of the interface's behaviour.

The interfacial performance is especially of interest, due to the presence of intermediate supports, hence negative bending moments and high shear forces. This implies that the stress conditions at the interface are different than in the case of simply supported prestressed concrete girder bridges.

One of the methods to assess the performance of existing structures is adopting the Nonlinear Finite Element Analysis (NLFEA) [4]. Properly executed NLFEA can not only be an aid in designing and specifying the experimental program of the research but also be a tool which enables the prediction of the structure's response and its failure load. In order to align modelling techniques and increase the reliability of NLFEA Dutch Ministry of Infrastructure and Water Management initiated the development of Guidelines for Nonlinear Finite Element Analysis of Concrete Structures [6]. The guidelines provide recommendations concerning the constitutive models, finite element discretization, loads and boundary conditions as well as analysis settings, among others load increments, iterative procedure and convergence criteria. It was noticed, however, that concrete-to-concrete interface constitutive models are not extensively covered, hence there is a necessity to investigate the subject to provide clear modelling solutions for the interfaces.

1.2 Problem statement

The main motivation for this research is the need for a more sophisticated reassessment of existing bridges in the Netherlands. Taking into account the scale of the problem, finding hidden capacities by a better understanding of the structural performance of the bridges will be highly beneficial. Strengthening or rebuilding the bridges may no longer be necessary, which is desirable from an environmental point of view. Moreover, the decrease in demand for extra labour and materials could possibly lead to financial savings.

For this specific type of structure, the interface behaviour should be studied since the composite action of structures is dependent on the effectiveness of the connection [7]. In addition, the cracking of the precast girders is assumed to influence the interface capacity [3]. What makes the problem even more complex is the influence of the hogging bending moment and substantially high shear forces in the vicinity of the intermediate supports. Another factor influencing the shear performance of the structure is the presence and amount of reinforcement crossing the interface. All the above-mentioned aspects need to be studied to gain an overall understanding of the interface behaviour [3].

What should be emphasised is that it is assumed that there are different stress conditions along the length of the interface. Above the intermediate support, tension perpendicular to the interface is expected, whereas compressive stresses are anticipated under the load application locations. Moreover, tangential tractions are also expected to vary along the beam's length. For this reasons, comprehensive research on the stress conditions is a crucial aspect. Based on the aforementioned investigation, in a later stage, it can be verified whether existing interface models can correctly predict the interface behaviour. If is not the case, it shall be pointed out what are their shortcomings and how they can be improved.

1.3 Thesis objective

1.3.1 General objective

Computational modelling is a powerful method for the safety assessment of concrete structures. Nevertheless, NLFEA is susceptible to variations in input parameters and is dependent on choices done by analysts [4]. To accurately simulate the structural performance, in this case, with emphasis on the behaviour of the interface, an appropriate solution strategy has to be developed to ensure consistency and increase the reliability of such assessment.

As the main goal of the research is to focus on computational modelling of the interfacial behaviour, the objective of the thesis would be to assess to what extent solution strategies for the NLFEA of the interface can be developed.

1.3.2 Research questions

- To what extent can the solution strategy for modelling the interface at concrete-to-concrete connections, between precast girders and cast-in-situ top layers, be developed?
 - · What are the stress conditions at the interface in the concrete-to-concrete connection with the emphasis on the vicinity of the intermediate supports? What are the stress conditions in the concrete elements, next to the interface, in this specific case?
 - · Are the available interface material models applicable for modelling the concrete-to-concrete connection in composite beams? What are the advantages and disadvantages of using certain material models, already available in FEA software packages? How the reinforcement crossing the interface can be incorporated in the model?

1.4 Methodology and thesis outline

The general outline of the report's structure is presented below.

Chapter 2: Literature review

• verification of current knowledge on the topic, existing design recommendations, previous experimental and numerical research, available material models and modelling guidelines.

Chapter 3: Linear analysis of the composite structure

- analytical verification of stresses in the beam for numerical model validation;
- numerical analysis analysis of the stresses in the concrete elements and at the interface along its length and at selected points;
- numerical analysis verification of the influence of the decrease of shear stiffness of the interface.

Chapter 4: Verification study of material models on a component level

- single element test verification of models accounting for coupling; sensitivity study of certain modelling aspects being top boundary condition, initial shear stiffness and residual friction angle;
- element assembly verification of the model accounting for coupling and beam, bond-slip reinforcements crossing the interface.

Chapter 5: Nonlinear analysis of the composite structure

• comparison of the performance of two material models and two sets of input parameters.

Chapter 6: Conclusions and recommendations

Literature review

2.1 Prefabricated beam bridges

2.1.1 History

Early development of prefabrication dates back to the beginning of the XX century. The first prefabricated, prestressed elements were introduced in the bridge construction field around the mid-30s, however, the largest expansion of the technology took place between 1950 and 1970. This was not only related to the development of prestressing techniques, but also an increased demand for rapid growth in road infrastructure [5]. On top of that, the scarcity of steel in Europe after the Second World War caused an increase in concrete use in bridge construction [8]. As prefabrication allows relatively quick assembly of the bridge structure, without causing disruption to the traffic, bridges and viaducts produced in this way were getting more and more utilised across many countries around the world. According to the Fib Bulletin [5] the Netherlands is among the countries where precast, prestressed structures establish over 50% of all of the bridges, however, that percentage could be suspected to be even as high as 90%.

An important aspect that contributed to the success of this technology was the introduction of high-strength steel wires which, in contrast to the initially used normal-strength steel tie rods, prevent excessive prestressing losses caused by elastic deformation, creep and shrinkage [8]. Over the years, produced elements were getting longer and more slender, which enabled the creation of larger spans. Moreover, the choice of elements kept getting wider, with types ranging from solid slabs, T, T, T, and inverted T beams, box beams to troughs [5] [9].



Figure 2.1 Prefabricated Y-beams [10]



Figure 2.2 Prefabricated U-beams [10]

Prestressed beams, being a very common type of precast element, have been in use in bridge construction for a few decades. Initially, they could be used as a part of a system where relatively small beams were placed close to each other, with flanges being in contact, forming the bottom of the slab and with the space between the beams and on top of them filled with concrete. Starting from the sixties large girders being 'I' or inverted 'T' beams have been widely applied in the construction of both simply supported and continuous bridges [5].

Among the advantages of building from precast elements, the economic savings due to a substantial level of repetition, high quality control, no need for formwork installation on site and speed of the construction may be listed. Nonetheless, there are also drawbacks of the technology, like non-appealing appearance and ambiguities concerning certain aspects of structural behaviour. As the aesthetics are a matter of subjective judgement and moreover are being handled by producers, who try to create more complex and slender elements, the structural attributes, such as uncertainty concerning stress transfer between precast parts and cast-in-situ concrete elements, still require more research [5] [3].

2.1.2 Production and assembly

The prefabricated beams used for bridges with moderate spans are usually produced as pre-tensioned elements [9]. The prestressing steel is stressed and anchored before casting the concrete. Commonly used are 7-wire strands made of six outer and one inner core wires [11]. The concrete is cast in proper, usually, steel moulds and after gaining sufficient strength the strands are released and cut. The prestressing is transferred through bond stress between steel and concrete [12]. The use of long casting beds facilitates the production of several elements as presented in Figure 2.3 [9].

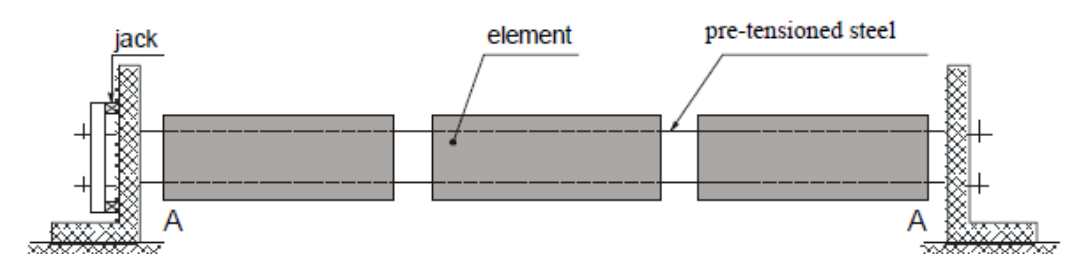


Figure 2.3 Scheme of production of pre-tensioned elements [12]

After being transported to the construction site, the beams are handled by a crane or an erection gantry in order to be placed on the bearings at a target position or the temporary supports. The scaffolding for the deck slab is usually placed in the small indentations in the web. It is a common practice to use permanent formwork, in the form of prefabricated concrete planks, especially for widely spaced beams. The example of a cross-section of the bridge constructed with the inverted "T" beams is presented in Figure 2.4 [9].

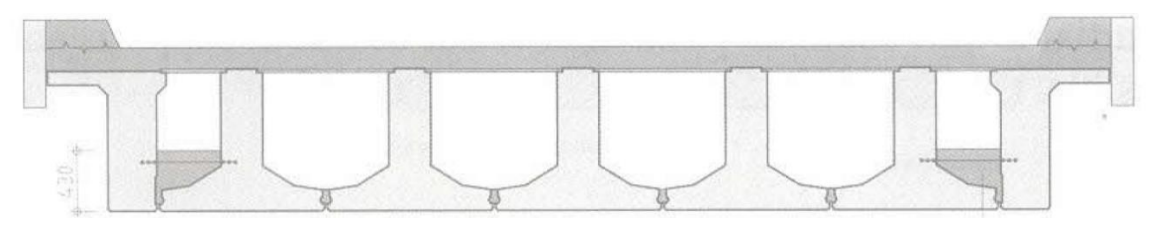


Figure 2.4 Example of the inverted 'T' beam bridge cross-section [5]

In the case of bridges with multiple spans, the beams can be simply supported on the piers, partially connected with a continuous slab or made continuous by in-situ cross-beams. There are a few ways how the continuity can be realised, nevertheless, irrespective of the procedure, the structural performance has to be considered at two stages. Firstly the beams are simply supported and have to carry their own weight and the weight of in-situ casted concrete, whereas after concrete hardening the structure, already regarded as continuous, has to withstand additional dead and live loads [5].

2.2 Concrete-to-concrete interface

When the structure consists of elements cast at different times one has to take the presence of the interface between the different structural components into account. Such a situation typically occurs in cast-in-place structures when the casting process is disrupted for scheduled, technical activities as well as in structures in which precast elements are connected with each other or with cast-in-situ components [13].





Figure 2.5 Interface between precast member and cast in situ concrete

Figure 2.6 Interface between precast members [14]

In the case of the abovementioned bridge types, consisting of prefabricated beams and a cast-in-situ deck, the interface between the girders and the slab plays a key role [15]. The deck not only provides the surface on which the vehicles can move but primarily, ensures the transfer of the load across multiple girders. Moreover, the cast-in-situ layer also constitutes part of the composite beam, enhancing its capacity. Therefore, the effectiveness of the connection is crucial, on one hand, to ensure load transfer across the beams, and on the other, to guarantee the composite action in the structure. If the bond between elements is weakened or broken, it can be highly detrimental to structural performance. The beams' capacity without the slab's contribution might not be sufficient to withstand the design loads and on top of that, in such a situation, the layer is only an additional weight being carried by the girders.

The lack of complete continuity not only triggers the necessity for special attention but also increases the vulnerability of the bond to various factors, such as improper roughening or excessive drying, which decrease its quality. Moreover, testing of the interface is not unambiguous as the results of the experiments are influenced by the scale of testing. Small-scale tests are easier to execute and can provide detailed information, however, they might not ensure that the behaviour will be the same in the case of the structure as a whole, with more complex loading, hence stress

conditions. The universality of the use on one hand and the intricacy of the subject on the other, have resulted in multiple researchers trying to investigate and deepen the topic [16].

2.2.1 Knowledge development

There have been numerous academics studying interface load transfer which resulted in several changes and adjustments in design formulas over the past few decades. Although it would be challenging to summarise the work of each and every one of them, a few academics are frequently pointed out, in more recent articles [16] [17], to have left a significant mark on the course of knowledge development on concrete interfaces.

The first crucial theory was presented in the late 60s. Shear-friction hypothesis was introduced by Birkeland, P. W. and Birkeland, H. W. [18] and it was established for interfaces crossed by reinforcement. The hypothesis is based on the assumption that in a cracked, rough connection subject to shear, not only a slip is observed, but also an opening of the crack. The opening produces tensile forces in the reinforcement, which generate clamping forces that provide friction, hence shear capacity. The authors compared the roughened interface to sawtooth ramps and related the strength to the tangent of the ramps' slope, the amount of reinforcement crossing the interface and its yield strength.

$$v_u = \rho f_y \tan \phi \text{ [MPa]} \tag{2.1}$$

Where:

 ρ is the reinforcement ratio

 f_{ν} is the yield strength of reinforcement crossing the interface

 $\tan \phi = \mu$ is the friction coefficient, dependent on the surface characteristics

1) $\mu = 1.7$ for monolithic concrete

2) $\mu = 1.4$ for artificially roughened joints

3) $\mu = 0.8 - 1.0$ for ordinary construction joints.

The hypothesis enables the calculation of the capacity in a simple way, however, it has certain shortcomings which were pointed out by other researchers [19]. In order to compensate for not including, among others, cohesion influence, the angle of internal friction has to be set to a high value, which does not represent reality. Experiments also revealed that for high values of ρf_y , the angle would have to be adjusted, hence the range of applicability of shear-friction theory is limited.

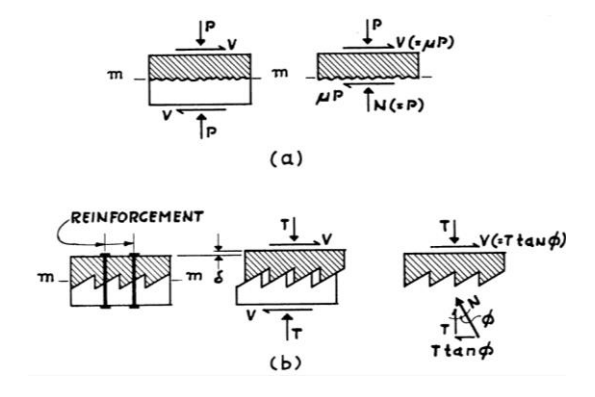


Figure 2.7 Shear friction theory [18]

The theory was further developed, which resulted in the modified shear friction theory, firstly proposed by Mattock and Hawkins [20]. They have conducted and analysed several series of tests on push-off, pull-off and modified push-off specimens to study shear transfer across interfaces with varying characteristics of the shear plane, size and spacing of reinforcement crossing the plane, concrete class, as well as stresses acting perpendicular and parallel to the plane. One of the conclusions that stemmed from the research was to include the influence of cohesion and external compression's contribution in the formula for shear capacity. The formula proposed by the authors is presented below.

$$v_u = 1.38 + 0.8(\rho f_v + \sigma_{Nx}) < 0.3 f_c \text{ [MPa]}$$
 (2.2)

Where:

 σ_{Nx} is the external stress acting across the shear plane, positive if compressive, negative if tensile is the concrete compressive strength.

Loov equation [21] is said to be the first one to take concrete strength into consideration and can be written as follows:

$$v_u = k \sqrt{f_c(\rho f_y + \sigma_n)} \quad [MPa]$$
 (2.3)

where k is constant, with a recommended value of 0.5 for uncracked interfaces.

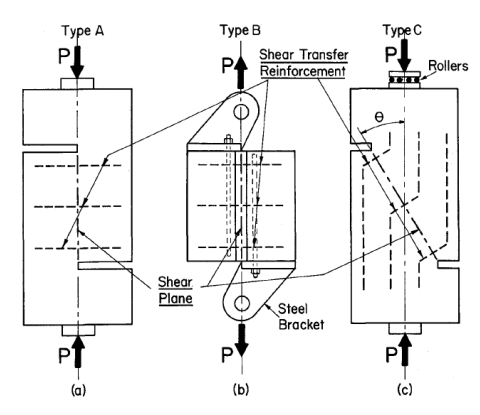


Figure 2.8 Test specimens used in [20] a) push-off b) pull-off c) modified push-off

Another researcher having had a major influence on the advancements in the understanding of the interface load transfer was Walraven [22] who focused his study on the aggregate interlock. Not only an experimental investigation was carried out, but also theoretical models were developed. The author emphasised the necessity to relate shear stresses with shear displacement as well as with normal stresses and crack opening. Another conclusion was that concrete strength influences the ultimate capacity.

In [23] the authors argued that shear friction and modified shear friction theory do not provide accurate results for high-strength concrete, as they were validated by tests carried out on normal-strength concrete specimens. It has been pointed out that shear transfer across two surfaces is intrinsically related to contact between aggregate particles and matrix surface, therefore concrete strength should be included in the equation. Based on experimental results evaluated in the research the following formula was proposed.

$$v_{y} = C_{1} (\rho f_{y})^{C_{2}} [MPa]$$

$$(2.4)$$

Where:

 $C_1 = 0.822 f_c^{0.406}$ [MPa] $C_2 = 0.159 f_c^{0.303}$ [MPa].

Further advancements concerning design expressions are results of the Randl's [24] [25] [26] [16] work. The suggested general design formula accounts for the bond induced by a chemical and physical force bond as well as aggregate interlock, the friction generated by both clamping stresses induced by reinforcing bars and external forces, along with dowel action which was not included by previous researchers [16].

$$v_u = \tau_a + \mu \cdot (\kappa_1 \cdot \rho \cdot f_y + \sigma_n) + \kappa_2 \cdot \rho \cdot \sqrt{f_{yd} \cdot f_{cd}} \le \beta_c \cdot v \cdot f_{cd}$$
 (2.5)

Where:

 τ_a is the strength generated by adhesion and/or aggregate interlock

 κ_1, κ_2 are the interaction coefficients

 μ is the friction coefficient

 σ_n is the external stress applied in a normal direction

 ρ is the interface's reinforcement ratio

 β_c is the coefficient related to the strength of the compression strut

v is the reduction factor.

2.2.2 Analytical formulas for concrete-to-concrete interface

2.2.2.1 NEN-EN 1992-1-1:2005

Eurocode 2 [2] specifies that the design value of shear stresses at the interface between concretes cast at different times should be lower than the design shear resistance given by the following formula.

$$v_{Rdi} = c \cdot f_{ctd} + \mu \cdot \sigma_n + \rho \cdot f_{vd} \cdot (\mu \sin \alpha + \cos \alpha) \le 0.5 \cdot v \cdot f_{cd}$$
 (2.6)

Where:

c and μ are factors related to adhesion and friction - dependent on the

roughness of the interface

 σ_n is the minimum stress per unit area initiated by the external normal force, that can act simultaneously with the shear force, positive for

compression and negative for tension

 $\rho = A_s/A_i$

 A_s is the area of the reinforcement crossing the interface, appropriately

anchored

 A_i is the interface area

 α is the angle of reinforcement inclination, measured between

the reinforcement's longitudinal axis and interface surface

 $v = 0.6 \left[1 - \frac{f_{ck}}{250} \right].$

The roughness classification can be simplified to very smooth, smooth, rough, and indented. The values of the factors c and μ are presented in Table 2.1.

Table 2.1 Adhesion and friction coefficient values according to NEN-EN 1992-1-1:2005 [2]

Surface roughness	С	μ
Very smooth	0.25	0.5
Smooth	0.35	0.6
Rough	0.45	0.7
Indented	0.50	0.9

2.2.2.2 NEN-EN 1992-1-1 draft version

In the draft version of Eurocode 2, which was referenced in [3], the formula for interface shear resistance varies from the one given in the currently used version [2]. Two design situations are recognised, based on the anchoring of the interfacial reinforcement. Equation (2.7) represents the case of unreinforced interfaces, or reinforced ones, but only with sufficient anchorage. The following (2.8) formula is given for the situation when the rebars crossing the interface are not adequately anchored, hence their yielding is not guaranteed.

$$\tau_{Rdi} = c_{v1} \cdot \sqrt{f_{ck}/\gamma_c} + \mu_v \cdot \sigma_n + \rho_i \cdot f_{yd} \cdot (\mu_v \cdot \sin \alpha + \cos \alpha) \le 0.5 \cdot v \cdot f_{cd}$$
 (2.7)

$$\tau_{Rdi} = c_{v2} \cdot \sqrt{f_{ck}/\gamma_c} + \mu_v \cdot \sigma_n + k_v \cdot \rho_i \cdot f_{yd} \cdot \mu_v + k_{dowel} \cdot \rho_i \cdot \sqrt{f_{yd}f_{cd}} \le 0.5 \cdot v \cdot f_{cd}$$
 (2.8)

Where:

are the coefficients dependent on the roughness of the interface $C_{v1}, C_{v2},$ $k_v, k_{dowel},$ μ_v is the characteristic concrete strength, taken as the minimum of the f_{ck} concretes' strengths is the normal stress caused by an external force acting simultaneously σ_n with the shear stress is the reinforcement ratio of the anchored reinforcement crossing the ρ_i interface is the angle of reinforcement inclination; $35^{\circ} \le \alpha \le 90^{\circ}$ α is the strength reduction factor; might be taken as 0.5.

As stated above, the values of certain coefficients are dependent on the roughness. The proposed values are provided in Table 2.2

Table 2.2 Coefficients dependent on surface roughness according to draft version of Eurocode 2 [3]

Surface roughness	c_{v1}	c_{v2}	k_v	k_{dowel}	μ_v
Very smooth	0.0095*	0	0	1.5	0.5
Smooth	0.075*	0	0.5	1.1	0.6
Rough	0.15*	0.075*	0.5	0.9	0.7
Very rough	0.19*	0.15*	0.5	0.9	0.9
Keyed	0.37	n.a	n.a.	n.a.	0.9

*in the case of the presence of tensile stresses, normal to the interface $c_{v1}=c_{v2}=0$

2.2.2.3 Fib Model Code for Concrete Structures 2010

Fib Model Code 2010 [27] also covers interface resistance calculations, and the code distinguishes two design situations. The distinction is made between rigid and non-rigid bond-slip behaviour. For interfaces without reinforcement, which are considered rigid, equation (2.9) is proposed. With regard to the interfaces crossed by dowels or reinforcing bars, the formula (2.10) is recommended. It should be highlighted that in contrast to Eurocode [2], fib Model Code 2010 considers the bending resistance of reinforcement or connectors crossing the interface.

$$\tau_{Rdi} = c_a \cdot f_{ctd} + \mu \cdot \sigma_n \le 0.5 \cdot v \cdot f_{cd} \tag{2.9}$$

$$\tau_{Rdi} = c_r \cdot f_{ck}^{\frac{1}{3}} + \mu \cdot \sigma_n + \kappa_1 \cdot \rho \cdot f_{yd}(\mu \sin \alpha + \cos \alpha) + \kappa_2 \cdot \rho \cdot \sqrt{f_{yd} \cdot f_{cd}} \le \beta_c \cdot \nu \cdot f_{cd} \qquad (2.10)$$

Where:

 c_a is the adhesive bond coefficient

 c_r is the factor accounting for aggregate interlock

 κ_1 is the tensile force interaction coefficient

 κ_2 is the flexural resistance interaction coefficient

 μ is the coefficient of friction

 σ_n is the minimal expected stress caused by an external normal force

acting on the interface

 ρ is the reinforcement ratio of the reinforcement crossing the interface

 α is the angle of reinforcement inclination

 β_c is the strength of the compression strut coefficient

$$v = 0.55 \left[1 - \frac{30}{f_{ck}} \right]^{1/3} < 0.55.$$

The coefficients used in the formula are dependent on the roughness of the interface. Appropriate values for certain roughness are listed in Table 2.3.

Table 2.3 Coefficients dependent on surface roughness according to Fib Model Code 2010 [27]

Surface roughness	c_a	c_r	κ_1	κ_2	eta_c	$\frac{\mu}{f_{ck} \ge 20 \mid f_{ck} \ge 35}$	
Very smooth	0.025	0	0	1.5	0.3	0.5	
Smooth	0.2	0	0.5	1.1	0.4	0.6	
Rough	0.4	0.1	0.5	0.9	0.5	0.7	
Very rough	0.5	0.2	0.5	0.9	0.5	0.8	1.0

2.2.3 Shear transfer mechanisms

Even though the behaviour of the concrete-to-concrete interface may vary depending on the existence of a crack prior to loading [28], the presence of the reinforcement crossing the interface or the surface preparation, certain shear transfer mechanisms can be recognized. Looking at currently used analytical formulas and taking into account previously mentioned developments, mechanical interlock and adhesive bonding, friction and dowel action are distinguished [16].

2.2.3.1 Adhesion and mechanical interlocking

The adhesive bonding is active since the very beginning of interface loading and for very rough interfaces between Normal-Strength Concretes (NSC), it was reported to provide even up to 3.5 N/mm2 of shear resistance [16]. Adhesion can develop irrespective of the surface roughness, owing to chemical and physical bonding, whereas for the aggregate interlock to be activated, the roughness has to be sufficiently high. It can be observed looking at the aggregate interlock factor values proposed by the fib Model Code 2010 [27], that for interfaces with peak-to-mean roughness lower than 1.5 mm the mechanical interlocking is not taken into account in shear resistance calculation. The influence of adhesion lasts only up until the bond is broken. The interlocking still has an impact, it is actually activated at this point, however, for larger slips, the protruding aggregates and other surface irregularities are being crushed, which reduces or even eliminates this mechanism's contribution [16] [27]. It should be noted at the same time, that the currently used version of Eurocode 2 [2] does not distinguish between the adhesive and interlocking transfer mechanisms, and certain, initial value of bonding is always accounted for, even for very smooth interfaces.

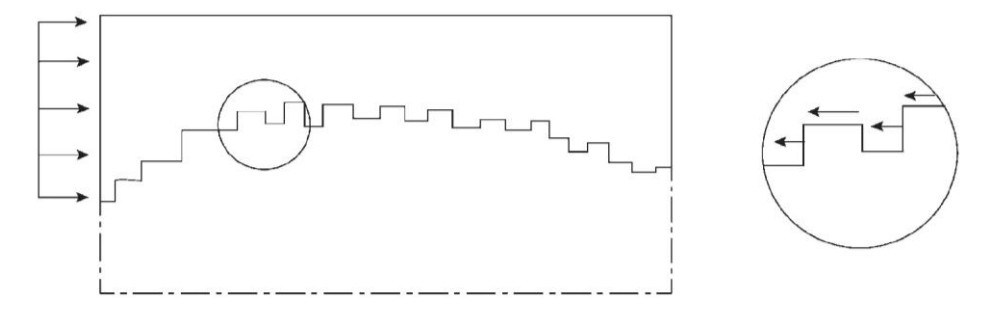


Figure 2.9 Scheme of the mechanism of interlocking [27]

2.2.3.2 Friction

There are two sources of friction in the concrete-to-concrete interfaces. Firstly, clamping forces are generated due to the presence of reinforcing bars or connectors. They restrain the opening of the crack when surfaces slip with respect to each other, which was essentially the basis for the shear friction theory proposed by Birkeland and Birkeland [18]. The second contribution stems from externally applied compressive stresses perpendicular to the interface surface. This mechanism is also dependent on the surface roughness, as previously outlined aggregate interlock is [16].

2.2.3.3 Reinforcement contribution

Reinforcement not only provides axial forces generating clamping stresses but also contributes by means of different mechanisms. The "dowel action" describes the bending capacity provided by the steel crossing the interface. Steel connectors or rebars also deliver shearing capacity and enable horizontal force transfer by kinking of the bar. It should be noted, however, that kinking can be activated only for relatively large slips, which may exceed serviceability limits. Shearing of the connectors is also unlikely to be governing, as it is more probable that concrete would crush first. Considering the above, mainly the axial and bending resistances influence the shear transfer across the interface [16]. The interaction of both actions has to be accounted for, as neither axial nor bending capacity can be fully utilised.

In the fib Model Code 2010 [27] the interaction is considered by the introduction of κ coefficients, for axial and flexural resistance contributions [16]. In the current version of Eurocode 2 [2], dowel action is not accounted for.

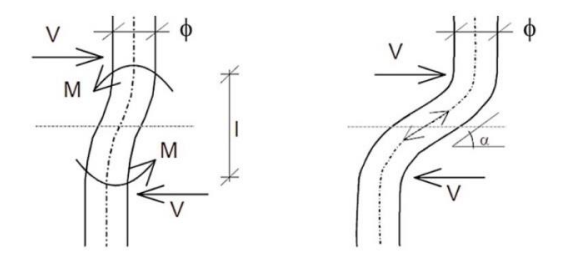
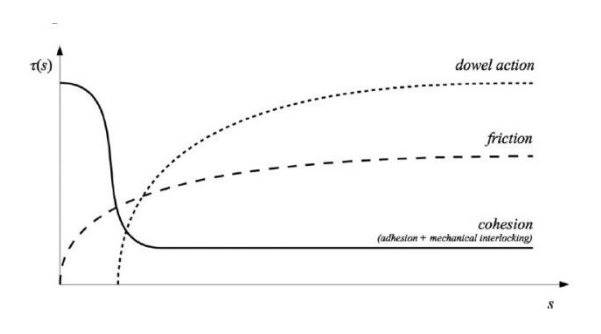


Figure 2.10 Bending and kinking of the reinforcing bar [16]

2.2.3.4 Resistance

The impact of the mechanisms cannot simply be added, as the level of contribution differs and is dependent on the relative displacements between concrete parts. The influence of each mechanism, as a function of slip, is schematically shown in Figure 2.11. In [17] authors compare design expressions given in Eurocode 2 [2], fib Model Code 2010 [27], and ACI 318 [29]. The only mechanism accounted for in all of them is friction. Fib Model Code 2010 [27] takes all contributions into account, however, two design situations are distinguished. It is argued that in the case, of joints with little or no reinforcement, the behaviour is primarily dependent on adhesion, hence the failure is brittle and should be considered differently than the heavily reinforced connections. Both design expressions are based on the Coulomb friction failure criterion, with the additional influence of dowel action in the case of non-rigid connections. There is a difference in initial shear resistance, which in rigid joints is owed to the adhesion and proven to be dependent on the tensile strength of concrete, whereas in non-rigid connections it is related to the interlocking, thus the compressive strength [16].



Reinforced joint, very rough τ_{max} No reinforcement, slightly roughened $w_1 \approx 0.55 \text{ mm}$ $w_1 \approx 0.5-1.5 \text{ mm}$

Figure 2.11 Scheme of contribution of transfer mechanism as a function of slip [17]

Figure 2.12 Traction-relative displacement curves for different join types [16]

Although it seems that the topic is sufficiently explored and the formulas were validated with experimental data, there are some points of concern. In the first place, Randl [16] highlighted that adhesion's impact was verified with NSC tests, while for High-Strength Concrete (HSC) the capacity could be higher. Similarly, friction coefficients in experiments with HSC were reported to be higher than suggested in fib Model Code 2010 [27]. On top of that, looking at Figure 14 from the same technical paper [16], the equation provides lower bound estimates for the shear capacity. Croes [30], who performed experimental research on unreinforced

concrete-to-concrete interfaces, drew a comparable conclusion, that the design expressions provided by both Eurocode 2 [2] and fib Model Code 2010 [27], yield conservative values for interface strength. Even though it is beneficial from the safety point of view, it can underestimate the true capacity of the structure, which is undesirable when reassessing existing structures. Moreover, it is also observed, that as far as initial bond is concerned, there is no uniformity among design codes.

2.2.4 Previous experimental research

The experimental studies on the force transfer at the interface, especially on component-level specimens, have been performed and described by several researchers, as already mentioned in Subchapter 2.2.1. A brief overview of tests which are commonly performed to assess the bond strength was done by Espeche and León [31] and the scheme that they prepared is presented below.

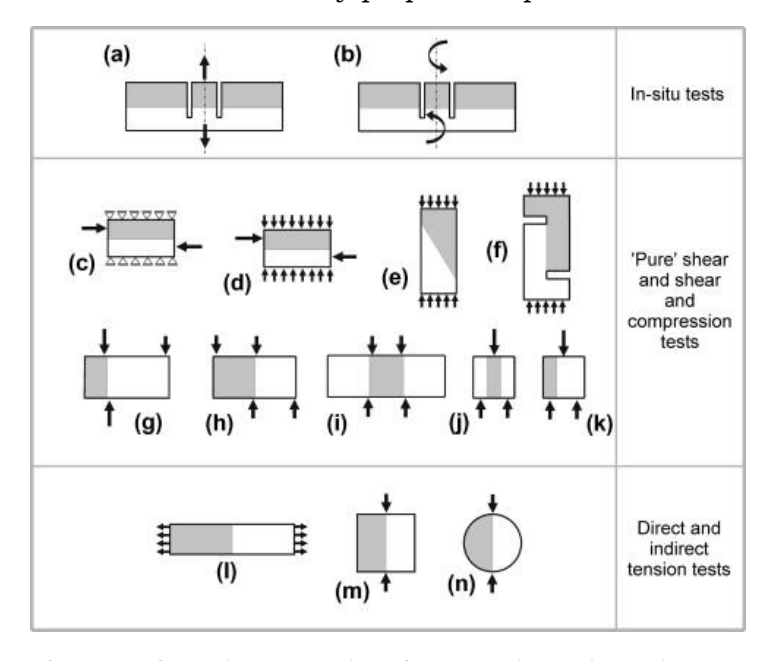


Figure 2.13 Types of tests performed to assess interface capacity under various stress conditions [31]

Figure 2.8 a) and Figure 2.13 (f) display the push-off specimen, which is the most typical test specimen for assessing shear capacity. Such samples, with slight changes concerning dimensions or presence and the amount of crossing reinforcement, have been tested, among others, by Hofbeck, Ibrahim and Mattock [19], Walraven and Reinhardt [22] or more recently by Júlio et al. [32] and Rahal, Khaleefi and Al-Sanee [33]. In that type of experimental setup, pure shear is aimed to be introduced at the interface. It is also the case, in the direct shear test presented in Figure 2.13 (c), the guillotine test displayed in (h, i, j) or the bisurface test shown under (k). It should be underlined, however, that the pure shear state is difficult to obtain, and some bending moments are usually present [31].

Tensile resistance is being verified in the pull-off, the direct tension or the splitting tension tests presented in Figure 2.13 (a) (l) and (m,n) respectively.

In order to verify the behaviour under more complex stress conditions, adjustments were made for example in the case of modified push-off proposed by Mattock and Hawkins [20], who wanted to establish the influence of compressive stresses. Another type of experiment, that is usually performed, is the slant shear test, sketched in Figure 2.13 (e), in which the interface is under shear and compression.

Such experimental setup was used among others by Santos and Júlio [17], and Randl and Zanotti [34].

Experiments focusing on the topic of the interface, conducted on bigger scale specimens have also been found.

2.2.4.1 Loov and Patnaik [15]

Loov and Patnaik performed tests on sixteen composite girders representing prefabricated concrete beams with a cast-in-situ slab. The beams had varying concrete strength and clamping stress values, as well as web thicknesses. There were two main groups of beams – half of them had the flange covering the whole length of the web, whereas the other half had a shorter flange, exposing 400 mm of the web on both sides of the beam. The specimens were tested under three-point bending. Load–slip relations were recorded using slip gauges and strains, in the reinforcement were measured by strain gauges.

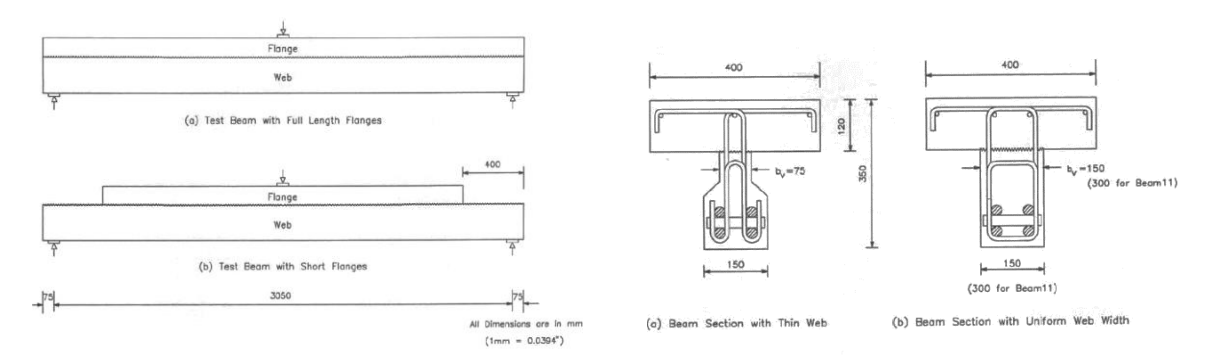


Figure 2.14 Side view of experimental setup [15]

Figure 2.15 Cross-sections of beams [15]

One of the conclusions that could be drawn is that slip was not substantial until traction reached 1.5 – 2 MPa, which is in line with adhesive bond strength values for slightly roughen surfaces presented by [16]. Maximum shear stresses were documented for slips between 0.3 to 0.8 mm which also partially corresponds to the slips presented in Figure 2.12. Moreover, it was recorded that the yielding of steel occurred at slips of around 0.5 mm, and slips at failure ranged from 2 to 7 mm. One of the beams set an example for the importance of surface characteristics, as due to lower roughness it developed considerably lower strength than other girders.

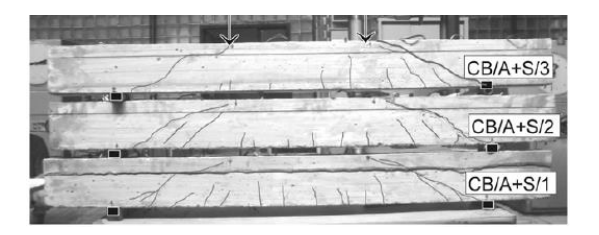
On one hand, the study provides a lot of insights into interface behaviour in composite concrete beams. On the other, there are some matters worth highlighting. Firstly, girders are subjected to a positive bending moment, which is in contrast to the point of concern of this research. Secondly, it is already reported, that the cracking did not develop above the support area and generally due to complex strain conditions interface behaviour was not well determined there. Moreover, it ought to be pointed out that beams were designed in a way, that they would not fail in flexure or diagonal shear so that the interface behaviour could be examined.

2.2.4.2 Halicka [7]

The author has conducted three series of four-point bending tests on simply supported composite beams, where the influence of the surface preparation and presence of stirrups on governing failure mechanism was verified. The relative displacement of concrete parts was measured, as well as the interface opening and the strains in the reinforcement.

In this case, the beams failed due to shear in support zones, and the horizontal slip values recorded in the experiments are not substantial or even not present as in the case of interfaces with adhesive bond. In the beams where adhesion was ensured, diagonal cracking appeared in the bottom part, further propagating horizontally towards the loading points and expanding in the new concrete layer. In the reinforced interface with no adhesion, cracking at the interface appeared at first and afterwards propagated towards the supports in the form of steep, diagonal cracks.

Even though in this case the interface is, almost entirely, in the compressed part of the beam, a conclusion can be drawn that the interfacial and beam behaviour affect each other. The overall performance depends on the stress conditions in the beam as well as at the juncture.



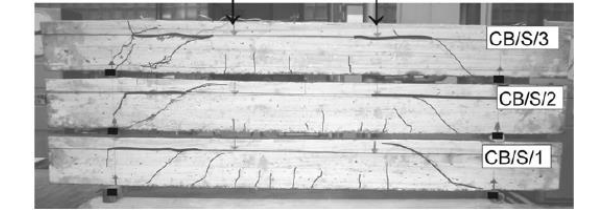


Figure 2.16 Crack pattern of beams with stirrups and ensured adhesion tested by Halicka [7]

Figure 2.17 Crack pattern of beams with stirrups but without adhesion tested by Halicka [7]

2.2.4.3 Harrass [35]

A series of experiments on composite concrete-to-strain hardening cementitious composites (SHCC) samples has been performed at TU Delft, with emphasis on interfacial behaviour. Seven different samples were tested, with varying interface roughness, curing methods and the presence of stirrups at the joint.

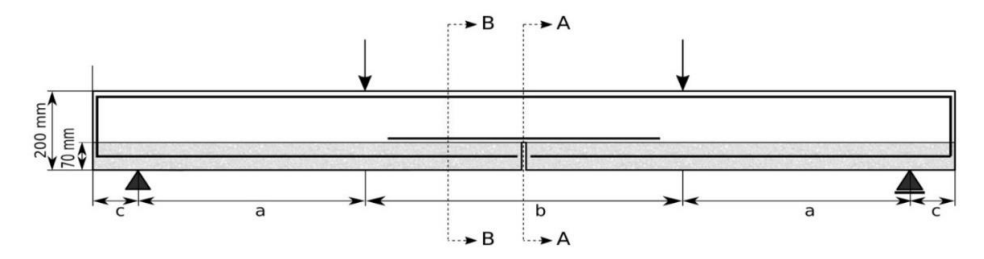


Figure 2.18 Experimental setup provided by Harras [35]

This research can prove to be useful as in this case the connection between concretes was in the tensioned part of the beam. It was confirmed among others that the roughness of the interface has an influence on the bearing capacity of the composite element. The positive effect of stirrups crossing the interface was also demonstrated. Based on the performed numerical research, it was shown, among others, that dilatancy angle had an effect on both interfacial and overall structural behaviour.

2.3 Computational modelling of the interfaces

2.3.1 Finite element modelling

Finite element analysis is a method of solving physical problems employing discretizing a continuum into a finite number of elements. It entails making approximations, which are to simplify the solution of the problem while providing

accuracy when increasing the number of elements [36]. In structural engineering considerations, a physical problem has to be schematized first to a mechanical model and subsequently to the finite element model [6]. Several assumptions have to be made in the process, starting from the choice of level of detail, through boundary conditions to material models [6].

In order to ensure a satisfactory level of reliability and results' independence from analysts' choices, the guidelines for NLFEA have been developed [4]. Experimental research on larger structures such as existing bridges can be said to either not be possible at all or be costly and highly invasive, as it leads to structural destruction. Nevertheless, experimental data is required to perform the validation studies and verify the applicability of specific solution strategies [4]. The results available in the literature may be useful for models' verification and calibration, but at the same time, particular tests on elements representing the structures in question can be performed in a laboratory, limiting the necessity for extensive, invasive testing.

DIANA FEA 10.5 software was used for all finite element analyses completed within the course of this research. Solution strategies should provide the analyst with modelling recommendations, which can be applied by engineers irrespective of the software they use and ensure that results are not dependent on the choice of the program [4]. Nevertheless, the applicability of certain solutions for use with other software than DIANA is not verified.

2.3.2 Interface element types in DIANA FEA

The most basic method of modelling the interface between two adjacent elements is to assume a rigid connection, thus connecting the nodes of the elements. However, when discontinuities influencing the overall structural behaviour, such as discrete cracks, joints in masonry or connections between concretes cast at different times, are to be modelled, the application of structural interface elements might be useful, or even necessary. DIANA offers several structural interface element types, depending on the field of application, among which three basic groups can be distinguished:

- · nodal interface elements,
- · line interface elements,
- · plane interface elements.

They vary between each other on the basis of the number of nodes, shape in case of plane elements, possible use in 2D or 3D and interpolation order. The example of structural interface elements can be observed in Figure 2.19 and Figure 2.20 with their topology on the left-hand side and allowed displacements on the right-hand side [37].

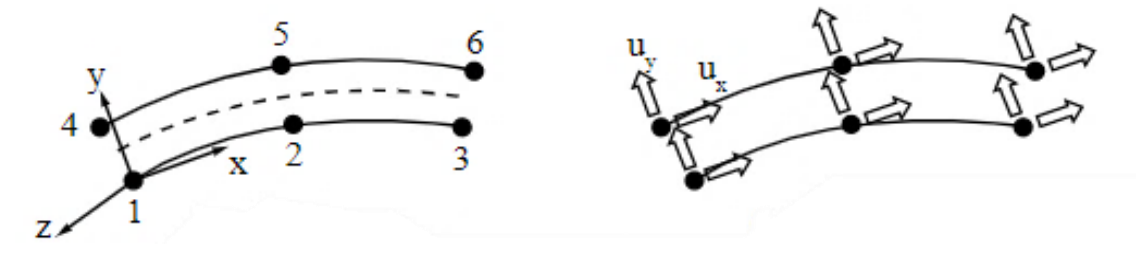


Figure 2.19 Line, 2D structural interface element, with 3+3 nodes [37]

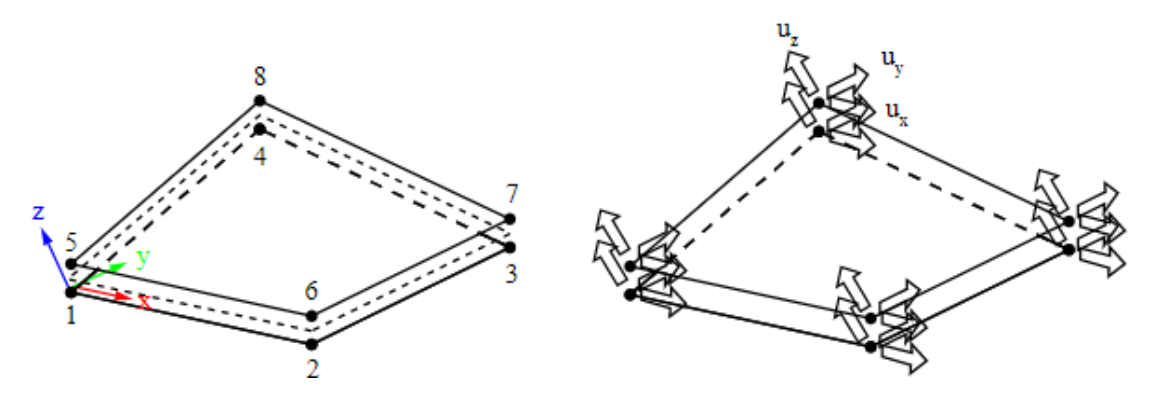


Figure 2.20 Plane, quadrilateral structural interface element with 4+4 nodes [37]

2.3.3 Interface material models available in DIANA FEA

The main purpose of the structural interface elements is to describe the relationship between shear and normal tractions and relative tangential and normal displacements, which is dependent on the chosen material model. The simplest, linear relation for a case of plane interface structural element can be described as follows:

$$\begin{pmatrix} t_n \\ t_s \\ t_t \end{pmatrix} = \begin{bmatrix} k_n & 0 & 0 \\ 0 & k_s & 0 \\ 0 & 0 & k_t \end{bmatrix} \begin{pmatrix} \Delta u_n \\ \Delta u_s \\ \Delta u_t \end{pmatrix}$$

where:

 t_n, t_s, t_t are the normal, and shear tractions respectively,

 k_n, k_s, k_t are the stiffnesses describing the relation between the tractions and the relative displacements in normal and tangential directions,

 $\Delta u_n, \Delta u_s, \Delta u_t$ are the relative displacements in normal and tangential directions [37].

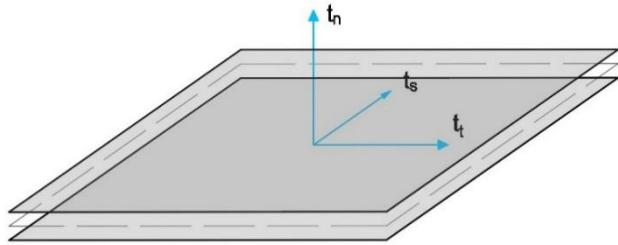


Figure 2.21 Sketch of three-dimensional interface element with indicated tractions

Nonlinearity can be introduced by means of diagrams, or functions that reduce the stiffness for certain interface opening or slip. In several cases, the coupling between normal and shear tractions might be necessary to be implemented, which is also facilitated by certain constitutive models. In such a case the non-diagonal entries of the stiffness matrix are no longer equal to zero. There are also more sophisticated models enabling the description of post-peak behaviour on the basis of, for instance, fracture energy. In Table 2.4 a brief overview of some of the available interface models is presented [37]. An extended table is included in Annex A.

Table 2.4 Overview of key material models for structural interfaces available in DIANA FEA [37]

Material model	Short description
Linear Elasticity	Only the linear behaviour of the interface can be described. Stiffness in normal and tangential directions is required as an input.
Nonlinear Elasticity	Nonlinearity is introduced by means of diagrams or functions reducing stiffnesses for certain, critical values of relative displacements.
Discrete Cracking	Constitutive relation to model discrete cracks. Stiffness in normal and shear directions have to be indicated, nevertheless, the behaviour in the normal direction is more significant. The post-peak behaviour can be specified to be either brittle or with an application of linear or nonlinear tension softening.
Crack Dilatancy	The model is activated when certain shear traction and crack opening is present. Tension softening can be specified for the development of the cracking stage. In the open-crack stage, the tractions in normal and tangential directions are coupled, hence non-diagonal entries of crack stiffness coefficients' matrix are non-zero. There are five mathematical models to choose from, which are based on either empirical results or assumptions and theoretical models [38].
Bond Slip	The model is used only with line interfaces utilised to describe contact between reinforcement and concrete. In the normal direction, the relation is assumed to be linear, while in shear nonlinearity is introduced by predefined or user-specified functions.
Coulomb Friction	Based on the Mohr-Coulomb plasticity model for continuum elements. The coupling between normal and tangential tractions and displacements is accounted for. Apart from initial stiffness parameters cohesion, friction and dilatancy angle, as well as interface opening model are to be specified.
Nonlinear Elastic Friction	Material model stemming from Coulomb Friction model, however, it is simplified as it only allows to model elastic behaviour. The model takes cohesion and friction angle into account. Properties can be either specified or based on properties of neighbouring elements.
Combined Cracking- Shearing-Crushing (CCSC)	Diana Manual [37] and reference study [39] emphasize the application of this model in masonry structures. CCSC also stems from Coulomb friction model. It encompasses modelling of the cracking, shearing and crushing along the interface or of the material that the elements represent. The constitutive relation involves a substantial amount of input parameters, some of which should be determined experimentally.

2.3.4 Previous numerical research

2.3.4.1 Component-level studies

Numerical calculations of small-scale experiments have been performed by several researchers, as it is needed to verify the applicability of the newly introduced material models to represent the interface behaviour. For instance, the Crack Dilatancy model proposed by Bažant and Gambarova [40] has been based on functions fitting Paulay and Loeber's [41] experimental results. The relations given by the authors were verified in numerical calculations fitting, among others, Mattock's tests, with rather satisfying results, especially for slips lower than 0.2 mm. Paulay and Loeber's [41] tests were also used to validate all five, existing crack dilatancy constitutive relations by Feenstra, de Borst and Rots [42]. The models with constant crack width, consisting of two plane stress elements and one interface element, yielded results which proved to be in acceptable agreement with experiments, with decreasing scatter for larger surfaces' opening in the normal direction.

Dias-da-Costa, Alfaiate and Júlio [43] performed numerical research on push-off specimens. The model they built was firstly validated with experimental results and further utilised to complete a parametric study on a few influencing parameters. A plasticity model with a Coulomb friction law yield surface was used for the interface elements. In the research, the concrete was considered as linear elastic in tension and elastic-perfectly plastic in compression. Reinforcement crossing the connection surface was modelled using truss elements. The bond-slip was accounted for by using interface elements with constitutive law based on the relation given in fib Model Code 2010. Values of input parameters like dilatancy angle, cohesion or stiffness values were given. The authors also highlighted the importance of applied boundary conditions. These pieces of information can serve as guidance, however, the stress conditions may vary from the considered case of prefab girder-to-top layer connection. Moreover, the simplifications being forcing the crack to appear along the interface, and disregarding shear and bending resistance of reinforcing bars which were modelled as trusses, are acknowledged.

Concrete-to-concrete interface modelling was also done with Abaqus code, by Dudziak, Jackiewicz-Rek and Kozyra [44] using the interface, cohesive elements with the elastic-damage traction-separation-type material model, which was enhanced by the authors. The authors provided values of input parameters utilised for models' calibration, hence magnitudes of such parameters as initial stiffness or Mode II fracture energy can be considered valuable for further modelling purposes. It should be highlighted that the modelled interfaces were unreinforced.

2.3.4.2 Structural-level studies

Van den Heever et al. [45] performed a FEA of 3D Concrete Printed (3DCP) element, employing, among others, a micro-modelling approach involving interface elements representing interfacial regions and continuum elements representing concrete layers. The combined Cracking-Shearing-Crushing model available in DIANA was used for the interfaces. The authors provided the input parameters that they used and what are they based on, as well as proved that results obtained from FEA are in good agreement with the experiments.

As already mentioned, Harrass [35] has performed the experimental analysis of SHCC-concrete composite beams and carried out inverse modelling using FE software DIANA. As the focus of the research was the structural SHCC-concrete interface, the author provided some recommendations concerning numerical analysis and input for the Coulomb Friction material model. Numerical studies on the interfacial behaviour of the beams tested by Harrass have been brought to a higher level of complexity by Setyanto [46]. The samples with smooth surfaces were modelled, moreover, the SHCC was used in the experiments. However, as already stated, the stress conditions at the interface are expected to be different than in the case of composite beams with the interface located in the compressed zone, hence the study was considered interesting. Table 2.5 shows the overview concerning the input for structural interfaces' material models, applied by other researchers, prepared by Setyanto [46]. The author, in his research, performed several numerical analyses, studying 2D and 3D models with varying parameters being interfacial stiffness, tensile strength, cohesion, friction angle, spacing of lap splice and connecting reinforcement, as well as applied lateral restraints. The reference models were validated with tests' results, and further, the numerical, sensitivity study was performed to analyse the influence of particular factors. In the case of unreinforced interfaces, stiffness and tensile strength of the interface had the biggest influence on the beam's capacity, whereas, for reinforced joints, cohesion was observed to have significant effect. Only two interface models were further studied - smooth interface based on the Coulomb Friction constitutive relation and perfectly bonded interface therefore there is still room for further investigation.

Table 2.5 Summary performed by Setyanto [46] of concrete-to-concrete interface properties used by researchers studying composite plank floor systems

Reference	Lundgren [22]	abt [26]	Harrass [1]	Bouwsema [27]
Material model	Coulomb	Coulomb	Coulomb	Non-linear
	friction	friction	friction	elastic friction
Normal stiffness modulus	1000	60000	1200	10
Shear stiffness modulus	100	6000	1200	10
Cohesion (MPa)	0.58	0.5	1.0	0.2
Friction angle (rad)	0.73	0.54	0.85	0.38
Dilatancy angle (rad)	0.1	0	1.0	Not applicable
Tensile strength (MPa)	Not available	0.5	0.5	Not applicable

Minalu [47] provided in his thesis quite an extensive literature review concerning the FEA of skew bridges. When the bridge is modelled as a three-dimensional structure and there is no emphasis on verifying interfacial behaviour, the connection is usually assumed to be rigid since such details are not considered to be that relevant. The author has created five models of the composite, precast beam bridge, using varying element types, among others, isotropic and orthotropic plates, beam elements or solids and it appears that in all cases the connection was always represented by sharing the nodes. Therefore, unless spring elements introducing certain stiffness to the connection between the girders and the deck are applied, the interface's impact is neglected.

2.3.4.3 Guidelines

As far as the guidelines [6] are concerned, the interface is only briefly mentioned, when describing the recommendations concerning boundary conditions. It is

advised to avoid stress concentrations by employing the loading and supporting plates, connecting them with the element under consideration through the interface elements. No-tension, low-friction material models should be applied, with substantially high stiffness in compression. When modelling a certain element, for instance, a thin layer of mortar, the interface elements can be used with the stiffness set to the quotient of material stiffness by its thickness.

2.4 Concluding remarks

A summary of the cohesion and friction coefficients for the interfaces with similar characteristics to the studied beam-to-top layer case, is presented below. The coefficients were assumed worth reviewing since design codes utilise them in the interface capacity calculations, and they are needed as an input for certain, interface material models. Part of the values was calibrated for numerical modelling purposes, for some the formulas were proposed, and others were obtained to fit the experimental data. It should be noted that some values were not explicitly given by the authors, thus some data processing was done before preparing the table. It is also to be highlighted, that the cohesion coefficient was selected in a way, to represent the bond between concretes, with the notion that when multiplied by mean tensile strength, it will yield the value of initial cohesion. The values of coefficients considered as a best guess are also in line with data given by Randl [16] for very rough surfaces.

Table 2.6 Cohesion and friction coefficients for interfaces with similar characteristics

Author	or Source Interface preparation Note		Note	С	μ
R.E. Loov, A.K. [15] wit		Left as cast with protruding aggregates	Calculation described in Annex B	0.73 1.26	0.98 1.53
P.M.D. Santos	[48]	[48] Shot-blasted; $c = 1.062 \cdot R_{vm}^{0.145}$ $R_{vm} = 0.809$ $\mu = 1.366 \cdot R_{vm}^{0.041}$		1.03	1.35
D. Dias-da- Costa J. Alfaiate, E.N.B.S. Júlio	[43]	Sand-blasted	Values obtained to fit the experimental data	1.38	0.95
M.E. Mohamad et al.	[49]		$c = 0.2363 \cdot e^{0.237R_{pm}}$ $\mu = 0.8766 \cdot R_{pm}^{0.3978}$	0.98	1.79
M. E Mohamad, I. S. Ibrahim	[1]	Wire-brushed	Values obtained to fit the experimental data	1.21	2.02
S. Dudziak, W. Jackiewicz- Rek, Z. Kozyra	[44]	Wire-brushed	Values calibrated for modelling purposes	1.10	1.19
Eurocode 2	[2]	Rough	Design code value	0.45	0.70
fib Model Code 2010	[27]	Rough	Design code value	0.40* 0.10**	0.70***
Assumed best guess				1.00	1.30

*value given for the case of interface without reinforcement; the coefficient for adhesive bond

**value given for the case of interface intersected by dowels or reinforcement; the code accounts for aggregate interlock mechanism; the coefficient shall be multiplied with $f_{ck}^{1/3}$ instead of tensile strength

***for the friction generated by reinforcement there are also interaction coefficients included

 $^{****}R_{pm}$ was calculated as a mean value for the results given for transversely and longitudinally roughen surfaces

With:

 R_{vm} is the roughness parameter - Mean Valley Depth R_{pm} is the roughness parameter - Mean Peak Height

On the basis of the literature analysis, it is concluded that there is still quite a big scatter concerning cohesion and friction values which shall be used, with design codes recommendations [2] [27] being quite conservative.

The general conclusion is that limited information has been found on the modelling of the interface in continuous, composite concrete girders. Most of the numerical studies concern either a very thorough analysis of component-level experiments, or they focus on simply supported elements with very few recommendations concerning modelling the connection between the elements, which are frequently assumed to be perfectly bonded, especially on a structural level. It shows that a certain balance between complexity and applicability has to be found.

As shown in Table 2.4, the selection of interfacial material models is rather broad. The use of linear or nonlinear elasticity constitutive relations, due to the limited number of input parameters and ease of use, seem a logical choice to start with. Nonetheless, it can be argued that such modelling does not reflect the real behaviour of the interface and that it is oversimplified. On the other hand, more sophisticated material models, like Combined Cracking-Shearing-Crushing, require not only a set of input parameters which are not as tangible and straightforward to test as compressive or tensile strength but also basic knowledge about the theoretical background of the model.

Composite beam structural behaviour – Linear Analysis

The assessment of the concrete-to-concrete interface performance was preceded by an initial analysis of the structural behaviour of the composite beam in question. The stress distribution in the vicinity and at the interface is crucial for assessing the behaviour and later performing computational analysis to analyse the behaviour of the interface itself. The knowledge of the interfacial stress conditions is also of importance when planning further experimental research. Component-level tests can be executed in a way to test the interface in similar conditions to the ones present in composite bridge structures, between precast beams and top layers. In order to evaluate the structural behaviour both, analytical, based on Euler-Bernoulli beam theory, and finite element analyses were performed. To simplify the task, the assumption of linearity of the specimens' behaviour was made at this stage.

3.1 Test specimen

3.1.1 Geometric and material properties

The specimen under consideration is a concrete, composite, statically indeterminate girder, representing an element being a part of existing bridge structures. The beam is constructed from two precast beam elements, connected with a cast in situ cross beam and top layer. The geometry of the sample is presented in Figure 3.1 and Figure 3.2. The beam's side view along with the position of supports and loading points is indicated in Figure 3.1. Cross-section dimensions and position of prestressing strands are presented in Figure 3.2. The strands have a 12.9 mm diameter. For the sake of simplicity, reinforcing bars are not included in the sketches as the alignment of reinforcement is quite complex. Moreover, as the analyses performed within this chapter are linear, just the prestressing strands were included in the models. The only information utilised at this point of the research is the reinforcement ratio of rebars crossing the interface. It ought to be highlighted, that the girder in question is a representative element of the extensive research program, comprising several specimens with various alignments and amounts of reinforcing bars. The ratio of the reinforcement crossing the interface is assumed to be equal to the minimal web shear reinforcement ratio $\rho_i = \rho_{w_{min}} = 0.12\%$.

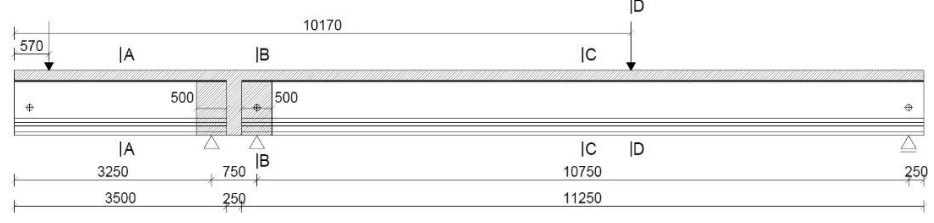


Figure 3.1 Beam geometry

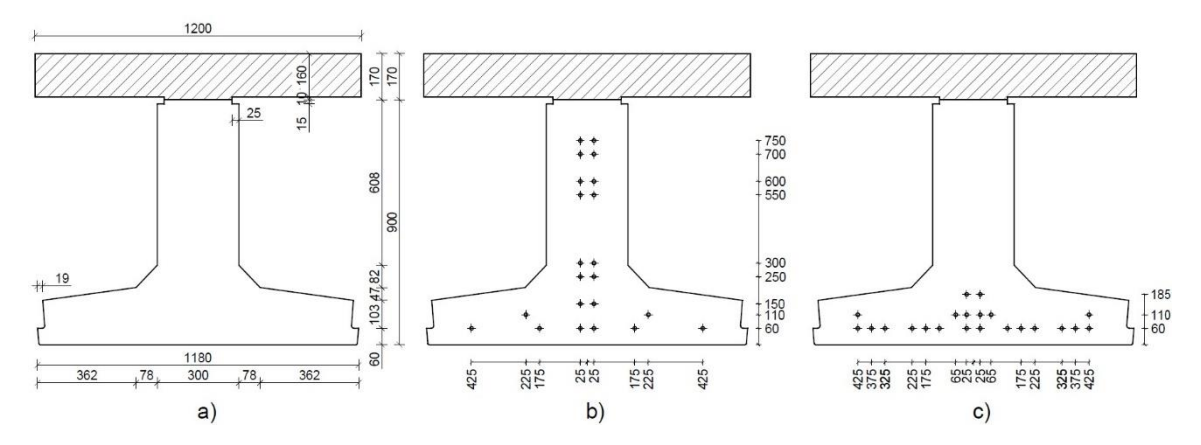


Figure 3.2 a) Dimensions of cross-section, along with b) position of prestressing tendons at the location A-A c) and B-B

Material properties used in the analyses of the beam are listed in Table 3.1. Cubic specimens were tested in the lab to assess the strength of the concrete used for the top layer. The results were in the range between 45 MPa and 50 MPa. Based on engineering judgement, the value of 47.5 MPa was divided by 1.25 to obtain the mean value of concrete cylinder compressive strength and further assign the concrete class of C30/37, in accordance with Eurocode 2 [2]. The concrete class of the girders, both, the ultimate one and when releasing the prestressing tendons, were given by the prefabricated beams' producer. For both compressive and tensile strength, the mean, characteristic and design values were defined according to Eurocode 2 [2] for given concrete classes. Precast beams' manufacturer also provided reinforcing and prestressing steel types. The tested yield strength of the reinforcing steel varied between 524 MPa and 593 MPa, hence the value of $f_y = 540$ MPa is assumed. The other assumed characteristics of rebars and strands follow the Eurocode 2 [2] and EN 10138-3 [50] recommendations.

Table 3.1 Material properties of the composite beam

Material	Class/Type
Concrete – top layer	C30/37
Concrete – precast beams	C55/C67
Concrete – precast beams (tendons' release)	C30/37*
Reinforcing steel	B500B
Prestressing steel	Y1860S7

*The producer guaranteed the class of C32/40 however, the class was assumed to be C30/37 to be consistent with Table 3.1 of Eurocode 2 [2].

3.1.2 Phases of construction

The girder consists of two, initially simply supported, prestressed elements, later connected to form a composite, continuous beam. It is essential to take that into account while assessing structural behaviour, as the phases of construction and loading play a key role in the development of stresses in the structure. The phases distinguished in the process are presented in Figure 3.3 and can be described as follows:

- 1. simply supported concrete beams
 - a. subject to prestressing loading
 - b. prestressed, under self-weight
 - c. prestressed, under self-weight and 5/8 weight of wet concrete
- 2. continuous, composite beam
 - a. under the whole dead load, supported in 3 points (demoulding of the top deck and removing left support)
 - b. under imposed live load

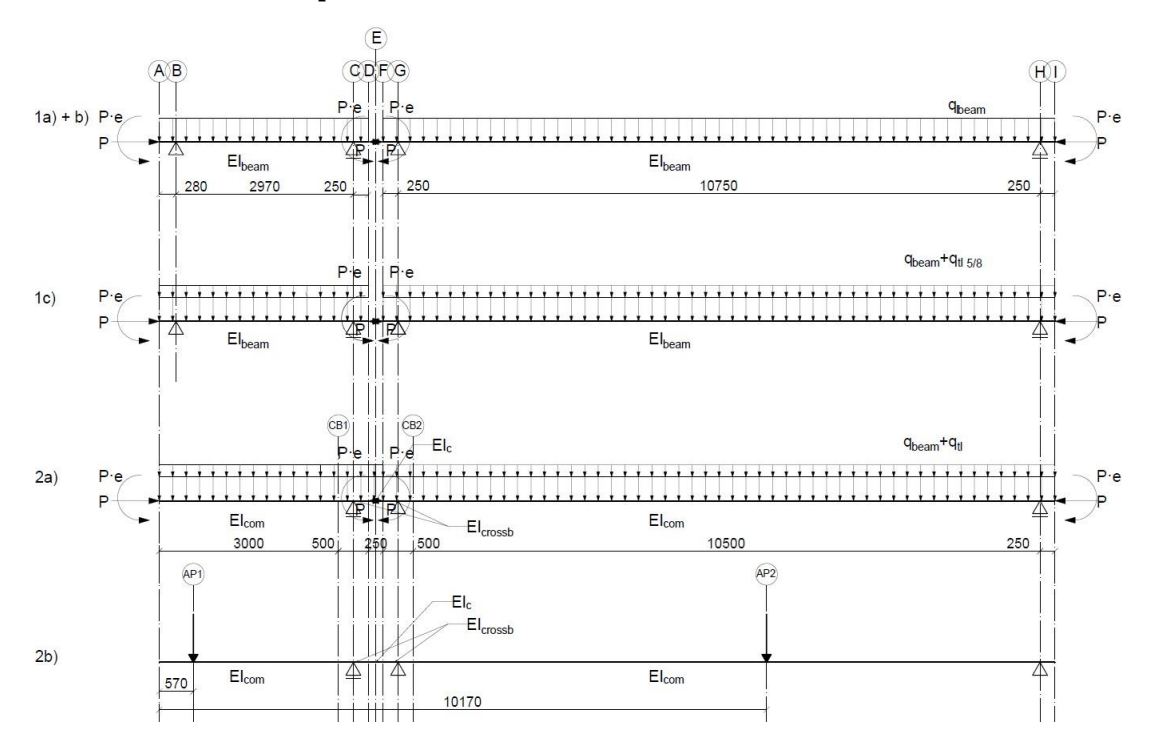


Figure 3.3 Phases of construction and loading

After placing the prefabricated elements at the bearings, a formwork is installed to enable the casting of the top layer and cross beam. Since the formwork was supported on one side of the beam's web and on the other by additional supports, it is assumed that the beam had to withstand only 5/8 of the top layer's weight in this construction stage. After the hardening of the concrete, the formwork was removed. The beam, which could already be regarded as a composite beam, had to withstand the whole weight of the concrete top layer. Moreover, the removal of the left support at axis B resulted in the change of static scheme, hence the increase of internal forces in the intermediate support area. The girder was further loaded with point loads at the locations of axis AP1 and AP2 indicated in the figure above.

3.2 Analytical calculations for validation purposes

The principal aim of performing analytical calculations was to verify, whether the numerical model was correctly assembled and if the results are within an expected range. The first step towards the assessment of the internal forces, hence stresses, in the considered specimen, was to perform analytical calculations. It was assumed that the beam can be verified according to the Euler-Bernoulli beam theory. It should be highlighted that such an approach is a simplification, which is related to disregarding the influence of shear deformation. Moreover, only the linear-elastic stage of structural performance will be compared.

3.2.1 Ordinary differential equations

The calculations were done on the basis of a set of Ordinary Differential Equations and appropriate boundary conditions representing beams' supporting and loading points, at particular stages of assembly and loading. The basic equation used is presented below.

$$\frac{d^2}{dx^2} \left(EI \frac{d^2 w}{dx^2} \right) = q$$

The code presenting all necessary calculations for solving ODEs, the boundary conditions, loads, as well as geometrical and material properties of the beam, can be found in Annex C.

3.2.2 Stress distribution in the composite beam

3.2.2.1 Longitudinal stresses

Having defined internal forces' distribution in the element, at all stages considered, the stresses could be calculated. For each stage, a different load case was considered. The stresses were calculated according to the formulas included in Table 3.2. Stresses along the height of particular cross-section could also be verified, using the moment of inertia and the distance from the neutral axis to the fiber considered. The resultant stresses at most critical cross-sections – above support, at midspan and at the point of load application – were presented and compared with FEA results in section 3.5.

Table 3.2 Stress calculations formulas for consecutive phases

Phase	Beam	Top Layer
1a	$\sigma = \frac{P_{m0}}{P_{m0}} P_{m0} \cdot e_p$	
	$\sigma_{bot} = -\frac{mc}{A_c} - \frac{mc}{W_{bot}}$	
	$\sigma_{bot} = \frac{A_c}{A_c} + \frac{W_{bot}}{W_{top}}$ $\sigma_{bot} = -\frac{P_{m0}}{A_c} + \frac{P_{m0} \cdot e_p}{W_{top}}$ $\sigma_{bot} = -\frac{P_{m0}}{A_c} - \frac{P_{m0} \cdot e_p}{W_{bot}} + \frac{M_{g_{beam}}}{W_{bot}}$ $\sigma_{top} = -\frac{P_{m0}}{A_c} + \frac{P_{m0} \cdot e_p}{W_{top}} - \frac{M_{g_{beam}}}{W_{top}}$ $\sigma_{bot} = -\frac{P_{m0}}{A_c} - \frac{P_{m0} \cdot e_p}{W_{bot}} + \frac{M_{g_{beam}} + M_{g_{tl_{5/8}}}}{W_{bot}}$ $\sigma_{top} = -\frac{P_{m0}}{A_c} + \frac{P_{m0} \cdot e_p}{W_{top}} - \frac{M_{g_{beam}} + M_{g_{tl_{5/8}}}}{W_{top}}$ $\sigma_{bot} = -\frac{P_{m0}}{A_c} - \frac{P_{m0} \cdot e_p}{W_{bot}} + \frac{M_{g_{beam}} + M_{g_{tl}}}{W_{bot}} + \frac{M_{sta}}{W_{bot,com}}$ $P_{m0} \cdot P_{m0} \cdot e_p - \frac{M_{g_{beam}} + M_{g_{tl}}}{M_{sta}} + \frac{M_{sta}}{W_{sta}}$	
1b	$P_{mo} = P_{mo} \cdot \rho_m M_a$	
10	$\sigma_{bot} = -\frac{1}{4}\frac{mo}{\sigma} - \frac{1}{W_{c}}\frac{mo}{\sigma} + \frac{1}{W_{c}}\frac{g_{beam}}{W_{c}}$	
	$P_{m0} P_{m0} \cdot e_n M_{a_{1},\ldots}$	
	$\sigma_{top} = -\frac{mo}{A_c} + \frac{mo}{W_{top}} - \frac{g_{peam}}{W_{top}}$	
1c	$P_{m0} P_{m0} \cdot e_n M_{g_{beam}} + M_{g_{tl_{5/8}}}$	
	$\sigma_{bot} = -\frac{mc}{A_c} - \frac{mc}{W_{hot}} + \frac{s/c}{W_{hot}}$	
	$P_{m0} P_{m0} \cdot P_{m0} \cdot e_p M_{g_{beam}} + M_{g_{tl_{5/8}}}$	
	$O_{top} = -\frac{1}{A_c} + \frac{1}{W_{top}} - \frac{1}{W_{top}}$	
2a	$ P_{m0} P_{m0} \cdot e_p M_{g_{beam}} + M_{g_{tl}} M_{sta} $	$\sigma = \frac{M_{sta}}{M_{sta}}$
	$W_{bot} = W_{bot} = W_{bot} = W_{bot} = W_{bot}$	$\sigma_{bot} = \frac{sta}{W_{bot,com}n}$ M_{sta}
		$\sigma = \frac{M_{sta}}{M_{sta}}$
	$W_{top} = -\frac{1}{A_c} + \frac{1}{W_{top}} - \frac{1}{W_{top}} - \frac{1}{W_{top,com}}$	$\sigma_{top} = \frac{M_{sta}}{W_{top,com}n}$
2b	$P_{m0} P_{m0} \cdot e_p M_{g_{beam}} + M_{g_{tl}} M_{sta} + M_{LL}$	
	$O_{bot} = -\frac{1}{A_c} - \frac{1}{W_{bot}} + \frac{1}{W_{bot}} + \frac{1}{W_{bot,com}}$	$V_{bot} - \overline{W_{bot,com}n}$
	$P_{m0} P_{m0} e_p M_{g_{beam}} + M_{g_{tl}} M_{sta} + M_{LL}$	$\sigma = \frac{M_{sta} + M_{LL}}{2}$
	$\sigma_{top} = -\frac{P_{m0}}{A_c} + \frac{P_{m0} \cdot e_p}{W_{top}} - \frac{M_{g_{beam}} + M_{g_{tl}}}{W_{top}} - \frac{M_{sta}}{W_{top,com}}$ $\sigma_{bot} = -\frac{P_{m0}}{A_c} - \frac{P_{m0} \cdot e_p}{W_{bot}} + \frac{M_{g_{beam}} + M_{g_{tl}}}{W_{bot}} + \frac{M_{sta} + M_{LL}}{W_{bot,com}}$ $\sigma_{top} = -\frac{P_{m0}}{A_c} + \frac{P_{m0} \cdot e_p}{W_{top}} - \frac{M_{g_{beam}} + M_{g_{tl}}}{W_{top}} - \frac{M_{sta} + M_{LL}}{W_{top,com}}$	$\sigma_{bot} = \frac{M_{sta} + M_{LL}}{W_{bot,com}n}$ $\sigma_{top} = \frac{M_{sta} + M_{LL}}{W_{top,com}n}$

Where:

 A_c is the area of the precast beam

 W_{top} are the section moduli at the top fiber of the precast and composite

 $W_{top,com}$

 W_{bot} are the section moduli at the bottom fiber of the precast and composite

 $W_{bot,com}$ beam

is the ratio of moduli of elasticity of precast beam and top layer

is the prestressing force after immediate losses (only elastic P_{m0} deformation was accounted for as the immediate loss)

is the eccentricity of resultant prestressing force e_p

 $M_{g_{\it beam}}$ is the moment generated by the self-weight of the beam is the moment generated by the self-weight of the top layer $M_{g_{t1}}$ is the moment generated by the change of static scheme M_{sta}

is the moment generated by the applied live load. M_{LL}

3.2.2.2 Shear stresses

Vertical shear stresses at the particular cross-section can be calculated according to the shear formula [51]:

$$\tau = \frac{VQ}{Ib}$$

where:

Vis the shear force at the considered cross-section

is the first moment of area directly above the point at which the

Q stresses are assessed

Ι is the moment of inertia of the cross-section

is the width of the element considered. b

An infinitesimally small element can be isolated from the beam, as shown in Figure 3.4. To maintain force and moment equilibrium in the element, the shear forces on vertical and horizontal faces has to balance each other, therefore, it can be observed that the horizontal and vertical shear stresses will be of the same magnitude [51]. Thus, knowing the value of the vertical shear at the level of the interface, it could be verified what the horizontal stresses at the interface are. It is noted, that due to the sudden change of cross-section properties, at the point between the girder's web and the flanges, the vertical shear stresses in flanges cannot be accurately analysed [51]. Moreover, it was also verified with FEA results, that such an approach can only be used at the locations far from supports or points of load application. This matter will be further discussed in subsequent paragraphs.

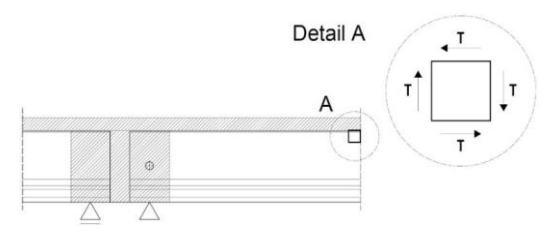


Figure 3.4 Shear stresses at the interface

3.3 Interface capacity according to design codes

The capacity calculation is the consecutive step towards the initial assessment of the interfacial behaviour. The maximum shear that the interface can withstand was calculated in accordance with the EN 1992-1-1 [2], as well as the new draft version of Eurocode 2 [3] and fib Model Code 2010 [27]. The results were later verified to determine if they are comparable. Two sets of input parameters were used - design (and/or characteristic) as well as mean values. Concrete strength values were taken as the average of the two concretes' classes used. Top segments of the tables do not account for the applied compression at the interface, whereas the sections at the bottom show the extreme case of capacity increase under the point of load application. The compressive stress was assumed to be generated by the load of 1 MN magnitude, applied in main span, and spread at the angle of 45 degrees, yielding the value of localised pressure of approximately 12 MPa.

3.3.1 NEN-EN 1992-1-1:2005

Formula provided in Eurocode 2 [2] was already presented in the subchapter 2.2.2. In the table below the results of the intermediate and final calculations are shown. The interface under consideration was classified as rough.

С	0.45	
μ	0.7	
	design values	mean values
	no external	pressure
$c f_{ctd}$	0.7500	1.5975
$\mu\sigma_n$	0.0000	0.0000
$\rho f_{yd}(\mu \sin \alpha + \cos \alpha)$	0.3611	0.4485
v_{Rdi}	1.1111	2.0460
	location under point	of load application
$c f_{ctd}$	0.7500	1.5975
$\mu\sigma_n$	8.4000	8.4000
$\rho f_{yd}(\mu \sin \alpha + \cos \alpha)$	0.3611	0.4485
v_{Rdi}	9.5111	10.4460
$0.5vf_{cd}$	7.0550	12.0897

Table 3.3 Interface capacity according to Eurocode 2 [2]

3.3.2 NEN-EN 1992-1-1 draft version

There are two different design situations proposed in the draft version of Eurocode 2 for the calculation of the interface capacity, as described in subchapter 2.2.2. The hairpins are assumed to be sufficiently anchored, therefore the (2.7) formula is used. The case of insufficiently anchored rebars was also verified, using equation (2.8), however, the calculations' presentation is omitted for the sake of clarity. The results of both cases, for mean values of material properties, are presented in Figure 3.5. As above, the interface is assumed to be rough.

c_{v1}	0.15	
μ_v	0.70	
c_{v2}	0.0750	
k_t	0.50	
k_f	0.90	
	design values	mean values
	no external	pressure
$c_{v1}\sqrt{\frac{f_{ck}}{\gamma_c}}$	0.7984	1.0660
$\mu_v \sigma_n$	0.0000	0.0000
$\rho_i f_{yd}(\mu_v \sin \alpha + \cos \alpha)$	0.3611	0.4485
$ au_{Rdi}$	1.1596	1.5145
	location under point	of load application
$c_{v1}\sqrt{\frac{f_{ck}}{\gamma_c}}$	0.7984	1.0660
$\mu_v \sigma_n$	8.4000	8.4000
$\rho_i f_{yd}(\mu_v \sin \alpha + \cos \alpha)$	0.3611	0.4485
$ au_{Rdi}$	9.5596	9.9145
$0.5vf_{cd}$	7.0550	12.0897

Table 3.4 Interface capacity according to new, draft version of Eurocode 2

3.3.3 Fib Model Code 2010

The code [27] also distinguishes two design situations, from which the non-rigid bond-slip behaviour was assumed to resemble the considered conditions more properly. The interface is regarded as rough.

Table 3.5 Interface capacity according to fib Model Code 2010 [27]

c_r	0.1	
κ_1	0.5	
κ_2	0.9	
β_c	0.5	
μ	0.7	
	design values	mean values
	no external	pressure
$c_r f_{ck}^{1/3}$	0.3490	0.3696
$\mu \sigma_n$	0.0000	0.0000
$\kappa_1 \rho f_{yd}(\mu \sin \alpha + \cos \alpha)$	0.1806	0.2243
$\kappa_2 \rho \sqrt{f_{yd} f_{cd}}$	0.1185	0.1764
$ au_{Rdi}$	0.6481	0.7702
	location under point	of load application
$c_r f_{ck}^{1/3}$	0.3490	0.3696
$\mu \sigma_n$	8.4000	8.4000
$\kappa_1 \rho f_{yd}(\mu \sin \alpha + \cos \alpha)$	0.1806	0.2243
$\kappa_2 \rho \sqrt{f_{yd} f_{cd}}$	0.1185	0.1764
$ au_{Rdi}$	9.0481	9.1702
$\beta_c v f_{cd}$	6.9376	11.6744

Table 3.6 Comparison of the interface capacity results

Code	Mean interface capacity without external pressure [MPa]
EN 1992-1-1 2005	2.0460
EN 1992-1-1 draft	1.5145
fib Model Code 2010	0.7702

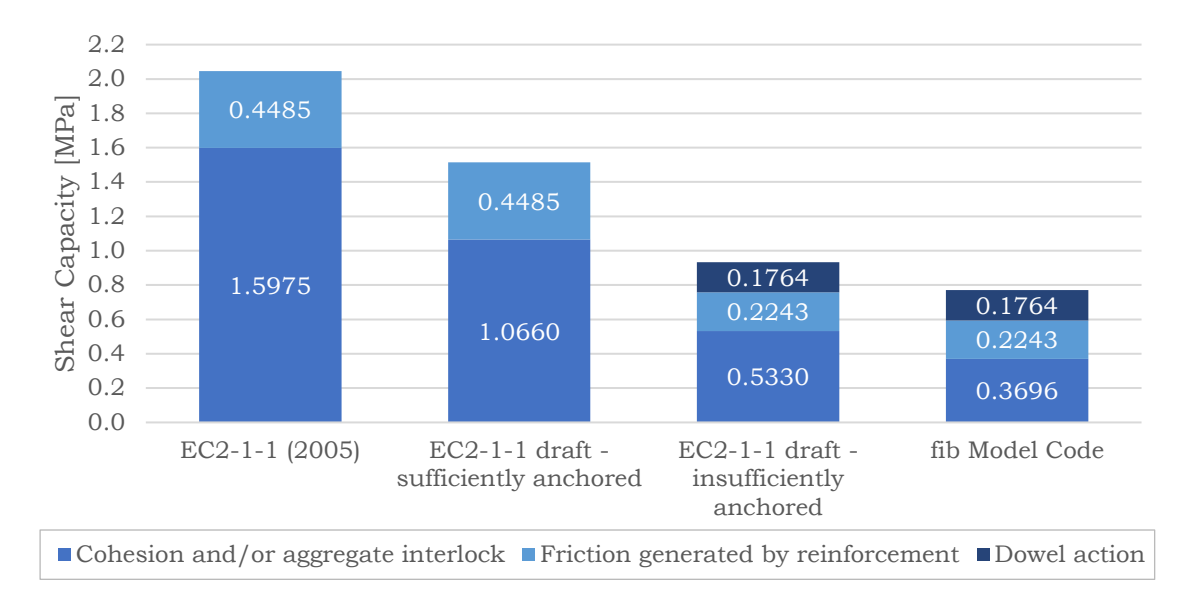


Figure 3.5 Contribution of working mechanisms on shear capacity - mean values

3.4 Finite element analysis

Following the analytical calculations, the finite element analyses were performed. In this subsection, three models of the beam are presented. Model 1.0, with prestressing, linear elastic material properties and without interface elements between prefabricated beams and top layer, was taken as a reference. This model was compared with analytical calculations for validation purposes. In further Models 1.1 and 1.2 interface elements were applied, however, material properties of the elements remain linear elastic. Details of the analyses are presented in the following subchapters.

3.4.1 Numerical setup

The finite element models were composed in accordance with experimental set-up. It was decided that a 2D model and application of plane stress elements will provide a sufficient level of detail in the study. As in the analytical calculations, all relevant stages of construction and loading were taken into account. The overview of the models can be found in Table 3.7. Models are presented in Figure 3.6 and Figure 3.7.

Table 3.7 Models' overview

Model Number	Concrete-to-concrete interface	Concrete	Prestressing Steel	Reinforcement Steel
1.0	X			
1.1	Linear Elastic - Penalty Stiffness	Linear Elastic	Linear Elastic	x
1.2	Linear Elastic - Realistic Stiffness			



Figure 3.6 Model 1.0 with linear elastic material properties and without interface elements between prestressed beams and top layer



Figure 3.7 Models 1.1-1.2 with linear elastic material properties and varying interface material models

3.4.2 Geometry and structural element types

The overall models' geometry is presented in Figure 3.6 and Figure 3.7. Regular plane stress elements were used, and their dimensions were chosen following the sketches provided in subchapter 3.1.1. The applied dimensions of bearings and loading plates are 40 mm x 220 mm and 20 mm x 300 mm respectively. In the case of loading plates, the dimensions correspond with the plates' sizes used in the experiments. As far as bearings are concerned, the plane stress elements are used to model the stiff plane, whereas the interface elements, applied on top, represent the elastomeric behaviour. For this reason the height of the plane stress elements was not relevant and was chosen arbitrarily.

As can be observed in the figures above, not only the plane stress elements were utilised, but also structural line interface elements. In all of the models, there are line interface elements between loading plates and the top layer as well as between supporting plates, representing the bearings and the beams. In Models 1.1 and 1.2, there are also line interface elements included between the beams and top layer, and between the bottom and the top part of the cross-beam in order to maintain the continuity of the interface along the whole length of the beam.

The thickness of the elements representing precast beams had to be defined as a function, due to the complex geometry of the elements. Table 3.8 contains the overview of the cross-section properties of the structural elements. It is noted that only the segment of the cross-beam, in the space between the beams, was included in the models, and the overlapping parts of concrete were disregarded. Details concerning the geometry of prestressing reinforcement are included in Table 3.9. Each tendon at a particular y-coordinate represents all the tendons at this level in accordance with Figure 3.2 b) and c). The coordinates are given, following the assumption of zero being at the bottom fibre of the beam.

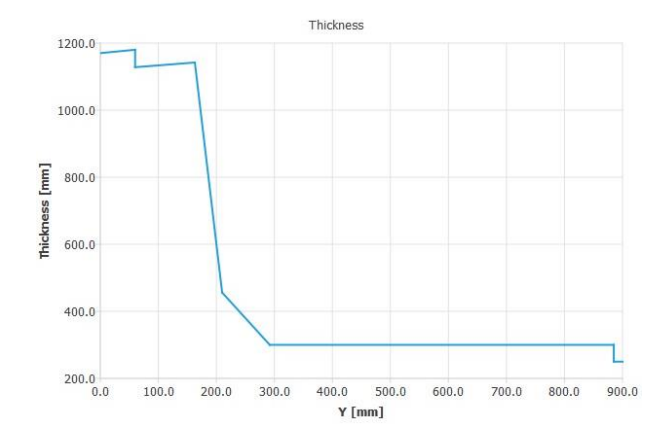


Figure 3.8 Beam's cross-section geometry

Table 3.8 Cross-section properties

Element	Element Class	Material	Geometry
Precast beams	Regular plane stress	Concrete C55/67	acc. to Figure 3.8
Top layer	Regular plane stress	Concrete C30/37	t = 1200 mm
Cross beam	Regular plane stress	Concrete C30/37	t = 1200 mm
Bearings	Regular plane stress	Bearings - steel	t = 455 mm
Loading plates	Regular plane stress	Loading plates - steel	t = 300 mm
Prestressing reinforcement	Embedded bar	Prestressing Steel	acc. to Table 3.9
Bearing - beam interface	Structural line interfaces	Interface - bearings	t = 455 mm
Loading plate - beam interface	Structural line interfaces	Interface - loading plate	t = 300 mm
Top layer – cross beam interface	Structural line interfaces	Interface - penalty stiffness	t = 1200 mm
Top layer - beam	Structural line	Interface - penalty stiffness	t = 250 mm
interface	interfaces	Interface - realistic stiffness	

Table 3.9 Geometrical properties of prestressing tendons

Cantilever Part		Main Span		
y coordinate	Cross-section area	y coordinate	Cross-section area	
[mm]	$[mm^2]$	[mm]	$[mm^2]$	
60	600	60	1400	
110	200	110	600	
150	200	185	200	
250	200			
300	200			
550	200			
600	200			
700	200			
750	200			

3.4.3 Material models

Material models applied in this part of the research were linear elastic for all the elements. The summary of the material properties utilized is outlined in Table 3.10

3.4.3.1 Concrete

For the concrete elements, the mass density had to be specified as the self-weight of the girder was accounted for in the analyses. The number was taken from Table A.1 of Eurocode 1 [52] for reinforced concrete. The moduli of elasticity were applied in accordance with the Eurocode 2 [2] for the assumed concrete classes included in Table 3.1. The value of 0.2 for Poisson's ratio is suggested by both [2] and [6].

3.4.3.2 Steel

Young's moduli for the steel elements were taken as recommended in Eurocode 2 [2]. However, if it comes to loading plates, the load was applied to the plates at a particular point, which does not accurately represent reality as loading jacks have certain dimensions. Therefore, to spread the loading over the plates, their stiffness was increased 100 times. The value of Poisson's ratio was taken from [6].

Table 3.10 Material properties of regular plane stress elements and embedded reinforcement

Material	Class	Material model	<i>E</i> [N/mm ³]	v [-]	Mass Density [T/mm³]
Concrete C30/37	Concrete and masonry	I	33 000	0.2	25E-9
Concrete C55/67	Concrete and masonry		38 000	0.2	25E-9
Bearings - steel	Steel	Linear elastic isotropic	200 000	0.3	-
Loading plates - steel	Steel	isotropic	20 000 000	0.3	-
Prestressing steel	Reinforcements		195 000	-	-

Where:

E is Young's modulus*v* is Poisson's ratio.

3.4.3.3 Interface between bearings and the girder

The properties of the interface elements between the bearing plates and the girder were adjusted to capture the behaviour of the elastomeric bearings utilised in the experiments. stiffness in normal direction approximation, the load-displacement curve by the intermediate bearing's location was used. The rubber's stiffness tends to increase when compression is applied. The secant line was drawn through two points of the load-displacement graph at the stage of more or less constant stiffness. The gradient of a line was later divided by the dimensions of the bearings. The no-tension constitutive law could have been applied however there are two reasons for choosing a linear elastic material model. Firstly, it was aimed to keep the analyses in this section linear and secondly, the bearings are expected to be fully in compression.

The shear stiffness was assumed based on the engineering judgement. The low value applied ensures that no unnecessary horizontal confinement will appear in the support zones.

3.4.3.4 Interface between loading plates and the girder

For the normal stiffness of the interface between the loading plates and the girder, a very high penalty value was chosen based on dividing the utilised stiffness of the loading plate elements by their thickness. In the tangential direction, the same principle as for bearings was applied.

3.4.3.5 Concrete-to-concrete interface

In Models 1.1 and 1.2, interface elements were applied between precast beams and concrete cast in situ. As the analyses conducted within this part of the research are linear, for the concrete-to-concrete interface the Linear Elasticity material model was chosen. It is also the most basic way of interface modelling, hence it is regarded as a favourable starting point. In Model 1.1, the high penalty stiffness was applied according to the formulas presented below.

$$k_n = \frac{1000 \cdot E_{cm}}{h} = \frac{1000 \cdot 35.5 \left[\frac{N}{mm^2} \right]}{50 \text{ [mm]}} = 710000 \left[\frac{N}{mm^3} \right]$$

$$k_s = \frac{1000 \cdot G_{cm}}{h} = \frac{1000 \cdot 14.8 \left[\frac{\text{N}}{\text{mm}^2}\right]}{50 \text{ [mm]}} = 296000 \left[\frac{\text{N}}{\text{mm}^3}\right]$$

Where:

 k_n is the normal stiffness modulus k_s is the shear stiffness modulus E_{cm} is Young's modulus, taken as a mean value of concretes' moduli is the shear modulus, taken as a mean value of concretes' moduli is the size of a neighbouring element, in this case, taken as 50 mm, as it is the applied mesh size.

In the following model, the stiffness in the normal direction was kept the same. It was decided that the shear stiffness will represent lower and, which was assumed, more realistic value. It was reported by Loov and Patnaik [15] that the relative displacement between concretes in tested beams is almost unnoticeable for shear values below 1.5 - 2 MPa. However, there was no drop in capacity up until 0.3 - 0.8mm of relative displacement, which can be related not only to friction generated by reinforcement but also to aggregates interlocking. Loov and Patnaik reported the values of horizontal stresses at three different slip magnitudes - 0.13 mm, 0.5 mm and at failure. The initial stiffness was approximated by dividing the shear stresses by the corresponding 0.13 mm slip. The mean value found was 26.58 N/mm³ and details can be seen in Annex B. The value of 18 N/mm³ was calibrated, based on experiments, and used in the numerical research on push-off, sand-blasted specimens performed by Dias-da-Costa, Alfaiate and Júlio [43]. The numerical study [46] on a smooth interface in a composite SHCC-concrete beam revealed that application of 10 N/mm³ yielded the best results. Following those values, the shear stiffness of 20 N/mm³ was chosen for the interface elements in Model 1.2.

Material	Class	Material model	$k_n [\text{N/mm}^3]$	k_s [N/mm ³]
Interface - bearings			12	0.03
Interface - loading plate	Interface		1000000	0.03
Interface - penalty stiffness	Elements		710000	296000
Interface - realistic stiffness			710000	20

Table 3.11 Material properties of interface elements

3.4.4 Boundary and loading conditions

The boundary conditions applied can be observed in Figure 3.6 and Figure 3.7. The bearing plates by the intermediate support were restrained along the edge in horizontal and longitudinal directions, whereas the side plates have only horizontal restraints. It should be kept in mind that the presence of interface elements on top of the plates, to a certain degree, facilitates the movement in the horizontal direction as well as rotations.

The live load in these analyses was applied in a force control manner, hence no additional supports had to be included in the model. The point loads were chosen to be utilised, however, with the increased stiffness of the loading plates, the compression was more evenly spread over the plate areas. The ratio of forces applied at the cantilever and at the main span was 0.63/1. As the analyses were linear, the magnitude of the load did not have to be chosen with a close attention. The stresses obtained from analytical and numerical calculations were compared at the level of total load equal to 1.63 MN, however, the entire applied load was two times higher as presented in Table 3.12.

As far as other loads are concerned in the first phase the prestressing of rebars was applied. The function was used to account for the transmission of prestress, based on the value of l_{pt} that can be found in Annex C. The elastic losses are already accounted for in DIANA, as the shortening of concrete elements leads to the loss of prestress in the tendons. Following, the self-weight of the concrete elements was applied as equivalent acceleration. Moreover, the part of the weight of wet concrete was applied as a line load to the top edges of elements representing prestressed beams. The line load was applied in the first phase, and later with the same magnitude but opposite direction in the second one because equivalent acceleration was applied to the top layer and cross beams when the elements were already active. Details concerning the magnitude of the loads can be observed in Table 3.12.

Dhaga	Applied load	Magnitude		
Phase Applied load		Cantilever Part	Main Span	
	Reinforcement bar prestress	1185 N/mm ²	790 N/mm ²	
1	Equivalent acceleration - precast	0810	mm /s2	
1	beams	-9810 mm/s ²		
	Distributed force – 5/8 wet concrete	-3 N/mm		
0.0	Distributed force	3 N/mm		
2a	Equivalent acceleration – cross beam,		2010 /-2	
	top layer	-9810 mm/s ²		
2b	Live load	-1 260 000 N	-2 000 000 N	

Table 3.12 Loads applied in consecutive phases

3.4.5 Mesh

The average mesh size applied is approximately 50 mm x 50 mm, with slight differences at loading or bearing plates. Meshes of Models 1.0-1.2 are the same, with the only difference being the presence of more interface elements in Models 1.1 and 1.2. In the figures below the meshes at certain phases are presented. Specifications concerning finite element types can be found in Table 3.13. The top values in the last two rows regard Model 1.0, whereas bottom ones Models 1.1 and 1.2.



Figure 3.9 Meshed model at Phase 1



Figure 3.10 Meshed model at Phase 2a

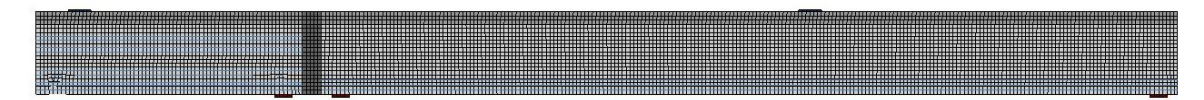


Figure 3.11 Meshed model at Phase 2b

Table 3.13 Finite elements used - specifications

Finite element type	CQ16M	CT12M	CL12I		
Degrees of freedom	$\begin{vmatrix} u_x, u_y \\ 8 \times 2 = 16 \end{vmatrix}$	$ \begin{vmatrix} u_x, u_y \\ 6 \times 2 = 12 \end{vmatrix} $	$ \begin{vmatrix} u_x, u_y \\ 6 \times 2 = 12 \end{vmatrix} $		
Interpolation scheme	Quadratic	Quadratic	Quadratic		
Integration scheme	2×2 Gauss	3-point	5-point Newton-Cotes		
Stress components	$\sigma_{xx}, \sigma_{yy}, \sigma_{xy}$	$\sigma_{xx}, \sigma_{yy}, \sigma_{xy}$	t_n, t_t		
Average element size [mm]	50×50	50	50		
Total number of elements	6324	1	28		
Total flumber of elements	0324	1	328		
Total number of nodes	20998				
Total Humber of Hodes	21603				

3.4.6 Analysis characteristics

The simulations were performed as a Phased analysis, hence in each phase, a new structural analysis was run. The analyses chosen were Structural Nonlinear, in order to apply certain loads separately, however, none of the nonlinear effects was activated. As already discussed and can be observed in Table 3.12, three main phases were distinguished. In the first one, two simply supported beams are loaded with prestressing load, self-weight, and further with the part of the weight of wet concrete. Each load was applied in a different load step. The next phase represents the phase 2a, where the static scheme is changing – the beam is made continuous, the left support under the cantilever part is subtracted from the model and the whole self-weight has to be carried by the structure. In the last phase, the loading plates are activated, and the live load is applied. The details are displayed in Table 3.14. The data concerning equilibrium iteration applies to all the analyses, however, only the live load was applied in 20 steps, and the loads in previous phases were applied using one step. The analyses specifics are valid for all of the three models distinguished and all analyses performed within the models.

Table 3.14 Analysis specifications

Iterative method	Regular Newton-Raphson
Maximum number of iterations	50
Convergence norms	Energy, Force – both satisfied
Energy – convergence tolerance	0.001
Displacement – convergence tolerance	0.01
Live load application – load steps	0.05 (20)

3.5 Comparison of the results of the analytical and numerical calculations

Longitudinal and shear stresses calculated analytically, based on Euler-Bernoulli beam theory, are compared with the numerical results obtained from the Model 1.0. The results of the stresses along the height of particular cross-sections – above support, in midspan, and under the point of load application – are presented in the following figures. Cross-section labels refer to Figure 3.1. The stresses in the phase 2b were compared, at the load level of 0.63 MN and 1 MN at the cantilever part and main span respectively. For the sake of the clarity of the report only that phase is analysed, however more details can be found in Annex D.

3.5.1 Longitudinal stresses

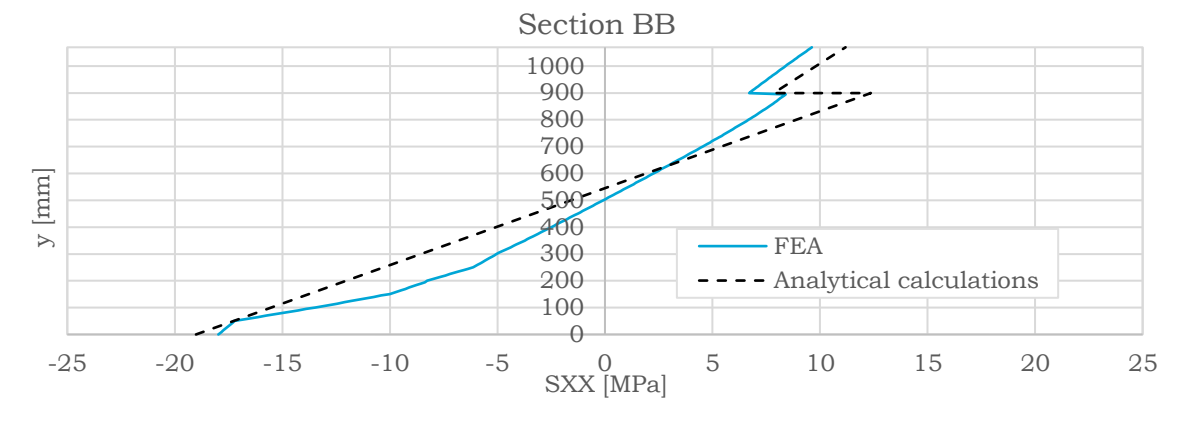


Figure 3.12 Stresses above the support, phase 2b

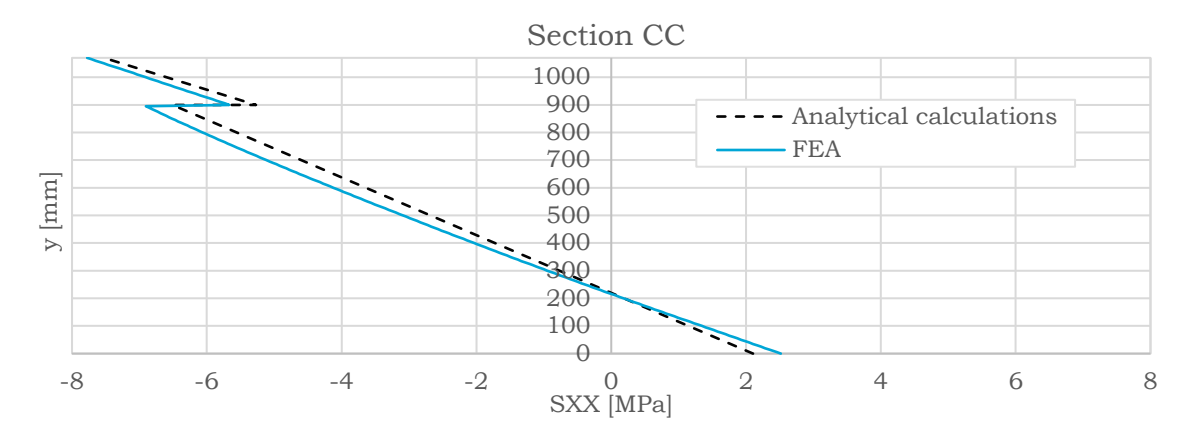


Figure 3.13 Stresses in midspan, phase 2b

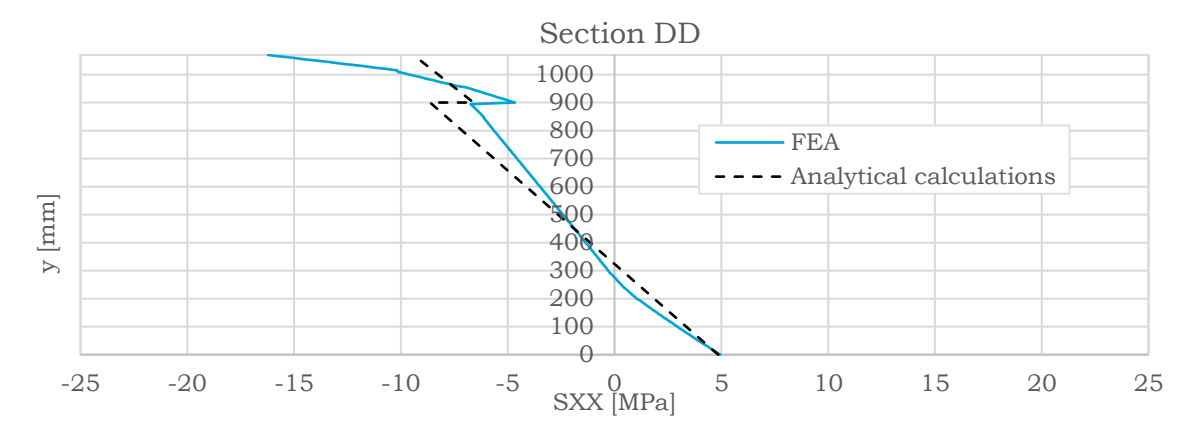


Figure 3.14 Stresses at the cross-section below the point of load application, phase 2b

3.5.2 Shear stresses

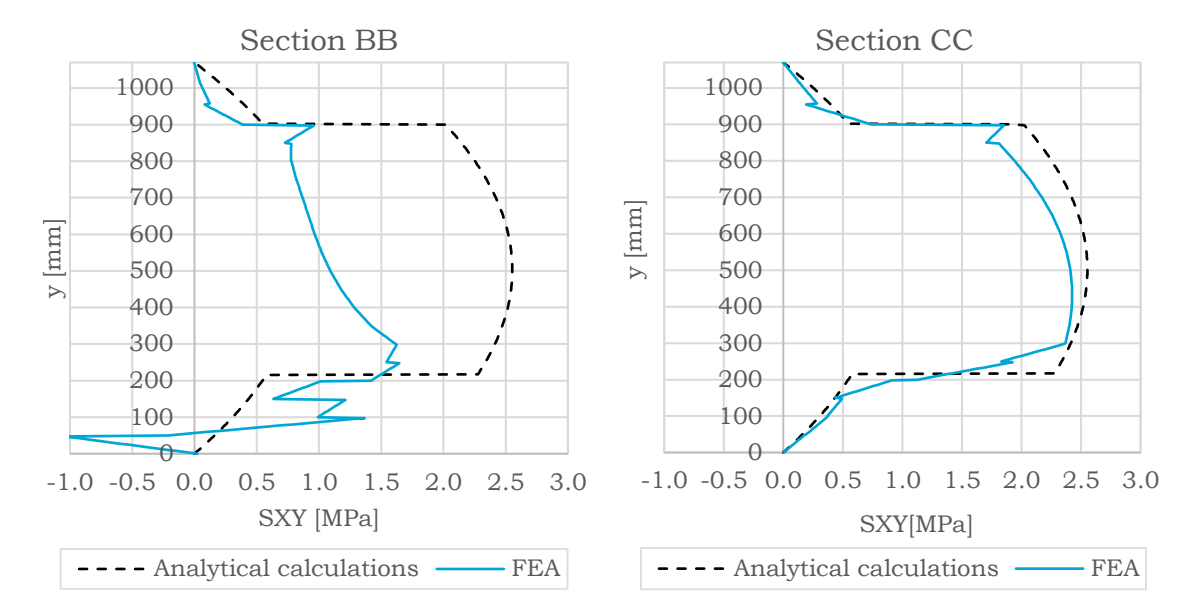


Figure 3.15 Shear stresses above the support, phase 2b

Figure 3.16 Shear stresses in midspan, phase 2h

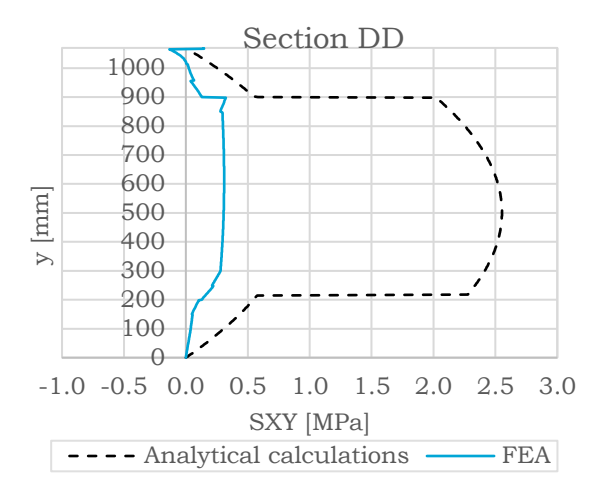


Figure 3.17 Shear stresses below the point of load application, phase 2b

3.6 Comparison of the results obtained from the finite element analyses

In this subchapter the numerical results of Models 1.0, 1.1 and 1.2 are compared. The assessment is made in order to verify how the presence, and the basic properties of the interface influence the girder's behaviour. Similarly to previous verification, the results of longitudinal and shear stresses are compared at the total load level of 1.63 MN. The same holds for comparison of the stresses and relative displacements at the interface along the beam's length, however, certain points are also verified under the point loads of magnitudes 1.26 MN and 2 MN (see Table 3.12) at the cantilever and main span respectively.

3.6.1 Longitudinal stresses

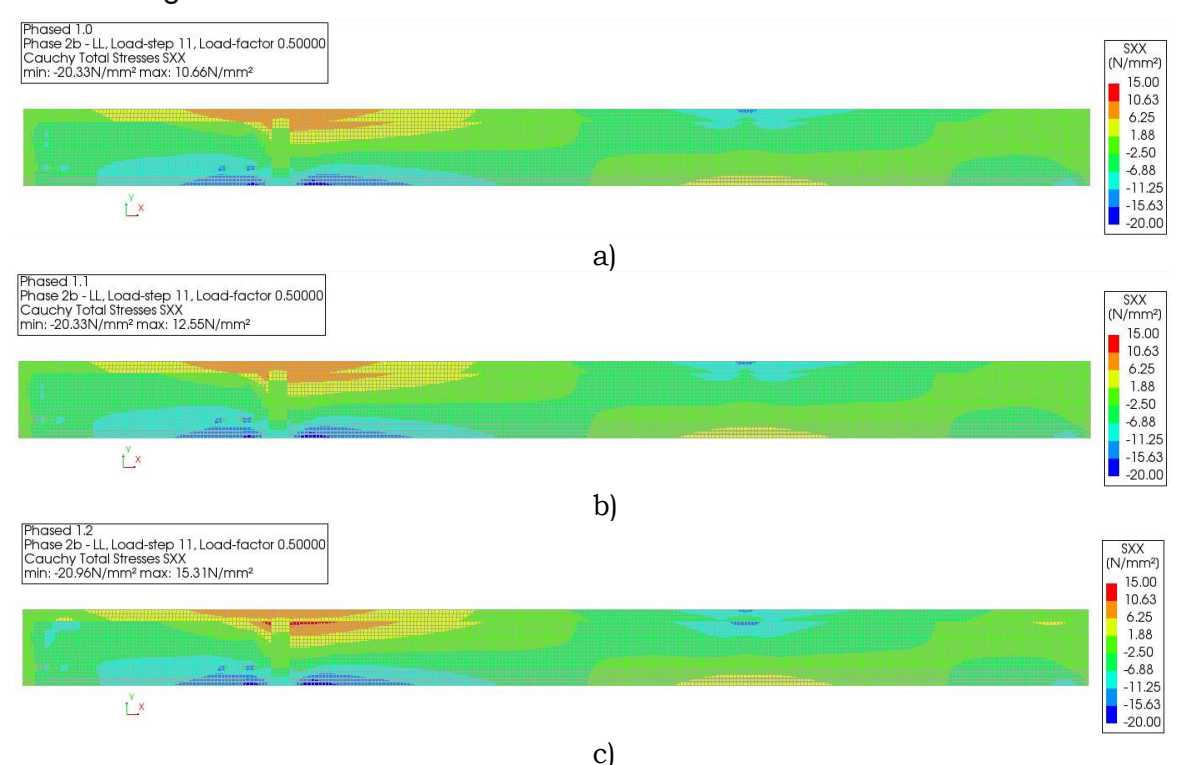


Figure 3.18 Horizontal stresses comparison a) Model 1.0 b) Model 1.1 c) Model 1.2

3.6.2 Shear stresses

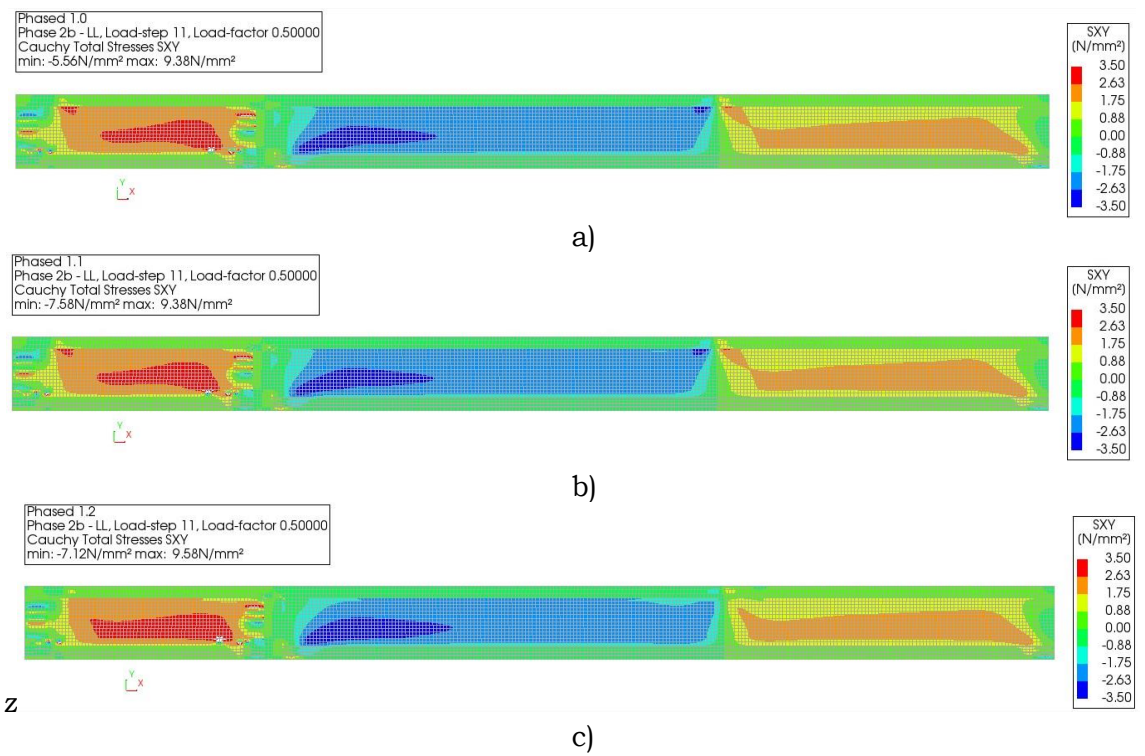


Figure 3.19 Horizontal stresses comparison a) Model 1.0 b) Model 1.1 c) Model 1.2

3.6.3 Normal tractions at the interface

In this and three following subchapters only Model 1.1 and 1.2 will be compared, as the presented type of graphs can only be obtained from the models with interface elements. A probing curve could be used to assess the shear and vertical stresses right below the interface, however it was verified that the results, were slightly different than those indicated as tractions at the interface. It was decided to show the stresses and relative displacements in normal direction for one model as the stiffness k_n was kept the same in both, hence the differences were almost unnoticeable in the global scale.

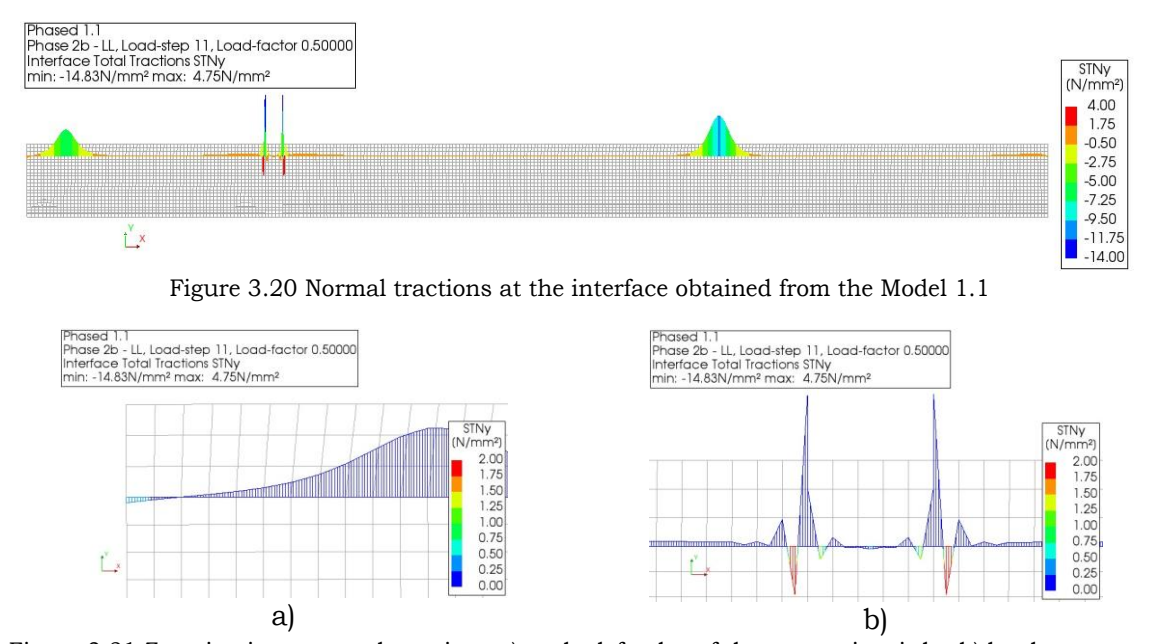


Figure 3.21 Zooming in to normal tractions a) at the left edge of the composite girder b) by the support

3.6.4 Relative displacement in normal direction at the interface

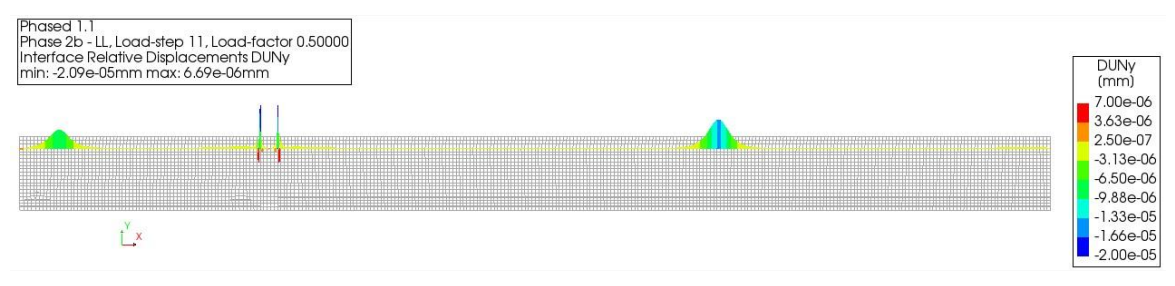


Figure 3.22 Relative displacements in normal direction at the interface obtained from the Model 1.1

3.6.5 Shear tractions at the interface

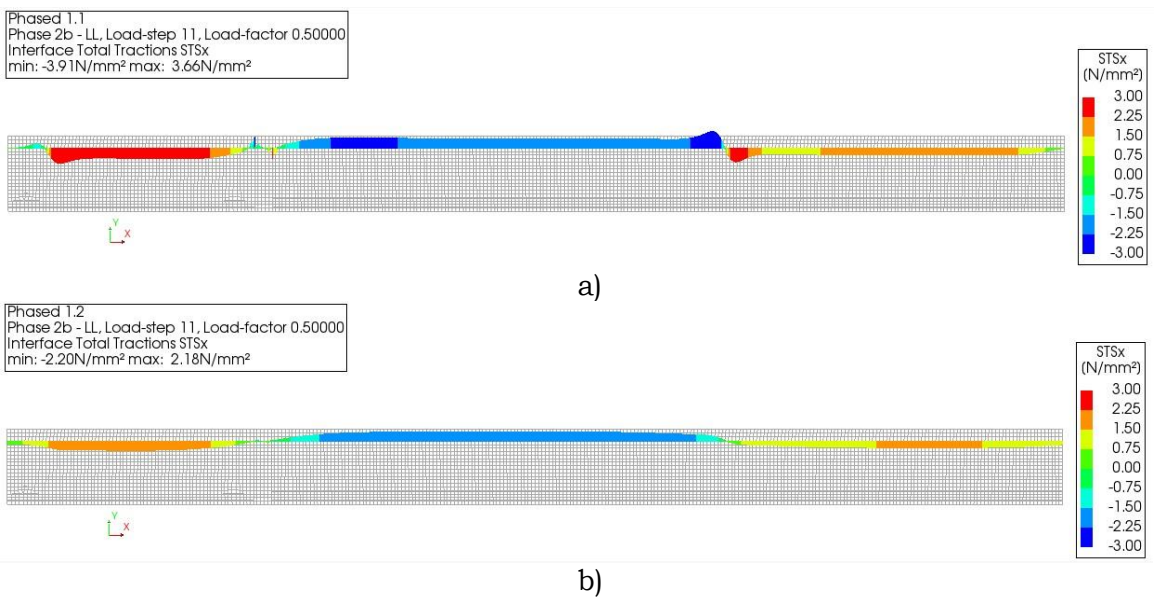


Figure 3.23 Shear tractions at the interface obtained from a) Model 1.1 b) Model 1.2

3.6.6 Relative displacement in tangential direction at the interface

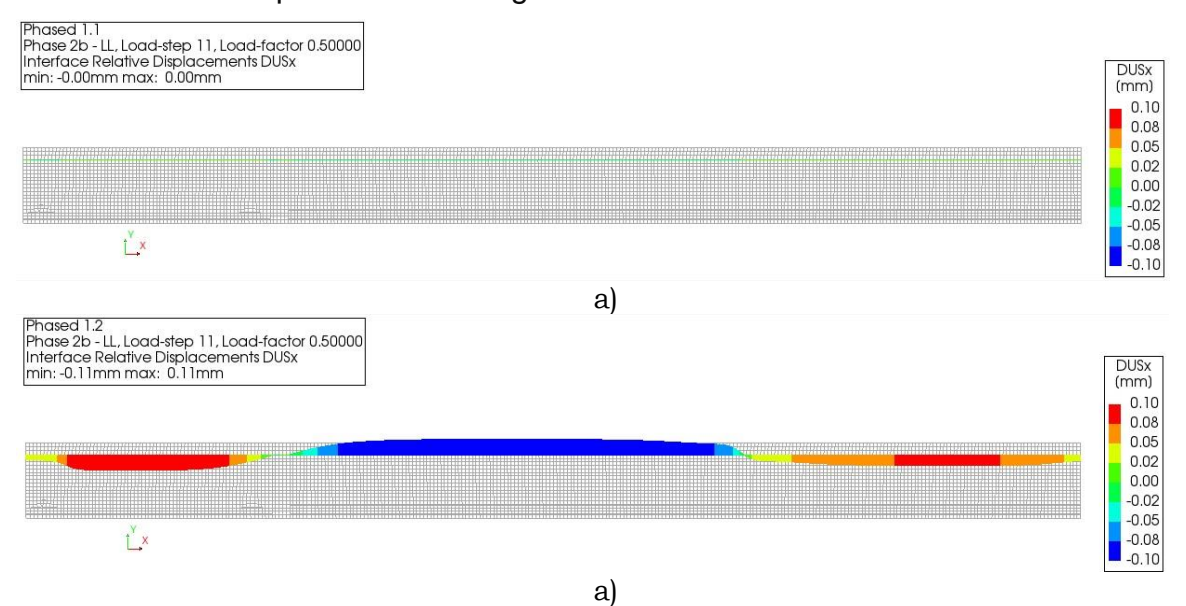


Figure 3.24 Relative displacements in tangential direction obtained from a) Model 1.1 b) Model 1.2

3.6.7 Development of stresses at the selected points at the interface

The observation of the normal and shear tractions along the length of the interface is beneficial, however it is worth taking closer look at the combination of those stresses. After analysing the graphs above, a few points were considered interesting to investigate. The nodes at the following locations were verified – above the intermediate support hence at section BB (red point in Figure 3.25), in midspan meaning at section CC (blue point), at the point of load application, in the section DD (yellow point), as well as at the local shear extremum in the vicinity of the load application point (green point). As mentioned before, the analysis was continued up until the total load reached 3.26 MN. To obtain the stresses from the Model 1.0, the SXY and SYY stress resultants were read from the nodes of the elements just below the interface. In case of Model 1.1 and 1.2 the shear and normal tractions could be obtained directly from the interface elements' nodes.

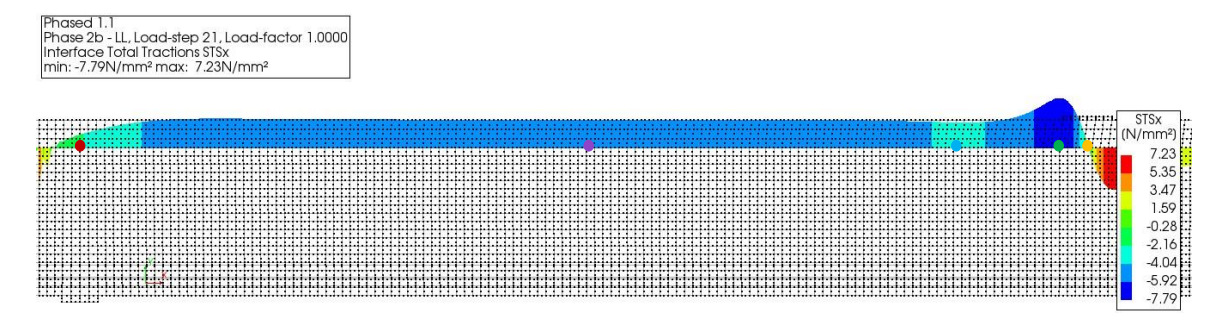


Figure 3.25 Close-up to the part of the beam between intermediate support and loading point, with highlighted nodes under consideration; plot presenting shear tractions at the interface of Model 1.1

The nodal results are displayed in Figure 3.26 and Figure 3.27. The stress development itself can be considered only partially valuable. It was decided that information on whether any of those spots is at risk of failure would be valuable.

The black, dashed lines crossing the graph's axis are the assumed failure envelope based on the Mohr-Coulomb failure theory. The cohesion and friction coefficients were selected as a best guess on the basis of the values found in the literature, which are displayed in Table 2.6. To obtain the magnitude of cohesion the coefficient was multiplied with f_{ctm} , taken as an average of the two concretes' strengths.

The black, solid lines represent the failure envelope constructed in accordance with cohesion and friction coefficients given by the Eurocode 2 [2], as calculated in section 3.3.1. Similarly to the assumed failure envelope, mean values were used as far as the concrete and steel strength is concerned.

The markers along the envelopes represent the point at which the envelope crosses the normal tractions axis, the state of zero clamping stress and the condition of clamping stress generated by $\rho_i = \rho_{w_{min}} = 0.12\%$, respectively. It shall be highlighted, however, that the compression at chosen points is generated by the external forces, not by the clamping of the reinforcement, since the rebars were not included in the models.

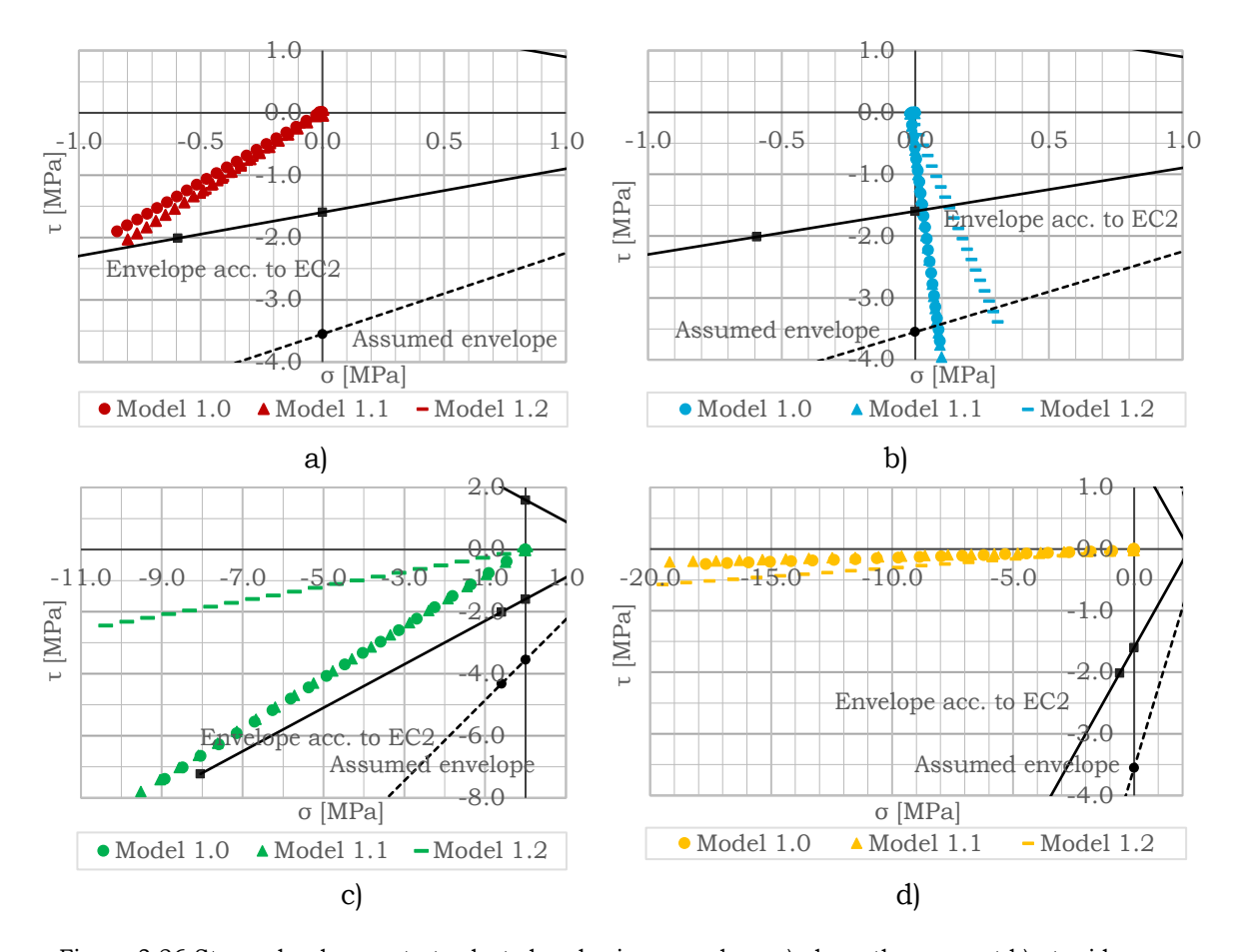


Figure 3.26 Stress development at selected nodes in $\sigma - \tau$ plane a) above the support b) at midspan c) at local shear extreme d) under the point of load application

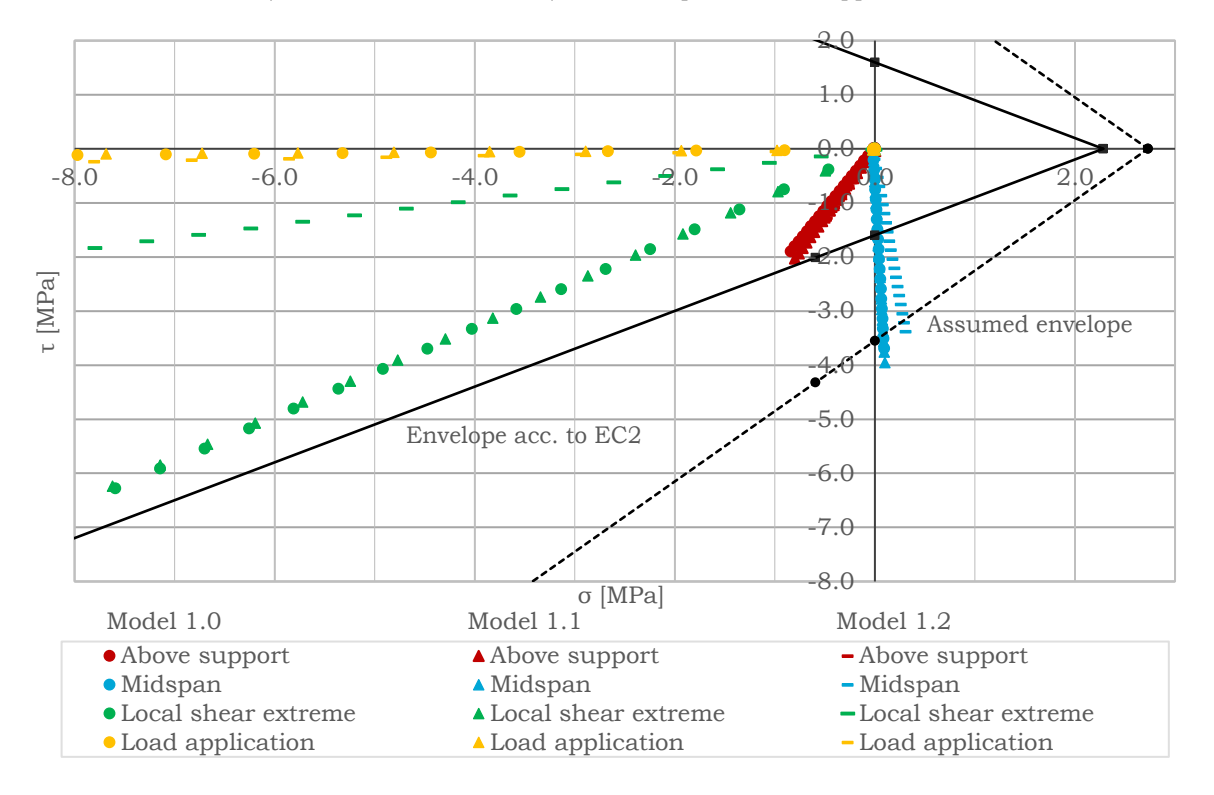


Figure 3.27 Stress development at selected nodes in $\sigma-\tau$ plane - overview

3.7 Discussion 45

3.7 Discussion

As far as the model validation, on the basis of Euler-Bernoulli beam theory, is concerned, it is observed that the longitudinal stresses calculated analytically and numerically are comparable, especially when looking at Figure 3.13. It can be concluded that the model was correctly assembled and it complies with basic principles of structural behaviour. The minor differences, visible at the section BB presented in Figure 3.12 and section DD in Figure 3.14, are undoubtedly related to the presence of support and loading points. As the occurrence of singularities was avoided through the use of bearing and loading plates, it can be assumed that the stress concentrations were properly analysed.

It is also noted that in the section above the support, the top part of the girder is in tension and that the values of tensile stresses considerably exceed the tensile capacity of concrete, for the analysed 1.63 MN of the applied load. It is expected that the cracking would appear in this section, which would influence the interfacial behaviour.

The analysis of shear stresses presented in Figure 3.16 revealed that there is a good agreement between the results in midspan, however, the outcome of FEA at both sections BB (Figure 3.15) and DD (Figure 3.17) is quite different from analytical calculations. Firstly, again, the difference lies in the presence of support and loading positions, however in this case the stress values obtained from FEA are smaller. It was verified that the stresses arise to their full magnitude over a certain distance along the beam's length, which reflects the expectations. Secondly, it is acknowledged that the Euler-Bernoulli beam theory is a simplification, hence it is anticipated not to obtain the same results. Due to the aforementioned aspects, it was decided that verification of stresses at the interface based on analytical calculations, as suggested in subchapter 3.2.2.2 would not be effective and could only be utilized for a rough assessment. Any local increases or decreases of stresses can only be identified with FEA.

If it comes to the comparison of the numerical results, the distributions of both, longitudinal and shear stress, presented in Figure 3.18 and 3.19, obtained from the Models 1.0 and 1.1 are almost the same. However, lowering the shear stiffness of the interface proved to introduce some changes in the behaviour. The composite action is weakened as the tensile forces in the top fibres of the prestressed beams, in the vicinity of the support, are higher than in previous models. Also, the compression of the beam's web under the point of load application is higher than in Models 1.0 and 1.1. The horizontal stresses' change is presented in Table 3.15. The nodes below the top left corner of the main, precast beam, where the tension was extreme, and in the beam's web under the point of load application, were chosen for the comparison. As can be noted, the change of interfacial shear stiffness from the penalty value of 296000 N/mm³ to 20 N/mm³, which was considered more realistic, resulted in the 1.21 higher maximum tensile stresses in the prefabricated element and 2.26 times higher compressive stresses under the point of load application.

Table 3.15 Analysis of stresses change with varying interface material properties

	SXX, support region [MPa]	SXX, load application region [MPa]
Model 1.1	12.55	-6.82
Model 1.2	15.22	-15.42

46 3.7 Discussion

As far as normal tractions displayed in Figure 3.20 and Figure 3.21 are concerned, as expected, there is an increase in compressive stresses under the point loads. In the performed analyses, no considerable tensile stresses were detected at the interface, except for some localised peaks near the cross-beams location. It is understood to be related to a sudden change of material and geometrical properties. The relative displacements are negligible, as a result of the very high normal stiffness of the interface elements.

It is acknowledged that such linear, 2D analysis has its limitations concerning identifying tensile stresses. First, it should be acknowledged that perpendicular cracking of concrete is not accounted for. Secondly, in reality, if the longitudinal crack appears at the interface, either due to progressing from the concrete elements or by insufficient shear strength of the interface, there would be certain sliding, hence the opening of the connection, which is also not taken into consideration. Moreover, the three-dimensional structure of a precast beam bridge is subject to torsional effects, as well as vertical, relative displacements of the girders, hence it is expected that if the whole structure was analysed, more pronounced differences would be revealed.

Analysing the shear tractions in Figure 3.23, it is observed that with lower stiffness of the interface the stresses are lower and the distribution is more smooth along the length of the beam. What was also observed is that the slip was approximately 10000 times higher, which is in line with expectations and approximately matches the ratio of shear stiffness decrease.

Looking at the stresses at chosen points, plotted in the $\sigma-\tau$ plane, shown in Figure 3.26 and Figure 3.27, it seems that for majority of the points, the failure is not expected. Nevertheless, the stresses at the midspan cross the assumed envelope at approximately 2.9 MN of the total applied force and the Eurocode 2 envelope at the total load magnitude of 1.5 MN. Moreover, for the lower stiffness of the interface, the stresses tend to shift towards the tensile part of the diagram. It was also verified that for even lower values of k_s the magnitude of tensile stresses at that point is higher, nonetheless, at the same time, the shear tractions become lower. It is recognised that the initial stiffness, before cracking of the interface, can be assumed infinitely high. However, after certain microcracking, or when the cracks from the top layer or the web reach the interface, locally the stiffness may be reduced, resulting in the change of behaviour. On the other hand, looking at the stresses development at the point of local shear extreme, it is noticed that the tangential tractions considerably exceed the assumed limit of 3.55 MPa, nevertheless, due to the presence of compression at that location, the failure is not expected.

Another point of concern is that the assumed Mohr-Coulomb failure envelope constructed based on best guess stemming from literature data and the one created using Eurocode 2 [2] values are quite different. As expected, the Eurocode one is safer, however, it is not necessarily desirable when looking for hidden capacities. Furthermore, analysing the factors given by the fib Model Code 2010 [27] and calculations performed in section 3.3.3, the failure envelope would be even more conservative. More, comprehensive information, such as the measured roughness parameter (Mean Peak Height or Mean Valley depth) of the interface surface, or experimental results of push-off tests, would be necessary to define the interface failure envelope with more assurance. It should be remarked that for the time being,

3.8 Conclusions 47

no tension cut-off was assumed. Certain values can be found in the literature, however, the splitting test could be performed to verify the tensile performance of the investigated surface and determine the tension cut-off with higher certainty.

A conclusion that could be drawn is that the models accounting for coupling between the horizontal and vertical tractions are considered to be worth to investigate, not only to account for the lowering of the capacity when tensile stresses are present, but also for the increase of interface strength under compression. Such models are especially valuable when clamping from the reinforcement is to be included. Otherwise, the constitutive law has to describe the behaviour of the reinforced joint and has to be adjusted for each reinforcement ratio of the rebars crossing the reinforcement. That could be problematic for instance when the hairpins are not uniformly distributed along the beam's length.

Moreover, a nonlinear analysis would give more insight into the real behaviour of this type of structural element, as the cracking and local unloading of concrete parts will undoubtedly influence the interface behaviour, especially in the support region.

3.8 Conclusions

- The results of longitudinal and shear stresses obtained from the linear-elastic numerical analysis of the beam were to some extent in line with the outcome of the analytical calculations based on the Euler-Bernoulli differential equations. The agreement of the results was higher at the locations relatively distant from supporting and loading points. It can be claimed to prove that the finite element model, with phased analysis, was correctly assembled and that it corresponds to basic principles of structural behaviour.
- Based on the results of finite element, linear analysis, no significant tensile stresses, perpendicular to the interface, were detected, except from localised peaks as the junction of the beam's and cross-beam's elements. Nonetheless, the parts of concrete in the support region, in the vicinity of the interface are in tension, hence analysis of the girder with nonlinear material properties of concrete is needed as cracking is expected to influence the results.
- The reduction of the interface shear stiffness k_s resulted in changes in the behaviour of the interface, as well as of the global structural behaviour. Lowering the stiffness from 296000 to 20 N/mm³ caused a reduction of composite action in the beam, leading to the increase of the maximum tensile stresses in the precast beam, in the support region, by a factor of 1.21 and the rise of compression in the beam's web, below the load application, by a factor of 2.26.
- Shear and normal stresses at the interface should not be analysed independently. Plotting the stress development in the $\sigma \tau$ plane provides more insight into behaviour of the interface. Even for elements subject to considerable shear tractions, the failure might not occur due to the presence of compressive stresses. Such a situation was observed for the point of local shear extremum by the load application location.
- Based on the linear analysis it was concluded that models accounting for coupling can prove to be beneficial for modelling the interface in the continuous girders, not only to account for the decrease of capacity under tensile forces, but also for the increase when compression is present.

Verification study on models on a component level - Nonlinear Analysis

In this part of the research, the interface behaviour is examined on a component level. It was decided to test more advanced interface material models on a smaller scale. A push-off test, with lateral compression, was modelled with the application of two different interface material models - Coulomb Friction and Combined Cracking-Shearing-Crushing - which take into consideration the coupling between shear and normal tractions. The modelling procedure, results and observations stemming from the numerical tests are included in this chapter.

4.1 Experimental reference - modified push-off test

4.1.1 Experimental setup and properties of the specimens

The specimens that were chosen for the component-level numerical analyses were taken from the research by Mohamad and Ibrahim [1]. The researchers performed a set of push-off experiments without and with applied pressure in a direction perpendicular to the interface. The picture, along with the sketch of the experimental setup, presented by the authors, is included in Figure 4.1 and Figure 4.2. The dimensions of the concrete elements are 300 mm x 300 mm with a height of 100 mm and 75 mm for the base and top layer respectively. Grid reinforcement is included in both concrete elements. A number of specimens also have nine, U-shaped reinforcing bars crossing the joint surface. The rebars utilized in this experimental program are plain, round mild steel bars of 6 mm diameter.



Figure 4.1 The photo of the experimental setup

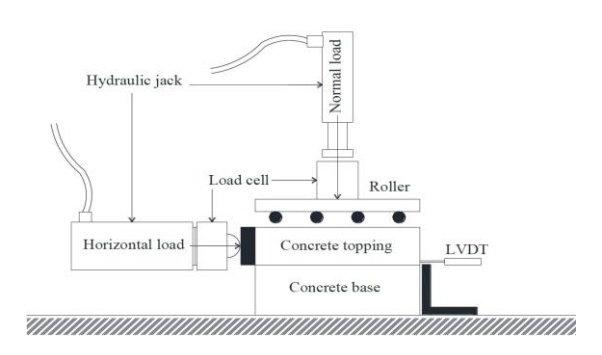


Figure 4.2 The sketch of the experimental setup [1]

In total 36 specimens were tested. Three main types of specimens can be distinguished:

- S specimens with a smooth surface between concretes
- T specimens with a rough surface between concretes
- L specimens with a smooth surface between concretes and reinforcement crossing the interface

Smooth specimens were simply left without any finishing after casting, whereas the rough ones were roughened by wire brushing in the direction transverse to the assumed direction of load application. Each specimen type was tested under 4 levels of perpendicular pressure being 0, 0.5, 1 and 1.5 MPa. Three specimens were tested for all types of performed experiments.

Material properties are summarised in Table 4.1. It was stated in the research that cube compressive strength was measured on three samples, on the day of testing. The mean values were given for each level of applied pressure. It was decided to calculate the average of those values and further translate them to the mean value of concrete cylinder compressive strength to be able to assign other properties in accordance with Eurocode 2 [2]. The splitting tensile strength of 2.99 MPa was documented, however, it is not entirely clear whether it is the strength of the concrete or the interface. Nevertheless, only one value was given.

Table 4.1 Material properties of tested specimens

Element	Average f_{cu} [MPa] [1]	$f_{cm}[MPa]$	$f_{yk}[MPa][1]$
Base	46.20 ≈ 45	36	
Topping	30.07 ≈ 30	24	
Steel bars			250

4.1.2 Experimental results

The authors have documented peak shear load along with the corresponding horizontal slip at the interface for all experiments performed. Average shear strength was also provided, which was the mean peak load divided by the shearing area. The table displaying mean values of peak load, corresponding stress and slip, calculated as an average of three specimens, is provided below. The researchers also supplied the horizontal load versus interface slip curves. However, the diagrams were only provided for one of the three specimens for the given setup. There were 12 graphs in total – for each surface type and each level of applied perpendicular pressure. The diagrams are presented in Figure 4.3.

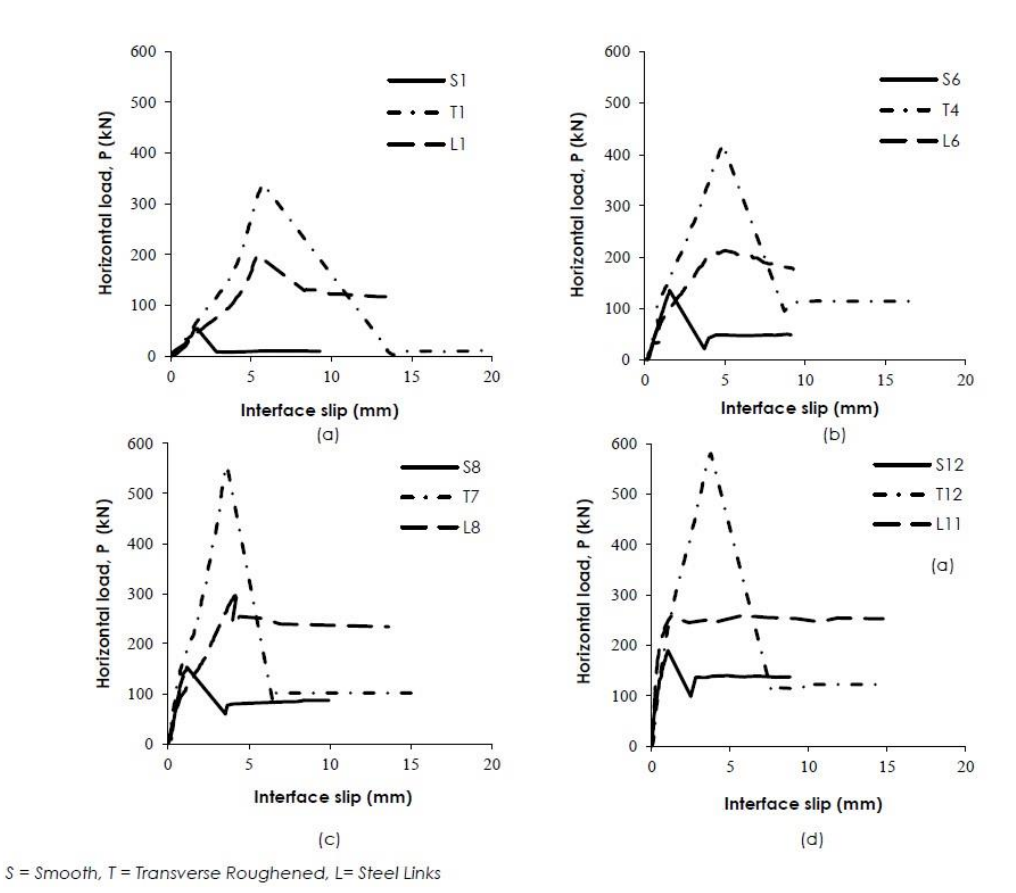


Figure 4.3 Horizontal load versus interface slip curves recorded and presented by Mohamad and Ibrahim [1]

Table 4.2 Results of experimental research [1] - mean values

Surface preparation		Smooth				
σ_n [MPa]	0	0.5	1	1.5		
P_{max} [N]	60300	125100	150733	178233		
$ au_{max} [\text{N/mm}^2]$	0.67	1.39	1.67	1.98		
slip at peak load [mm]	1.39	1.96	1.62	1.36		
Surface preparation	Rough					
σ_n [MPa]	0	0.5	1	1.5		
P_{max} [N]	311767	422100	536867	577400		
$ au_{max} [\text{N/mm}^2]$	3.46	4.69	5.97	6.42		
slip at peak load [mm]	4.52	4.70	4.27	3.97		
Surface preparation		Smooth with	n reinforcemen	t		
σ_n [MPa]	0	0.5	1	1.5		
P_{max} [N]	170100	215367	264167	283800		
$ au_{max} [\text{N/mm}^2]$	1.89	2.39	2.94	3.15		
slip at peak load [mm]	3.48	3.88	3.35	2.68		

The authors of the research have plotted the obtained values of stresses in the $\sigma - \tau$ plane to derive the cohesion and friction coefficients based on the Mohr-Coulomb failure criterion. The researchers have summarised the values, and compared them with Eurocode 2 [2] requirements, in a table, which is displayed below.

				Friction coef	Friction coefficient, μ		ohesion, c
Surface type $\begin{array}{c} \text{Normal} \\ \text{stress, } \sigma_n \\ \text{(N/mm}^2) \end{array}$	Clamping stress $(\rho \cdot f_{yd})$ (N/mm^2)	Splitting tensile strength, f_{ct} (N/mm ²)	Experimental in Figure 5, μ_{exp} (from best fit line)	Cl. 6.2.5(2) Eurocode 2	Experimental in Figure 5, c_{exp} $(c = C/f_{ct})$ (from best fit line)	Cl. 6.2.5(2) Eurocode 2	
	0	e e					
Smooth or "left as-cast" 1.5			0.84	0.60	0.27	0.20	
			0.64				
	1) 20		4				
	0				•		
Transverse	0.5	[4] 20	2.99	2.02	0.70	1.01	0.40
roughened	1		2.77	2.02	0.70	1.21	0.40
3	1.5	N.		ay and a second		va .	
Desir eller	0	8					
Projecting 0.5	0.5	1.41		0.87	0.60	0.04	0.20
steel reinforcement	1	1.41		0.87		0.24	0.20
1.5	1.5						

Table 4.3 Cohesion and friction coefficients derived from experiments, along with Eurocode 2 values [1]

4.1.3 Choice motivation

The choice of this particular research can be justified by a few arguments. Firstly, the tests were performed on specimens with two types of interface roughness, smooth and rough, hence the behaviour of the joint, depending on the surface preparation, could be observed, compared, and later modelled. Moreover, the authors studied the specimens with reinforcement crossing the interface, which constitutes another experiment useful for model verification. On top of that, different levels of compressive stress, perpendicular to the interface, were adopted, thus the coupling between shear and normal tractions could be investigated. Based on the results, the authors have already determined cohesion and friction coefficients, for both roughness levels. The coefficients could be utilised in interfacial material models, since they are both based on the Coulomb friction model.

However, there are also certain shortcomings. The uplift versus normal traction relation was not documented in the study, hence modelling of the behaviour in the direction normal to the interface could not be studied. Moreover, the boundary conditions used in the experiment are not entirely clear. From the preliminary boundary conditions study, it was observed that when preventing the uplift, hence using vertical supports at the top edge of the model, considerably higher capacities were recorded, when using models including coupling. Furthermore, it was observed, that when such an experimental setup was applied, it would be particularly difficult to obtain uniform, horizontal movement while maintaining 0 MPa of the pressure on top of the specimen. Another shortcoming is the uncertainty about the measurement of the relative, horizontal displacement. The slip values at the peak shear stresses, recorded in the research, are in the range of 1-5 mm. The results are of an order of magnitude higher than reported in other sources, especially when smooth, unreinforced interfaces are concerned.

Nevertheless, despite the abovementioned drawbacks, it was decided to proceed with this experiment, based on the outlined positive aspects.

4.2 Numerical model - single element test

A simplified model consisting of two plane stress and one interface element was utilised for initial model verification and comparison. Such an approach was employed, for instance, by Feenstra, de Borst and Rots [42]. It was decided to test two different material models – Coulomb Friction(CF) and Combined Crashing-Shearing-Cracking (CCSC) model. Both models are related to the Mohr-Coulomb failure criterion, however, the second one is more sophisticated as it takes into account more parameters. Such parameter is among others fracture energy in mode I, which allows the model to capture the softening in tension. Mode II fracture energy, along with parameter specifying the increase of the energy under pressure, is also to be specified, as well as residual friction angle. Cohesion and friction softening are accounted for in the model, based on the abovementioned parameters. On top of that the dilatancy-related parameters can be specified, in order to account for the dilatancy dependency on normal stresses. The specimens with both smooth and rough interfaces were modelled. The samples with reinforcement crossing the joint surface were not included in this part of the modelling activities.

4.2.1 Numerical setup

As already stated the models in this part of the research consisted of three elements – two regular plane stress and one structural line interface. The plane stress elements represented the concrete base and topping, whereas the interface element was to capture the behaviour of the connection between them. Additional models were run to study the influence of boundary conditions and initial stiffness, as well as to observe the response with decreased residual friction angle. The model's view is presented in Figure 4.4.

Table 4.4 Single element study - models' overview

Model Name	Surface preparation	Concrete-to-concrete interface material model
S-CF	Smooth	Coulomb Friction
S-CCSC	Sillootii	Combined Cracking-Shearing-Crushing
R-CF	5 1	Coulomb Friction
R-CCSC	Rough	Combined Cracking-Shearing-Crushing

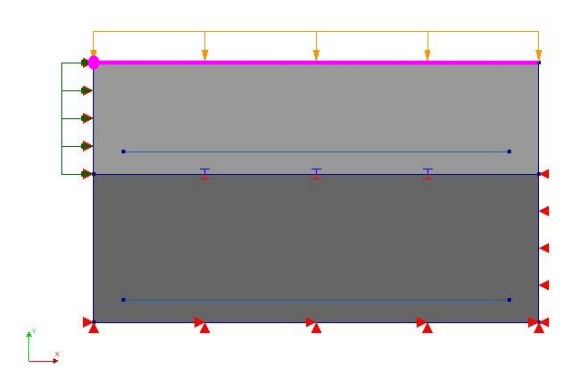


Figure 4.4 Single element model

Model Name	Variation type	Note
R-CF-NR/T/C	Top Boundary	No restrain Tyings Constrained top
R-CCSC-NR/T/C	Condition	boundary
R-CF-k1/k5/k10	Shear	$k_s = 1 \text{ N/mm}^3 \mid k_s = 5 \text{ N/mm}^3 \mid$
R-CCSC-k1/k5/k10	stiffness	$k_s = 10 \text{ N/mm}^3$
R-CCSC-RF	Residual	$\phi_{res} = \phi_0 \mid \phi_{res} = 36^\circ$
	Friction angle	

Table 4.5 Single element study - additional models

4.2.2 Geometry and structural element types

The general model's geometry is presented in Figure 4.4. As stated above, the plane stress elements were used, as well as the structural line interface element. The embedded bars were also utilised, to represent the reinforcing grid, included in the concrete elements. However, in this case, it does not influence the behaviour considerably, as the reinforcement only increases the stiffness. The dimensions of the plane stress elements correspond with the dimensions of the base and the topping. The elements' properties are summarised in Table 4.6.

Table 4.6 Cross-section properties

Element	Element Class Material		erial	Geometry
Concrete base	Regular plane stress	Concrete base		
Concrete topping	Regular plane stress	Concrete topping		t = 300 mm
Interface	Structural line	S-CF	R-CF	t - 300 mm
Interface	interfaces	S-CCSC	R-CCSC	
Reinforcement	Embedded bar	Reinforcement		$A = 56.55 \text{ mm}^2$

4.2.3 Material models

The overview of material properties for steel and concrete is included in Table 4.7. As far as the interface elements are concerned, separate tables were made, including all input parameters applied.

4.2.3.1 Concrete

Concrete material properties were assumed to be linear elastic, as in such a simplified model no localised crushing or cracking can be captured – the whole continuum element would fail. The Young's Moduli were calculated based on the Eurocode 2 [2] for the f_{cm} values included in Table 4.1. Poisson ratio and mass density are applied as explained in the previous chapter.

4.2.3.2 Steel

Linear elastic properties for steel rebars were applied.

Table 4.7 Material properties of concrete and steel elements

Material	Class	Material model	<i>E</i> [N/mm ³]	v [-]	Mass Density [T/mm ³]
Concrete base	Concrete and masonry	Linear	32 000	0.2	2.5E-9
Concrete topping	Concrete and masonry	elastic isotropic	29 000	0.2	2.5E-9
Reinforcement	Steel		200 000	0.3	-

4.2.3.3 Interface

For the interface element, two material models were utilised – Coulomb Friction (CF) and Combined Crushing-Shearing-Crushing (CCSC). In total, four different material models were used, as two types of surface roughness were analysed. The input parameters applied are included in Table 4.9 and Table 4.10. Certain parameters are repeated in both models since both of them stem from Coulomb friction hypothesis.

As far as the shear stiffness k_s is concerned, the analyses were originally performed with the values with a purpose to ideally resemble the experimentally obtained, initial slope of the traction-slip curves. Nevertheless, due to two main reasons, it was decided to proceed with the value of 10 N/mm^3 . Firstly, it was noted that the magnitudes of slip at failure recorded in the reference experiments were considerably higher than expected, especially for smooth, unreinforced specimens. Slips for this type of surfaces, according to [16], should be as low as 0.05 mm. As was already highlighted in the previous chapter, there is no consensus concerning the initial shear stiffness for modelling the concrete-to-concrete interfaces, and the initial value could be theoretically assumed as very high to represent the adhesive bonding. The magnitude of around 1 N/mm^3 , which would have to be used to fit the experimental data, seems far too low, which can be confirmed by the values used by other researchers summarised in Table 4.8. Secondly, with very low shear stiffness, there were some convergence issues observed.

Table 4.8 Shear and	normal els	astic stiffness	values for	ound in	literature
Table 7.0 bilear and	. mormai cic	asuc sumicos	varues n	ouna m	nicialuic

Author	Source	Interface type	Note	$k_n \left[\frac{N}{\text{mm}^3} \right]$	$k_s \left[\frac{N}{\text{mm}^3} \right]$
S.B. Setyanto	[46]	Concrete- SHCC Smooth interface	CF Model DIANA	10	10
D. Dias-da- Costa J. Alfaiate, E.N.B.S. Júlio	[43]	Sand-blasted	Mohr – Coulomb friction law yield surface	1.8E+5*	18
M. van den Heever et al.	[45]	IRs** in 3D printed concrete	CCSC Model DIANA	1.0E+6	4.17E+5
S. Dudziak, W. Jackiewicz- Rek, Z. Kozyra	[44]	Wire-brushed	Cohesive elements with traction- separation law Abaqus	3.63E+4	1.51E+4
Assumed				10000	10

*It was not given explicitly, the authors only stated that they used high penalty value.

The cohesion and friction coefficients were already provided by the authors of the reference research, and those values were used in the model. Cohesion coefficient

^{**}IRs - interfacial regions

was multiplied by f_{ct} in accordance with Eurocode 2 [2], which was also done by Mohamad and Ibrahim, to obtain the magnitude of cohesion.

The dilatancy angle was neglected in this part of the study. It is acknowledged that such a value does not correctly represent interfacial behaviour. However, the displacements in the normal direction could not be studied as they were not documented in the reference research. Additionally, it was observed that the model is sensitive to the boundary conditions applied and deformations in the direction perpendicular to the load application.

Tensile cut-off, even if applied, would not limit the failure envelope. The splitting tensile strength given by the authors equals 2.99 N/mm², which exceeds the envelopes for both, smooth and rough specimens. It was not clear, however, whether it is a concrete or interface tensile strength.

For the CCSC model, in the cracking part, the tensile strength of 2.99 N/mm² was applied, however, this value is most probably overestimated. The fracture energy was calculated according to the guidelines [6]. The weaker concrete strength was used in the formula, according to the approach pursued in [44].

In the CCSC, model the residual friction angle has to be specified. At first, the value was chosen as equal to the initial friction angle. After observing that for roughened surfaces, especially for higher levels of applied lateral pressure, the post-peak capacity is overestimated, it was decided to decrease the angle's value.

For the fracture energy in shear, the values were initially chosen based on the relation $G_{f_{II}} = 10G_{f_I}$ given in [43], proposed by Neto et al. [53]. For the specimens with a smooth interface, the value was in good accordance with the approximated area under the traction-slip curve [1], however, for the rough surfaces it was not the case and the fracture energy was increased.

As far as the input parameters related to the compression cap are concerned, they were adjusted in a way to move the cap away. Crushing behaviour is not relevant when modelling the interface between two concretes since, if any compressive failure was to occur, the continuum elements should indicate the failure.

Table 4.9 Input	parameters :	for	Coulomb	Friction	interface	material 1	model

Input parameter	Symbol	Va	lue	Unit	Source	
	Symbol	Smooth	Rough	Omt	Source	
	Linear Material Properties					
Normal stiffness modulus-y	k_n	10000	10000	$\frac{N}{mm^3}$	Assumed - penalty stiffness	
Shear stiffness modulus-x	k_s	10	10	$\frac{N}{mm^3}$	Based on Table 4.8	
Coulomb Friction						
Cohesion	С	0.8073	3.6179	$\frac{N}{mm^2}$	[1] calculated based on experimental results	
Friction angle	φ	40.0303	63.6623	٥	[1] calculated based on experimental results	
Dilatancy angle	ψ	0	0	0	Assumed	

Table 4.10 Input parameters for Combined Cracking-Shearing-Crushing interface material model

	Symbol	Value		Unit	Source	
	Syllibol	Smooth	Rough	Omi	Source	
		Linear Ma	terial Prop	erties		
Normal stiffness modulus-y	k_n	10000	10000	$\frac{N}{mm^3}$	Assumed - penalty stiffness	
Shear stiffness modulus-x	k_s	10	10	$\frac{N}{mm^3}$	Based on Table 4.8	
		Coulo	mb Friction	n		
Cracking						
Tensile strength	f_t	2.99	2.99	$\frac{N}{mm^2}$	[1]	
Fracture energy	G_{f_I}	0.0905	0.0905	$\frac{N}{mm}$	[6] $G_{Fk} = 0.7 \cdot 0.073 f_{cm}^{0.18}$ $f_{cm} = f_{cm_{weak}}$	
Shearing	l .	l .		I.	, wan	
Cohesion	С	0.8073	3.6179	$\frac{N}{mm^2}$	[1] derived based on experimental results	
Friction angle	φ	40.0303	63.6623	0	[1] derived based on experimental results	
Dilatancy angle	ψ	0	0	0	Assumed	
Residual friction angle	$\phi_{residual}$	40.0303	36.5000	0	Assumed - equal to init. friction angle adjusted	
Mode II fracture en	nergy	·		I.		
Parameter a	а	0	0	mm	Assumed – no influence of σ on fracture energy	
Fracture energy	G_{f}_{II}	1	20	$\frac{N}{mm}$	Approximated acc. to [1] [43] [53] as explained above	
Crushing						
Compressive strength	f_c	10000	10000	$\frac{N}{mm^2}$	Values chosen to move the compression cap	
Factor C_s	C_{S}	1	1	-	away	
Compressive inelastic law						
Compressive fracture energy	G_{f_c}	10000	10000	$\frac{N}{mm}$	Values chosen to move the compression cap	
Eq. plastic relative disp.	κ	0.0025	0.0025	mm	away	

4.2.4 Boundary and loading conditions

As presented in Figure 4.4, vertical restrain was applied along the bottom edge of the base element. Horizontal restraints were used along the bottom and right-side edges of the base element. Such conditions are supposed to represent the conditions used when performing the experiment. The top boundary condition was a topic of the discussion initiated in subchapter 4.1.3. In the final model, it was decided to apply a set of tyings connecting vertical translation of the top nodes, with the top left node being the master. The pink line and dot were added in Figure 4.4 to represent the tying. Horizontal supports were added along the left-side edge of the topping element to facilitate the displacement application.

As far as the loads applied are concerned, the self-weight was accounted for, by applying an equivalent acceleration. Then, the perpendicular pressure was applied in the consecutive step, as a line load in a force-control manner. In the following step, the displacement was applied along the topping element's edge.

Table 4.11 Loads applied

Applied load	Load type	Magnitude			
Self-weight	Equivalent acceleration	-9810 mm/s ²			
Perpendicular pressure	Distributed force	0 N/mm	150 N/mm	300 N/mm	450 N/mm
Horizontal movement	Prescribed displacement	1 mm			

4.2.5 Mesh

The meshed model consists of only three finite elements, as presented in Figure 4.5. Two, 8-node, quadrilateral elements, representing concrete elements, are connected employing the line, 3+3 node interface element. The interface element is however not visible in such a view. The elements' specifics are included in Table 4.12.



Figure 4.5 Meshed single element model

Table 4.12 Finite elements used - specifications

Finite element type	CQ16M	CL12I	
Degrees of freedom	u_x, u_y	u_x, u_y	
Degrees of freedom	8×2=16	6×2=12	
Interpolation scheme	Quadratic	Quadratic	
Integration scheme	2×2 Gauss	5-point Newton-Cotes	
Stress components	$\sigma_{xx}, \sigma_{yy}, \sigma_{xy}$	t_n, t_t	
Element size [mm]	75×300 100×300	300	
Total number of elements	2	1	
Total number of nodes	20		

4.2.6 Analysis characteristics

The structural nonlinear analysis with physical nonlinearities was applied for all considered models. The energy and force convergence norms were chosen, with tolerances according to Table 4.13. Both norms had to be satisfied, however, it was allowed for the analysis to continue even if the convergence was not reached. In order to improve the convergence rate the line search algorithm was used. The self-weight and pressure were applied with a single load step, and the horizontal movement was applied in 230 steps to obtain the total of 15 mm horizontal displacement. It should be noted that phased analysis was used. It was done since for the models with restrains along the top edge, the lateral pressure was applied in

the first phase, and in the second one, the top-edge vertical supports were activated. Following, the horizontal displacement was applied. In other models the phased analysis was not required, however, it does not affect the outcome.

Table 4.13 Analysis specifications

Iterative method	Regular Newton-Raphson
Maximum number of iterations	50
Convergence norms	Energy, Force – both satisfied
Energy – convergence tolerance	0.001
Displacement – convergence tolerance	0.01
Load steps	0.02 (100) 0.1 (130)*

*The step size was slightly altered for the analysis with $k_s = 1 N/mm^3$ to maintain relatively small step size up until the peak is reached - 0.05 (100) 0.1 (100)

4.2.7 Results

The results that can be compared with the reference research are the load-horizontal displacement relations. As already discussed, there is uncertainty concerning the recorded displacements. Therefore the load-slip relations obtained from the numerical models were compared with the peak and post-peak loads presented as horizontal lines. The peak capacity is taken as the mean value recorded for the three specimens, according to Table 4.2. The markers indicate the peak shear load and corresponding slip for each specimen tested by Mohamad and Ibrahim [1]. The post-peak capacity was not documented in detail, thus it was estimated based on the load-slip curves recorded only for one specimen - Figure 4.3.

The numerical results were obtained by measuring the horizontal reactions at the nodes where the displacement was applied. The sums of the reactions were presented as functions of horizontal displacements of the right bottom node of the topping element. The sample reading is presented in the following figures.

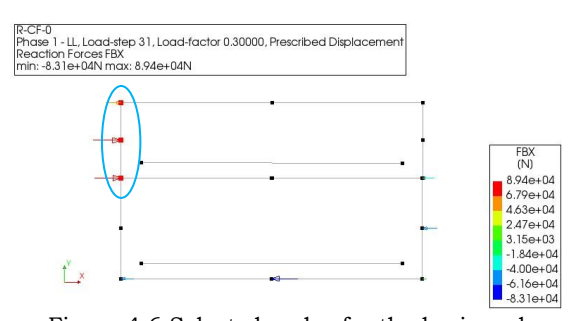


Figure 4.6 Selected nodes for the horizonal reactions reading

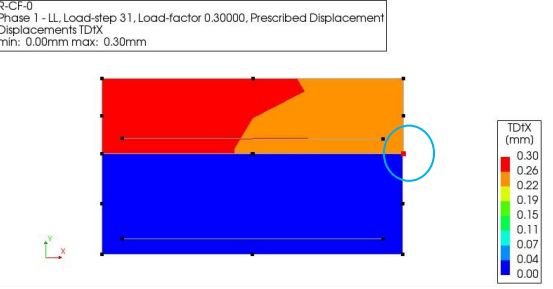


Figure 4.7 Selected node for the horizontal displacement reading

4.2.7.1 Boundary conditions study

Firstly, a study on boundary conditions was performed. Three types of boundary conditions were applied:

- Tyings set of tyings connecting vertical translation of the top nodes, with the top left node being the master;
- Supports supports restraining vertical movement applied along the top edge;
- No restraints at the top edge.

The results for both CF and CCSC models, using input parameters for the rough interface, according to Table 4.9 and Table 4.10, were compared. For the sake of clarity only the results for 0 MPa and 1 MPa of applied pressure are compared.

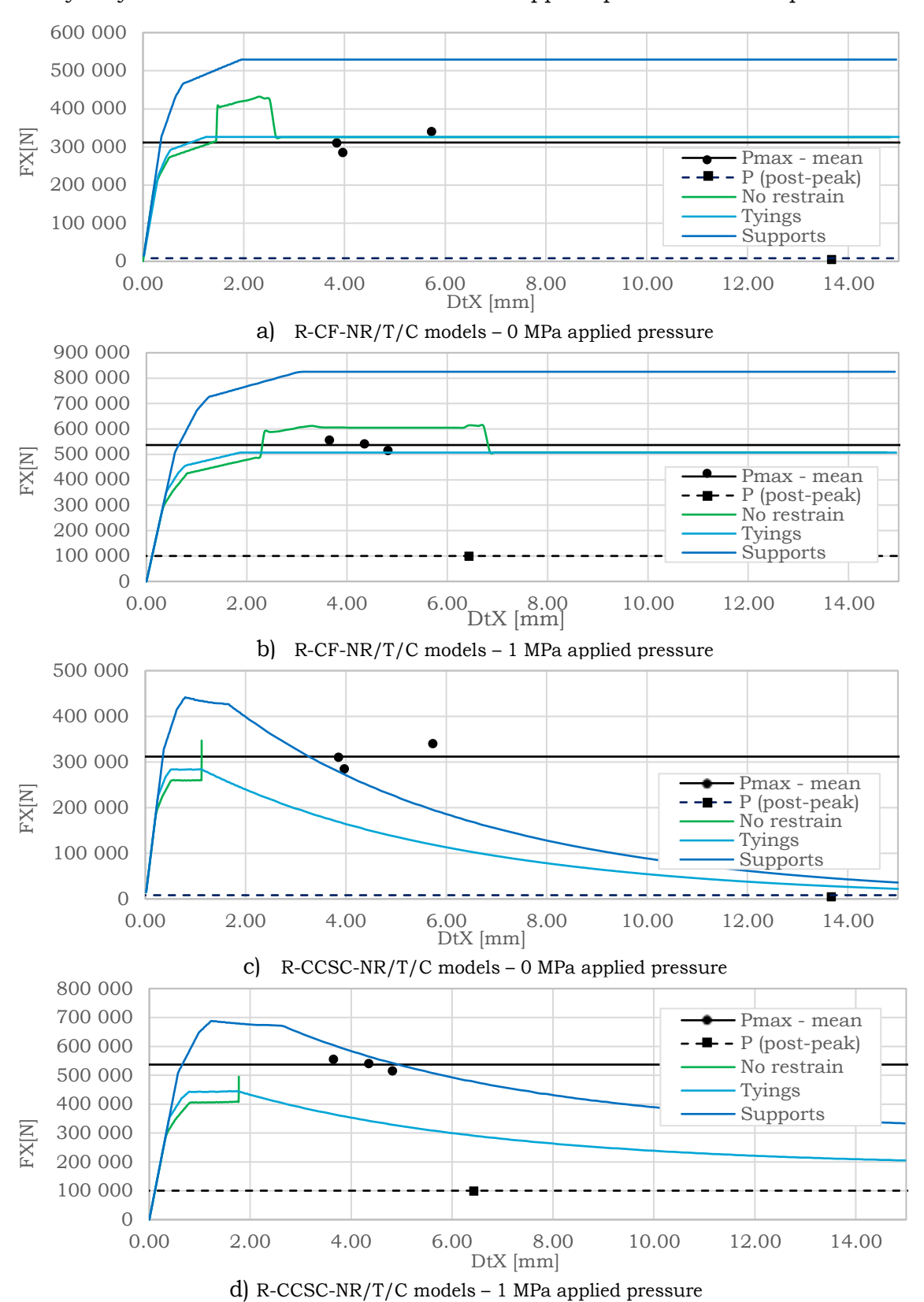
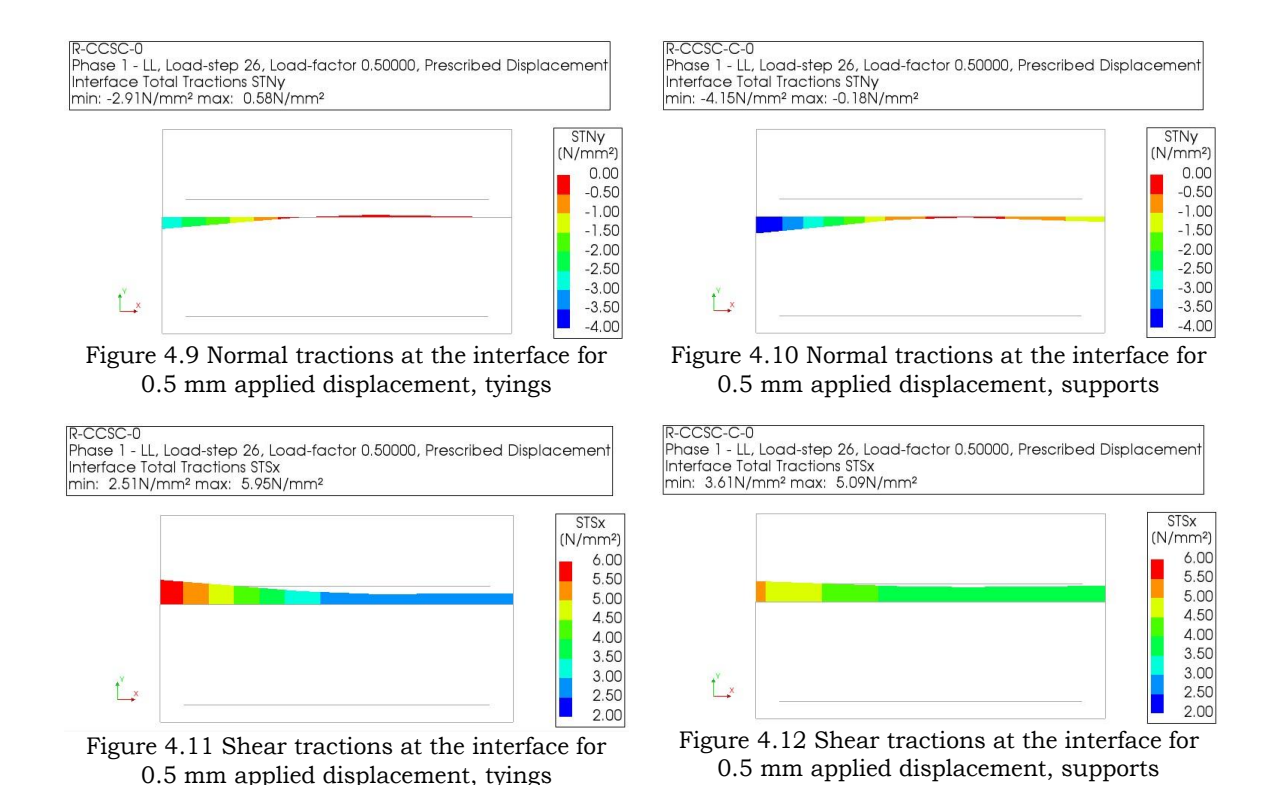
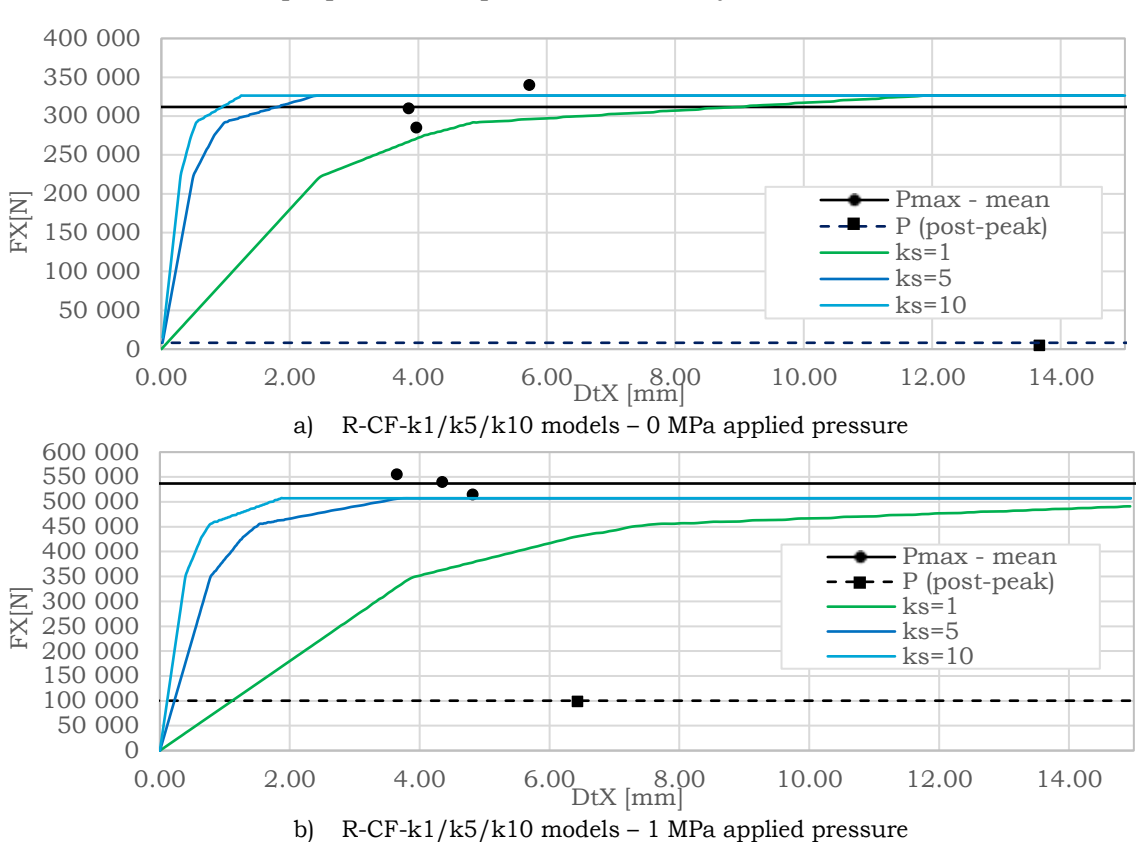


Figure 4.8 Results comparison for varying boundary conditions



4.2.7.2 Elastic stiffness ks study

Taking into account the debate over elastic shear stiffness, it was decided to observe how the response changes with varying stiffness input. As above, only the results for 0 MPa and 1 MPa of perpendicular pressure are analysed.



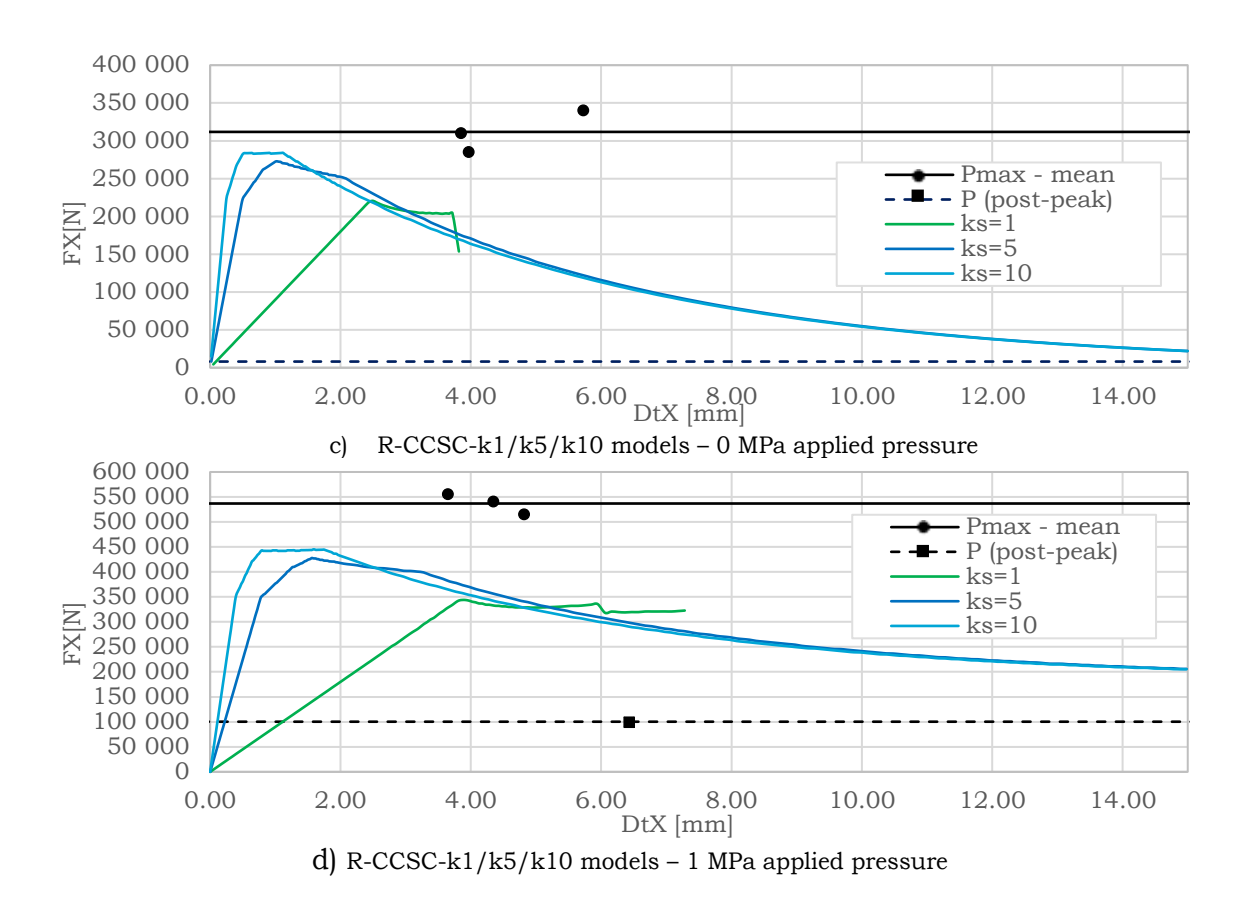


Figure 4.13 Results comparison for varying elastic shear stiffness

4.2.7.3 Residual friction angle study

The results for the variation in residual friction angle are compared only for CCSC model, for 1 MPa perpendicular pressure.

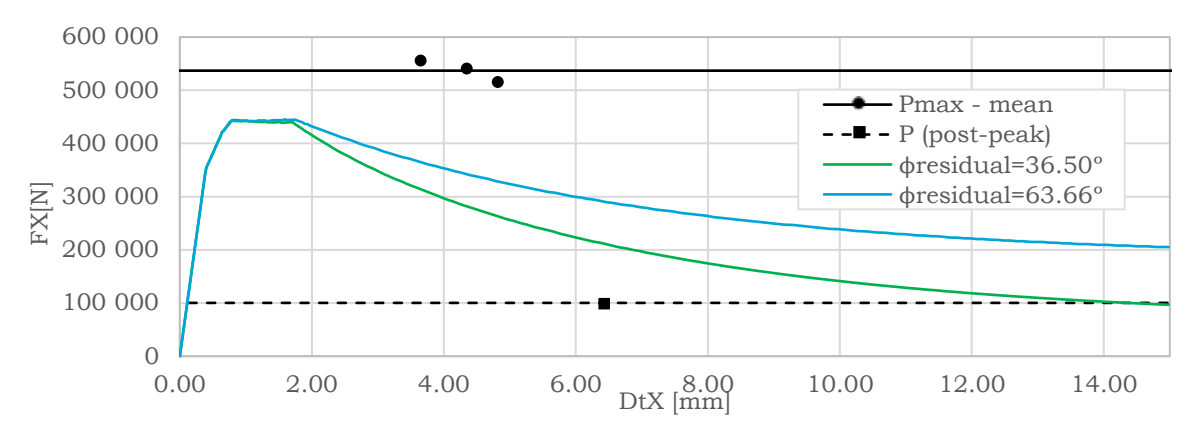


Figure 4.14 R-CCSC and R-CCSC-RF Models - 1 Ma applied pressure - results comparison

4.2.7.4 Reference model results

Accounting for the studies performed above, the results of the reference models with the input parameters according to Table 4.9 and Table 4.10 and the tyings applied along the top edge, are presented below.

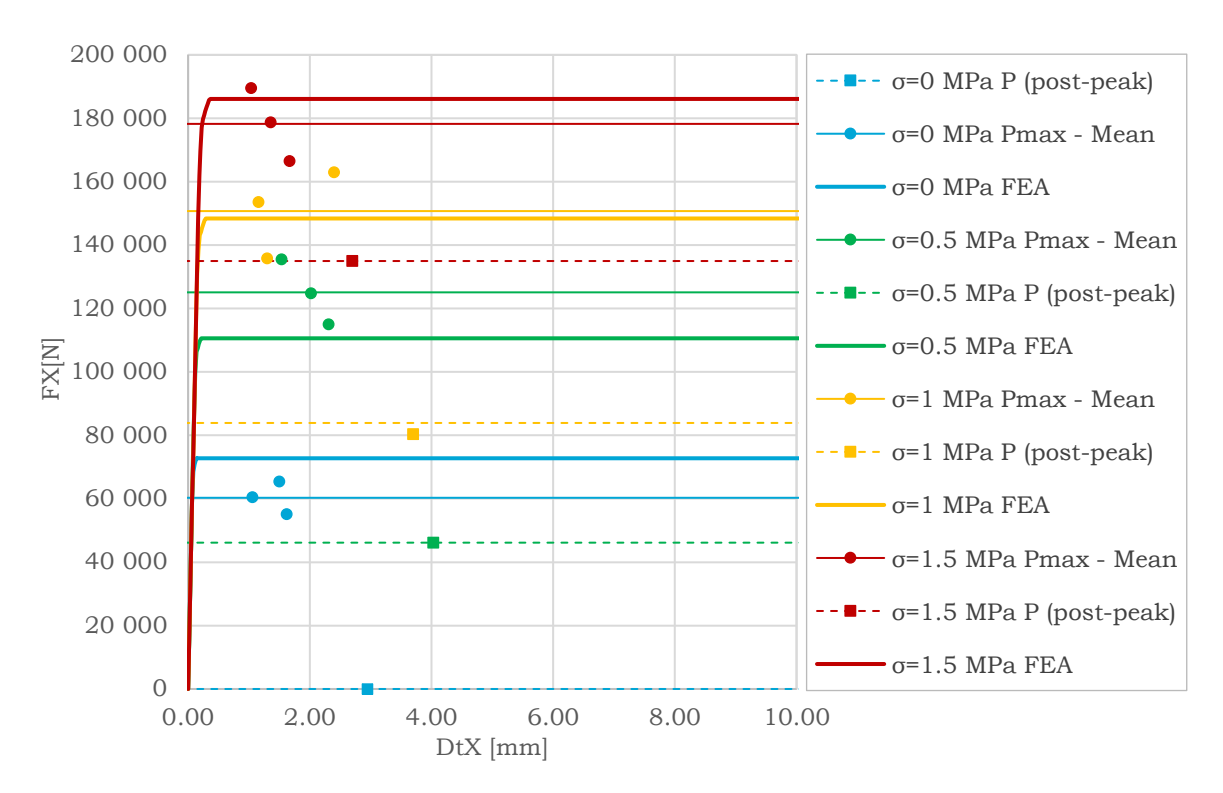


Figure 4.15 Load-slip curves for the specimens with smooth interface, using CF material model

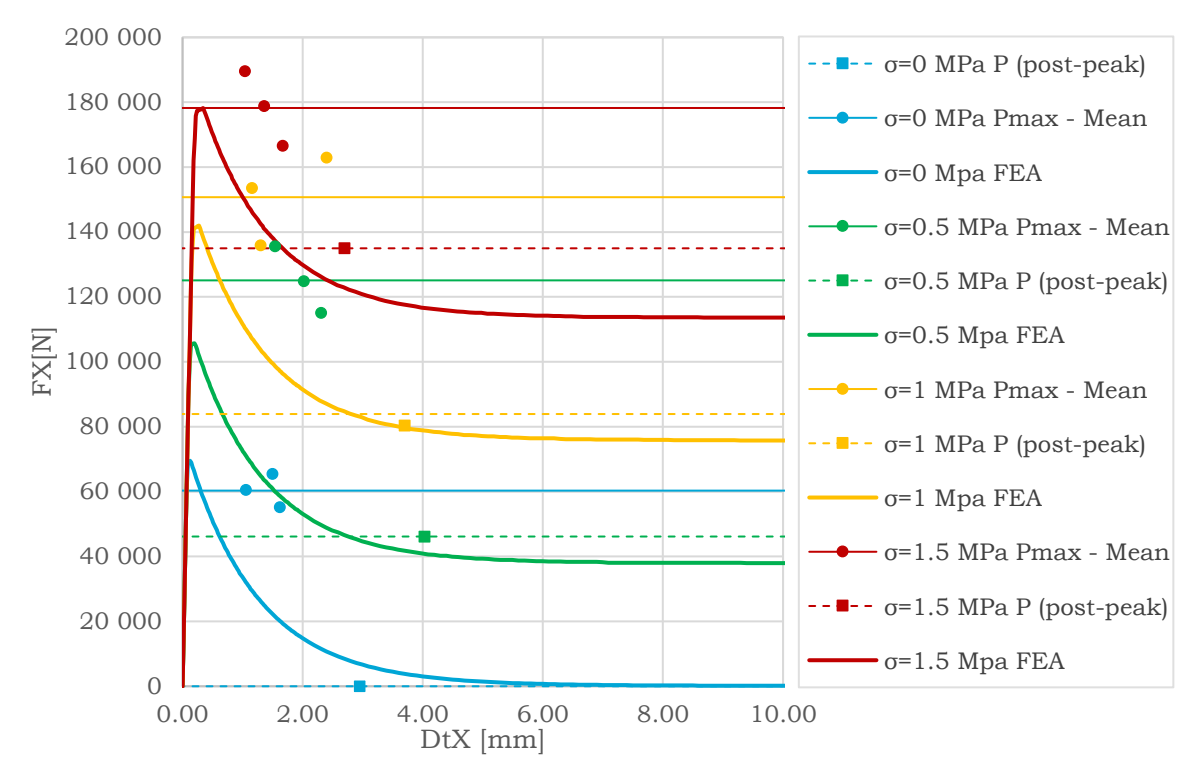


Figure 4.16 Load-slip curves for the specimens with smooth interface, using CCSC material model

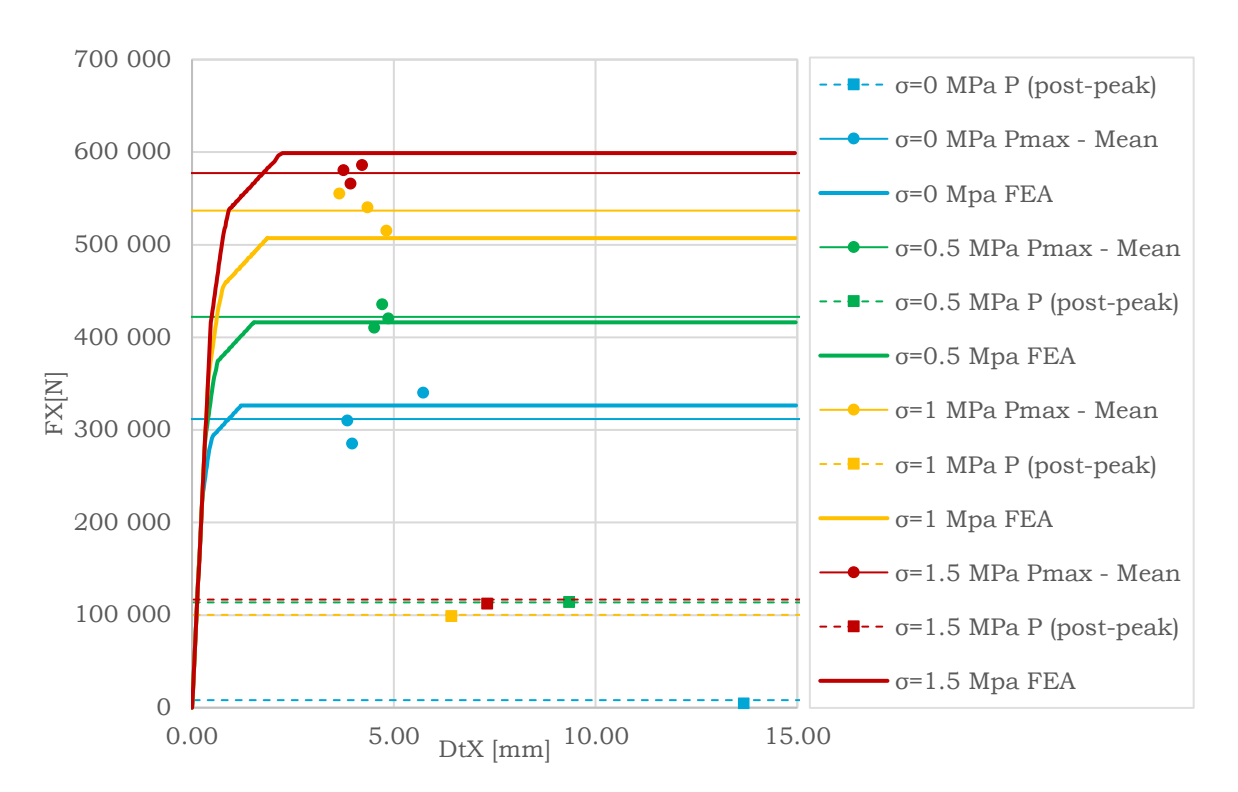


Figure 4.17 Load-slip curves for the specimens with rough interface, using CF material model

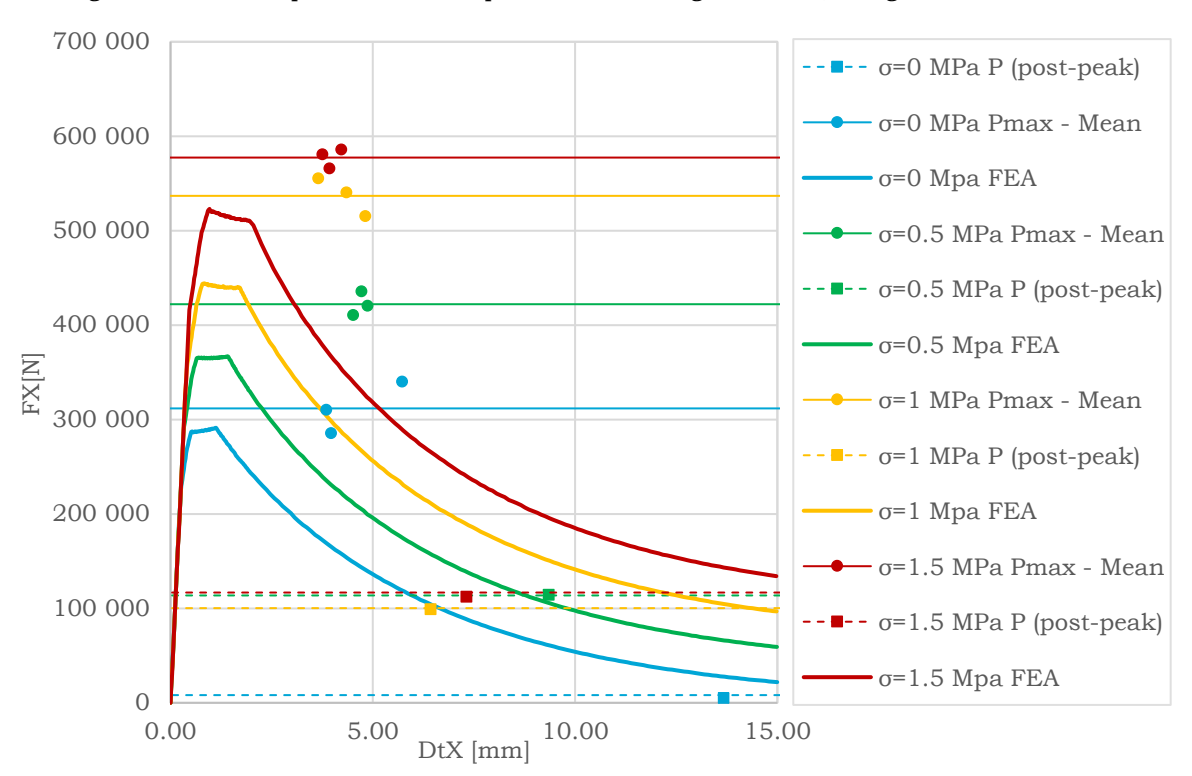


Figure 4.18 Load-slip curves for the specimens with rough interface, using CCSC material model

4.3 Numerical model – element assembly

The principle reason for creating a model with an assembly of the elements was to study the behaviour of the specimens with rebars crossing the interface. It was analysed how refined strain distribution, presence of circular beam bond-slip reinforcement, as well as nonlinear concrete properties influence the analysis of the samples.

4.3.1 Numerical setup

Only one model was tested within this part of the research. The Combined Cracking-Shearing-Crushing material model was used for the interface. The reinforcement was modelled as a circular beam bond slip bar to capture not only the clamping generated by the reinforcement but also the influence of the bending and shear resistance of the rebars. The material properties of concrete were set to be nonlinear, to allow cracking of the concrete bulk.

Table 4.14 Element assembly - models' overview

Model Name	Surface preparation	Concrete-to-concrete interface material model
S-CCSC-RC		Combined Cracking-Shearing- Crushing

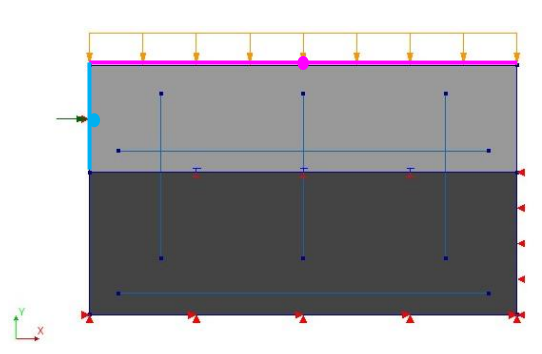


Figure 4.19 Component study – S-CCSC-RC Model

4.3.2 Geometry and structural element types

The model's geometry is displayed in Figure 4.19. The structural elements used are the same as already presented in subchapter 4.2.2 with the only exception being additional elements for rebars crossing the interface.

Table 4.15 Cross-section properties

Element	Element Class	Material	Geometry
Concrete base	Regular plane stress	Concrete base NL	
Concrete topping	Regular plane stress	Concrete topping NL	t = 300 mm
Interface	Structural line interfaces	S-CCSC	t - 300 mm
Reinforcement	Embedded bar	Reinforcement	A = 56.55 mm ²
Interface reinforcement	Circular beam bond slip bar	Reinforcement – bond slip	φ = 6 mm*

*To represent that there are in fact six bars across the thickness, instead of looking for an equivalent bar, it was decided to copy each element and paste it at the same location five times.

4.3.3 Material models

Material models, again, stem from the properties outlined in the previous subchapters. It was decided to use nonlinear properties for concrete and steel. Details are presented in the next sections. Derivation of the material properties was performed following Eurocode 2 [2] and guidelines for nonlinear FEA of concrete structures [6].

4.3.3.1 Concrete

Young's moduli and tensile strength values were calculated based on the compressive strength magnitudes given in Table 4.1. Fracture energies were calculated following the formulas given in the guidelines [6]. Other input parameters were also chosen on the basis of the guidelines [6].

Table 4.16 Material properties of concrete

		Inj	put	
Input parameter	Symbol	Concrete	Concrete	Unit
		base NL	topping NL	
Young's Modulus	Ε	32000	29000	N/mm ²
Poisson's ratio	v	0.2		-
Mass density	ρ	2.5E-9		T/mm ³
Crack orientation		Rotating		
Tensile curve		Hordijk		
Tensile strength	f_{ct}	2.8	1.9	N/mm ²
Mode-I tensile fracture energy	G_F	0.0974	0.0905	N/mm
Crack bandwidth specification		Rots		
Poisson's ratio reduction		Damage base	d	
Compression curve		Parabolic		
Compressive strength	f_c	36	24	N/mm ²
Compressive fracture energy	G_C	27.0553	21.5581	N/mm
Reduction model due to lateral		Vecchio and Collins 1993		
cracking		veccino and	Commo 1990	
Lower bound reduction curve	eta_{σ}^{min}	0.4		-

4.3.3.2 Steel

Linear elastic material properties were chosen in accordance with Guidelines for NLFEA of Concrete Structures [6]. As far as Von Mises plasticity input is concerned, the graph presenting the total strain-yield stress relation applied is presented in Figure 4.20. 250 MPa was specified by the authors [1], whereas the ultimate value and corresponding strain follow Eurocode 2 [2] and guidelines' [6] recommendations for steel Class B.

For steel rebars crossing the interface not only linear elastic and Von Mises parameters had to be specified, but also the bond-slip behaviour of the steel-to-concrete interface. The failure model based on fib Model Code 2010 [27] was selected. The s, τ and α values follow the code's recommendations for hot-rolled bars, assuming good bond conditions, following Table 6.1-2 of that code. The concrete strength for the formula for $\tau_{bmax} = \tau_{bf}$ was taken as the lower of the compressive capacities. The normal stiffness modulus applied in the model was obtained assuming that the rebar embedded in concrete behaves like a beam on an elastic foundation. Normal stiffness was calculated as a concrete bearing stiffness

using the formula (4.1) provided by Soroushian, Obaseki and Rojas [54] also referenced, among others, by [55] [56].

$$k_n = \frac{127c_1\sqrt{f'_c}}{d_b^{2/3}} \tag{4.1}$$

Where:

 c_1 is the coefficient ranging from 0.6 for a clear bar spacing of 25 mm to

1.0 for larger bar spacing

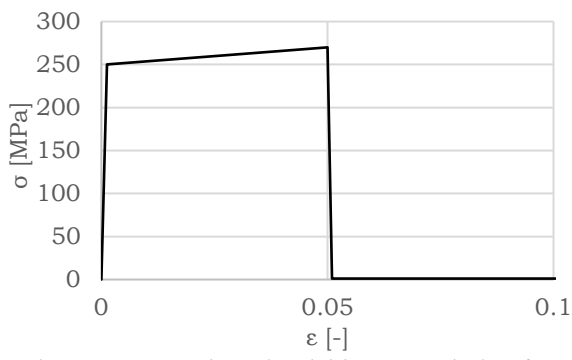
 f'_c is the concrete compressive strength in MPa

 d_b is the diameter of a bar crossing the interface.

Steel-to-concrete interaction in the normal direction is assumed to be ideal – only linear elastic behaviour described by the stiffness k_n is represented. The shear stiffness modulus was assumed as equal to the secant modulus at a slip of 0.01 mm. However, the value is less significant as the behaviour in the shear direction is represented by the bond-slip relation. The shear stiffness is only relevant until s_0 is reached, and for unloading which may happen. To represent the fact that the bars are U-shaped, the reinforcement was anchored at the top, by setting the penalty values to the anchor stiffness.

Table 4.17 Material properties for steel rebars crossing the interface

Input parameter	Symbol	Input	Unit	
Young's Modulus	Е	200 000	N/mm ²	
Poisson's ratio	v	0.3	-	
Mass density	ρ	7.9E-9	T/mm ³	
Nonlinear Model		Von Mises plasticity		
Von	Mises par	rameters		
Plastic hardening		Total strain-yield stress		
Total strain-yield stress		Acc. to Figure 4.20		
Hardening hypothesis		Strain hardening		
Hardening type		Isotropic hardening		
Bo	nd-slip in	terface		
Normal stiffness modulus	k_n	190	N/mm ³	
Shear stiffness modulus	k_s	46.5	N/mm ³	
Bond-slip interface failure model		CEB-FIB 2010 bond-slip		
		function		
Maximum shear stress	$ au_{max}$	1.47	N/mm ²	
Ultimate shear stress	$ au_f$	1.47	N/mm ²	
Linearized initial slip section	s_0	0.01	mm	
Relative slip section s1	s_1	0.1	mm	
Relative slip section s2	s_2	0.1	mm	
Relative slip section s3	s_3	0.1	mm	
Exponent alpha	α	0.5	-	
Reinforcement anchor				
Normal stiffness in anchor	K_n	1E+9	N/mm	
direction	¹ N	110.9	14/111111	
Shear stiffness normal to anchor direction	K_{s}	1E+9	N/mm	



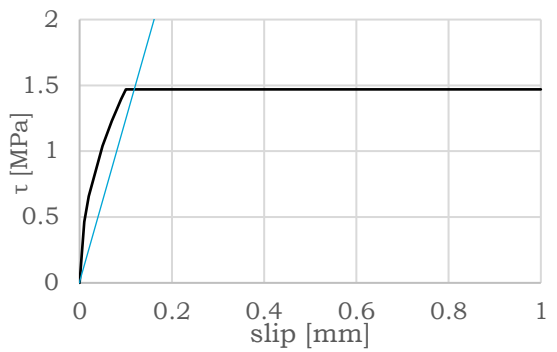


Figure 4.20 Total strain-yield stress relation for reinforcement crossing the interface

Figure 4.21 Applied $\tau - s$ relationship of steel rebars

4.3.3.3 Interface

For the interface elements, the CCSC material model was applied, with input parameters for the smooth interface according to Table 4.10. However, there is a minor exception. To activate the clamping of the rebars, certain opening of the interface had to be incorporated into the model. The dilatancy angle was set to be equal to 15° . According to Vermeer and de Borst [57] the magnitudes of the dilatancy angle for concretes, are observed to be below 20° . In research [43] where authors modelled push-off experiments with sand-blasted surfaces, the 10° angle was applied. Therefore, $\psi = 15^{\circ}$ seemed like a reasonable assumption. Moreover, the confining normal stress at which the dilatancy becomes zero had to be specified. The relatively high value of -10 MPa was assumed, as it was aimed to disregard any dilatancy degradation. The exponential coefficient that allowed to get more or less stable results was equal to 1. It shall be observed that the lower the value, the lower the dilatancy's degradation. It is highlighted, however, that the abovementioned values are assumed and are not supported by any experimental results.

Table 4.18 Additional input parameters applied in CCSC material model

Input parameter	Symbol	Input	Unit
Dilatancy angle	ψ	15	0
Confining normal stress	σ_n	-10	$\frac{N}{mm^2}$
Exponential degradation coefficient	δ	1	_

4.3.4 Boundary and loading conditions

Boundary conditions applied are similar to the ones used in single-element tests, already outlined in section 4.2.4. The difference is that in the assembly two sets of tyings were applied, which are depicted as pink and blue lines and dots in Figure 4.19. In order to apply the shear load uniformly to the left edge of the topping, it was decided to use tyings rigidly connecting all the nodes along that edge, with the node in the centre. It should be highlighted that it is also just an assumption. The horizontal support for displacement application was applied in the centre, master node. Tyings connecting translations in the y-direction were applied to the top edge according to Figure 4.19. The master node had to be specified in the centre as it could not coincide with the already tied left edge.

The loads applied were the same as in previous subchapter, hence are in accordance with Table 4.11.

4.3.5 Mesh

The mesh size applied is approximately 10 mm x 10 mm. Mesh of the S-CCSC-RC Model is presented in Figure 4.22. Specifications concerning finite element types can be found in Table 4.19.

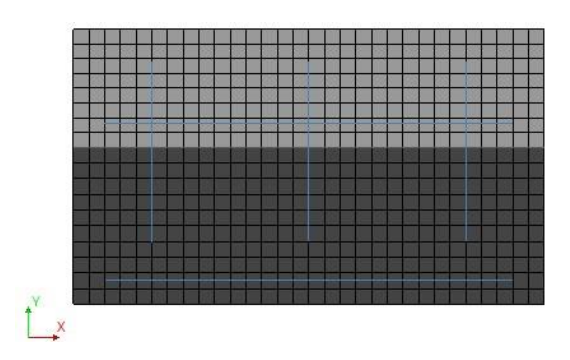


Figure 4.22 Mesh of the S-CCSC-RC Model

Table 4.19 Finite elements used - specifications

Finite element type	CQ16M	CL12I
Degrees of freedom	u_x, u_y	u_x, u_y
	8×2=16	6×2=12
Interpolation scheme	Quadratic	Quadratic
Integration scheme	2×2 Gauss	5-point Newton-Cotes
Stress components	$\sigma_{xx}, \sigma_{yy}, \sigma_{xy}$	t_n, t_t
Element size [mm]	10×10	10
Total number of elements	540	30
Total number of nodes	23	327

4.3.6 Analysis characteristics

The analysis characteristics were almost the same as in the single-element test part. However, the maximum number of iterations was increased from 50 to 100. Moreover, the step size after 2 mm of applied displacement was reduced from 0.1 to 0.05. Nonetheless, it was observed, that none of the models run for more than 110 load steps, hence in none of the analyses, the 15 mm displacement was reached. Again, the line search option was employed.

Table 4.20 Analysis specifications

Iterative method	Regular Newton-Raphson
Maximum number of iterations	100
Convergence norms	Energy, Force – both satisfied
Energy – convergence tolerance	0.001
Displacement – convergence tolerance	0.01
Load steps	0.02 (100) 0.05 (260)

4.3.7 Results

The analysed results are the load-horizontal displacement relations, as in the previous study. The graphs representing experimental reference [1] are presented in the same manner as in section 4.2.7.4, using horizontal lines representing mean peak capacity and approximated post-peak capacity, along with markers indicating experimental results.

The finite element model results were generated by plotting the horizontal reaction at the node of displacement application, as a function of horizontal displacement read at the right-edge node, slightly above the interface surface, to comply with the experimental setup presented in Figure 4.2.

Additional results displaying more details concerning the model's behaviour can be found in Annex E.

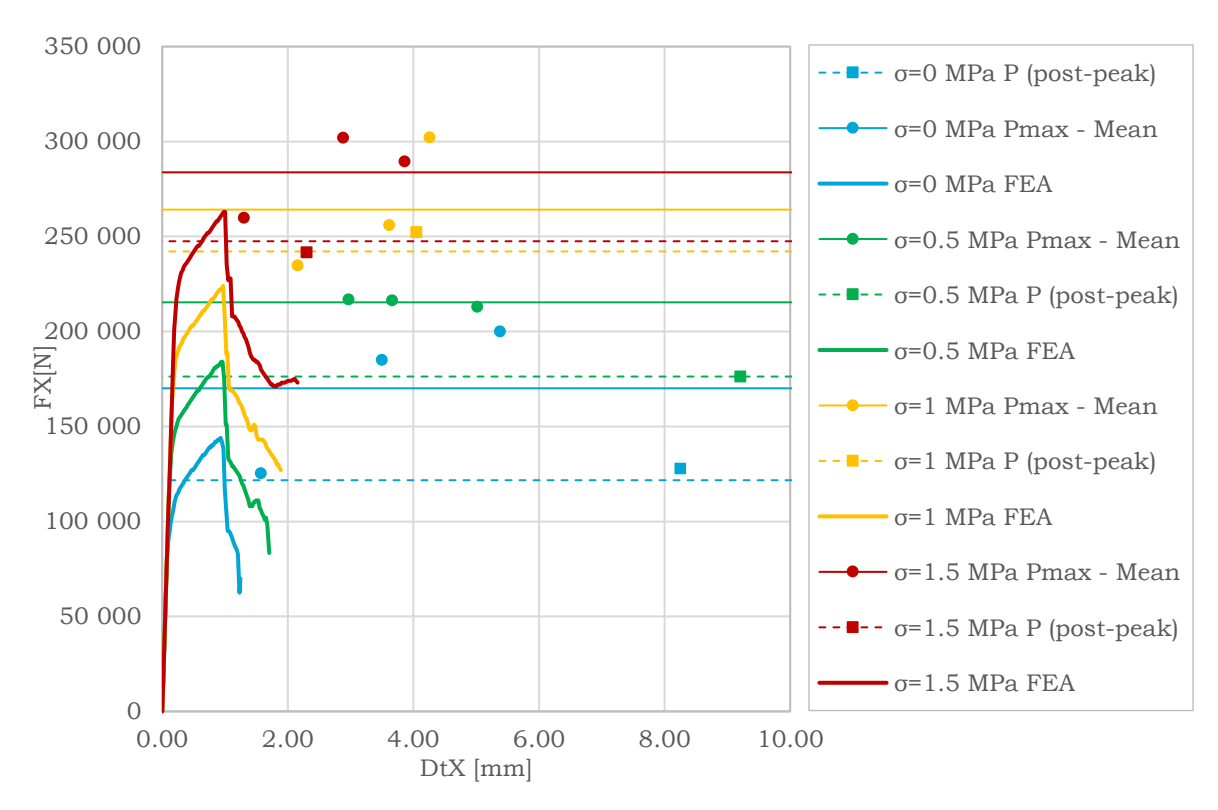


Figure 4.23 Load-slip curves for the specimens with smooth interface and reinforcing bars

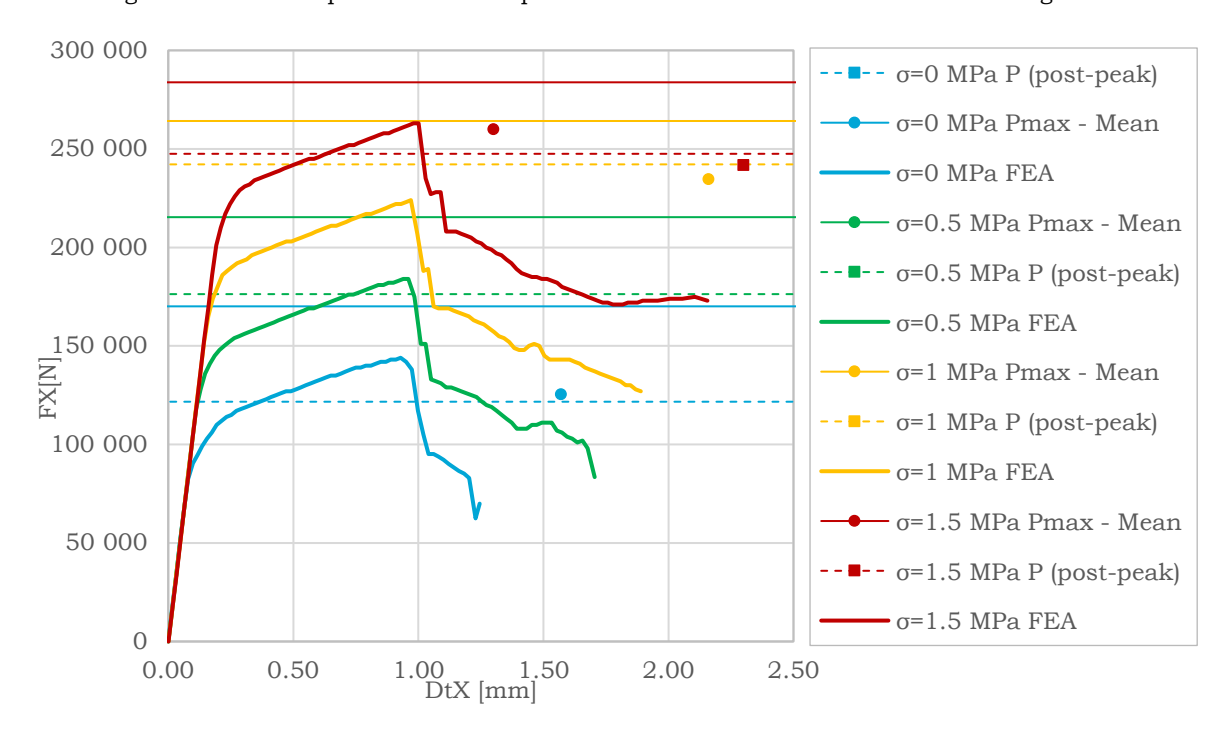


Figure 4.24 Load-slip curves for the specimens with smooth interface and reinforcing bars - zooming in

70 4.4 Discussion

4.4 Discussion

Looking at a single element tests results, the elastic stiffness study confirmed that the ultimate capacity is not highly dependent on the k_s . The slip at the peak load differs, but the peak capacity is maintained. With a very small value of k_s , however, there were some convergence issues and model R-CCSC-k1 did not yield satisfactory results.

The boundary conditions' test revealed that the most suitable top boundary for this particular case was the application of tyings, connecting vertical displacements of the nodes. The use of the supports restraining any horizontal movement, resulted in the increase of the capacity, as the compressive stresses at the interface were higher in that case. Such behaviour is undoubtedly related to the confinement of the concrete. Due to Poison's ratio the concrete expands perpendicularly to the direction of the load application, creating higher compressive stresses at the interface, which generate higher shear capacity. This tendency is well demonstrated in Figure 4.9-Figure 4.12. In the analysis of the model with supports, for the same load step, the normal tractions are more elevated, with respect to the model with tyings. The corresponding shear stresses are higher as well.

The effect would be even more pronounced if the dilatancy at the interface was accounted for. However, it was not possible to study that effect and calibrate the input parameters due to two reasons. Firstly, no experimental data concerning uplift or the crack opening was provided by the authors of reference research. Moreover, if the uplift was prevented, as was implied in the reference research, it would be difficult to maintain constant stresses at the interface. Secondly, it was also observed that the single element model with CF interface material model is very sensitive as far as the combination of dilatancy and boundary conditions is concerned. The analyses employing higher dilatancy angles generated convergence issues and unstable results, thus it was decided to simplify the input. For the angle of dilatancy equal to 0°, when no uplift is present, the models with the top nodes having equal translations in the y-direction, yielded the results which were in good accordance with experiments.

It is observed that with such an experimental setup it is difficult to maintain uniform normal and shear stresses along the interface, as there is a certain bending moment present. The use of tyings is synonymous with the assumption that the vertical displacements at the top edge are not restrained, but have to be uniform. It is also acknowledged that such an approach is also not entirely correct as the possible rotations of the top edge are restrained.

Similar observations to the study of Dias-da-Costa et al. [43] were made, that the boundary conditions are of key importance. The support and loading conditions can significantly influence the results, both experimental and numerical. It can be concluded that the component level tests for interface investigation should be thoroughly planned with close attention to boundary conditions, as well as to the measurements of the relative displacements. Furthermore, later, if calibration of material models based on performed experiments is needed, the restrains applied in the finite element model should closely resemble the boundary conditions utilised in the laboratory tests. Moreover, for the calibration of such material models as CCSC or CF more detailed data ought to be recorded, especially concerning the performance in the normal direction.

4.4 Discussion 71

Another observation is that, since there were concerns related to the load-slip curves documented in the reference research [1], the applied fracture energy for models with rough interface ($G_{f_{II}} = 20 \text{ N/mm}$) have probably been overestimated in the analysis. This value is not recommended for further use as it is substantially higher than the input for smooth interface and values used by other researchers [43] [44].

Adjusting the residual friction angle in the case of the models representing specimens with rough surfaces is considered a good choice. It can be also related to the real behaviour when shearing two surfaces with respect to each other – the irregularities and protruding aggregates crush with the increase of relative displacements, which decreases the friction between concrete elements. It should be borne in mind that the post-peak capacities were not documented in detail in the reference research, and the magnitudes are based only on the graphs presented in Figure 4.3.

Table 4.21 Comparison of the peak load magnitudes obtained from single-element models and lab tests

	$\sigma = 0 \text{ MPa}$	$\sigma = 0.5 \text{ MPa}$	$\sigma = 1 \text{ MPa}$	$\sigma = 1.5 \text{ MPa}$		
Experiment [1] [N]	60300	125100	150733	178233		
		S-CF				
FEA [N]	72800	110600	148400	186100		
Difference [N]	-12500	14500	2333	-7866		
Difference [%]	-20.73	11.59	1.55	-4.41		
Average [%]		-3	.00			
		S-CCSC				
FEA [N]	69500	105700	142000	178200		
Difference [N]	-9200	19400	8733	33		
Difference [%]	-15.26	15.51	5.79	0.02		
Average [%]		1.	52			
Experiment [1] [N]	311766	422100	536866	577400		
	•	R-CF		•		
FEA [N]	326400	416300	507200	599000		
Difference [N]	-14633	5800	29667	-21600		
Difference [%]	-4.69	1.37	5.53	-3.74		
Average [%]		-0.	.38			
R-CCSC						
FEA [N]	291300	366800	444200	523000		
Difference [N]	20467	55300	92667	54400		
Difference [%]	6.56	13.10	17.26	9.42		
Average [%]	11.59					

Despite some abovementioned concerns, the results of single element study presented in Figure 4.15 to Figure 4.18 show rather good correspondence with the experimental data. The peak capacity is quite well predicted for models with both CF and CCSC interface material models, what is portrayed in Table 4.21. The CCSC model which accounts for the softening, also proved to be suitable for predicting the post-peak capacity. For the smooth interfaces, the post-peak capacity obtained from FEA is slightly lower than the experimental one. Since the specified input of CF material model did not allow for any type of softening, it was decided that for the

72 4.4 Discussion

assembly of elements the CCSC model will be used. Otherwise the capacity could be overestimated as after the stresses at the interface would reach the capacity generated by the bond between concretes, they would continue to rise with the opening of the interface, thus clamping generated by the rebars.

Looking at the results of the elements assembly, with bond-slip reinforcements, presented in Figure 4.23, there are certain differences as far as the experimental and finite element responses are concerned. The biggest disagreement is related to the relative displacements. It should also be mentioned that there is quite big scatter between the experimentally observed slips at the peak load and, as already debated, there is uncertainty concerning the documented slip values. Nonetheless, for 0 MPa and 1.5 MPa the FEA results predict one of the experimentally obtained peak loads and corresponding displacements quite well. Looking at the graph given by Randl [16] included in Figure 2.12 in this research, for the reinforced, very rough joints the peak load is reached at slips of around 0.5 - 1.5 mm, whereas for smooth joints there is no pronounced peak but the capacity continues to grow but with less steep slope also after reaching around 2 to 5 mm relative displacement. Therefore, the value of 1 mm obtained from the S-CCSC-RC model can be claimed to be within certain expected range. In this case, the capacity was reached at around 1 mm displacement for all of the applied perpendicular pressures. To verify which input parameters are the most relevant and how they change the outcome if it comes to, not only the peak capacity, but also corresponding slip, an extensive sensitivity analysis would have to be performed.

Figure 4.24 shows the same results, however with magnified FEA results. It shall be observed that the peak magnitudes of the horizontal load correspond with the experimental data to an acceptable degree. Nevertheless, in all of the cases the results are underestimated by 7-15% with respect to the mean, experimentally obtained capacities. The post-peak capacities are significantly underestimated.

Table 4.22 Comparison of the peak load magnitudes obtained from the S-CCSC-RC model and lab tests

	$\sigma = 0 \text{ MPa}$	$\sigma = 0.5 \text{ MPa}$	$\sigma = 1 \text{ MPa}$	$\sigma = 1.5 \text{ MPa}$
Experiment [1] [N]	170100	215366	264166	283800
FEA [N]	144139	184333	223872	263433
Difference [N]	25961	31033	40294	20367
Difference [%]	15.26%	14.41%	15.25%	7.18%

Two sources that cause the differences are identified. Firstly, the model is highly complex and each input parameter can influence the results. It was observed that the first drop in the load-slip curves was obtained at the moment of a major crack appearing in the vicinity of the reinforcement crossing the interface. Therefore, potentially the material model for concrete should be adjusted. At the same time, either the bond-slip relation for reinforcement, or the interface constitutive law may require adjustments. Secondly, especially the post-peak capacity obtained from the experiments is based on the results obtained from one specimen only.

Analysing the results included in Annex E, the behaviour of the specimen matches the expectations quite well. The normal tractions increase in the regions where reinforcement crosses the interface and correspondingly there is a rise in shear stresses at the interface. It was also observed that the bars are not only under tension but also bent and subjected to shear. It is noted that yielding occurs in the

4.5 Conclusions 73

rebars, in the close vicinity of the interface. The slip along the rebars was analysed as well. It was observed that the anchoring of the bars at the top, to simulate the U-shaped hairpins behave as expected. Only the bottom parts of the rebars are slipping, thus being pulled out of the concrete while the interface is opening. Nevertheless, as stated above, the performance can be analysed only based on expectations and no quantitative consideration is possible. More data is required to judge with more confidence whether the behaviour of the sample obtained from a model corresponds with experiments.

It is undoubtedly a drawback of such a modelling strategy that a comprehensive data set is needed to assemble and further calibrate the model. The complexity increases when the surface is crossed by reinforcements as the behaviour is not exactly the same as in the case of the externally applied pressure – for the clamping generated by the reinforcements the interface has to dilate [16] [18]. Moreover, from the computational point of view, the node connectivity of the beam elements (as that's what DIANA converts the circular beam bond-slip elements to [58]) connected to surrounding concrete through bond-slip interface elements, and on top of that, crossing the interface between two concretes, is very complex. Additionally, the analyses diverged before all the assumed load steps were applied, however, a peak and certain post-peak capacity were captured for all the analyses. A simplification could be made by introducing truss elements instead of beam elements or even resigning from modelling the bond-slip relation. Nevertheless, the simplifications have to be borne in mind when analysing the results.

In conclusion, it was proven that the complex models can provide reasonable results. First and foremost the coupling was well preserved by both, CF and CCSC material models, as with the same input parameters the numerically obtained capacities for all applied pressure levels were in good agreement with experiments. It was also demonstrated that when applying lateral pressure in a form of clamping stress generated by reinforcement modelled as beam elements with bond-slip steel-to-concrete relation, the capacity was to some extent correctly predicted, with underestimation of 7-15%. It can be concluded that the models used are a powerful tool to perform detailed analysis of interfaces. It is expected that when having comprehensive data concerning the experimental setup and results, the models could be calibrated to give results which are in very close correspondence with the lab tests. Nevertheless, it is also observed that the amount of input parameters, as well as the sensitivity of component-level test to the applied boundary conditions make the assembly, calibration, and later upscaling to macro-scale modelling, of the considered material models challenging.

4.5 Conclusions

• Inadequate choice of boundary conditions in the numerical model can significantly alter the results of the analysis. In the presented case, the model with supports restraining vertical movements generated 1.62 times higher interfacial strength for the analysis of a rough surface, with no additional pressure, using Coulomb Friction material model. The increases for the analyses with 1 MPa of added pressure and analyses with the other interfacial material model were of a similar order of magnitude.

74 4.5 Conclusions

• It was proven by single element tests that both, Coulomb Friction and Combined Cracking-Shearing-Crushing models are well suited for capturing the coupling between shear and normal stresses. With the same set of input parameters, but added external normal pressure at the interface, the shear capacity increased, representing well the reference, experimental data.

- The specified input of the Coulomb Friction material model is not suitable for modelling interfaces with clamping provided by reinforcing bars. Unless the cohesion and friction softening is captured, the results might be overestimated.
- The model with beam bond-slip reinforcements and Combined Cracking-Shearing-Crushing interface material model to certain degree corresponds to experimental results. It is promising, since the peak loads were underestimated by 7-15% with respect to the mean, experimentally obtained values. The drawback is that all the analyses diverged at approximately 2 mm of prescribed displacement.
- The Combined Cracking-Shearing-Crushing material model, if properly calibrated, can undoubtedly be used in the analysis of the unreinforced interfaces.

Composite beam structural behaviour – Nonlinear Analysis

The analysis of the composite girders, with an emphasis on the behaviour of the interface, was already performed in Chapter 3 with linear material properties. In this part of the research, the nonlinear analysis of the experiment introduced in Chapter 3 is presented. Based on the findings of the component-level verification study of chosen interface material models, it was decided to use the Combined Cracking-Shearing-Crushing (CCSC) model for the beam-to-top layer interface. However, due to the material model's complexity, the Nonlinear Elasticity (NE) constitutive law, with corresponding input, introduced through diagrams, is also tested and compared with the models utilising CCSC. In total, four models are analysed. For both CCSC and NE two sets of input parameters were introduced, one is based on Eurocode 2 [2] recommendations and the other one on assumptions stemming from the literature study.

5.1 Test specimen

In this part of the research, the nonlinear analysis was performed. More detailed information concerning the reference sample, such as the alignment of reinforcement, was necessary. The specimen examined is the S10H1A sample, with low interfacial reinforcement ratio, in the section between intermediate support and loading point.

The general information concerning the specimen in question, was already introduced in Chapter 3. The basic geometric properties, the position and cross-section dimensions of concrete elements, as well as alignment of prestressing strands are the same and were presented in Figure 3.1 and Figure 3.2. To be consistent, the positions of loading points are kept the same as in Chapter 3, however, they are slightly different than the locations given in the latest drawings of the experimental setup. Material properties of concrete and prestressing strands are assumed the same as included in Table 3.1.

The only difference is the alignment and properties of reinforcing bars which in the linear-elastic analysis were assumed, but in this case, more comprehensive data was employed. Detailed drawing can be found in Annex F [59]. As the focus of the analysis is the interface, the table summarising the hairpin layout is presented below.

76 5.2 Numerical model

Distance from the left edge of the beam [mm]	0- 3000	3000- 3500	3750- 4250	4250- 10170	10170- 14500	14500- 15000
Hairpin diameter and spacing [mm]	Ø16-100	5 × Ø16	5 × Ø6	Ø6-200	Ø16-100	5 × Ø16
Reinforcement ratio [%]	1.	61	0.	11	1.	61
ρf_{ν} [MPa]	8.	69	0.	61	8.	69

Table 5.1 Hairpin layout

5.2 Numerical model

5.2.1 Numerical setup

The models analysed in this part of the research were built based on the S10H1A experimental sample. The dimensions of the elements and positions of the supporting and loading points were chosen in accordance with Figure 3.1. The differences with respect to the numerical setup presented in Chapter 3 are the presence of reinforcing bars, the beam introducing loads to the loading plates as well as the utilised material models.

Four models were analysed, which overview is shown in Table 5.2. The variation between the models lies in the modelling of the interface. In two of the models the Nonlinear Elasticity (NE) material model for the interface was introduced, utilising diagrams to prescribe behaviour in tangential and normal directions. In the other two, the Combined Cracking-Shearing-Crushing (CCSC) material model with bond-slip reinforcements crossing the interface was applied. In models designated with -EC2 the input was based on Eurocode 2 [2], whereas the name -Lbg is related to best guess stemming from the literature. All stages of the construction and loading were accounted for through phased analysis.

Table 5.2 Model's overview

Model	odel Concrete-to-concrete interface Concre		Prestressing Steel	Reinforcing
	Interface	iteriace		Steel
M-CCSC-EC2	Combined Cracking-			Nonlinear and
M-CCSC-Lbg	Shearing-Crushing	Nonlinear	Linear	bond-slip
M-NE-EC2	Nonlinear Elasticity	Nommean	Elastic	Nonlinear
M-NE-Lbg	Norminear Elasticity			Inominear

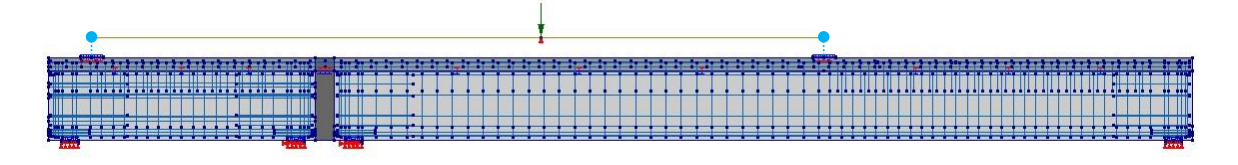


Figure 5.1 Model based on S10H1A sample

5.2.2 Geometry and structural element types

The models' geometry is presented in Figure 5.1. The geometry of the model was already introduced in subchapter 3.4.2. The only variations are the presence of reinforcing bars and the beam element for the introduction of the load, along with

tyings. The tyings connect vertical (and horizontal in the case of the main span) translations of the nodes of the loading beam with the nodes at the centres of loading plates located at the girders' flange. Table 5.3 displays the updated cross-section properties of the structural elements. It is emphasised again that the cross-beam parts that overlap with the precast elements were disregarded in the FE model.

Hairpins in models with the NE material model for the interface were modelled as embedded reinforcement. In the case of the M-CCSC-EC2 and M-CCSC-Lbg, the circular beam bond slip bar was chosen as the element class of the hairpins. Other reinforcing bars were modelled as embedded reinforcement. The diameters follow the drawing included in Annex F [59].

Table 5.3 Cross-section properties

Element	Element Class	Material	Geometry
Precast beams	Regular plane stress	Concrete C55/67 NL	acc. to Figure 3.8
Top layer	Regular plane stress	Concrete C30/37 NL	t = 1200 mm
Cross beam	Regular plane stress	Concrete C30/37 NL	t = 1200 mm
Bearings	Regular plane stress	Bearings - steel	t = 455 mm
Loading plates	Regular plane stress	Loading plates - steel	t = 300 mm
Prestressing reinforcement	Embedded bar	Prestressing steel	acc. to Table 3.9
Haimina	Embedded bar	Embedded reinforcement NL	acc. to Annex F
Hairpins	Circular beam bond slip bar	Bond-slip reinforcement	acc. to Annex F
Other reinforcing bars	Embedded bar	Embedded reinforcement NL	acc. to Annex F
Bearing - beam interface	Structural line interfaces	Interface - bearings	t = 455 mm
Loading plate - beam interface	Structural line interfaces	Interface - loading plate	t = 300 mm
Top layer – cross beam interface	Structural line interfaces	Interface – high stiffness	t = 1200 mm
Top layer - beam interface	Structural line interfaces	Acc. to Table 5.7	t = 250 mm
Loading bar	Class-III Beams 2D	Loading bar	A = 500×500 mm ²

5.2.3 Material models

In this part of the research, nonlinearity was introduced in the constitutive relations of the materials used.

5.2.3.1 Concrete

Concrete properties were chosen based on the concrete classes C30/37 for the top layer and cross beam, and C50/57 for precast girders. The input was selected in accordance with Eurocode 2 [2] and Guidelines for NLFEA of Concrete Structures [6].

78 5.2 Numerical model

773 1 1 F		3.5 1	. •	c	
Table :	5.4	Material	properties	ot	concrete

Innut noromator	Symbol	Inj	Unit	
Input parameter		C30/37 NL	C55/67 NL	Ollit
Young's Modulus	Е	33000	38000	N/mm ²
Poisson's ratio	v	0.2		-
Mass density	ρ	2.5E-9		T/mm ³
Crack orientation		Rotating		
Tensile curve		Hordijk		
Tensile strength	f_{ct}	2.9	4.2	N/mm ²
Mode-I tensile fracture energy	G_F	0.0984	0.1077	N/mm
Crack bandwidth specification		Rots		
Poisson's ratio reduction		Damage based		
Compression curve		Parabolic		
Compressive strength	f_c	38	63	N/mm ²
Compressive fracture energy	G_C	27.73	33.58	N/mm
Reduction model due to lateral		Vecchio and Collins 1993		
cracking				
Lower bound reduction curve	eta_{σ}^{min}	0.4		-

5.2.3.2 Steel

The properties of loading and bearing plates, as well as of prestressing strands were applied as presented in Table 3.10.

For nonlinear analysis more comprehensive data concerning reinforcing bars was available. Tested yield strengths varied between 524 and 593 MPa, the ultimate ones between 603 and 702 MPa. The ultimate strain values ranged between 5.32 and 10.65 %. To simplify the input, one set of values was used for all rebars. The constitutive law for the embedded bars is outlined in Table 5.5.

Linear elastic and Von Mises parameters for hairpins are the same as for other rebars, however, the bond-slip relation had to be additionally specified for M-CCSC-EC2 and M-CCSC-Lbg. Material properties are provided in Table 5.6. Fib Model Code 2010 [27] failure model was employed. All properties were selected based on code instructions [27] for ribbed bars in good bond conditions. For the calculation of τ_{bmax} the lower concrete strength was used. The clear distance between ribs was assumed as 0.8Ø and 0.6Ø for the 6 and 16 mm diameter bars respectively [60]. Normal stiffness was calculated based on equation (4.1). As explained in section 4.3.3.2, the k_s was taken as the secant modulus at 0.01 mm slip.

The beam for displacement application was assumed to be a steel beam, however, in order to maintain the high stiffness of this element, Young's modulus was increased, as in the case of loading plates. The constitutive law was linear elastic.

Table 5.5 Properties of the Embedded reinforcement NL material model

Input parameter	Symbol	Input	Unit		
Young's Modulus	E	200 000	N/mm ²		
Nonlinear Model		Von Mises plasticity			
Von Mises parameters					
Plastic hardening		Total strain-yield stress			
Total strain-yield stress		Acc. to Figure 5.2			
Hardening hypothesis		Strain hardening			
Hardening type		Isotropic hardening			

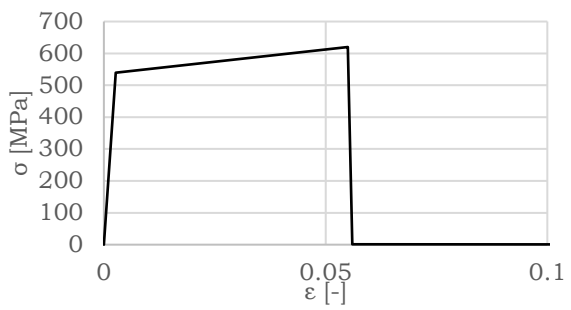
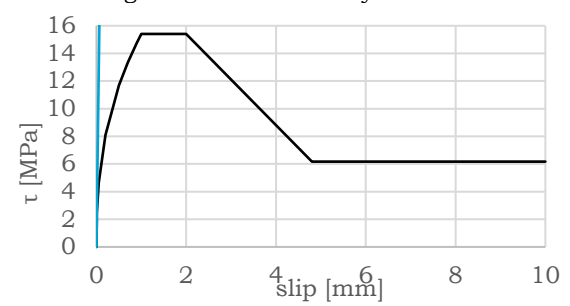


Figure 5.2 Total strain-yield stress relation for embedded and bond-slip reinforcements



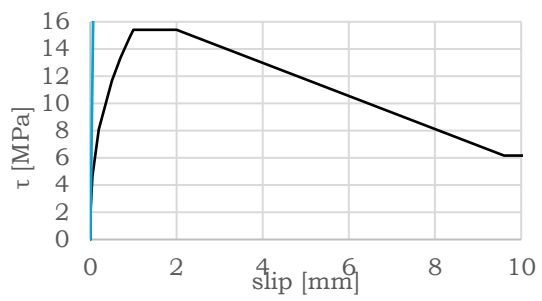


Figure 5.3 Applied $\tau - s$ relationship for steel Ø6 rebars

Figure 5.4 Applied $\tau - s$ relationship for steel Ø16 rebars

Table 5.6 Properties of the Bond-slip reinforcement material model

Toward managed an	01	Input		TT :
Input parameter	Symbol	Ø6	Ø16	Unit
Young's Modulus	Е	200 000		N/mm ²
Poisson's ratio	v	0.3		-
Mass density	ρ	7.9E-9		T/mm ³
Nonlinear Model		Von Mises pla	asticity	
Von	Mises par	rameters		
Hardening function		Total strain-y	ield stress	
Hardening hypothesis		Strain harder	ning	
Total strain-yield stress		Acc. to Figure	5.2	
Hardening type		Isotropic hard	lening	
Bo	nd-slip in	terface		
Normal stiffness modulus	k_n	240	125	N/mm ³
Shear stiffness modulus	k_s	240	240	N/mm ³
Bond-slip interface failure model		CEB-FIB 20	10 bond-slip	
		function		
Maximum shear stress	$ au_{max}$	15.4110		N/mm ²
Ultimate shear stress	$ au_f$	6.1644		N/mm ²
Linearized initial slip section	s_0	0.01		mm
Relative slip section s1	s_1	1		mm
Relative slip section s2	s_2	2		mm
Relative slip section s3	s_3	4.8	9.6	mm
Exponent alpha	α	0.4		-
Reinforcement anchor				
Normal stiffness in anchor	K_n	1E+9		N/mm
direction	11n	112.5		11/11111
Shear stiffness normal to anchor direction	K_{s}	1E+9		N/mm

80 5.2 Numerical model

5.2.3.3 Concrete-to-concrete interface

Beam-to-bearings and beam-to-loading plates interface properties were set in accordance with subchapters 3.4.3.3 and 3.4.3.4, hence they follow Table 3.11.

For the beam-to-top layer interface two main types of interface material models were applied – Nonlinear Elasticity and Combined Cracking-Shearing-Crushing. The models were built based on similar assumptions, so that the composite beam behaviour using different material models built in an analogous way, could be compared. At the connection between the cross-beam and top layer elements, the structural line interface elements, with high stiffness were applied to maintain the continuity of the interface. The scheme of applied material models for the interface elements is included in Table 5.7.

Table 5.7 Interface material models' location

	Distance from the left edge of the beam [mm]				
Model	0-	3500-	3750-	10170-	
	3500	3750	10170	15000	
M-CCSC-EC2	CCSC-EC2		CCSC-EC2		
M-CCSC-Lbg	CCSC-Lbg	Interface –	CCSC	C-Lbg	
M-NE-EC2	NE-EC2-Ø16	high stiffness	NE-EC2-Ø6	NE-EC2-Ø16	
M-NE-Lbg	NE-Lbg-Ø16		NE-Lbg-Ø6	NE-Lbg-Ø16	

High stiffness, cross-beam connection

The stiffness in the normal direction was chosen to have a relatively high value. The 710000 N/mm³ assumed in section 3.4.3.5 was suspected to generate some convergence difficulties. Therefore, slightly lower, yet still fairly high magnitude, was utilised. The shear stiffness was assumed to be the same.

$$k_n = 10000 \left[\frac{N}{\text{mm}^3} \right]$$
$$k_s = 10000 \left[\frac{N}{\text{mm}^3} \right]$$

Combined Cracking-Shearing-Crushing Models

The input for stiffnesses in normal directions was uniform in all of the models. The shear stiffnesses were assumed in a way that the capacity generated by cohesion is reached at 0.05 mm. Such slip values is in line with the figure provided by [16] for slightly roughened non-reinforced interfaces. As also already mentioned in section 3.4.3.5, in the experiments carried out on beams by Loov and Patnaik [15] the relative displacement was not noticeable below the value of 1.5-2 MPa of the interface traction. The inputs of 30 and 70 N/mm³ are also in the similar range as the 18 N/mm³ calibrated by [43] based on a push-off test, hence it seems like a reasonable approach.

The tensile cut-off was also applied in this case. Looking at Figure VI.11 and VI.12 provided by Santos in [48], the bond strength in tension for both, sand-blasted and shot-blasted surfaces, cured in the lab and external conditions was slightly higher than 2MPa after 56 days. As the composite beams were tested at approximately 65 days after connection, this assumption can be considered sensible. For that value of

5.2 Numerical model 81

mean tensile strength, the mean compressive strength was determined using relations included in Table 3.1 of Eurocode 2 [2] to further calculate the fracture energy, using the formula included in RTD guidelines [6].

For the cohesion, two sets of values were used, based on the Eurocode 2 [2] and the literature review findings. The Eurocode value was based on the coefficient given in the code [2] for the rough interfaces. The cohesion value used in the performed verification study on the component-level, was considered too high, due to uncertainties regarding boundary conditions applied in the reference test. The coefficient equal to 1 was chosen according to Table 2.6. Both coefficients were multiplied with the mean tensile strength taken as an average of the C30/37 and C55/67 concretes.

Similarly, the value of friction angle varied between the models. One value is based on the Eurocode 2 [2] recommendations and the other one on the best guess made on the basis of literature review. As far as residual friction angle is concerned the magnitude indicated by Eurocode 2 [2] was considered safe and was applied as equal to the initial one, whereas for the other model, the value was adjusted. It was observed that the capacity generated by such input could be too high, as for the clamping stresses equal to 8.69 MPa (Table 5.1) the capacity provided by the friction only, would be equal to 11.30 MPa. Considering Figure 11 given by Loov and Patnaik [15] the capacities obtained were not that high. The $\mu = 1$ was assumed, being in line with some of the values included in Table 2.6.

The input parameters concerning dilatancy were presumed equal to the values applied in the component-level study, already included in Table 4.18. It ought to be highlighted that it is an assumption and a detailed study on those parameters was not performed.

The fracture energy input parameter used for modelling the specimens with a rough surface in Chapter 4 was considered too high. The formula found in the literature [61] yielded a value of 2.3 N/mm, which seemed more reasonable.

$$G_{IIf} = 0.429 d_a^{0.1461} f_{ck}^{0.3042} (5.1)$$

Where:

 d_a maximum size of aggregate; taken as 16 mm

 f_{ck} is the concrete cube compressive strength in MPa; the average value of f_{cm} was applied to remain consistent.

As already discussed while performing the component-level study, the Crushing part of the CCSC model is not relevant, hence the input was again adjusted to move the compression cap away.

Nonlinear Elasticity Models

The constitutive relation was prescribed by the use of diagrams. In the normal direction, the stiffness was assumed the same as in the CCSC model. For 2 MPa of tensile stresses, the yielding was applied through bi-linear curve, to correspond with the case of CCSC.

The behaviour in the shear direction was prescribed based on the cohesion and friction coefficients as well as Mode-II fracture energy included in Table 5.8. In total

82 5.2 Numerical model

four material models had to be constructed because the clamping stresses were higher in the sections where the higher reinforcement ratio was used. The graphs presenting the construction of the shear traction-slip diagrams are presented in Figure 5.5.

It should be noted that it was assumed that after reaching the shear traction equal to cohesion, the interface will have a certain capacity generated by the aggregates interlocking. That magnitude of stresses could be considered constant up until slip reaches the 0.5 mm. Such value is expected based on Figure 2.12, or the experimental results analysed in [43]. An assumption was made that after the loss of cohesion, the ultimate capacity is related only to friction generated by clamping, not the sum of those two contributions. Such an approach can be considered too conservative, as according to Eurocode 2 [2] the capacity provided by both mechanisms can be summed up. However, for the coefficients based on the literature such methodology can be regarded as sensible. The descending branch was built assuming there is no compressive stresses and the area under the graph has to be equal to fracture energy.

Table 5.8 Input parameters for Combined Cracking-Shearing-Crushing interface material model

	Crembol	V	Unit		
	Symbol	EC2	Lbg	Unit	
	Linear M	aterial Properties		<u> </u>	
Normal stiffness modulus-y	k_n	10000	10000	$\frac{N}{mm^3}$	
Shear stiffness modulus-x	k_s	30	70	$\frac{N}{mm^3}$	
	Coul	omb Friction	·		
Cracking					
Tensile strength	f_t	2	2	$\frac{N}{mm^2}$	
Fracture energy	G_{f_I}	0.0914	0.0914	$\frac{N}{mm}$	
Shearing				·	
Cohesion	С	0.45×3.55 =	1×3.55 =	N	
Collesion	C	1.5975	3.55	mm ²	
Friction angle	ϕ	35	52.43	0	
Dilatancy angle	ψ	15	15	0	
Residual friction angle	$\phi_{residual}$	35	45	0	
Confining normal stress	σ_c	-10	-10	$\frac{N}{mm^2}$	
Exponential degradation coefficient	δ	1	1	-	
Mode-II fracture energy					
Parameter a	а	0	0	mm	
Fracture energy	$G_{f_{II}}$	2.3	2.3	$\frac{N}{mm}$	

5.2 Numerical model 83

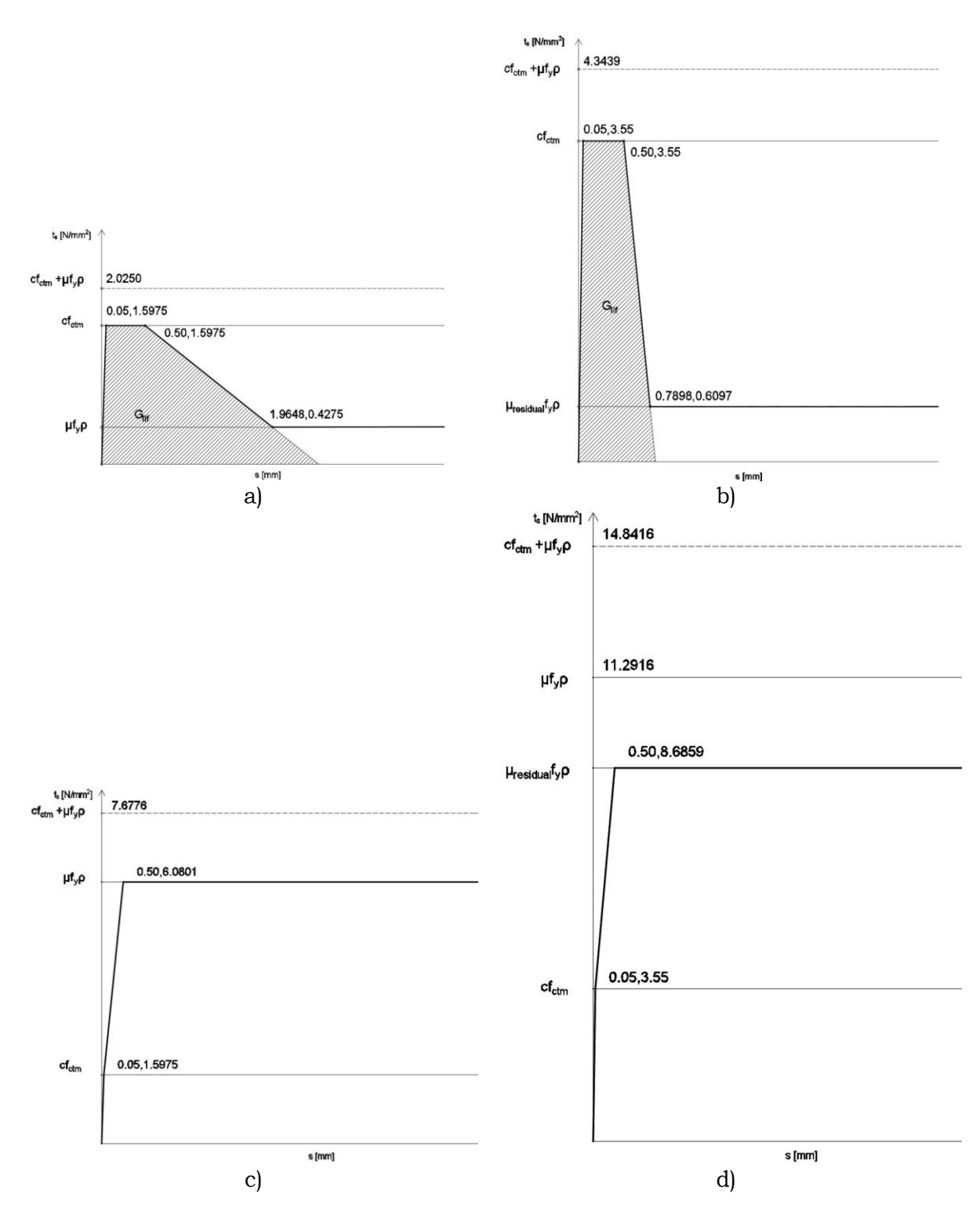


Figure 5.5 Prescribed t_s-s relation for a) NE-EC2-Ø6 material model b) NE-Lbg-Ø6 material model c) NE-EC2-Ø16 material model d) NE-Lbg-Ø16 material model

84 5.2 Numerical model

5.2.4 Boundary and loading conditions

The boundary conditions applied are in line with subchapter 3.4.4. However, the live load was applied differently. The restrains utilized are presented in Figure 5.1. It is highlighted that the blue connections which represent tyings were added to the figure.

To be able to observe possible post-peak behaviour of the sample it was intended to have the displacement-controlled analysis. Nevertheless, the experiments were performed in a way that the ratio of forces applied in the cantilever and main span was 0.63:1. Therefore, a stiff beam, attached by tyings to the loading plates was introduced. The tyings related the vertical (and horizontal in case of main span) displacements of the beam ends with displacements of the nodes at the centres of the loading plates. The point at which the displacement was applied to the beam, was chosen in a way that the ratio of reaction forces at the beam ends was as in the experiments.

Other applied loads are the same as in linear analysis, thus they follow Table 3.12.

5.2.5 Mesh

The mesh size was applied in accordance with assumptions made in Chapter 3. The average mesh dimension is 50 mm. The total number of nodes for models with bond-slip reinforcements is higher, since DIANA generates additional nodes for those elements.



Figure 5.6 Meshed model at Phase 2b

Table 5.9 Finite elements used - specifications

Finite element type	CQ16M	CT12M	CL12I	CL9BE	
Degrees of freedom	$u_x, u_y \\ 8 \times 2 = 16$	$u_x, u_y $ $6 \times 2 = 12$	u_x, u_y $6 \times 2 = 12$	$u_x, u_{y,} \phi_z$ $3 \times 3 = 9$	
Interpolation scheme	Quadratic	Quadratic	Quadratic	Quadratic	
Integration scheme	2×2 Gauss	3-point	3-point Newton-Cotes	2-point Gauss	
Stress components	$\sigma_{xx}, \sigma_{yy}, \sigma_{xy}$	$\sigma_{xx}, \sigma_{yy}, \sigma_{xy}$	t_n, t_t	σ_{xx}, σ_{xy}	
Average element size [mm]	50×50	50	50	50	
Total number of elements	6324	1	328	192	
Total number of	32662				
nodes	30810				

5.2.6 Analysis characteristics

The Phased analysis was adopted. All the chosen analyses within the phases were Structural Nonlinear with physical nonlinear effects. Distinguished phases along with applied loads are the same as in the linear analysis described in Chapter 3. The

5.2 Numerical model 85

difference lies in the additional activation of the loading bar, the tyings and the support for displacement application in Phase 2b.

Energy and force norms were selected, with the convergence tolerances according to Table 5.10. It was decided that the step is considered converged when either one of the norms is satisfied. The line search algorithm was applied to potentially improve convergence.

The rate of applied displacement was 0.1 mm per step. For models with the Eurocode 2 input parameters, the analyses continued up until the model diverged, as in the case of M-CCSC-EC2, or until a considerable drop was reached, as for M-NE-EC2. For the models based on the literature-related best guess, the analyses were running until 30 mm of applied displacement was reached or until models' divergence.

Table 5.10 Analysis specifications

Iterative method	Regular Newton-Raphson		
Maximum number of iterations	50		
Convergence norms	Energy, Force		
Energy – convergence tolerance	0.001		
Displacement – convergence tolerance	0.01		
Load steps	0.1 (100) 0.	1 (300)	

5.3 Results

In the following sections, the results of the analyses are compared. Based on the obtained load-displacement graph, specific points along the curves were chosen and further investigated.

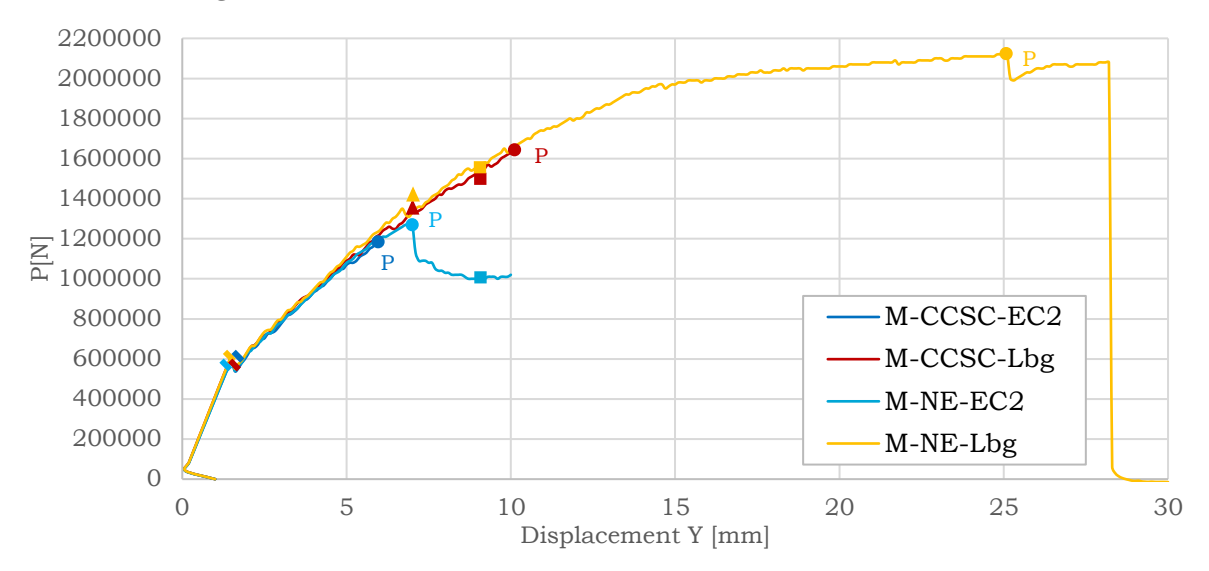


Figure 5.7 Load-displacement graphs for analysed models

The dashes signify the end of the elastic regime of the girder's behaviour, which occurred at 1.5 mm applied displacement. A further significant point was recognised at 7 mm of applied displacement, as it is a peak capacity of the M-NE-EC2 model. The next point worth investigating is the post-peak drop at 9 mm displacement. Since the other models do not have such pronounced peaks and drops, the results at 7 and 9 mm of applied displacement are compared for other models as well. The results at peak (or ultimate in the case of the M-CCSC-EC2/-Lbg) capacities are also analysed. The M-CCSC-EC2 model has only reached 5.9 mm and diverged, hence the results, at only two load levels, could be compared.

The results presented below display certain outputs for the part of the beam between the intermediate support and the main span loading point.

5.3.1 Crack pattern

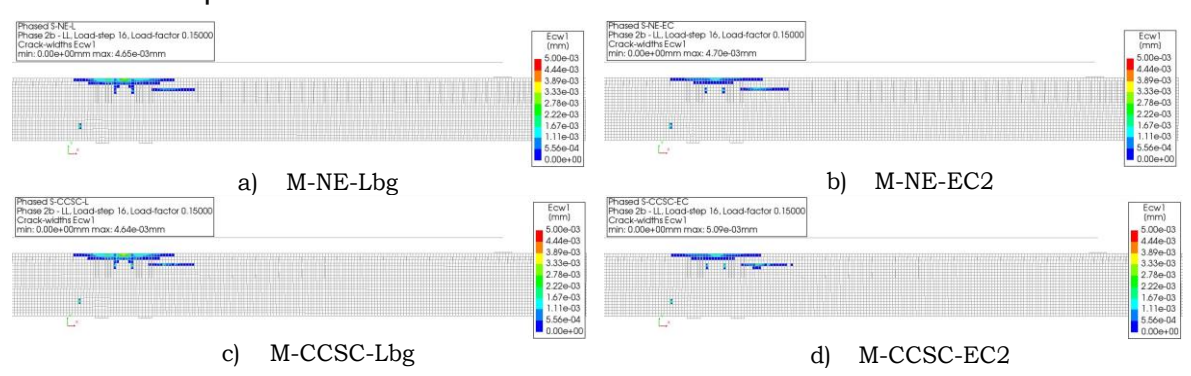


Figure 5.8 Crack pattern at applied 1.5 mm displacement (end of global elastic regime)

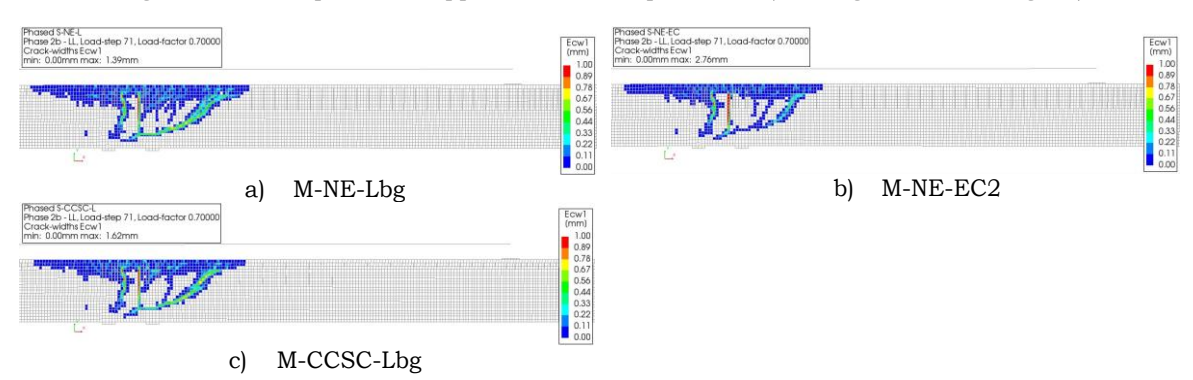


Figure 5.9 Crack pattern at applied 7 mm displacement

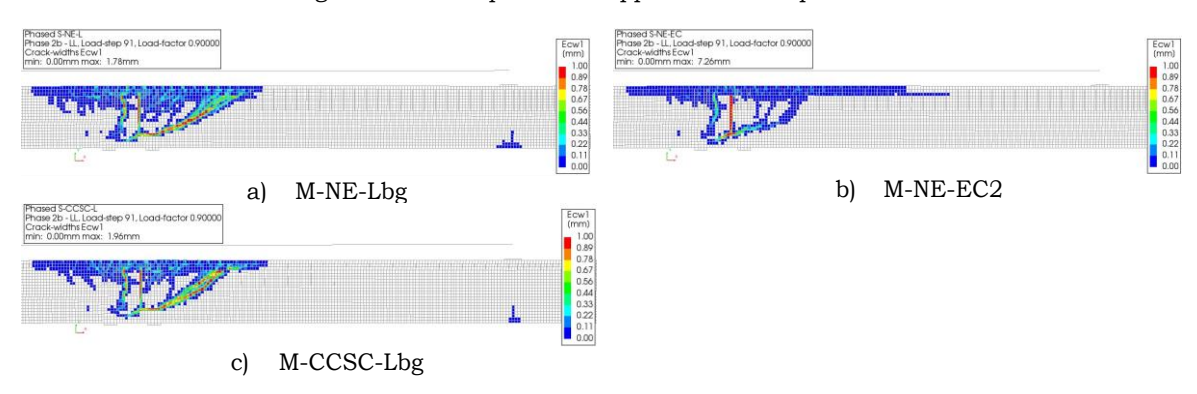


Figure 5.10 Crack pattern at applied 9 mm displacement

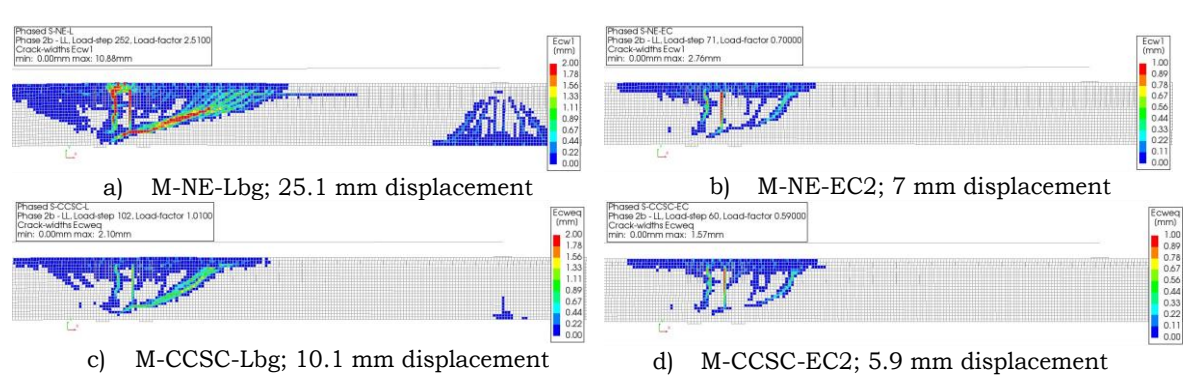


Figure 5.11 Crack pattern at peak capacity

5.3.2 Shear tractions at the interface

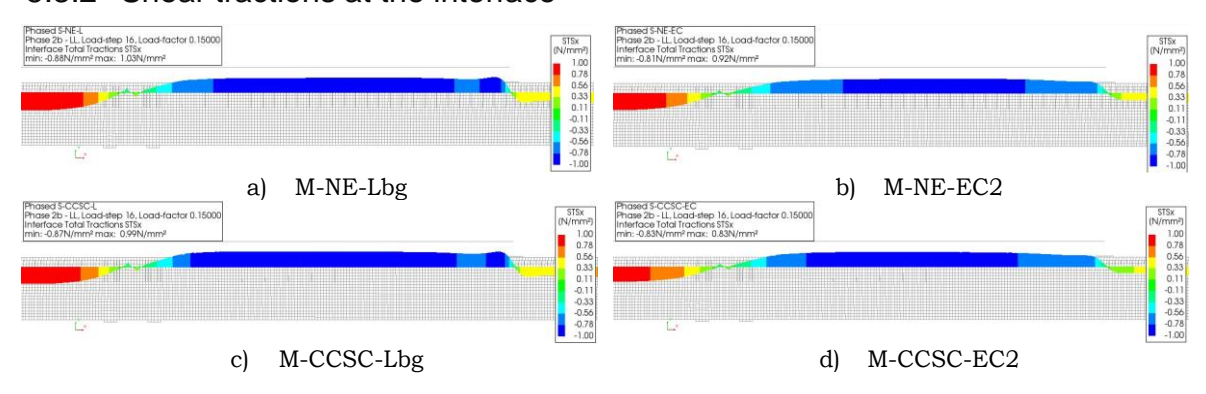


Figure 5.12 Interface shear tractions at applied 1.5 mm displacement (end of global elastic regime)

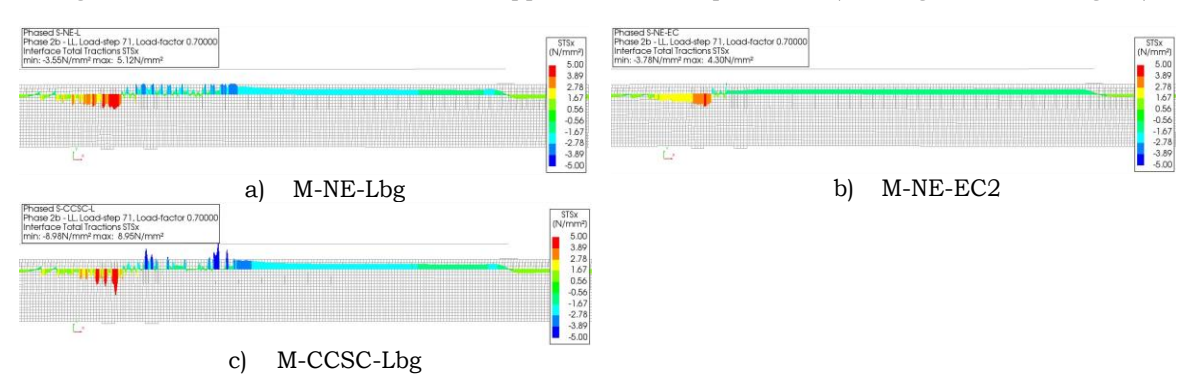


Figure 5.13 Interface shear tractions at applied 7 mm displacement

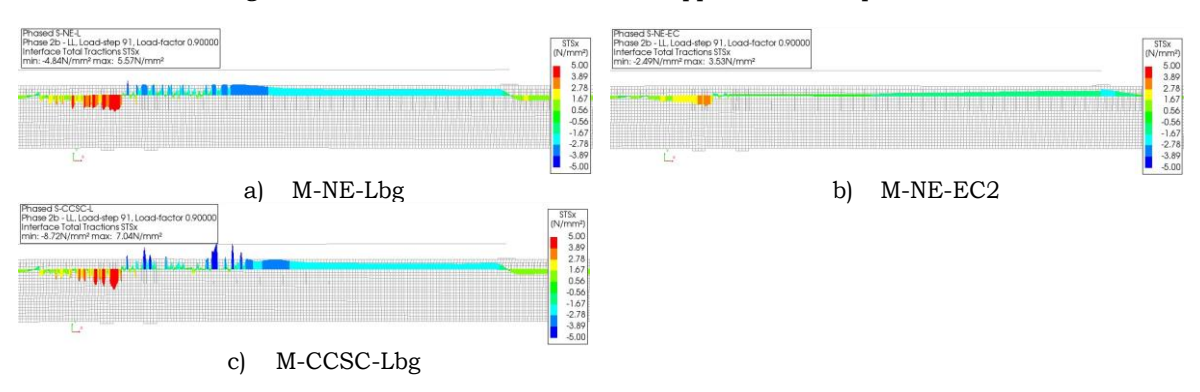


Figure 5.14 Interface shear tractions at applied 9 mm displacement

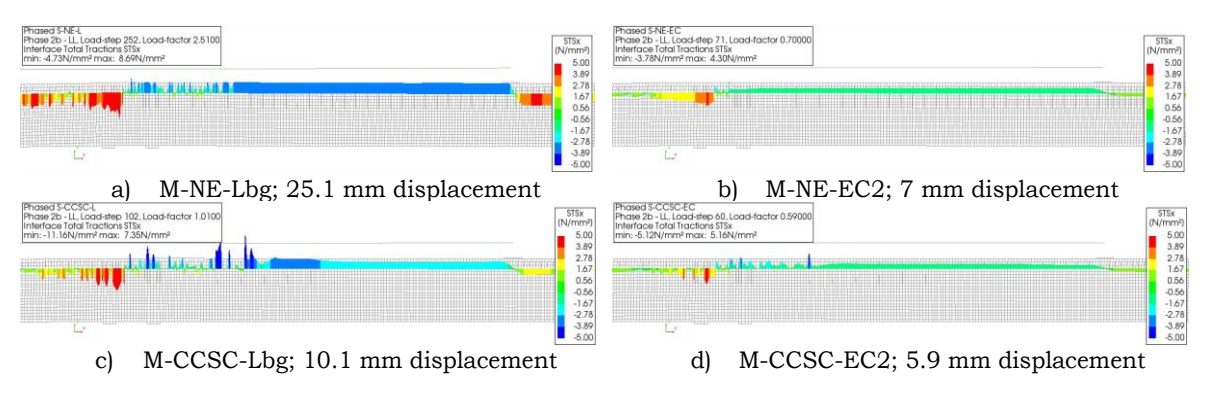


Figure 5.15 Interface shear tractions at peak capacity

5.3.3 Normal tractions at the interface

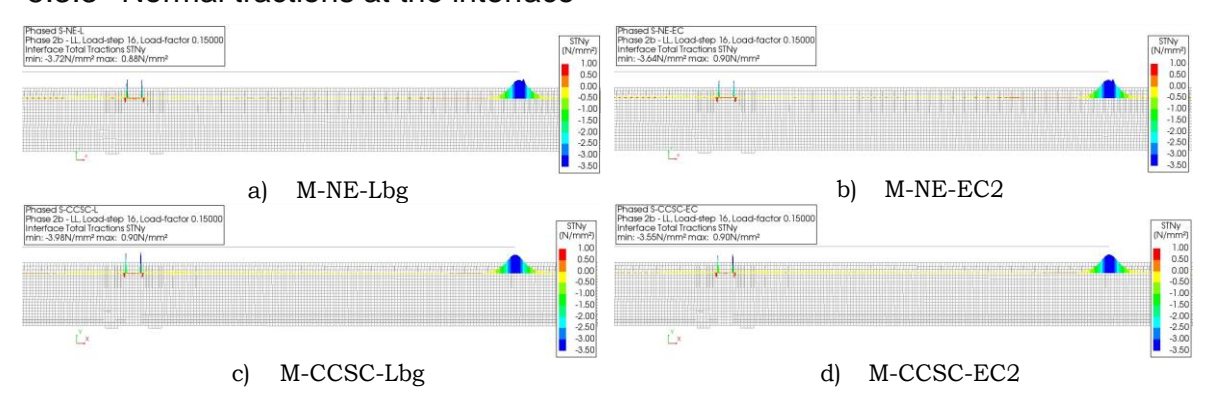


Figure 5.16 Interface normal tractions at applied 1.5 mm displacement (end of global elastic regime)

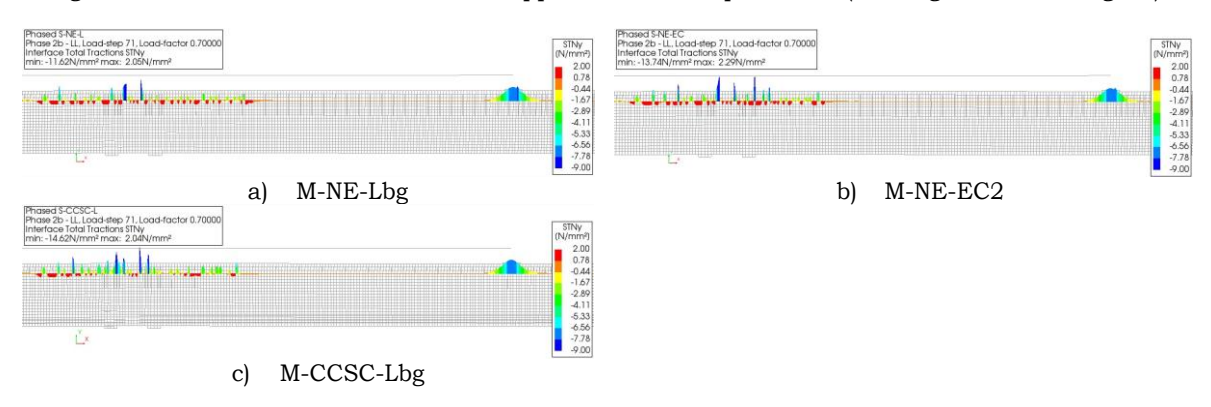


Figure 5.17 Interface normal tractions at applied 7 mm displacement

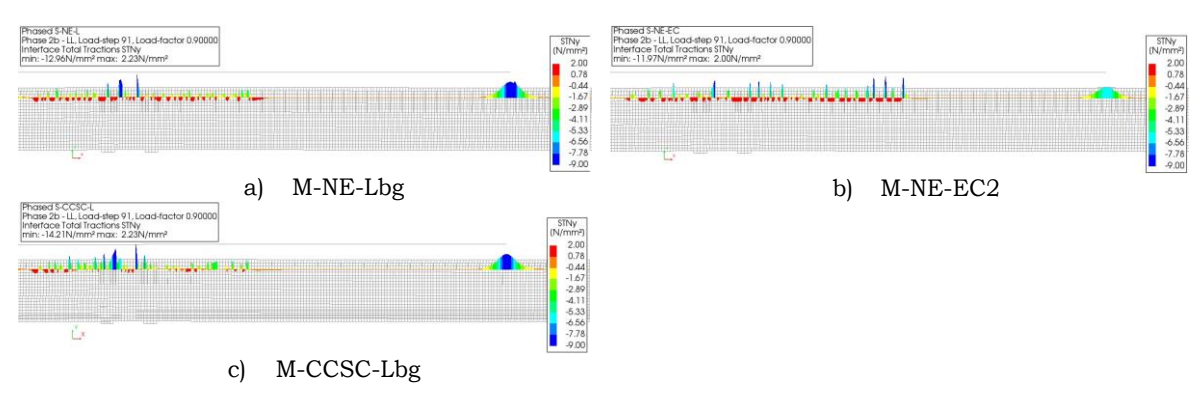


Figure 5.18 Interface normal tractions at applied 9 mm displacement

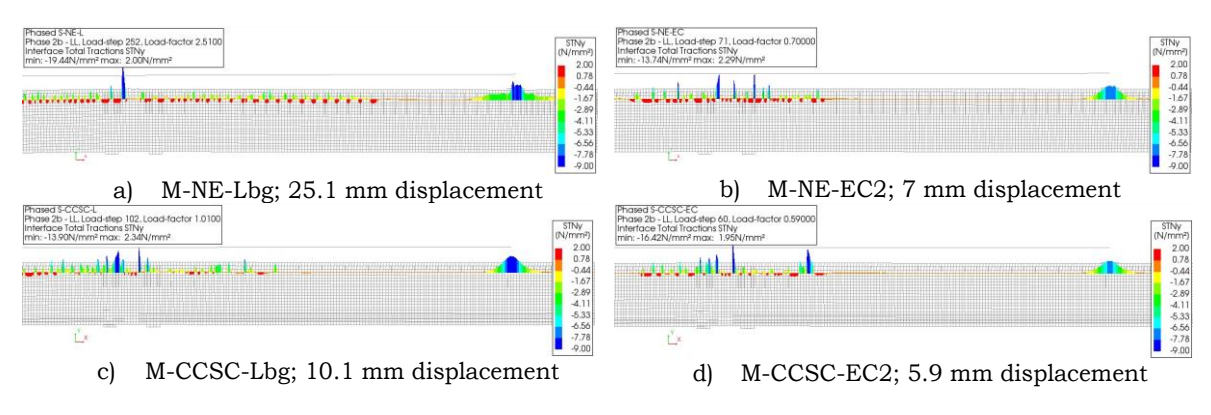


Figure 5.19 Interface normal tractions at peak capacity

5.3.4 Shear relative displacements

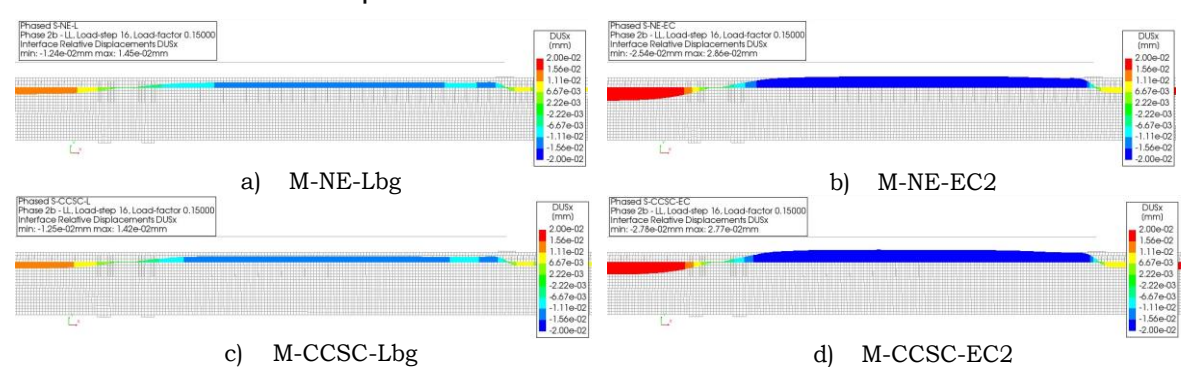


Figure 5.20 Interface relative displacements in tangential direction at applied 1.5 mm displacement (end of global elastic regime)

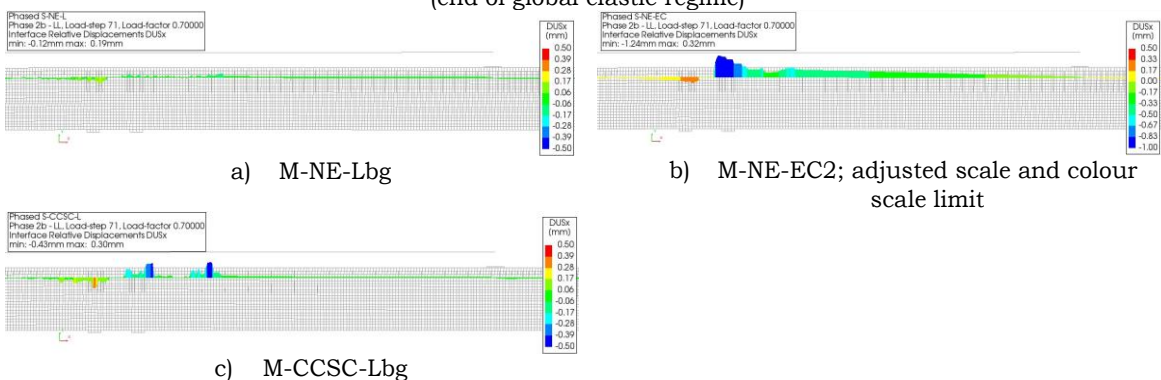


Figure 5.21 Interface relative displacements in tangential direction at applied 7 mm displacement

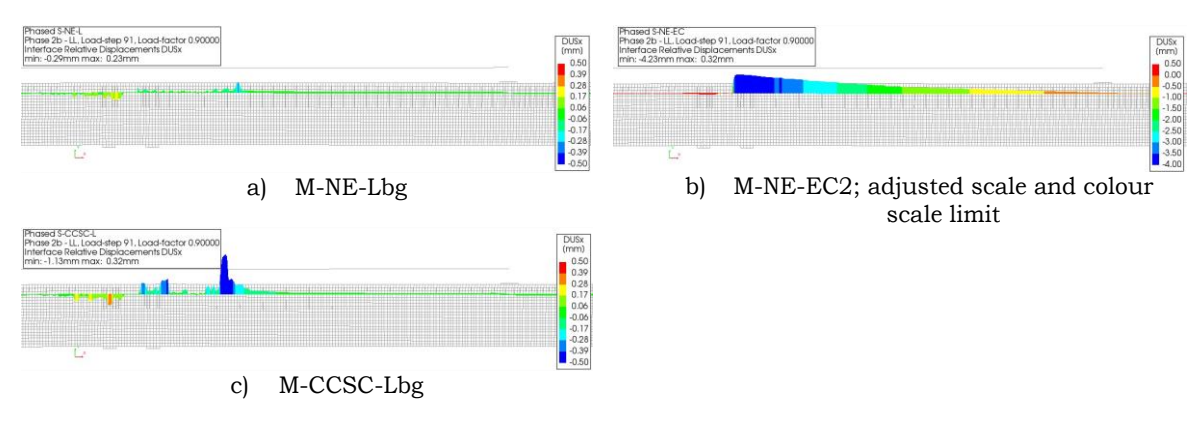


Figure 5.22 Interface relative displacements in tangential direction at applied 9 mm displacement

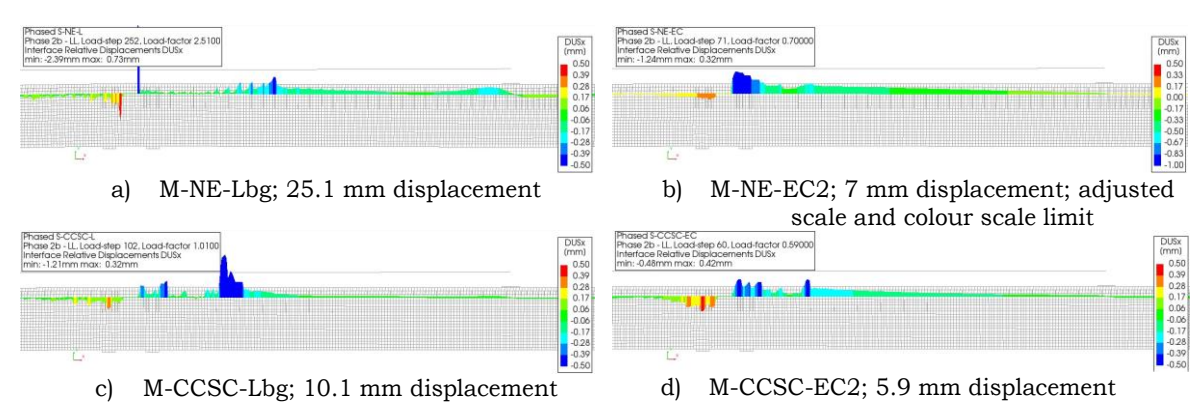


Figure 5.23 Interface relative displacements in tangential direction at peak capacity

5.3.5 Normal relative displacements

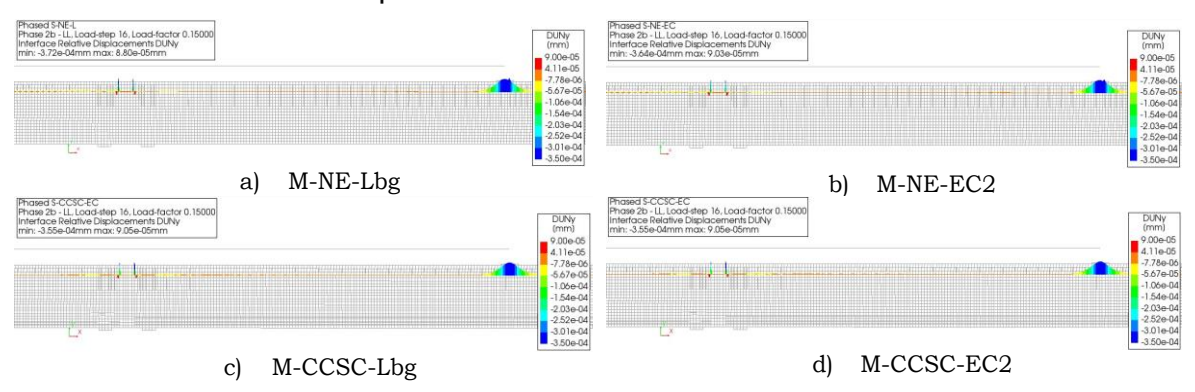


Figure 5.24 Interface relative displacements in normal direction at applied 1.5 mm displacement (end of global elastic regime)

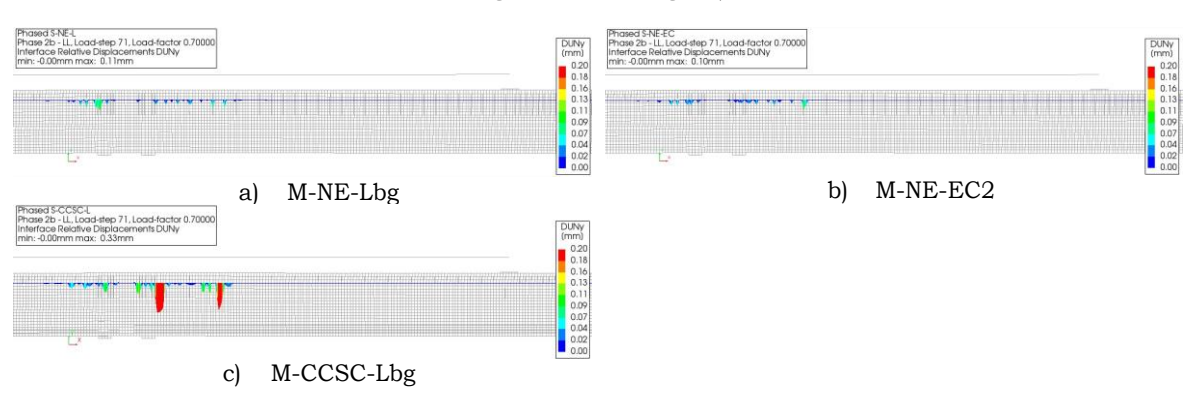


Figure 5.25 Interface relative displacements in normal direction at applied 7 mm displacement

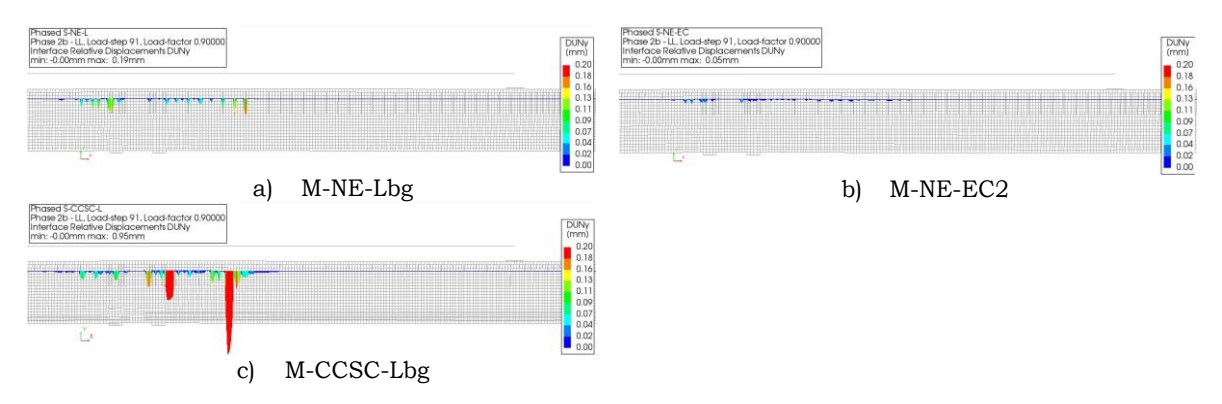


Figure 5.26 Interface relative displacements in normal direction at applied 9 mm displacement

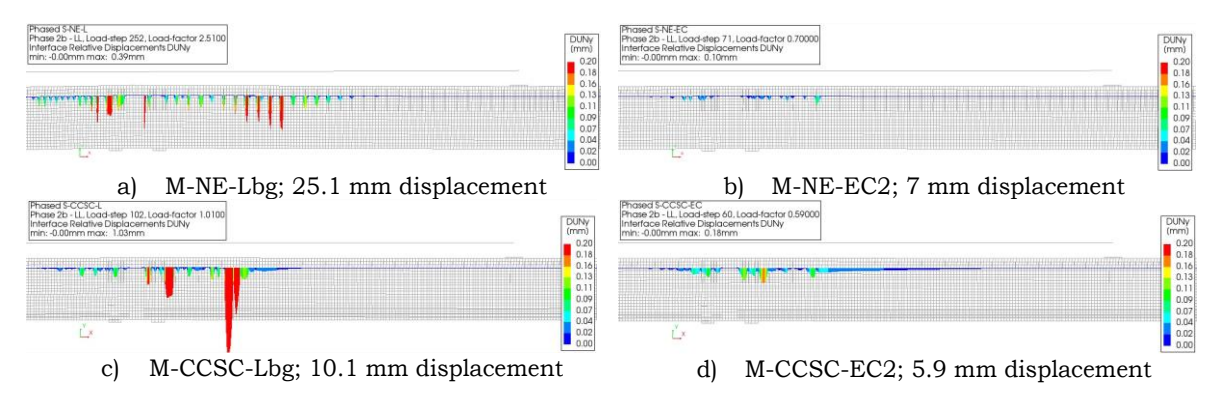


Figure 5.27 Interface relative displacements in normal direction at peak capacity

5.3.6 Development of stresses in selected points

The stresses at chosen points were plotted in the $\sigma - \tau$ plane. For each model, the data was presented for all the load steps of the analysis, thus corresponding with Figure 5.7. In this case, the plots display stress conditions above the support and at the location between the support and loading point (points red and purple in Figure 3.25). From the linear analysis, it appeared that the midspan location could be worth looking at, however, after initial verification, the point in the centre of the support-loading distance was considered more interesting. The envelopes were created based on Eurocode 2 [2] and literature-related best guess. The values of cohesion and friction are the same as used in Chapter 3 for the envelopes' assembly.

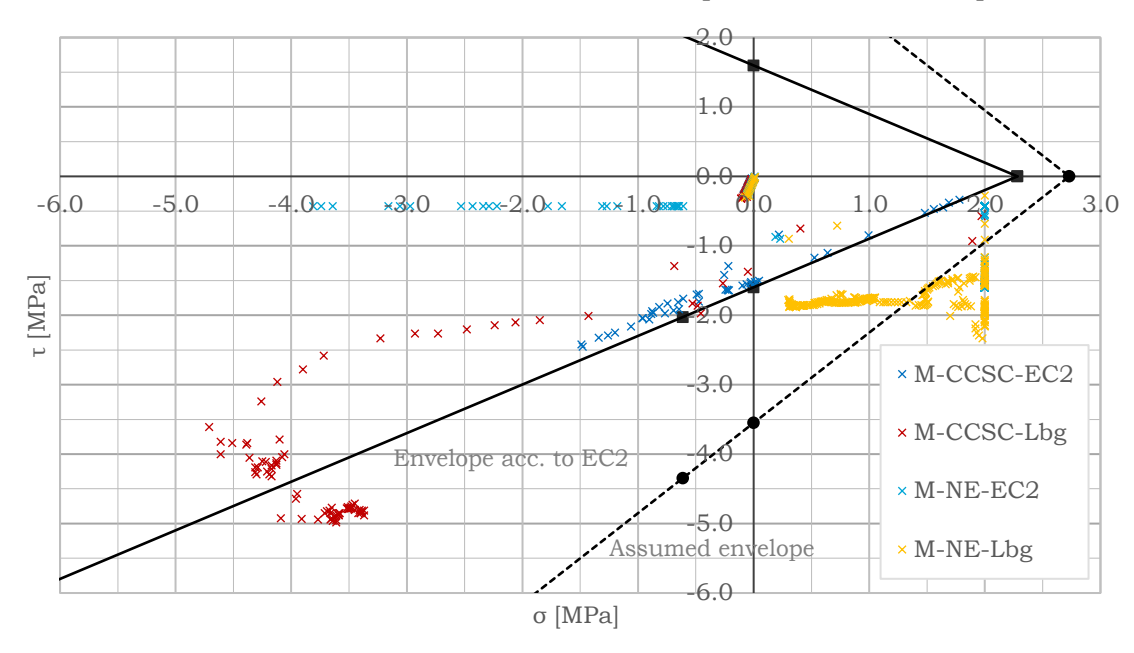


Figure 5.28 Stresses development above the support in $\sigma - \tau$ plane

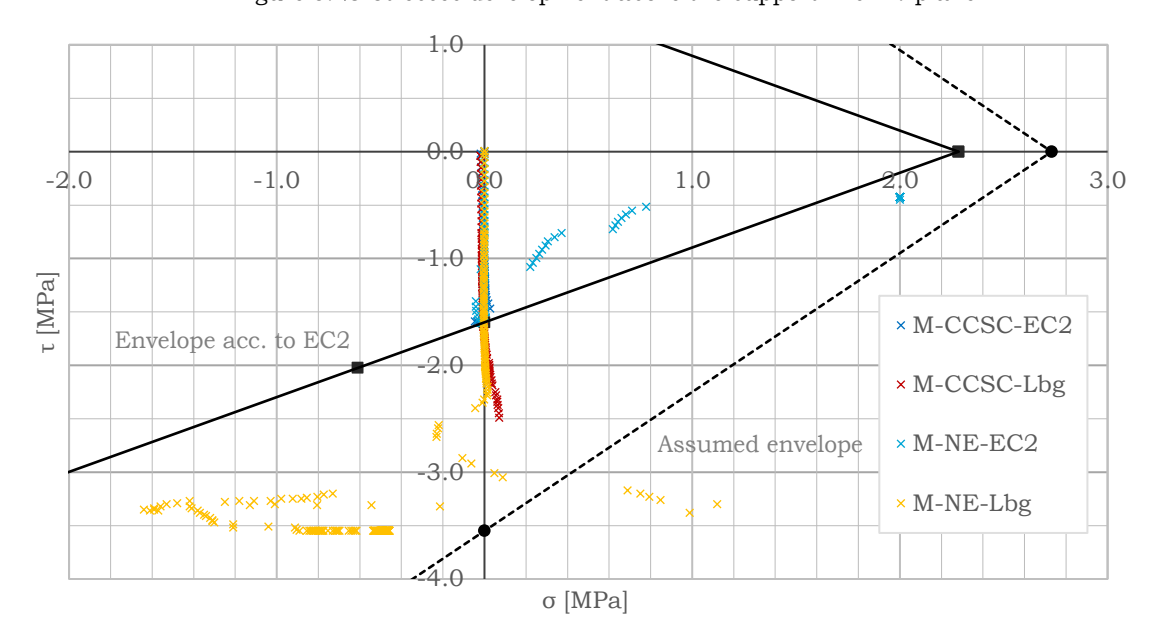


Figure 5.29 Stresses development at the point between support and loading points (x=7.075 m) in σ – τ plane

5.4 Discussion 93

5.4 Discussion

The composite concrete girder with varying material models for structural interfaces - Combined Cracking-Shearing-Crushing (CCSC) and Nonlinear Elasticity (NE) - was analysed within this Chapter. The Combined Cracking-Shearing-Crushing was chosen to be used with bond-slip beam element reinforcements as in this way, all contributing shear transfer mechanisms could in theory be captured. The cohesion (or aggregate interlock in the case of very rough surfaces) is accounted for by the interface material model which is based on the Mohr-Coulomb yield criterion and allows cohesion softening. Similarly, friction is included through the interface material model, which also enables the specification of a residual friction angle. The crushing of interfacial irregularities, hence friction softening can therefore be simulated. In the surfaces crossed by the reinforcements, the frictional resistance not only can be activated by the external forces but also by the reinforcement bars. As the bars were modelled using circular beam bond-slip type of reinforcements, they could provide axial, shear and bending resistance, along with certain slip with respect to the surrounding concrete. Therefore they could, theoretically, fully simulate the clamping and the dowel action. In contrast to this sophisticated material model, the Nonlinear Elasticity material model for the interface was composed, utilising diagrams to specify the traction-relative displacement relations in both, shear and normal directions. This material model does not account for the coupling between shear and normal tractions and relative displacements. The reinforcement contribution to the interfacial force transfer was already included in the material model of the interface itself. The hairpins were modelled as embedded bars, not crossing the interface, only adding stiffness to the surrounding concrete elements. The aim was to provide analogous inputs for both model types, to be able to assess and compare the outcomes.

With respect to the load-deflection diagram, presented in Figure 5.7, it is apparent that analyses of models with CCSC interface material model were less stable as in both cases the analyses were terminated due to divergence. Capturing the post-peak behaviour in the models M-CCSC-EC2 and M-CCSC-Lbg was not possible. The analyses with applied NE were able to proceed to the point that all given load steps were applied or when a total drop in the capacity occurred. In case of the M-NE-EC2 it was possible to further continue the analysis, however, it was decided that it is not necessary to do so. It was assumed that failure load has been reached since the peak capacity dropped by 21%. For the M-CCSC-EC2, the ultimate capacity is close to the peak of the M-NE-EC2 load-displacement graph. The load obtained was only 7% lower than the result obtained from the model with the NE interface material model. As far as the M-CCSC-Lbg is concerned, the analysis continued up until 10.1 mm of displacement was applied, reaching approximately 1.64 MN of the total load. The corresponding model with NE constitutive law reached a load almost 0.50 MN higher. It was also observed that the global stiffness of all the models is quite similar.

Looking at the crack patterns of models with literature-based input of cohesion and friction angles, for all distinguished load steps, the M-CCSC-Lbg and M-NE-Lbg portray good correspondence with each other. The -EC2 models are more difficult to compare, however, Figure 5.11 b) and d) present a comparable cracking patterns. It was observed that in all of the models, there is a pronounced crack forming at the junction of the precast beam and the element representing cross beam. As the

94 5.4 Discussion

cracking at that location might be expected due to a change of material and geometrical properties, it should be mentioned that the model was simplified. The parts of the cross beam that overlap for 0.5 m with the precast beam were not modelled, hence the behaviour of the test specimen in that region could be to some extent altered.

From the Figure 5.12-Figure 5.19 presenting shear and normal tractions at the interface, it is evident that cracking has considerably influenced the interfacial behaviour. The tractions in the support region are not varying smoothly, there are sudden changes between tensile and compressive stresses perpendicular to the interface. Since the CCSC model accounts for the coupling of stresses it is assumed that the shear stresses generated by models with CCSC constitutive relation are more sensitive to those variations, which can be observed for instance in Figure 5.15 b) and d). The peaks in the output of M-CCSC-EC2 are more pronounced and change more rapidly.

As far as tangential relative displacements are concerned, it is apparent that the drop in the capacity in the M-NE-EC2 model was related to the slip at the interface. At the level of 7 mm of applied displacement, the slip close to the support exceeded 1 mm, which according to Figure 5.5 a) is already the descending branch of the slip-traction diagram. At the level of 9 mm of applied displacement (Figure 5.22 b)), the slip at the interface is already higher than 4 mm. Looking at Figure 5.23 d), the M-CCSC-EC2 at the last step before divergence also displays an increase of the slip near the support, however, it was not possible to investigate what occurs beyond this point. There are also localised increases in relative shear displacement in the M-CCSC-Lbg.

It is noteworthy to observe, that at the locations of the increased slip, the interface is opening accordingly, when looking at the results obtained from models accounting for coupling. It is well represented when relating Figure 5.23 c) and d) with Figure 5.27 c) and d). At the same time, the models with the NE material model did not yield any considerable opening of the interface, except for some localised, modest peaks. Such a response is expected, as the behaviour in the normal and shear direction in the assembled NE material model are not related to each other – they are prescribed by separate diagrams.

It would be difficult to investigate the development of stresses at all the points along the interface, hence similarly to Chapter 3, certain locations along the beam's length were chosen. Again, the point above the support was selected and the stresses in the $\sigma-\tau$ plane for this point are plotted in Figure 5.28. The global performance of the girder is rapidly altering in the support area, where a small difference in chosen location would probably yield different results. Nevertheless, some observations can be made based on the given plot. Another selected point is the location exactly in between support and loading points and the stresses are displayed in Figure 5.29. It is apparent that in the case of the models with coupling accounted for, all the points lie within the envelopes' boundaries. As far as the M-NE-EC2 and M-NE-Lbg are concerned, it is no longer the case. It can be noted that the points do not cross the given limits, being 2 MPa of tensile stress or the shear boundaries according to Figure 5.5 a) and b). What is interesting to see is that the stresses above the support obtained from M-NE-EC2 are aligned at approximately $\tau=0.5$ MPa. Such behaviour is in line with the prescribed shear-slip relation shown in Figure 5.5 a). As already

5.5 Conclusions 95

discussed, there is a considerable slip present by the support, therefore the shear tractions for slips equal or higher than 1.96 mm will be equal to 0.43 MPa. Similarly, at the location between support and loading point, several points lie at $\tau = 3.5$ MPa which is related to reaching the flat plateau of the graph presented in Figure 5.5 b). However, the combination of normal and shear stresses for several load steps, especially obtained from the analysis of the M-NE-Lbg model, is already outside of the envelope.

Even though the CCSC material model allows for a very detailed representation and analysis of the interfacial behaviour, it was not possible to obtain comprehensive load-deflection beam performance. It is acknowledged that the model setup was based on several assumptions and, perhaps, with either a more detailed literature study, or with calibration of the model on the push-off specimens tested specifically for this interface type, the outcome of the analysis would be more successful. It is uncertain but might be probable that the convergence problems could be avoided if a less complex reinforcement modelling approach was adopted. For instance, truss elements with bond-slip relation, or even embedded reinforcements without any prescribed bond-slip, which are continuous at the interface, could be an alternative. Although, in such a case, the bending and shear of the connectors would not be taken into account. It may also be suggested that less elaborate material model, which, at the same time, is still able to account for the coupling and the cohesion and friction softening, could be employed for the interface elements.

In contrast, the first and main benefit of the NE material model is the fact that it allowed for the analysis to proceed in the post-peak stage. What is promising about the models with NE is that the global cracking pattern is comparable to the patterns presented by the corresponding models with CCSC interfacial material models, before they diverged. Nevertheless, as already argued, this model is less reliable as it does not account for the combinations of stresses that might be detrimental. Moreover, it was built with an assumption that the tensile capacity of the reinforcement bars crossing the interface surface is fully activated, which might not necessarily be accurate. On the other hand, no bending or shear capacity of dowels is accounted for, which can lead to a lower capacity. Another point of concern is that no localized concrete crushing around the hairpins could be depicted with such an approach.

In order to recommend one of the material models and either of the input sets, further validation of the models would have to be performed.

5.5 Conclusions

• With a change of input parameters of the interface material only, being an increase of initial cohesive strength by a factor of 2.2 (and accordingly the shear stiffness to maintain the same relative displacement at the loss of cohesion) and an increase of the friction angle of 35° by 17.43° and 10° for the initial and residual input, the difference in the capacity obtained from the analyses was substantial. For the models with the CCSC interfacial material model, the ultimate, total load was $\frac{1.64 \text{ MN}}{1.18 \text{ MN}} = 1.39$ higher, while, for the analyses with the NE material model, the ratio of the peaks was $\frac{2.12 \text{ MN}}{1.27 \text{ MN}} = 1.67$.

96 5.5 Conclusions

• The increase in the interface capacity has also proven that the global behaviour of the girders is highly dependent on it. With lower capacity, the cracking continued to develop in the top layer, while in models marked with -Lbg, the more significant part of the composite structure was activated.

- With this particular numerical setup, it was not possible to obtain the
 post-peak behaviour of the girders using the Combined Cracking-ShearingCrushing material model for the interface. It is undesirable as one of the
 reasons behind using a more sophisticated model, would be to have a more
 detailed insight into the overall structural behaviour, including the post-peak
 stage.
- The Nonlinear Elasticity material model performed more stable and allowed for the analyses to continue, which is its main advantage. Another benefit is the ease of implementation, in comparison with the Combined Cracking-Shearing-Crushing model.
- Based on Figure 5.28 and Figure 5.29 it was observed that at certain load steps, the models with Nonlinear Elasticity material model display results which lie outside the assumed failure envelopes. It could be concluded that the overall beam capacity might be overestimated.
- It cannot be stated whether the capacities obtained from the analyses can be related to reality as the outcome would have to be compared with the experimental results.

Conclusions and recommendations

6.1 Conclusions

Based on the review of the literature, performed analyses and results evaluation, a number of conclusions were already drawn in the preceding Chapters. In this subchapter the most significant conclusions are integrated and summarised.

- Results of the linear elastic analysis of the beam, with adopted modelling assumptions, revealed that no significant tensile stresses perpendicular to the interface were found, except the localised peaks in the vicinity of the beam, cross beam and top layer connection. It was shown, however, by the example of midspan location, that even minor values of tension, might be detrimental when shear tractions are present. Moreover, it was acknowledged that linear analysis has certain limitations if it comes to identifying tensile tractions at the interface, as it does not account for cracking of the concrete elements.
- Based on the linear verification of the influence of the interface shear stiffness k_s , it can be stated that the parameter has undoubtedly an impact on both the interfacial and the global structural behaviour. With a decrease of stiffness from a penalty value of 296000 to 20 N/mm³, which, according to literature findings, was considered more realistic, the composite action of the girder has deteriorated. The extreme tensile stresses in the precast beam in the support region increased by a factor of 1.21. The rise of compression in the beam's web, below the load application, by a factor of 2.26, was observed.
- Examination of the interfacial stresses development, at selected points, in the $\sigma \tau$ plane led to an observation that it is worthwhile to take into account the combination of normal and shear tractions. It is particularly desirable in the continuous elements, where the stress conditions vary along the structure's length. According to the linear analysis, the interface at the location near the point of load application, even though under shear stresses exceeding the assumed limit, is not expected to fail, due to substantial compressive stresses.
- Single-element tests revealed that both, Coulomb Friction and Combined Cracking-Shearing-Crushing interface material models are well suited for capturing the coupling between shear and normal stresses. With the same set of input parameters and a rising level of applied pressure at the interface, the shear capacity increased, representing the reference, experimental data on a satisfactory level. For the specimens with a rough, unreinforced surface, the average difference between numerically and experimentally obtained peak capacity was 0.38% and 11.59% using the Coulomb Friction and the Combined Cracking-Shearing-Crushing models respectively. The advantage

98 6.1 Conclusions

of the applied input for the Combined Cracking-Shearing-Crushing interface material model over the specified setup of the Coulomb Friction model, is the possibility to capture not only the initial but also the residual yield surface.

- The component-level analysis of the assembly of elements has proven that the model with interface elements with the Combined Cracking-Shearing-Crushing material model, the bond-slip reinforcements crossing interface and nonlinear properties of concrete, was able to reproduce the peak capacity with 7-15% underestimation. It was also observed that the post-peak strength was not well captured and that the analyses diverged after a certain applied load step. It has to be stated that there are uncertainties concerning reference data, especially the post-peak capacity and the horizontal relative displacements, therefore it was not possible to assess the model's performance with complete assurance.
- During the composite-level studies, the importance of boundary conditions, as well as accurate data recording, were noted. This is also crucial if any component-scale specimens were to be designed and tested in the course of further research.
- the verification of the application the Based on of Combined Cracking-Shearing-Crushing interface material model with bond-slip reinforcements crossing the connection, at the macro-level nonlinear analysis, it was concluded that the models with the assumed set of input parameters included in Table 5.6 and Table 5.8 did not allow for the capturing of the complete load-deflection path of the composite girder. Either more research on the input parameters has to be performed, or the model has to be simplified through, for instance, the application of a less complex numerical setup for hairpins. Nevertheless, judging by the acceptable results of the component-level single-element tests, it is assumed that the Combined Cracking-Shearing-Crushing model could be successfully used for modelling the interfaces not crossed by the reinforcements. It is highlighted, however, that the input parameters used within this research were largely based on assumptions and literature findings, and thus can only serve as guidance.
- The Nonlinear Elasticity material models, which were built based on the analogous input parameters, performed a more stable analysis and allowed for the analyses to continue. This is the model's main advantage. Another benefit is the more straight-forward definition of input parameters, in comparison with the Combined Cracking-Shearing-Crushing model. On the other hand, the shortcoming of the material model, which is not accounting for the coupling between the tractions, was demonstrated while analysing the results. Interfacial stresses plotted in the $\sigma-\tau$ plane indicated that at some load steps the tractions' combinations lie outside of the assumed failure envelopes, which might indicate that the beam's capacity is overestimated.
- With a change of input parameters of the interface material only, being an increase of initial bond strength by a factor of 2.2 and an increase of the friction angle of 35° by 17.43° and 10° for the initial and residual input, the differences in the capacity obtained from the analyses were considerable. For the models with the Combined Cracking-Shearing-Crushing interface material model and bond-slip reinforcements, the ultimate, total load was 1.39 times higher. For the analyses with the Nonlinear Elasticity interface material model, the ratio of the peaks was 1.67.

• It cannot be stated whether the capacities obtained from the analyses can be related to reality as the outcome would have to be validated with the experimental results. Neither of the modelling approaches can be fully recommended as one requires a lot of calibration and has issues with convergence, while the other might yield unreliable results. If the Combined Crushing-Shearing-Cracking model was to be further used, more research on input parameters and ways to improve analysis convergence would have to be performed. In the case of using the Nonlinear Elasticity material model for the interfaces, attention has to be given to whether the combination of stresses does not result in a stress state being outside of the assumed boundaries.

6.2 Recommendations

Recommendations concerning future research are listed below.

- Performing push off tests, modified push off with laterally applied compression, or, if possible, crack opening, turned out to be a crucial step in order to accurately describe the behaviour of this particular interface type and to calibrate the models. It would be then possible to obtain the parameters like cohesion, friction angle and initial shear stiffness. For the calibration of other parameters, concerning dilatancy, the data related to the interface opening has to be recorded.
- It is recommended to compare the outcomes of the nonlinear analyses of the composite girder performed within this research with experimental data, to assess the reliability of the results and judge whether either of the models provided trustworthy results.
- It is recommended to verify the modelling approaches with other large-scale experiments, for instance documented by Loov and Patnaik [15]. In the recommended research the beams were designed to fail at the interface, hence it might be beneficial to test the models on given samples as other influences are limited.
- Performing an analysis with the Combined Cracking-Shearing-Crushing interface material model but simplified numerical setup for hairpins is advised to test, as it might result in yielding more stable results.
- If the Combined Cracking Shearing-Crushing model was to be further investigated, it is recommended to perform sensitivity analysis, which might be done even on the structural-level, to detect how changes in certain input parameters would influence the performance of this particular continuous, composite girder.

- [1] M. E. Mohamad and I. S. Ibrahim, "Interface shear strength of concrete-to concrete bond with and without projecting steel reinforcement," *Jurnal Teknologi*, vol. 75, no. 1, pp. 169 172, 2015.
- [2] E. C. for Standardization, NEN-EN 1992-1-1 Eurocode 2: Design of concrete structures Part 1-1: General ruels and rules for buildings, Brussels: CEN, 2005.
- [3] Y. Yang, M. Park, N. Kostense and E. Lantsoght, "Analytical and numerical models for the shear behavior of precast concrete bridges at intermediate support A research proposal," Delft, 2021.
- [4] B. Belletti, C. Damoni and M. A. Hendriks, "Development of guidelines for nonlinear finite element analyses of existing reinforced and pre-stressed beams," *European Journal of Environmental and Civil Engineering*, vol. 15, no. 9, pp. 1361-1384, 2011.
- [5] J. Calavera, A. De Chefdebien, D. Fernández-Ordóñez, A. Gasperi, J. Ley, F. Mönnig, P. Passeman, C. Quartel, L. Sasek, G. Tootell and A. Van Acker, "Precast concrete bridges," International Federation for Structural Concrete (fib), Lausanne, 2004.
- [6] M. A. N. Hendriks and M. A. Roosen, "Guidelines for Nonlinear Finite Element Analysis of Concrete Structures," Rijkswaterstaat Centre for Infrastructure, Utrecht, 2020.
- [7] A. Halicka, "Influence new-to-old concrete interface qualities on the behaviour of support zones of composite concrete beams," *Construction and Building Materials*, vol. 25, no. 10, p. 4072–4078, 2011.
- [8] N. Hewson, "Prestressed concrete in bridgeworks," in *Prestressed Concrete Bridges: Design and Construction*, London, ICE Publishing, 2012, pp. 1-21.
- [9] N. Hewson, "Beam-and-slab bridges," in *Prestressed Concrete Bridges: Design and Construction*, London, ICE Publishing, 2012, pp. 171-195.
- [10] "www.banagherprecast.com," Inspiration Marketing and Walsh Design and Marketing, [Online]. Available: https://banagherprecast.com/projects/plymouth-road-bridge/. [Accessed 29 July 2022].
- [11] N. Hewson, "Prestressing components and equipment," in *Prestressed Concrete Bridges: Design and Construction*, London, ICE Publishing, 2012, pp. 23-37.
- [12] J. C. Walraven and C. R. Braam, CIE3150/4160 Prestressed Concrete, Delft: Faculty of Civil Engineering and Geosciences, TU Delft, 2019.
- [13] E. Cavaco, I. Pacheco and J. Camara, "Detailing of concrete-to-concrete

- interfaces for improved ductility," *Engineering Structures*, vol. 156, pp. 210-223, 2018.
- [14] C. Facilitator, "Constrofacilitator," Constrofacilitator, 19 February 2021. [Online]. Available: https://www.constrofacilitator.com/structural-connection-used-in-precast-building-part-1/. [Accessed 4 August 2022].
- [15] R. E. Loov and A. K. Patnaik, "Horizontal Shear Strength of Composite Concrete Beams With a Rough Interface," *PCI Journal*, vol. 39, no. 1, pp. 48-69, 1994.
- [16] N. Randl, "Design recommendations for interface shear transfer in fib Model Code 2010," *Structural Concrete*, vol. 14, no. 3, pp. 230-241, 2013.
- [17] P. M. D. Santos and E. N. B. S. Júlio, "Interface Shear Transfer on Composite Concrete Members," *ACI Structural Journal*, vol. 111, no. 1, pp. 113-122, 2014.
- [18] P. W. Birkeland and H. W. Birkeland, "Connections in Precast Concrete Construction," *ACI Journal*, vol. 11, no. 42, pp. 345-368, 1966.
- [19] J. A. Hofbeck, I. O. Ibrahim and A. H. Mattock, "Shear Transfer in Reinforced Concrete," *ACI Journal*, vol. 66, no. 2, pp. 119-128, 1969.
- [20] A. H. Mattock and N. M. Hawkins, "Shear transfer in reinforced concrete recent research," *Prestressed Concrete Institute*, *PCI Journal*, vol. 17, no. 2, pp. 55-75, 1972.
- [21] R. E. Loov, *Design of Precast Connections*, Singapore: Paper presented at a seminar organized by Compa International Pte, Ltd., 1978.
- [22] J. C. Walraven and H. W. Reinhardt, "Theory and Experiments on the Mechanical Behaviour of Cracks in Plain and Reinforced Concrete Subjected to Shear Loading," *HERON*, vol. 26, no. 1A, p. 68, 1981.
- [23] J. C. Walraven, F. Jerome and A. F. Pruijssers, "Influence of Concrete Strength and Load History on the Shear Friction Capacity of Concrete Members," *Prestressed Concrete Institute, PCI Journal*, vol. 32, no. 1, pp. 66-84, 1987.
- [24] N. Randl, "Investigations on load transfer between old and new concrete at different surface roughnesses. Dissertation," Leopold-Franzens-Universität, Innsbruck, 1997.
- [25] N. Randl and M. Wicke, "Schubübertragung zwischen Alt- und Neubeton. Experimentelle Untersuchungen, theoretischer Hintergrund und Bemessungsansatz," *Beton- und Stahlbetonbau*, vol. 95, no. 8, pp. 461-473, 2000.
- [26] N. Randl, F. Münger and M. Wicke, "Verstärkung von Brückentragwerken durch Aufbeton," *Bauingenieur*, vol. 80, no. 4, pp. 207-214, 2005.
- [27] International Federation for Structural Concrete, Fib Model Code for Concrete Structures 2010, Lausanne, 2010.

[28] R. Park and T. Paulay, "Strength and Deformation of Members in Shear," in *Reinforced concrete structures*, New York, John Wiley & Sons, 1975, pp. 270-345.

- [29] A. C. 318, Building Code Requirements for Structural Concrete (ACI 318M-08) and Commentary, Farmington Hills: American Concrete Institute, 2008.
- [30] L. Croes, "Behavior of unreinforced concrete-to-concrete interfaces under shear loading," Eindhoven University of Technology, Eindhoven, 2019.
- [31] A. D. Espeche and J. León, "Estimation of bond strength envelopes for old-tonew concrete interfaces based on a cylinder splitting test," *Construction and Building Materials*, vol. 25, no. 3, pp. 1222-1235, 2011.
- [32] E. N. Júlio, D. Dias-da-Costa, F. A. Branco and J. M. Alfaiate, "Accuracy of design code expressions for estimating longitudinal shear strength of strengthening concrete overlays," *Engineering Structures*, vol. 32, no. 8, pp. 2387-2393, 2010.
- [33] K. N. Rahal, A. L. Khaleefi and A. Al-Sanee, "An experimental investigation of shear-transfer strength of normal and high strength self compacting concrete," *Engineering Structures*, vol. 109, pp. 16 25, 2016.
- [34] N. Randl and C. Zanotti, "Are concrete-concrete bond tests comparable?," *Cement and Concrete Composites*, vol. 99, pp. 80-88, 2019.
- [35] O. Harrass, "Interfacial behavior of hybrid SHCC-Concrete beams with a joint at midspan," TU Delft, Delft, 2020.
- [36] O. C. Zienkiewicz, R. L. Taylor and J. Z. Zhu, "The standard discrete system and origins of the finite element method," in *The Finite Element Method: Its Basis and Fundamentals. Sixth edition*, Boston, Elsevier Butterworth-Heinemann, 2005, pp. 1-18.
- [37] J. Manie and D. Ferreira, "DIANA User's Manual -- Release 10.5," 24 January 2022. [Online]. Available: https://dianafea.com. [Accessed 1 August 2022].
- [38] P. H. Feenstra, R. De Borst and J. G. Rots, "Numerical Study on Crack Dilatancy Part 1: Models and Stability Analysis," *Journal of Engineering Mechanics*, vol. 117, no. 4, pp. 733-753, 1991.
- [39] P. B. Lourenço and J. G. Rots, "Multisurface interface model for analysis of masonry structures," *Journal of Engineering Mechanics ASCE*, vol. 123, no. 7, pp. 660-668, 1997.
- [40] P. Gambarova and Z. P. Bažant, "Rough Cracks in Reinforced Concrete," Journal of the Structural Division, vol. 106, no. 4, pp. 819-842, 1980.
- [41] T. Paulay and P. J. Loeber, "Shear Transfer By Aggregate Interlock," *ACI-Special Publications*, vol. 42, pp. 1-16, 1974.
- [42] P. H. Feenstra, R. de Borst and J. G. Rots, "Numerical Study on Crack

- Dilatancy Part 2: Applications," *Journal of Engineering Mechanics*, vol. 117, no. 4, pp. 754-769, 1991.
- [43] D. Dias-da-Costa, J. Alfaiate and E. Júlio, "FE modeling of the interfacial behaviour of composite concrete members," *Construction and Building Materials*, vol. 256, no. 1, pp. 233-243, 2012.
- [44] S. Dudziak, W. Jackiewicz-Rek and Z. Kozyra, "On the Calibration of a Numerical Model for Concrete-to-Concrete Interface," *Materials*, vol. 14, no. 23, 2021.
- [45] M. van den Heever, F. Bester, J. Kruger and G. van Zijl, "Numerical modelling strategies for reinforced 3D concrete printed elements," *Additive Manufacturing*, vol. 50, 2022.
- [46] S. B. Setyanto, "Numerical Study of Interface Behaviour in Composite SHCC-Concrete beams," Delft University of Technology, Delft, 2021.
- [47] K. K. Minalu, "Finite Element Modelling of Skew Slab-Girder Bridges," TU Delft, Delft, 2010.
- [48] P. M. D. Santos, "Assessment of the Shear Strength between Concrete Layers," Faculdade de Ciências e Tecnologia da Universidade de Coimbra, Coimbra, 2009.
- [49] M. E. Mohamad, I. S. Ibrahim, R. Abdullah, A. B. Abd. Rahman, A. B. H. Kueh and J. Usman, "Friction and cohesion coefficients of composite concrete-to-concrete bond," *Cement and Concrete Composites*, vol. 56, pp. 1-14, 2015.
- [50] E. C. for Standarization, DRAFT prEN 10138-3 Prestressing steels Part 3: Strand, Brussels: CEN, 2000.
- [51] J. M. Gere and S. P. Timoshenko, Mechanics of Materials, Cheltenham: Stanley Thornes (Publishers) Ltd, 1999.
- [52] E. C. for Standardization, NEN-EN 1991-1-1 Eurocode 1: Actions on structures Part 1-1: General actions Densities, self-weight, imposed loads for buildings, Brussels: CEN, 2002.
- [53] P. Neto , J. Alfaiate , J. R. Almeida and E. B. Pires , "The influence of mode II fracture on concrete strengthened with CFRP," *Computers and Structures*, vol. 82, no. 17–19, pp. 1495-1502, 2004.
- [54] P. Soroushian, K. Obaseki and M. C. Rojas, "Bearing Strength and Stiffness of Concrete under Reinforcing Bars," ACI Materials Journal, vol. 84, no. 3, pp. 179-184, 1987.
- [55] X. G. He and A. K. H. Kwan, "Modeling dowel action of reinforcement bars for finite element analysis of concrete structures," *Computers and Structures*, vol. 79, no. 6, pp. 595-604, 2001.
- [56] B. El-Ariss, "Behavior of beams with dowel action," Engineering Structures, vol.

- 29, no. 6, pp. 899-903, 2007.
- [57] P. A. Vermeer and R. de Borst, "NON-ASSOCIATED PLASTICITY FOR SOILS, CONCRETE AND ROCK," *Heron*, vol. 29, no. 3, 1984.
- [58] G.-J. Schreppers, "Bond-slip Reinforcements and Pile Foundations," TNO DIANA BV, 2015.
- [59] M. Ibrahim, N. Kostense, M. Poliotti, Y. Yang, M. Hendriks, J. Rots and M. Roosen, 2023 TU-Delft Concrete prediction contest, Delft: TU Delft, 2023.
- [60] E. C. for Standardization, NEN-EN 10080 Steel for the reinforcement of concrete Weldable reinforcing steel General, Brussels: CEN, 2005.
- [61] C. Naga Satish Kumar and T. D. Gunneswara Rao, "An Empirical Formula for Mode-II Fracture Energy of Concrete," KSCE Journal of Civil Engineering, vol. 19, no. 3, pp. 689-697, 2015.

Annex A

Table A.1 Extended overview of key material models for structural interfaces available in DIANA FEA [37]

Material model	Linear/ Nonlinear	Coupling	Short description				
Linear Elasticity	Linear	×	Only the linear behaviour of the interface can be described. Stiffness in normal and tangential directions is required as input.				
Nonlinear Elasticity	Nonlinear	×	Nonlinearity is introduced by means of diagrams or functions reducing stiffnesses for certain critical values of relative displacements.				
Discrete Cracking	Nonlinear	*	Constitutive relation to model discrete cracks. Stiffness in normal and shear directions have to be indicated, nevertheless, the behaviour in the normal direction is more significant. The post peak behaviour can be specified to be either brittle or with an application of linear or nonlinear tension softening.				
Crack Dilatancy	Nonlinear	√	The model is activated when certain shear traction and crack opening is present. Tension softening can be specified for the development of the cracking stage. In the open-crack stage, the tractions in normal and tangential directions are coupled, hence non-diagonal entries of crack stiffness coefficients' matrix are non-zero. There are five mathematical models to choose from, which are based on either empirical results or assumptions and theoretical models [38].				
Bond Slip	Nonlinear*	×	The model is used only with line interfaces utilised to describe contact between reinforcement and concrete. In the normal direction, the relation is assumed to be linear, while in shear nonlinearity is introduced by predefined or user-specified functions.				
Coulomb Friction	Nonlinear	✓	Based on the Mohr-Coulomb plasticity model for continuum elements. The coupling between normal and tangential tractions and displacements is accounted for. Apart from initial stiffness parameters cohesion, friction and dilatancy angle as well as interface opening model are to be specified.				

106 Annex A

Nonlinear Elastic Friction	Nonlinear	✓	Material model stemming from Coulomb Friction model, however, it is simplified as it only allows to model elastic behaviour. The model takes cohesion and friction angle into account. Properties can be either specified or based on properties of neighbouring elements.
Combined Cracking- Shearing- Crushing (CCSC)	Nonlinear	√	Diana Manual [37] and reference study [39] emphasize the application of this model in masonry structures. CCSC also stems from Coulomb friction model. It encompasses modelling of the cracking, shearing and crushing along the interface or of the material that the elements represent. The constitutive relation involves a substantial amount of input parameters, some of which should be determined experimentally.

^{*}Linear in normal direction

Annex B

B.1 Estimation of shear stiffness, cohesion and friction coefficients based on research by Love and Patnaik [15]

Table B.1 Estimation of initial shear stiffness, cohesion and friction coefficients [15].

Beam No.	clamping stress [MPa]	web f _{cm} [Mpa]	flange f _{cm} [Mpa]	mean f _{cm} [Mpa]	mean f _{ctm} [Mpa]	stress at 0.13 mm [Mpa]	stress at 0.5 mm [Mpa]	stress at failure [Mpa]	С	μ	k _{sinit} [N/mm ³]
1	4.36	42.7	37.4	40.05	3.03	4.81	7.5	7.76	1.59	0.68	37.00
2	1.66	39.2	34.9	37.05	2.83	3.22	4	4.27	1.14	0.63	24.77
3	2.73	40.2	30.5	35.35	2.72	3.32	5.95	6.82	1.22	1.28	25.54
5	1.63	42.6	34.8	38.7	2.94	2.95	5.08	5.54	1.00	1.59	22.69
6	1.62	40.4	37.1	38.75	2.94	2.95	5.04	5.25	1.00	1.42	22.69
7	6.06	38	35.8	36.9	2.83	4.55	8.57	9.25	1.61	0.77	35.00
8	0.77	38	35.6	36.8	2.82	2.35	2.89	3.12	0.83	1.00	18.08
9	1.62	37.6	37.1	37.35	2.85	3.59	4.54	4.64	1.26	0.65	27.62
10	0.77	37.6	38.7	38.15	2.91	2.46	3.46	3.46	0.85	1.30	18.92
12	7.72	36.2	34.6	35.4	2.73	5.71	8.04	9.2	2.09	0.45	43.92
13	0.82	23.7	19.2	21.45	1.70	2.1	2.92	2.92	1.24	1.00	16.15
Mean value	2.71	37.84	34.15	36.00	2.75	3.46	5.27	5.66	1.26	0.98	26.58
								*	0.73	1.53	

108 Annex B

Only the beams which failed in horizontal shear were taken into account. The magnitude of clamping stresses, concrete strength of web and flange, as well as shear stresses at given slip values, were obtained from Tables 2 and 3 from considered research [15]. Firstly, the mean concrete strength was calculated as the average of the strengths of the web and flange. Following, the mean tensile strength was calculated based on the formula provided by the Eurocode 2 [2].

$$f_{ctm} = 0.3 f_{ck}^{\frac{2}{3}}$$
; $f_{ck} = f_{cm} - 8MPa$

It was assumed that the magnitude of stress at the slip of $0.13 \, \text{mm}$ can be considered as the value of cohesion. The stresses were divided by the f_{ctm} to calculate the coefficient c. The friction coefficient was taken as a difference of shear magnitudes at failure and at $0.13 \, \text{mm}$, divided by the clamping stress value.

$$c = \frac{\tau_{s=0.13}}{f_{ctm}}; \mu = \frac{\tau_{u} - \tau_{0.13}}{\rho_{v} f_{v}}$$

The additional value with a star was calculated as the 2 MPa indicated by the authors to be the strength of the unreinforced surface, divided by mean tensile strength. Accordingly, friction coefficient could be approximated assuming the difference of ultimate stress and the 2MPa to be the capacity increase generated by friction.

$$c^* = \frac{2 \text{ MPa}}{f_{ctm}} = 0.73; \; \mu^* = \frac{\tau_u - 2 \text{MPa}}{\rho_v f_y} = 1.53$$

The friction coefficient could be also calculated as an ultimate capacity divided by the clamping stress, as a result of an assumption that the post-peak capacity is provided only by the friction generated by rebars. In that case the value would be even higher.

Initial stiffness is estimated by dividing the shear stress magnitude by the corresponding slip of 0.13 mm.

$$k_{s_{init}} = \frac{\tau_{s=0.13}}{0.13 \text{ mm}}$$

C.1 Solutions to analytical calculations

```
> restart:
> with (plots):
> q_D_1:=Pl*Dirac(x-AP1):
> q_D_2:=P2*Dirac(x-AP2):
 ODEs
Main Span - concrete, simply supported beam under prestressing load and, depending on the value of q, under self-weight or self-weight and 5/8 weight of wet concrete > ODE_mal:=Bl_ma*diff(w_mal(x),x$4)=q;
                                                                                                                                                                                                                                                                                                                                                                                                                                                                                                                                                                            (1)
'> ODE_ms2:=EI_ms*diff(w_ms2(x),x$4)=q;
                                                                                                                                                                                                                                   ODE\_ms2 := EI\_ms \left( \frac{d^4}{dx^4} w\_ms2(x) \right) = q
\stackrel{:}{>} \ \text{ODE\_ms3} := \! \text{EI\_ms*diff(w\_ms3(x),x$$4) = } q;
                                                                                                                                                                                                                                   ODE\_ms\beta := EI\_ms\left(\frac{d^4}{dx^4} w\_ms\beta(x)\right) = q
Cantilever Part of the Beam - concrete, simply supported beam under prestressing load and, depending on the value of q, under self-weight and 5/8 weight of wet concrete > OBE_opl:=E1_op*diff(w_opl(x),x$4)=q;
                                                                                                                                                                                                                                     ODE\_cpl := EI\_cp\left(\frac{d^4}{dx^4} w\_cpl(x)\right) = q
:
> ODE_cp2:=EI_cp*diff(w_cp2(x),x$4)=q;
                                                                                                                                                                                                                                     ODE\_cp2 := EI\_cp\left(\frac{d^4}{dx^4} w\_cp2(x)\right) = q
> ODE_cp3:=EI_cp*diff(w_cp3(x),x$4)=q;
                                                                                                                                                                                                                                     ODE\_cp3 := EI\_cp \left( \frac{d^4}{dx^4} w\_cp3(x) \right) = q
Continuous beam under the whole selfweight
> ODE_c1:=EI_com*diff(w_c1(x),x$4)=q_com;
                                                                                                                                                                                                                                ODE\_c1 := EI\_com\left(\frac{d^4}{dx^4} w\_c1(x)\right) = q\_com
\stackrel{:}{>} \ \mathtt{ODE\_c2} := \mathtt{EI\_crossb*diff(w\_c2(x),x\$4)} = \mathtt{q\_crossb};
                                                                                                                                                                                                                           ODE\_c2 := EI\_crossb\left(\frac{d^4}{dx^4} w\_c2(x)\right) = q\_crossb
> ODE_c3:=EI_crossb*diff(w_c3(x),x$4)=q_crossb;
                                                                                                                                                                                                                           ODE\_c\beta := EI\_crossb\left(\frac{d^4}{dx^4} w\_c\beta(x)\right) = q\_crossb
> ODE_c8:=EI_c*diff(w_c8(x),x$4)=q_c;
                                                                                                                                                                                                                                       ODE\_c\delta := EI\_c \left( \frac{d^4}{dx^4} w\_c\delta(x) \right) = q\_c
> ODE c4:=EI crossb*diff(w c4(x),x$4)=q crossb;
                                                                                                                                                                                                                           ODE\_c4 := EI\_crossb\left(\frac{d^4}{dx^4} w\_c4(x)\right) = q\_crossb
                                                                                                                                                                                                                                                                                                                                                                                                                                                                                                                                                                             (11)
> ODE c5:=EI crossb*diff(w c5(x),x$4)=q crossb;
                                                                                                                                                                                                                           ODE\_c5 := EI\_crossb\left(\frac{d^4}{dx^4} w\_c5(x)\right) = q\_crossb
                                                                                                                                                                                                                                                                                                                                                                                                                                                                                                                                                                            (12)
> ODE_c6:=EI_com*diff(w_c6(x),x$4)=q_com;
                                                                                                                                                                                                                               ODE\_c6 := EI\_com \left( \frac{d^4}{dx^4} w\_c6(x) \right) = q\_com
                                                                                                                                                                                                                                                                                                                                                                                                                                                                                                                                                                            (13)
> ODE_c7:=EI_com*diff(w_c7(x),x$4)=q_com;
                                                                                                                                                                                                                                ODE\_c7 := EI\_com \left( \frac{d^4}{dx^4} w\_c7(x) \right) = q\_com
                                                                                                                                                                                                                                                                                                                                                                                                                                                                                                                                                                            (14)
"> ODE_c1_LL:=EI_com*diff(w_c1_LL(x),x$4)=q__D_1;
                                                                                                                                                                                                     ODE\_cl\_LL := El\_com \left( \frac{d^4}{dx^4} w\_cl\_LL(x) \right) = Pl \operatorname{Dirac}(-x + APl)
                                                                                                                                                                                                                                                                                                                                                                                                                                                                                                                                                                            (15)
> ODE_c2_LL:=EI_crossb*diff(w_c2_LL(x),x$4)=0;
                                                                                                                                                                                                                          ODE\_c2\_LL := EI\_crossb\left(\frac{d^4}{dx^4} w\_c2\_LL(x)\right) = 0
                                                                                                                                                                                                                                                                                                                                                                                                                                                                                                                                                                            (16)
> ODE_c3_LL:=EI_crossb*diff(w_c3_LL(x),x$4)=0;
                                                                                                                                                                                                                          ODE\_c3\_LL := EI\_crossb\left(\frac{d^4}{dx^4} w\_c3\_LL(x)\right) = 0
                                                                                                                                                                                                                                                                                                                                                                                                                                                                                                                                                                            (17)
"> ODE_c8_LL:=EI_c*diff(w_c8_LL(x),x$4)=0;
                                                                                                                                                                                                                                ODE\_cs\_LL := EI\_c \left( \frac{d^4}{dx^4} w\_cs\_LL(x) \right) = 0
"> ODE_c4_LL:=EI_crossb*diff(w_c4_LL(x),x$4)=0;
                                                                                                                                                                                                                          ODE\_c4\_LL := EI\_crossb\left(\frac{d^4}{dx^4} w\_c4\_LL(x)\right) = 0
> ODE_c5_LL:=EI_crossb*diff(w_c5_LL(x),x$4)=0;
                                                                                                                                                                                                                          ODE\_c5\_LL := EI\_crossb\left(\frac{d^4}{dx^4} w\_c5\_LL(x)\right) = 0
                                                                                                                                                                                                                                                                                                                                                                                                                                                                                                                                                                             (20)
> ODE_c6_LL:=EI_com*diff(w_c6_LL(x),x$4)=q_D_2;
                                                                                                                                                                                                     ODE\_c6\_LL := EI\_com \left( \frac{d^4}{dv^4} w\_c6\_LL(x) \right) = P2 \operatorname{Dirac}(-x + AP2)
'> ODE_c7_LL:=EI_com*diff(w_c7_LL(x),x$4)=0;
                                                                                                                                                                                                                             ODE\_c7\_LL := EI\_com\left(\frac{d^4}{dx^4} w\_c7\_LL(x)\right) = 0
Solving ODEs
     NOVING ODES

sol:=dealve((ODE mai,ODE mai,ODE mai,ODE mai,ODE cp1,ODE cp2,ODE cp3,ODE c1,ODE c2,ODE c3,ODE c4,ODE c5,ODE c6,ODE c7,ODE c8,ODE c1 LL,ODE c2 LL,ODE c3 LL,ODE c4 LL,

ODE c5 LL,ODE c6 LL,ODE c7 LL,ODE c6 LL); (w mai (x), w mai(x), w mai(x), w cp1(x), w cp2(x), w cp3(x), w cf(x), w c2(x), w c3(x), w c5(x), w c5(x), w c6(x), w c7(x), w c6(x), w c7(x), w c6(x), w c7(x), w c6(x), w c7(x), w c7(x)
      phi ms1:=-diff(w ms1,x): kappa_ms1:= diff(phi ms1,x): M ms1:=EI ms*kappa_ms1: V ms1:=diff(M ms1,x): phi ms2:--diff(w ms2,x): kappa_ms2: - diff(phi ms2,x): M ms2:=EI ms*kappa_ms2: V ms2:-diff(M ms2,x): phi ms3:--diff(y ms3,x): kappa_ms3: diff(phi ms3,x): M ms3:=EI ms*kappa_ms3: V ms2:-diff(M ms3,x): M ms3:-diff(M ms3,
      phi_o1:=-diff(w_o1,x): kappa_o1:= diff(phi_o1,x): M_o1:=EI_com*kappa_o1: V_o1:=diff(M_o1,x): phi_o2:=-diff(w_o2,x): kappa_o2:= diff(phi_o2,x): M_o2:=EI_crossb*kappa_o2: V_o2:=diff(M_o2,x): phi_o3:=-diff(w_o3,x): kappa_o3:= diff(phi_o3,x): M_o3:=EI_crossb*kappa_o3: V_o3:=diff(M_o3,x): phi_o3:=diff(w_o4,x): phi_o3:=diff(w_o4,x): phi_o3:=diff(w_o4,x): phi_o3:=diff(w_o4,x): phi_o3:=diff(w_o4,x): kappa_o4:=diff(phi_o4,x): phi_o3:=diff(w_o4,x): kappa_o5:=diff(m_o4,x): phi_o3:=diff(w_o4,x): kappa_o5:=diff(phi_o5,x): M_o6:=EI_com*kappa_o6: V_o6:=diff(M_o6,x): phi_o3:=-diff(w_o7,x): kappa_o7:=diff(phi_o7,x): M_o7:=EI_com*kappa_o7: V_o7:=diff(M_o7,x): phi_o8:=-diff(w_o8,x): kappa_o8:=diff(phi_o8,x): mo8:=EI_o*kappa_o8: V_o8:=diff(M_o8,x):
```

```
> phi_o1_LL:=-diff(w_c1_LL,x): kappa_c1_LL:= diff(phi_c1_LL,x): M_c1_LL:=EI_com*kappa_c1_LL: V_c1_LL:=diff(M_c1_LL,x):  
> phi_o2_LL:=-diff(w_c2_LL,x): kappa_c2_LL:= diff(phi_c2_LL,x): M_c2_LL:=EI_com*kappa_c2_LL: V_c2_LL:=diff(M_c2_LL,x):  
> phi_o2_LL:=-diff(w_c3_LL,x): kappa_c3_LL:= diff(phi_c3_LL,x): M_c3_LL:=EI_com*kappa_c3_LL: V_c3_LL:=diff(M_c3_LL,x):  
> phi_o4_LL:=-diff(w_c4_LL,x): kappa_c3_LL:= diff(phi_c4_LL,x): M_c4_LL:=EI_com*kappa_c4_LL: V_c4_LL:=diff(M_c4_LL,x):  
> phi_o4_LL:=-diff(w_c4_LL,x): kappa_c5_LL:= diff(phi_c4_LL,x): M_c4_LL:=EI_com*kappa_c4_LL: V_c4_LL:=diff(M_c5_LL,x):  
> phi_o4_LL:=-diff(w_c4_LL,x): kappa_c5_LL:= diff(phi_c4_LL,x): M_c4_LL:=EI_com*kappa_c4_LL: V_c4_LL:=diff(M_c5_LL,x):  
> phi_o4_LL:=-diff(w_c4_LL,x): kappa_c4_LL:= diff(phi_c4_LL,x): M_c4_LL:=EI_com*kappa_c4_LL: V_c4_LL:=diff(M_c4_LL,x):  
> phi_o4_LL:=-diff(w_c4_LL,x): kappa_c4_LL:= diff(phi_c4_LL,x): M_c4_LL:=EI_com*kappa_c4_LL: V_c4_LL:=diff(M_c4_LL,x):  
> phi_o4_LL:=-diff(w_c4_LL,x): kappa_c4_LL:= diff(phi_c4_LL,x): M_c4_LL:=EI_c*kappa_c6_LL: V_c4_LL:=diff(M_c4_LL,x):  
> phi_o4_LL:=-diff(w_c4_LL,x): kappa_c4_LL:= diff(phi_c4_LL,x):  
> phi_o4_LL:=-diff(w_c4_LL,x):  
> phi_o4
  Boundary conditions:
  > x:=A: eq1:=V_cp1=0: eq2:=M_cp1=0:
> x:=A: eq25:=V_c1=0: eq26:=M_c1=0:
> x:=A: eq53:=V_c1_LL=0: eq54:=M_c1_LL=0:
      x:=B: eq3:=w_cp1=0: eq4:=w_cp2=0: eq5:=M_cp1=M_cp2: eq6:=phi_cp1=phi_cp2:
                                   =CB1: eq27:=w c1=w c2: eq28:=V c1=V c2: eq29:=M c1=M c2: eq30:=phi c1=phi c2:
=CB1: eq55:=w c1 LL=w c2 LL: eq56:=V c1 LL=V c2 LL: eq57:=M c1 LL=M c2 LL: eq58:=phi c1 LL=phi c2 LL:
  > 
> x:=C: eq7::=w_op2=0: eq8::=w_op3=0: eq9::=M_op3=M_op2: eq10::=phi_op3=phi_op2: 
> x:=C: eq31::=w_o2=0: eq32::=w_o3=0: eq33::=M_o3=M_o2: eq34::=phi_o3=phi_o2: 
> x:=C: eq59:=w_o2_LI-O: eq60:=w_o3_LI-O: eq61:=M_o3_LI-M_o2_LI-(op2_LI-(op3::=phi_o3_LI-phi_o2_LI-)
             x:=D: eq11:=V_cp3=0: eq12:=M_cp3=0: x:=D: eq35:=M_c93=0: x:=D: eq35:=M_c03=M_c08: eq38:=phi_c03=phi_c08: x:=D: eq36:=W_c03 LL=M_c08 LL: eq66:=M_c03 LL=M_c08 LL: eq66:=M_c08 LL: eq66:=
             x:=F: eq13:=V ms1=0: eq14:=M ms1=0:
x:=F: eq39:=V c4=V c6: eq40:=V c4=V c6: eq41:=M c4=M c6: eq42:=phi_c4=phi_c6=phi_c6=phi_c6=phi_c6=phi_c6=phi_c6=phi_c6=phi_c6=phi_c6=phi_c6=phi_c6=phi_c6=phi_c6=phi_c6=phi_c6=phi_c6=phi_c6=phi_c6=phi_c6=phi_c6=phi_c6=phi_c6=phi_c6=phi_c6=phi_c6=phi_c6=phi_c6=phi_c6=phi_c6=phi_c6=phi_c6=phi_c6=phi_c6=phi_c6=phi_c6=phi_c6=phi_c6=phi_c6=phi_c6=phi_c6=phi_c6=phi_c6=phi_c6=phi_c6=phi_c6=phi_c6=phi_c6=phi_c6=phi_c6=phi_c6=phi_c6=phi_c6=phi_c6=phi_c6=phi_c6=phi_c6=phi_c6=phi_c6=phi_c6=phi_c6=phi_c6=phi_c6=phi_c6=phi_c6=phi_c6=phi_c6=phi_c6=phi_c6=phi_c6=phi_c6=phi_c6=phi_c6=phi_c6=phi_c6=phi_c6=phi_c6=phi_c6=phi_c6=phi_c6=phi_c6=phi_c6=phi_c6=phi_c6=phi_c6=phi_c6=phi_c6=phi_c6=phi_c6=phi_c6=phi_c6=phi_c6=phi_c6=phi_c6=phi_c6=phi_c6=phi_c6=phi_c6=phi_c6=phi_c6=phi_c6=phi_c6=phi_c6=phi_c6=phi_c6=phi_c6=phi_c6=phi_c6=phi_c6=phi_c6=phi_c6=phi_c6=phi_c6=phi_c6=phi_c6=phi_c6=phi_c6=phi_c6=phi_c6=phi_c6=phi_c6=phi_c6=phi_c6=phi_c6=phi_c6=phi_c6=phi_c6=phi_c6=phi_c6=phi_c6=phi_c6=phi_c6=phi_c6=phi_c6=phi_c6=phi_c6=phi_c6=phi_c6=phi_c6=phi_c6=phi_c6=phi_c6=phi_c6=phi_c6=phi_c6=phi_c6=phi_c6=phi_c6=phi_c6=phi_c6=phi_c6=phi_c6=phi_c6=phi_c6=phi_c6=phi_c6=phi_c6=phi_c6=phi_c6=phi_c6=phi_c6=phi_c6=phi_c6=phi_c6=phi_c6=phi_c6=phi_c6=phi_c6=phi_c6=phi_c6=phi_c6=phi_c6=phi_c6=phi_c6=phi_c6=phi_c6=phi_c6=phi_c6=phi_c6=phi_c6=phi_c6=phi_c6=phi_c6=phi_c6=phi_c6=phi_c6=phi_c6=phi_c6=phi_c6=phi_c6=phi_c6=phi_c6=phi_c6=phi_c6=phi_c6=phi_c6=phi_c6=phi_c6=phi_c6=phi_c6=phi_c6=phi_c6=phi_c6=phi_c6=phi_c6=phi_c6=phi_c6=phi_c6=phi_c6=phi_c6=phi_c6=phi_c6=phi_c6=phi_c6=phi_c6=phi_c6=phi_c6=phi_c6=phi_c6=phi_c6=phi_c6=phi_c6=phi_c6=phi_c6=phi_c6=phi_c6=phi_c6=phi_c6=phi_c6=phi_c6=phi_c6=phi_c6=phi_c6=phi_c6=phi_c6=phi_c6=phi_c6=phi_c6=phi_c6=phi_c6=phi_c6=phi_c6=phi_c6=phi_c6=phi_c6=phi_c6=phi_c6=phi_c6=phi_c6=phi_c6=phi_c6=phi_c6=phi_c6=phi_c6=phi_c6=phi_c6=phi_c6=phi_c6=phi_c6=phi_c6=phi_c6=phi_c6=phi_c6=phi_c6=phi_c6=phi_c6=phi_c6=phi_c6=phi_c6=phi_c6=phi_c6=phi_c6=phi_c6=phi_c6=phi_c6=phi_c6=phi_c6=phi_c6=p
             x:=G: eq15:=w_ms1=0: eq16:=w_ms2=0: eq17:=M_ms1=M_ms2: eq16:=phi_ms1=phi_ms2:
x:=G: eq81:=w_c4=0: eq82:=w_c5=0: eq83:=M_c4=M_c5: eq84:=phi_c4=phi_c5:
x:=G: eq85:=w_c4_LL=0: eq86:=w_c5_LL=0: eq87:=M_c4_LL=M_c5_LL: eq88:=phi_c4_LL=phi_c5_LL:
                 x:=CB2: eq43:=w_c5=w_c6: eq44:=V_c5=V_c6: eq45:=M_c5=M_c6: eq46:=phi_c5=phi_c6:
x:=CB2: eq71:=w_c5_LI-w_c6_LL: eq72:=V_c5_LI-V_c6_LL: eq73:=M_c5_LI-M_c6_LL: eq74:=phi_c5_LI-phi_c6_LL:
             x:=H: eq23:=w_ms2=0: eq24:=w_ms3=0: eq19:=M_ms3=M_ms2: eq20:=phi_ms3=phi_ms2: x:=H: eq47:=w_c6=0: eq48:=w_c7=0: eq49:=M_c6=M_c7: eq50:=phi_c6=phi_c7: c=x:=H: eq27:=w_c6=LD:=eq76:=w_c7: LD:=eq77:=M_c6=LD:=M_c7: LD:=eq78:=phi_c6=LD:=phi_c7: LD:=eq78:=phi_c7: LD:=eq78:=eq78:=eq78:=eq78:=eq78:=eq78:=eq78:=eq78:
Beam properties
  Beam Axis:
  > L_beam:=11250:
> A:=0: API:=570: B:=280: C:=3250: CBI:=3000: D_:=3500: E:=D_+125: F:=3750: G:=4000: CB2:=4250: AP2:=10170: H:=14750: J:=15000:
    Material properties:
Standard properties:

Standard properties:

Standard properties:

Standard properties:

Standard properties:

Standard properties:

Standard properties:

Standard properties:

Standard properties:

Standard properties:

Standard properties:

Standard properties:

Standard properties:

Standard properties:

Standard properties:

Standard properties:

Standard properties:

Standard properties:

Standard properties:

Standard properties:

Standard properties:

Standard properties:

Standard properties:

Standard properties:

Standard properties:

Standard properties:

Standard properties:

Standard properties:

Standard properties:

Standard properties:

Standard properties:

Standard properties:

Standard properties:

Standard properties:

Standard properties:

Standard properties:

Standard properties:

Standard properties:

Standard properties:

Standard properties:

Standard properties:

Standard properties:

Standard properties:

Standard properties:

Standard properties:

Standard properties:

Standard properties:

Standard properties:

Standard properties:

Standard properties:

Standard properties:

Standard properties:

Standard properties:

Standard properties:

Standard properties:

Standard properties:

Standard properties:

Standard properties:

Standard properties:

Standard properties:

Standard properties:

Standard properties:

Standard properties:

Standard properties:

Standard properties:

Standard properties:

Standard properties:

Standard properties:

Standard properties:

Standard properties:

Standard properties:

Standard properties:

Standard properties:

Standard properties:

Standard properties:

Standard properties:

Standard properties:

Standard properties:

Standard properties:

Standard properties:

Standard properties:

Standard properties:

Standard properties:

Standard properties:

Standard properties:

Standard properties:

Standard properties:

Standard properties:

Standard properties:

Standard properties:

Standard properties:

Standard properties:

Standard properties:

  Prestressing steel
    > gamma s:=1.15: f ptk:=1860: f ptd:=f ptk/gamma s: A p:=100: phi:=12.9: E p:=195*1000:
    Prestressing:
           dum 5pm - n_strands:=n_1+n_2+n_3: axis_1:=60: n_1:=14: axis_2:=110: n_2:=6: axis_3:=185: n_3:=2: z_p:=(axis_1*n_1+axis_2*n_2+axis_3*n_3)/n_strands: e_p:=y_c-z_p: n_strands: n_strands: e_p:=y_c-z_p: n_strands: e_p:=y_c-z_p
**Combon For a strands: "n cp 1+n cp 2+n cp 3+n cp 4+n cp 5+n cp 6+n cp 7+n cp 8+n cp 9: 
** a xis cp 1:=60: n cp 1:=6: 
** a xis cp 2:=110: n cp 2:=2: 
** a xis cp 3:=150: n cp 3:=2: 
** a xis cp 3:=150: n cp 4:=2: 
** a xis cp 4:=250: n cp 4:=2: 
** a xis cp 6:=550: n cp 6:=2: 
** a xis cp 6:=550: n cp 6:=2: 
** a xis cp 6:=550: n cp 7:=2: 
** a xis cp 6:=700: n cp 7:=2: 
** a xis cp 6:=700: n cp 7:=2: 
** a xis cp 6:=700: n cp 8:=2: 
** a xis cp 6:=700: n cp 9:=2: 
** a xis cp 6:=700: n cp 5:=30: 
** a xis cp 6:=700: n cp 5:=30: 
** a xis cp 6:=700: n cp 9:=2: 
** a xis cp 6:=700: n cp 9:=2: 
** a xis cp 6:=700: n cp 5:=30: 
** a xis cp 6:=700: n cp 5:=30: 
** a xis cp 6:=700: n cp 9:=2: 
** a xis cp 6:=700: n cp 7:=2: 
*
                                                                                                                                                             ______.

1*n op 1+axis op 2*n op 2+axis op 3*n op 3+axis op 4*n op 4+axis op 5*n op 5+axis op 6*n op 6+axis op 7*n op 7+axis op 8*n op 8+axis op 9*
nds:
        Section properties :
    Pefabricated_concrete beams:

> EI ms:=E beam*! beam: EI cp:=EI ms: E beam:=E C55: I beam:=31268941782.7168: A beam:=437543.49: y c:=314.8709: h beam:=900: z b:=y c: z t:=h beam-y c: bw beam:=300: w b:=I beam beam:=25:
300: w b:=I beam beam:=25:
Top layer properties:

> garman ti=25: E ti=E c30: b ti=1200: h ti=170: z ti=88.91: I ti=427451134.9781: A ti=194499.9959:

Composite beam properties:

> n:=E beam/g ti: b tl transformed:=evalf(b tl/n): #simplified

> n:=E tz ti tl:

> A tl transformed:=A tl/n: I tl transformed:=371207172.0282: #taken from AutoCAD

> A con transformed:=A beam*a tl transformed:
> I com:=I beam*A beam*g (z b-z com)*2+1 tl transformed*h (h beam*z tl) / A com transformed:
> I com:=I beam*A beam*g (z b-z com)*2+1 tl transformed*h tl
                                                                                                                                                                                                                                                                                                                                                                                                                                                                                                                                                                                                                                                                                                                                                                                                                                                                                                                                                                                                                                                                                                                                                                                                                                                                                                                              (23)
El c:=E tl*I c: b c:=1200: h c:=h beam*h tl: z t c:=h c/2: z b c:=h c-z t c: El c: A c:=b c*h c: I c:=b c*h c*3/12:

> W t c:=I c/z t c: N b c:=I c/z b c: evalf(W t c): evalf(W b c):

> N t c:=I c/z t c: N b c:=I c/z b c: evalf(W t c): evalf(W b c):

> N:=B beam*L beam*s tl*I fill*(E beam*A beam*E tl*A fill)*r crossb*2/(E beam*A beam*E tl*A fill): I fill:=58490580290.6867; A fill:=844947.4638:

A fill transformed.*s fill*n: s fill:=20.1038: z b fill*l=h c*z t fill*z b: El crossb:=I crossb:=I crossb*E beam: z crossb:=(A beam*z b+A fill transformed*z b fill*)/(A beam*A fill transformed): z b crossb:=z crossb:=z crossb:=beam=crossb:=L crossb/E beam: z crossb:=(A beam*z b+A fill transformed*z b fill*)/(A beam*A fill transformed): z b crossb:=z crossb:=z crossb:=beam=crossb:=L crossb/E beam: z crossb:=L crossb/E beam: z crossb:=L crossb:=L crossb/E beam: z crossb:=L crossb:=L crossb/E beam*z crossb:=L crossb:=L crossb/E beam: z crossb:=L crossb:=L
      Prestressing load in the cantilever part:
    > M_cp_p:=P_cp_m0*e_cp_p:
> P_cp_max:=118500*n_cp_strands;
                                                                                                                                                                                                                                                                                                                                                                                                                                                                                                                                                                                                P_{cp_max} := 2607000
                                                                                                                                                                                                                                                                                                                                                                                                                                                                                                                                                                                                                                                                                                                                                                                                                                                                                                                                                                                                                                                                                                                                                                                                                                                                                                                            (24)
> alpha_op_e:=E_p/E_030:
> rho_op_p:=A_pFn_op_strands/A_beam:
> f_op:=(1/4 beam*e_op_p*2/I_beam):
> deltaP_op_el:=P_op_max*alpha_op_e*rho_op_p*f_op/(1*alpha_op_e*rho_op_p*f_op):
> P_op_m0:=P_op_max*deltaP_op_el;
                                                                                                                                                                                                                                                                                                                                                                                                                                                                                                                                                                       P_cp_m0 := 2.531642508 \times 10^6
                                                                                                                                                                                                                                                                                                                                                                                                                                                                                                                                                                                                                                                                                                                                                                                                                                                                                                                                                                                                                                                                                                                                                                                                                                                                                                                              (25)
```

```
P2 := 1.000 \times 10^6
                                                                                                                                                                                               P1 := 630000
                                                                                                                                                                                                                                                                                                                                                                                                                        (28)
Distributed load - Phase 1a and 1b
> #q:=A_beam*gamma_beam/1000000;
Distributed load - Phase 1a, 1b and 1c
> n_g tl:=(bw beam*2*(btl-2*bw beam)/4)/b_tl:
> q:=A_beam*gamma_beam/I000000+A_tl*n_g_tl*gamma_tl/1000000;
                                                                                                                                                                                           a := 13.97764968
                                                                                                                                                                                                                                                                                                                                                                                                                       (29)
Distributed load - Phase 2
    • q_com:=A_beam*gamma_beam/1000000+A_t1*gamma_t1/1000000;
                                                                                                                                                                                       q_com := 15.80108715
                                                                                                                                                                                                                                                                                                                                                                                                                       (30)
; q_c:=A_c*gamma_beam/1000000;
                                                                                                                                                                                               q_{c} := \frac{321}{10}
                                                                                                                                                                                                                                                                                                                                                                                                                        (31)
;
> q_crossb:=(A_beam+A_fill)*gamma_beam/1000000;
                                                                                                                                                                                    q\_crossb := 32.06227385
                                                                                                                                                                                                                                                                                                                                                                                                                        (32)
 Horizontal stresses distribution
                                                                                                                                                                                 Horizontal stresses distribution
                                                                                                                                                                                                                                                                                                                                                                                                                        (33)
  Stresses - Phase 1
Stresses enerated by prestressing

> sigma t P cp:=-P cp m0/A beam:

> sigma b P cp:=-P cp m0/A beam:
     sigma_t_P:=-P_m0/A_beam:
sigma_b_P:=-P_m0/A_beam:
     sigma_t_M_p_cp:=M_cp_p/W_t:
sigma_b_M_p_cp:=-M_cp_p/W_b:
     sigma_t_M_p:=M_p/W_t:
sigma_b_M_p:=-M_p/W_b:
 > stgma_b_M_p:—M_p/w_b:
Stresse generated by distributed load
x:='x':
stgma_b_M_g1_cp:=M_cpl/w_b:
stgma_b_M_g2_cp:=M_cpl/w_b:
stgma_b_M_g2_cp:=M_cp2/w_b:
stgma_b_M_g2_cp:=M_cp2/w_b:
stgma_b_M_g3_cp:=M_cp3/w_b:
stgma_b_M_g3_cp:=M_cp3/w_b:
     sigma t M g1:=-M ms1/W t:
sigma b M g1:=M ms1/W b:
sigma t M g2:=-M ms2/W t:
sigma b M g2:=-M ms2/W b:
sigma t M g3:--M ms3/W t:
sigma b M g3:--M ms3/W b:
  Stresses generated by prestressing and distributed load

sigma_tl_op:=sigma_tp_op+sigma_tM_p_op+sigma_tM_gl_op:
sigma_bl_op:=sigma_bp_op+sigma_bM_p_op+sigma_bM_gl_op:
sigma_bl_op:=sigma_tp_op+sigma_tM_p_op+sigma_tM_gl_op:
sigma_bl_op:=sigma_bp_op+sigma_bM_p_op+sigma_bM_gl_op:
sigma_bl_op:=sigma_bp_op+sigma_bM_p_op+sigma_bM_gl_op:
sigma_bl_op:=sigma_bp_op+sigma_bM_p_op+sigma_bM_gl_op:
sigma_bl_op:=sigma_bp_op+sigma_bM_p_op+sigma_bM_gl_op:
     sigma tl:=sigma t Pesigma t M pesigma t M g1:
sigma b1:=sigma b Pesigma b M pesigma b M g1:
sigma b1:=sigma b Pesigma t M pesigma t M g2:
sigma t 2:=sigma t M pesigma t M pesigma t M g2:
sigma b2:=sigma b Pesigma t M pesigma t M g3:
sigma t3:=sigma t M pesigma t M g3:
sigma t3:=sigma b Pesigma b M pesigma b M g3:
  Stresses in cantilever part of the beam - Phase 1c
     Ai-plot([sigma_t1_op,sigma_b1_op],x=A.B,title=stresses,labels=[x,sigma],legend=[typeset("sigma_top"),typeset("sigma_bottom")],color=[12,4]):
Bi:-plot([sigma_t2_op,sigma_b2_op],x=B..C,title=stresses,labels=[x,sigma],legend=[typeset("sigma_top"),typeset("sigma_bottom")],color=[12,4]):
CC:-plot([sigma_t3_op,sigma_b3_op],x=C..D_,title=stresses,labels=[x,sigma],legend=[typeset("sigma_top"),typeset("sigma_bottom")],color=[12,4]):
  Stresses in main span of the beam - Phase 1c
Stesses mann span of the Deam - Phase ic 

$ x:='x': 

$ DD:-plot([sigma_1t],x=F..G,title=stresses,labels=[x,sigma],legend=[typeset("sigma_top"),typeset("sigma_bottom")],color=[12,4]); 

$ EE:-plot([sigma_t2,sigma_b2],x=G..H,title=stresses,labels=[x,sigma],legend=[typeset("sigma_top"),typeset("sigma_bottom")],color=[12,4]); 

$ FF:-plot([sigma_t3,sigma_b3],x=H..J,title=stresses,labels=[x,sigma],legend=[typeset("sigma_top"),typeset("sigma_bottom")],color=[12,4]); 

$ display([AA,BB,CG,D,D,E,FFF),view=[0.15000,-B..4])
                                                                                          0
                                                                                                                                                                           5000
                                                                                                                                                                                                                                                           10000
                                                                                                                                                                                                                                                                                                                                            15000
                                                                                      -6
                                                                                      -8-
                                                                                                                                                                     sigma_top sigma_bottom
```

```
Stresses in the cross section at midspan - Phase la

| sigma 1:=-P m0/A beam*M p*y/_ beam:
| sigma 1:=-P m0/A beam.
| sigma 1
                                                                                                                                                                                                                   Stresses at midspan of a main beam - presressing
                                                                                                                                                                                                                                                            500
                                                                                                                                                                                                                                                           400
                                                                                                                                                                                                                                                          300
                                                                                                                                                                                                                                                           200
                                                                                                                                                                                                                                                           100
                                                                                                                                                                                                                                                      -100
                                                                                                                                                                                                                                                                                               sigma
                                                                                                                                                                                                                                                      - 200
> plots:-display(tf(S1_2), view=[-8..8,-z_b..z_t],title="Stresses at midspan of a main beam - moment from presressing",labels=["sigma","y"]);
                                                                                                                                                                           Stresses at midspan of a main beam - moment from presressing
                                                                                                                                                                                                                                500
                                                                                                                                                                                                                                400
                                                                                                                                                                                                                              300
                                                                                                                                                                                                                              200
                                                                                                                                                                                                                              100
                                                                                                                                                                        -8 -6 -4
                                                                                                                                                                                                                      -2
🍃 plots:-display(tf(S1),view=[-8..8,-z_b..z_t],title="Stresses at midspan of a main beam - phase la",labels=["sigma","y"]);
                                                                                                                                                                                                       Stresses at midspan of a main beam - phase 1a
                                                                                                                                                                                                                                                          500
                                                                                                                                                                                                                                                        400
                                                                                                                                                                                                                                                        300
                                                                                                                                                                                                                                                        100
                                                                                                                                                                                                       -6
                                                                                                                                                                                                                                                    -100
                                                                                                                                                                                                                                                    -200
                                                                                                                                                                                                                                                    -300-
:
> x:=F+0.5*L_beam: -P_m0/A_beam+M_p/W_t; -P_m0/A_beam-M_p/W_b;
                                                                                                                                                                                                                                                 3.331693880
                                                                                                                                                                                                                                                 -7.602319353
*

Note: stresses from this phase are uniform along the whole length of the beam (they grow from zero to certain value over the transmission length), hence in cross at the G axis they are assumed to be the same, although in fact they might be slightly lower

it is a lightly lower.
| slightly lower
|>
| Stresses in the cross section at midspan - Phase 1b
                                                                                                                                                                                                                                            q := 10.93858725
                                                                                                                                                                                                                                                                                                                                                                                                                                                                                                                               (35)
> sigma Mg beam:=-M ms2*y/I beam:

> sigma 2:=-P m0/A beam:M p*y/I beam-M ms2*y/I beam:

> $2 l:=plot([sigma Mg beam],y=-z b.z_t):

> $2:=plot([sigma 2],y=-z b.z_t):

> $2:=plot([sigma 2],y=-z b.z_t):

> tf:=plottools:-transform((x,y)>[y,x]): tf($2:1): tf($2):

> plots:-display(tf($2:1),view=[-8..8,-z_b..z_t],title="Stresses from the selfweight of the beam",labels=["sigma","y"]);
                                                                                                                                                                                                         Stresses from the selfweight of the beam
                                                                                                                                                                                                                                                   500
                                                                                                                                                                                                                                                   400
                                                                                                                                                                                                                                                    300-
                                                                                                                                                                                                                                                   100
                                                                                                                                                                                 -8 -6 -4
                                                                                                                                                                                                                                              -100
                                                                                                                                                                                                                                              -200
```

```
; > plots:-display(tf(S2),view=[-8..8,-z_b..z_t],title="Stresses at midspan of a main beam - Phase lb",labels=["sigma","y"]);
                                                                    Stresses at midspan of a main beam - Phase 1b
                                                                                      300-
                                                                                     200-
                                                                                     100-
                                                                                    -100-
                                                                                    - 200
                                                                                    -300
                                                                                   2/w_b;
0.381258214
-6.014624717
'> x:=F+0.5*L_beam: -P_m0/A_beam+M_p/W_t-M_ms2/W_t; -P_m0/A_beam-M_p/W_l
                                                                                                                                                                               (36)
Stresses from the selfweight of the beam
                                                                                        400
                                                                                       300-
                                                                                        200
                                                                                        100
                                                                       -0.10
                                                                                                   0.05
                                                                                                             0.10
                                                                                      -100
                                                                                                   sigma
                                                                                      -200
                                                                                      -300<sup>H</sup>
; plots:-display(tf(S2),view=[-8..8,-z_b..z_t],title="Stresses at G axis of a main beam - Phase 1b",labels=["sigma","y"]);
                                                                        Stresses at G axis of a main beam - Phase
                                                                                        400
                                                                                        100
                                                                                      -100
                                                                                       -200
                                                                                      - 300
> x:=G+0.00001: -P_m0/A_beam+M_p/W_t-M_ms2/W_t; -P_m0/A_beam-M_p/W_b+M_ms2/W_b; -3,338090478 -7.667561504
                                                                                                                                                                                    (37)
Stresses in the cross section at midspan - Phase 1c
> x:='x': y:='y':
> x:=F+0.5*L_beam:
> q:=A_tl*n_g_tl*gamma_tl/1000000;
                                                                                   q := 3.039062435
                                                                                                                                                                                    (38)
> sigma Mg_tl:=-M_ms2*y/I_beam:
> s3_1:=plot([sigma_Mg_tl],y=-z_b..z_t):
> tf:=plottools:-transform((x,y)->[y,x]): tf(s3_1):
plots:-display(tf(S3_1),view=[-2..2,-z_b..z_t],title="Stresses from the selfweight of the top layer",labels=["sigma","y"]);
                                                                       Stresses from the selfweight of the top layer
                                                                                        400
                                                                                         300
                                                                                        100
                                                                  _2
                                                                                                      sigma
                                                                                      - 100·
                                                                                      -200
                                                                                      - 300
"> x:=F+0.5*L_beam: -M_ms2/W_t; M_ms2/W_b;
                                                                                    - 0.8197181210
0.4411084366
                                                                                                                                                                                    (39)
$ x:='x': y:='y':
> x:=F+0.5*L beam:
> q:=A_beam*gamma_beam/1000000+A_tl*n_g_tl*gamma_tl/1000000;
                                                                                   q := 13.97764968
```

```
> sigma_3:=-P_m0/A_beam+M_p*y/I_beam-M_ms2*y/I_beam:
> S3:=plot([sigma_3],y=-z_b..z_t,-6..6):
> tf:=plottools:-transform((x,y)->[y,x]): tf(s3):
 > plots:-display(tf(S3),view=[-8..8,-z_b..z_t],title="Stresses at midspan of a main beam - phase lo",labels=["sigma","y"]);
                                                                                                                  Stresses at midspan of a main beam - phase 1c
                                                                                                                                                400
                                                                                                                                                300
                                                                                                                                               200
                                                                                                                                               100
                                                                                                                                            -100
                                                                                                                                            -200
                                                                                                                                            - 300-
> x:=F+0.5*L_beam: -P_m0/A_beam+M_p/W_t-M_ms2/W_t; -P_m0/A_beam-M_p/W_b+M_ms2/W_b; -0.33845990
                                                                                                                                          -5.573516282
                                                                                                                                                                                                                                                                                                     (41)
> x:='x': y:='y':
Stresses above the support - Phase 1c
 > x:=G+0.00001:
> q:=A_tl*n_g_tl*gamma_tl/1000000;
                                                                                                                                       q:= 3.039062435
> sigma_Mg_tl:=-M_ms2*y/I_beam:
> S3_1:=plot([sigma_Mg_tl],y=-z_b..z_t):
> tf:=plottools:-transform((x,y)->[y,x]): tf(S3_1):
> plots:-display(tf(S3_1),view=[-0.1..0.1,-z_b..z t],title="Stresses from the selfweight of the top layer",labels=["sigma","y"]);
                                                                                                                   Stresses from the selfweight of the top layer
                                                                                                                                                500
                                                                                                                                               400
                                                                                                                                               300
                                                                                                                                               200
                                                                                                                                               100
                                                                                                             -0.10
                                                                                                                               -0.05
                                                                                                                                                                      0.05
                                                                                                                                                                                        0.10
                                                                                                                                            -100
                                                                                                                                             -200
                                                                                                                                            - 300
> x:=G+0.00001: -M ms2/W t; M ms2/W b;
                                                                                                                                                                                                                                                                                                     (43)
> x:='x': y:='y':
> x:=G+0.00001:
> q:=A_beam*gamma_beam/1000000+A_tl*n_g_tl*gamma_tl/1000000;
                                                                                                                                        q := 13.97764968
> sigma_3:=-P_m0/A_beam+M_p*y/I_beam-M_ms2*y/I_beam:
> S3:=plot([sigma_3],y=-z_b..z_t,-6..6):
> tf:=plottools:-transform((x,y)->[y,x]): tf(S3):
 > plots:-display(tf(S3),view=[-8..8,-z_b..z_t],title="Stresses at G axis of a main beam - Phase 1c",labels=["sigma","y"]);
                                                                                                                     Stresses at G axis of a main beam - Phase
                                                                                                                                                500
                                                                                                                                                400
                                                                                                                                                300
                                                                                                                                                200
                                                                                                                                                100
                                                                                                                                                                  sigma
                                                                                                                                             -200
> x:=G+0.00001: -P_m0/A_beam+M_p/W_t-M_ms2/W_t; -P_m0/A_beam-M_p/W_b+M_m
                                                                                                                                    s2/W_b;
3.339867644
                                                                                                                                                                                                                                                                                                      (45)
 > x:='x': y:='y':
> q:=A_beam*gamma_beam/1000000+A_tl*n_g_tl*gamma_tl/1000000;
                                                                                                                                        q := 13.97764968
                                                                                                                                                                                                                                                                                                      (46)
 > q_com:=A_beam*gamma_beam/1000000+A_t1*gamma_t1/1000000;
                                                                                                                                    q\_com := 15.80108715
                                                                                                                                                                                                                                                                                                      (47)
PagaBad

x:='x':

AA:=plot([-M_c1+M_cpl],x=A..B,title="Moments' difference",labels=[x,M],color=12):

BB:=plot([-M_c1+M_cp2],x=B..CBl,title="Moments' difference",labels=[x,M],color=12):

CC:=plot([-M_c2+M_cp2],x=CBl..C,title="Moments' difference",labels=[x,M],color=12):

DD:=plot([-M_c2+M_cp2],x=CBl..C,title="Moments' difference",labels=[x,M],color=12):

EB:=plot([-M_c3+M_cp2],x=C..B,title="Moments' difference",labels=[x,M],color=12):

FF:=plot([-M_c3+M_s2],x=F..G;title="Moments' difference",labels=[x,M],color=12):

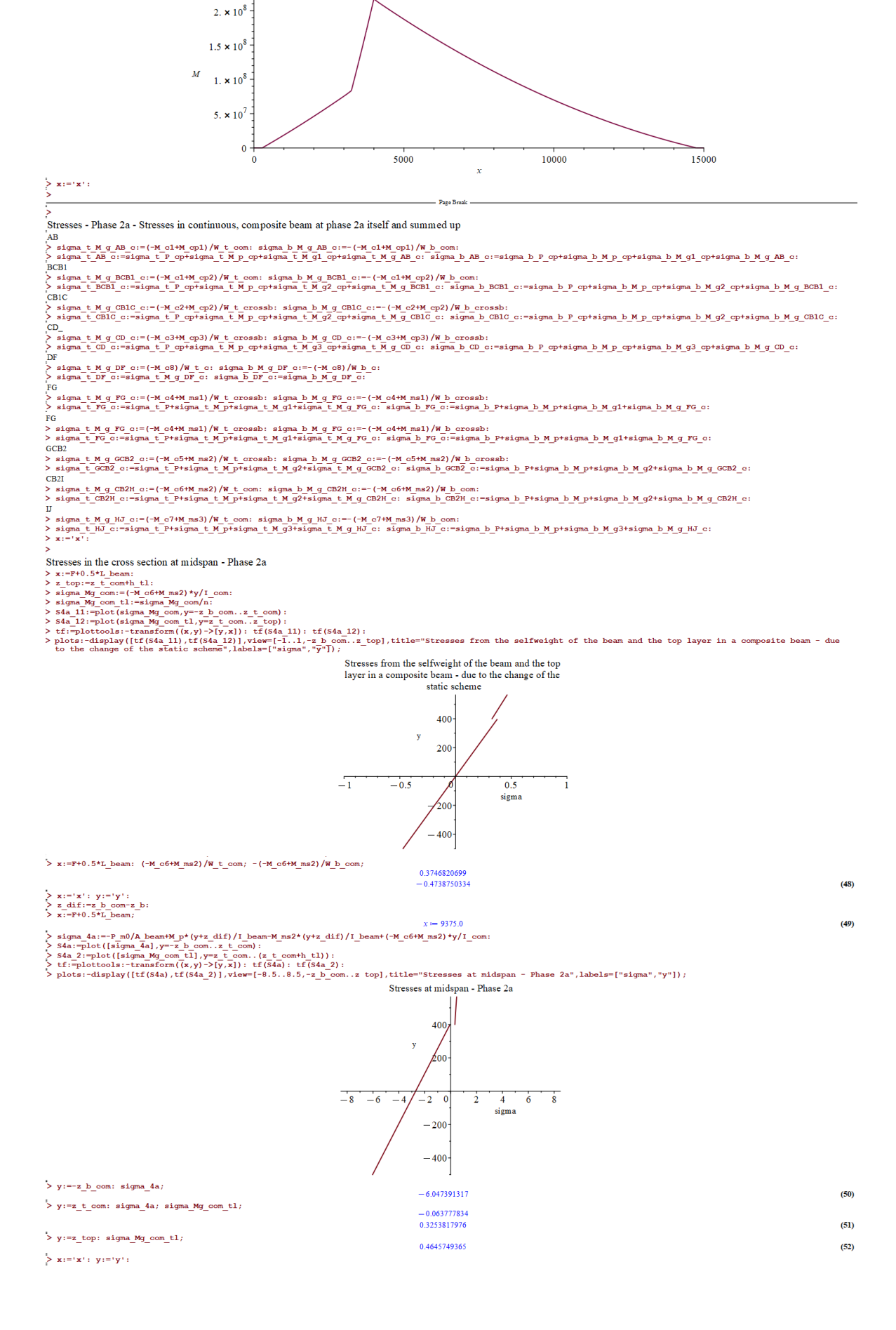
GG:=plot([-M_c3+M_s2],x=C..B;title="Moments' difference",labels=[x,M],color=12):

HN:=plot([-M_c3+M_s3],x=H..J,title="Moments' difference",labels=[x,M],color=12):

> HN:=plot([-M_c3+M_s3],x=H..J,title="Moments' difference",labels=[x,M],color=12):

> display((AA,BB,CC,DD,EB,FF,GG,HH,II));
```

Moments' difference



```
Stresses above the support - Phase 2a
 Sitesses above the support "rimes 2a' > x:=640.0001: |
> sigma Mg com:=(-M_c5+M_ms2)*y/I_com: |
> sigma Mg com ti:=sigma Mg com/n: |
> S4a 21:=plot(sigma Mg com, y-=z b com.z t com): |
> S4a 22:=plot(sigma Mg com ti,y=z t com.z top): |
> tf:=plottools:=transform((x,y)-7[y,x]): tf(S4a 21): tf(S4a 22); tisplot(sigma Mg com ti,y=z t com.z top): |
> tf:splottools:=transform((x,y)-7[y,x]): tf(S4a 21): tf(S4a 22); top): |
> tothe change of the static scheme", labels=["sigma", "y"]); |
                                                                                                                 .z_top],title="Stresses from the selfweight of the beam and the top layer in a composite beam - due
                                                                                                               Stresses from the selfweight of the beam and the top layer in a composite beam - due to the change of the static scheme
                                                                                                                                              400
                                                                                                                                              200
                                                                                                                                   -2
                                                                                                                                                                    sigma
                                                                                                                                              /400
200
                                                                                                                  -8 -6 -4
                                                                                                                                          -200
                                                                                                                                           -400
 ; y:=-z_b_com: sigma_4a;
                                                                                                                                        -8.861386475
                                                                                                                                                                                                                                                                                                  (53)
 > y:=z_t_com: sigma_4a; sigma_Mg_com_t1;
                                                                                                                                         4.331905153
 > y:=z_top: sigma_Mg_com_t1;
                                                                                                                                                                                                                                                                                                  (55)
 > x:='x': y:='y':
  Stresses - Phase 2b - Stresses in continuous, composite beam beam at phase 2b itself and summed up
 AB > sigma_t_AB_c_LL:=(-M_cl_LL)/W_t_com: sigma_b_AB_c_LL:=M_cl_LL/W_b_com: > sigma_t_AB:=sigma_b_AB_c+sigma_t_AB_c+sigma_t_AB_c_LL:
 > sigma t CD c LL:=(-M c3 LL)/W t com: sigma b CD c LL:=-(-M c3 LL)/W b com:
> sigma t CD:=sigma t CD c+sigma t CD c LL: sigma b CD:=sigma b CD c+sigma b CD c LL:
     r
sigma t DF c LL:=(-M c8 LL)/W t c: sigma b DF c LL:--(-M c8 LL)/W b c:
sigma t DF:=sigma t DF c+sigma t DF c LL: sigma b DF:=sigma b DF c+sigma b DF c LL:
  > sigma t FG c LL:=(-M c4 LL)/W t com: sigma b FG c LL:=-(-M c4 LL)/W b com:
> sigma t FG:=sigma t FG c+sigma t FG c LL: sigma b FG:=sigma b FG c+sigma b FG c LL:
GCB2
     sigma t GCB2 c LL:=(-M c5 LL)/W t com: sigma b GCB2 c LL:=-(-M c5 LL)/W b com:
sigma t GCB2:=sigma t GCB2 c+sigma t GCB2 c LL: sigma b GCB2:=sigma b GCB2 c+sigma b GCB2 c LL:
  CB2I
     sigma t CB2H c LL:=(-M c6 LL)/W t com: sigma b CB2H c LL:=-(-M c6 LL)/W b com:
sigma t CB2H:=sigma t CB2H c+sigma t CB2H c LL: sigma b CB2H:=sigma b CB2H c+sigma b CB2H c LL:
     sigma t HJ c LL:=(-M c7 LL)/W t com: sigma b HJ c LL:=(-M c7 LL)/W b com: sigma t HJ:=sigma t HJ c+sigma t HJ c LL: sigma b HJ c+sigma b HJ c LL: x:='x':
  Stresses in the cross section at midspan - Phase 2b
    x:=P40.5t; beam:
z top:=z t com*h tl:
z top:=z t com*h tl:
sigma_com_fL:=(-M_cof_LL)*y/I_com:
sigma_com_fL_LL:=(-M_cof_LL)*y/I_com.z t_com):
s4b_11:=plot(sigma_com_fL_y=-z_b_com.z_t_com):
s4b_12:=plot(sigma_com_tL_Ly=-z_b_com.z_t_com):
s4b_12:=plot(sigma_com_tL_Ly=-z_b_com.z_t_com):
s4b_12:=plot(sigma_com_tL_Ly=-z_b_com.z_t_com):
s4b_12:=plot(sigma_com_fL_y=-z_b_com.z_t_com):
s4b_12:=plot(sigma_com_f(x,y)-5(x,y)): tf(s4b_11): tf(s4b_12):
plots:-display([tf(s4b_11),tf(s4b_12)],view=[-20..20,-z_b_com.z_top],title="Stresses from live load at midspan",labels=["sigma","y"]);
                                                                                                                           Stresses from live load at midspan
                                                                                                                      -20
                                                                                                                                                                                20
                                                                                                                                                                sigma
```

-400

```
> x:=F+0.5*L beam: (-M c6 LL)/W t com; -(-M c6 LL)/W b com;
                                                                                                                                                                                                                                                                                                                                                                                         -6 444435457
 > x:='x'; y:='y':
| z_dif:=z_b_com-z_b:
| z:=Ft0.5T_beam:
| sigma_db:=P=m0/A_beam+M_p*(y+z_dif)/I_beam-M_ms2*(y+z_dif)/I_beam+(-M_c6+M_ms2)*y/I_com+(-M_c6_LL)*y/I_com:
| sigma_db:=P=m0/A_beam+M_p*(y+z_dif)/I_com/n*(-M_c6_LL)*y/I_com/n:
| sigma_db::=T_M_c6*M_ms2)*y/I_com/n*(-M_c6_LL)*y/I_com/n:
| sigma_db::=T_M_c6*M_ms2)*y/I_com/n*(-M_c6_LL)*y/I_com/n:
| sigma_db::=T_M_c6*M_ms2)*y/I_com/n*(-M_c6_LL)*y/I_com/n:
| sigma_db::=T_M_c6*M_ms2)*y/I_com/n*(-M_c6_LL)*y/I_com/n*(-M_c6_LL)*y/I_com/n:
| sigma_db::=T_M_c6*M_ms2)*y/I_com/n*(-M_c6_LL)*y/I_com/n*(-M_c6+M_ms2)*y/I_com+(-M_c6_LL)*y/I_com*(-M_c6_LL)*y/I_com*(-M_c6_LL)*y/I_com*(-M_c6_LL)*y/I_com*(-M_c6_LL)*y/I_com*(-M_c6_LL)*y/I_com*(-M_c6_LL)*y/I_com*(-M_c6_LL)*y/I_com*(-M_c6_LL)*y/I_com*(-M_c6_LL)*y/I_com*(-M_c6_LL)*y/I_com*(-M_c6_LL)*y/I_com*(-M_c6_LL)*y/I_com*(-M_c6_LL)*y/I_com*(-M_c6_LL)*y/I_com*(-M_c6_LL)*y/I_com*(-M_c6_LL)*y/I_com*(-M_c6_LL)*y/I_com*(-M_c6_LL)*y/I_com*(-M_c6_LL)*y/I_com*(-M_c6_LL)*y/I_com*(-M_c6_LL)*y/I_com*(-M_c6_LL)*y/I_com*(-M_c6_LL)*y/I_com*(-M_c6_LL)*y/I_com*(-M_c6_LL)*y/I_com*(-M_c6_LL)*y/I_com*(-M_c6_LL)*y/I_com*(-M_c6_LL)*y/I_com*(-M_c6_LL)*y/I_com*(-M_c6_LL)*y/I_com*(-M_c6_LL)*y/I_com*(-M_c6_LL)*y/I_com*(-M_c6_LL)*y/I_com*(-M_c6_LL)*y/I_com*(-M_c6_LL)*y/I_com*(-M_c6_LL)*y/I_com*(-M_c6_LL)*y/I_com*(-M_c6_LL)*y/I_com*(-M_c6_LL)*y/I_com*(-M_c6_LL)*y/I_com*(-M_c6_LL)*y/I_com*(-M_c6_LL)*y/I_com*(-M_c6_LL)*y/I_com*(-M_c6_LL)*y/I_com*(-M_c6_LL)*y/I_com*(-M_c6_LL)*y/I_com*(-M_c6_LL)*y/I_com*(-M_c6_LL)*y/I_com*(-M_c6_LL)*y/I_com*(-M_c6_LL)*y/I_com*(-M_c6_LL)*y/I_com*(-M_c6_LL)*y/I_com*(-M_c6_LL)*y/I_com*(-M_c6_LL)*y/I_com*(-M_c6_LL)*y/I_com*(-M_c6_LL)*y/I_com*(-M_c6_LL)*y/I_com*(-M_c6_LL)*y/I_com*(-M_c6_LL)*y/I_com*(-M_c6_LL)*y/I_com*(-M_c6_LL)*y/I_com*(-M_c6_LL)*y/I_com*(-M_c6_LL)*y/I_com*(-M_c6_LL)*y/I_com*(-M_c6_LL)*y/I_com*(-M_c6_LL)*y/I_com*(-M_c6_LL)*y/I_com*(-M_c6_LL)*y/I_com*(-M_c6_LL)*y/I_com*(-M_c6_LL)*y/I_com*(-M_c6_LL)*y/I_com*(-M_c6_LL)*y/I_com*(-M_c6_LL)*y/I_com*(-M_c6_LL)*y/I_com*(-M_c6_LL)*y/I_com*(-M_c6_LL)*y/I_com*(-M_c6_LL)*y/I_com*(-M_c6_LL
                                                                                                                                                                                                                                                                                                                                                                                                          200
                                                                                                                                                                                                                                                                                                                                 -15 -10
                                                                                                                                                                                                                                                                                                                                                                                                                                                                              10
                                                                                                                                                                                                                                                                                                                                                                                                                                                                                                        15
                                                                                                                                                                                                                                                                                                                                                                                                                                                            sigma
                                                                                                                                                                                                                                                                                                                                                                                                  -400
 > y:=-z_b_com: sigma_4b;
                                                                                                                                                                                                                                                                                                                                                                                            2.103137661
 > y:=z_t_com: sigma_4b; sigma_4b_2;
                                                                                                                                                                                                                                                                                                                                                                                        -6.508213295
-5.271101627
                                                                                                                                                                                                                                                                                                                                                                                                                                                                                                                                                                                                                                                                                                                                                                                                                                   (59)
 > y:=z_top: sigma_4b_2;
                                                                                                                                                                                                                                                                                                                                                                                         -7.525994760
                                                                                                                                                                                                                                                                                                                                                                                                                                                                                                                                                                                                                                                                                                                                                                                                                                   (60)
    Shear stresses in the cross section at midspan - Phase 2b
  \begin{array}{l} x_{1} = x_{1} \cdot y_{1} = y_{1} \cdot y_{2} \cdot y_{1} \\ \text{b } 1 = 1180 \text{ b } 2 := 300 \text{ b } 3 := 1200 \text{ ; } z_{1} = z_{2} \text{ b } \text{ com-} 216.5 \text{ ; } z_{2} = c_{2} \text{ com+} t_{1} \cdot z_{2} \\ \text{b } 1 := (y - 0.5^{*}(z_{1} \text{ b } \text{ com+} y)) * (z_{2} \text{ b } \text{ com+} y) * b_{1} \cdot z_{2} \\ \text{c} 2 := (y - 0.5^{*}(z_{1} \text{ b } \text{ com+} y)) * (z_{2} \text{ b } \text{ com-} z_{2} \cdot z_{2} + z_{2} \cdot y_{2} + z_{2} \cdot z_{2} \\ \text{c} 3 := (y + 0.5^{*}(z_{1} \text{ c } \text{ com+} t_{1} - y)) * (z_{2} t_{2} \text{ com+} t_{1} - y) * b_{2} \cdot z_{2} \\ \text{c} 2 := (y + 0.5^{*}(z_{1} \text{ b } \text{ com-} z_{2} \cdot z_{2}) + z_{2} \cdot z_{2} \cdot z_{2} \\ \text{c} 2 := (y + 0.5^{*}(z_{1} \text{ b } \text{ com+} z_{2}) + z_{2} \cdot z_{2} \cdot z_{2} \cdot z_{2} \\ \text{c} 2 := (y + 0.5^{*}(z_{1} \text{ b } \text{ com+} z_{2}) + z_{2} \cdot z_{2} \cdot z_{2} \cdot z_{2} \cdot z_{2} \\ \text{c} 2 := (y + 0.5^{*}(z_{1} \text{ b } \text{ com} z_{2}) + z_{2} \cdot z_{2} \cdot z_{2} \cdot z_{2} \cdot z_{2} \\ \text{c} 2 := (y + 0.5^{*}(z_{1} \text{ b } \text{ com} z_{2}) + z_{2} \cdot z_{2} \cdot z_{2} \cdot z_{2} \cdot z_{2} \cdot z_{2} \\ \text{c} 3 := (y + 0.5^{*}(z_{1} \text{ b } \text{ com} z_{2}) + z_{2} \cdot z_{2} \cdot z_{2} \cdot z_{2} \cdot z_{2} \\ \text{c} 3 := (y + 0.5^{*}(z_{1} \text{ b } \text{ com} z_{2}) + z_{2} \cdot z_{2} \cdot
                                                                                                                                                                                                                                                                                                                                                                                           589591.1340
                                                                                                                                                                                                                                                                                                                                                                                                                                                                                                                                                                                                                                                                                                                                                                                                                                      (61)
 > tau 4b 1:=(V c6 LL)*S 1/(I com*b 1):
> tau 4b 2:=(V c6 LL)*S 2/(I com*b 2):
> tau 4b 3:=(V c6 LL)*S 2/(I com*b 3)/n:
> tau 4b 3:=(V c6 LL)*S 3/(I com*b 3)/n:
> T4b 1:=plot([tau 4b 1], y=-z b com. -z 1):
> T4b 2:=plot([tau 4b 2], y=-z 1..z t com):
  > T4b_3:=plot([tau_4b_3],y=z_t_com..(z_t_com+h_t1)):

> tt:=plottools:-transform((x,y)->[y,x]): tf(T4b_1): tf(T4b_2): tf(T4b_3):
> plots:-display([tf(T4b_1).tf(T4b_2).tf(T4b_3)], view=[-4..4,-z b com.z top], title="Shear stresses at midspan - phase 4b", labels=["tau", "y"]);
                                                                                                                                                                                                                                                                                                                                               Shear stresses at midspan - phase 4b
                                                                                                                                                                                                                                                                                                                                                                                                          400-
                                                                                                                                                                                                                                                                                                                                                                                                       200
                                                                                                                                                                                                                                                                                                                       -4 -3 -2 -1 0
                                                                                                                                                                                                                                                                                                                                                                                                  -200
                                                                                                                                                                                                                                                                                                                                                                                                  - 400·
  > x:=AP2-0.5: (-M_c6_LL)/W_t_com; -(-M_c6_LL)/W_b_com;
                                                                                                                                                                                                                                                                                                                                                                                               - 8.583962794
                                                                                                                                                                                                                                                                                                                                                                                               10.85647268
                                                                                                                                                                                                                                                                                                                                                                                                                                                                                                                                                                                                                                                                                                                                                                                                                                          (6)
 > sigma_com_LL:=(-M_c6_LL)*y/I_com
> sigma_com_tl_LL:=sigma_com_LL/n:
 > S4b_11:=plot(sigma_com_LL,y=-z_b_com.z_t_com):
> S4b_12:=plot(sigma_com_LL,y=-z_b_com.z_t_com):
> S4b_12:=plot(sigma_com_tL_LL,y=-z_t_com.z_tcp):
> tf:=plot(tsigma_com_tL_LL,y=-z_t_com.z_tcp):
> tf:=plot(tsigma_com_tL_L,y=-z_t_com.z_tcp):
> plots:-display([tf(S4b_11),tf(S4b_12)],view=[-20..20,-z_b_com..z_tcp],title="Stresses from live load at AF2 axis",labels=["sigma","y"]);
                                                                                                                                                                                                                                                                                                                                                     Stresses from live load at AP2 axis
                                                                                                                                                                                                                                                                                                              -20
                                                                                                                                                                                                                                                                                                                                                                   -10
                                                                                                                                                                                                                                                                                                                                                                                                                                                                              10
                                                                                                                                                                                                                                                                                                                                                                                                     - 200
                                                                                                                                                                                                                                                                                                                                                                                                     -400
```

```
Stresses in the cross section at AP2 axis -
                                                                                                                                                                                                                                                                                        phase 4b
                                                                                                                                                                                                                                -20
                                                                                                                                                                                                                                                                 -10
                                                                                                                                                                                                                                                                                                                                   10
                                                                                                                                                                                                                                                                                                                                                                   20
 ; y:=-z_b_com: sigma_4b;
                                                                                                                                                                                                                                                                                4.853820882
                                                                                                                                                                                                                                                                                                                                                                                                                                                                                                                                                                                               (63)
 > y:=z_t_com: sigma_4b; sigma_4b_2;
                                                                                                                                                                                                                                                                                                                                                                                                                                                                                                                                                                                                (64)
  > y:=z_top: sigma_4b_2;
                                                                                                                                                                                                                                                                              -9.413362504
                                                                                                                                                                                                                                                                                                                                                                                                                                                                                                                                                                                                (65)
> x:='x': y:='y':
Shear stresses under point of load application - Phase 2b
> b1:=1180: b2:=300: b3:=1200: z1:=zb_com-216.5: zt_com+b_t1:
> 5.1:=(y-0.5*(zb_com+y))*(z.b_com+y)*b.1:
> 5.2:=-(y-0.5*(zb_com+y))*(z.b_com+y)*b.1:
> 5.3:=-(y-0.5*(zb_com+b_t1-y))*(zb_com+y)*b.2(0.5*(zb_com-z1)*z-1)*(zb_com-z-1)*b.1):
> 5.3:=(y+0.5*(zb_com-z))*(zb_com+b_t1-y)*b.3:
> zdif:=zb_com-z.b: bc_com-z.b:
> x:=AP2-0.5: evalf(y_cob_LL);
                                                                                                                                                                                                                                                                              589591.1340
                                                                                                                                                                                                                                                                                                                                                                                                                                                                                                                                                                                               (66)

}
tau 4b 1:=(V c6 LL)*s 1/(1 com*b 1);

tau 4b 2:=(V c6 LL)*s 2/(1 com*b 1);

tau 4b 3:=(V c6 LL)*s 2/(1 com*b 1);

tau 4b 3:=(V c6 LL)*s 2/(1 com*b 2);

tau 4b 3:=(V c6 LL)*s 3/(1 com*b 3)/n;

tab 1:=nbc([tau 4b 1],y=-z b com.-z 1);

tab 2:=nbc([tau 4b 2],y=-z 1..z t com);

tab 2:=nbc([tau 4b 3],y=z t com.(z t com*b tl));

tab 3:=nbc([tau 4b 3],y=z t com.(z t com*b tl));

tf:=plottcols:-transform((x,y)-v[y,x]); tf(T4b 1); tf(T4b 2); tf(T4b 3);

}

plots:-display([tf(T4b 1), tf(T4b 2), tf(T4b 3)], view=[-4..4,-z b com..z top], title="Shear stresses at midspan - phase 4b", labels=["tau", "y"]);

Shear stresses at midspan - phase 4b", labels=["tau", "y"]);

Shear stresses at midspan - phase 4b", labels=["tau", "y"]);

                                                                                                                                                                                                                                                  Shear stresses at midspan - phase 4b
                                                                                                                                                                                                                                                                                        400
                                                                                                                                                                                                                                                                                          200-
                                                                                                                                                                                                                                       -4 -3 -2 -1 0
                                                                                                                                                                                                                                                                                      -200
                                                                                                                                                                                                                                                                                      -400
  >
> x:='x': y:='y':
    Stresses above the support - Phase 2b
         sigma_com_LL:=(-M_c5_LL)*y/I_com:
sigma_com_tL:=sigma_com_LL/n:
         S4b 11:=plot(sigma com LL,y=z b com.z t com):
S4b 12:=plot(sigma com tL LL,y=z t com.z top):
S4b 12:=plot(sigma com tL LL,y=z t com.z top):
tir=plottoola:=transform(x,y)=2(x,1): tf(s4b 11): tf(s4b 12):
plots:=display([tf(s4b 11),tf(s4b 12)],view=[-20..20,-z b com.z top],title="Stresses from live load at G axis",labels=["sigma","y"]);
                                                                                                                                                                                                                                                        Stresses from live load at G axis
                                                                                                                                                                                                                                                                                            400
                                                                                                                                                                                                                                                                                          200
                                                                                                                                                                                                                                                  -20
                                                                                                                                                                                                                                                                           -10
                                                                                                                                                                                                                                                                                                                              10
                                                                                                                                                                                                                                                                                                                          sigma
                                                                                                                                                                                                                                                                                    <del>/</del>400-
  \begin{tabular}{ll} $>$ x:=G+0.5: $ (-M_a5_{LL})/W_t_{com}; $ -(-M_a5_{LL})/W_b_{com}; \end{tabular}
                                                                                                                                                                                                                                                                                                                                                                                                                                                                                                                                                                                                (67)
 | X:='x': y:='y':
| X:='x': y:='y':
| X:='G+0.5:
| X:='x': y:='y':
| X:='G+0.5:
| X:='x': y:='y':
| X:='G+0.5:
| X:='G+0.5
                                                                                                                                                                                                                                            Stresses in the cross section at G axis - Phase 2b
                                                                                                                                                                                                                                                                                            400
                                                                                                                                                                                                                                        -20
                                                                                                                                                                                                                                                                      -10
                                                                                                                                                                                                                                                                                                                                                                20
                                                                                                                                                                                                                                                                                        - 200
                                                                                                                                                                                                                                                                                      -400
  "> y:=-z_b_com: sigma_4b;
                                                                                                                                                                                                                                                                                -19.01509611
 > y:=z_t_com: sigma_4b; sigma_4b_2;
                                                                                                                                                                                                                                                                                 12.35980564
7.833781906
 "> y:=z_top: sigma_4b_2;
                                                                                                                                                                                                                                                                                11.18494875
                                                                                                                                                                                                                                                                                                                                                                                                                                                                                                                                                                                                (70)
  > x:='x': y:='y':
   Shear stresses in the cross section above the support - Phase 2b
b 1:=1180: b 2:=300: b 3:=1200: z 1:=z b com-216.5: z t com+h t1:
 5 b 1:=1180: b 2:=300: b 3:=1200: z 1:=z b com=216.5: z t com+h t1:
2 5 1:=-(y-0.5*(z b com+y))*(z b com+y)*b 1:
2 5 2:=-(y-0.5*(z b y))*(z 1+y)*b 2-(0.5*(z b com=z 1)+z 1)*(z b com=z 1)*b 1):
```

```
> s_3:=(y+0.5*(z_t_com+h_tl-y))*(z_t_com+h_tl-y)*b_3:
> z_dif:=z_b_com-z_b:
> x:=G+0.5: evalf(V_c5_LL);
                                                                                                    589590.9383
                                                                                                                                                                                                                   (71)
tau 4b 1:=(V o5 LL)*S 1/(I com*b 1):

tau 4b 2:=(V o5 LL)*S 2/(I com*b 2):

tau 4b 3:=(V o5 LL)*S 3/(I com*b 3)/n:

tau 4b 3:=(V o5 LL)*S 3/(I com*b 3)/n:

tab 1:=plot([tau 4b 1],y--z b com..-z 1):

tab 1:=plot([tau 4b 2],y--z 1..z t com):

tab 3:=plot([tau 4b 3],y-z t com.(z t com*h tl)):

tab 3:=plot([tau 4b 3],y-z t com.(z t com*h tl)):
 tf:=plottools:-transform((x,y)->[y,x]): tf(T4b_1): tf(T4b_2): tf(T4b_3):
> plots:-display([tf(T4b_1),tf(T4b_2),tf(T4b_3)],view=[-4..4,-z_b_oom.z_top],title="Shear stresses above the support - phase 4b",labels=["tau","y"]);
                                                                                         Shear stresses above the support -
phase 4b
                                                                                                       200-
                                                                                                      -200
                                                                                                      -400-
 \#Transmission length according to EC2 -1-1 8.10.2.2:
> sigma_pm0:=P_m0/A_p/n_strands;
                                                                                             sigma_pm0 := 751.1792668
                                                                                                                                                                                                                   (72)
> gamma_c:=1; #partial factor for concrete assumed as 1 for the time being, as mean, not the design, value is to be found gamma_c:=1
                                                                                                                                                                                                                   (73)
> #eta_p1:=2.7: #for indented and orimped wires
> eta_p1:=3.2; #for 7 wire strands
> eta_1:=1.0; #good bond conditions
                                                                                                    eta_1 := 1.0
                                                                                                                                                                                                                   (75)
> #eta_1:=0.7: #otherwise
f\_ctd\_t := 2.03
                                                                                                                                                                                                                   (76)
"> f_bpt:=eta_p1*eta_1*f_ctd_t; #design bond strength
                                                                                                  f_bpt := 6.4960
                                                                                                                                                                                                                   (77)
> alpha_p1:=1; #for gradual release
                                                                                                   alpha\_p1 := 1
                                                                                                                                                                                                                   (78)
alpha p2 := 0.19
                                                                                                                                                                                                                   (79)
}
Basic value
> i_pt:=alpha_p1*alpha_p2*phi*sigma_pm0/f_bpt;
                                                                                                l_pt := 283.4267831
                                                                                                                                                                                                                   (80)
"> 1_pt1:=1_pt*0.8;
                                                                                                l_pt1 := 226.7414265
                                                                                                                                                                                                                   (81)
> 1_pt2:=1_pt*1.2;
                                                                                                l_pt2 := 340.1121397
> 1_disp:=(1_pt^2+(h_beam-z_cp_p)^2)^0.5;
                                                                                                l_disp := 639.8354625
```

D.1 Longitudinal stresses

Intermediate support - Section BB

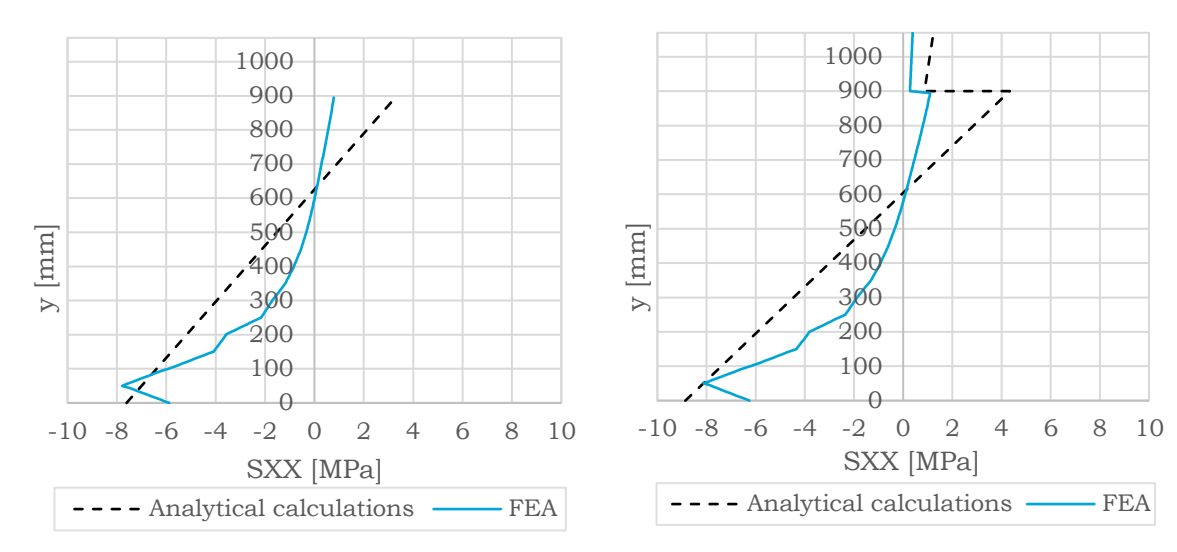


Figure D.1 Stresses above the support, phase 1

Figure D.2 Stresses above the support, phase 2a

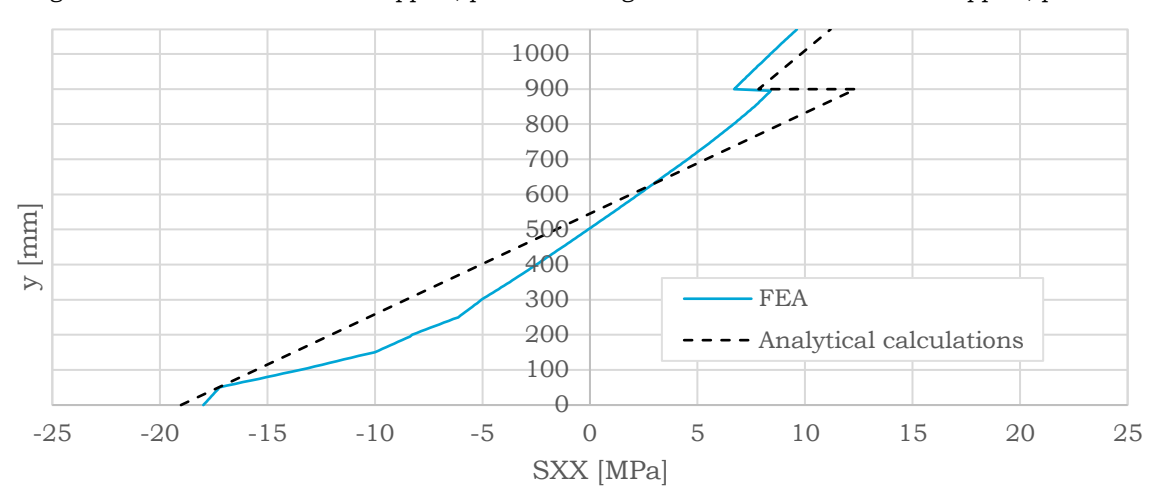


Figure D.3 Stresses above the support, phase 2b

Annex D 121

Midspan of the main span – section CC

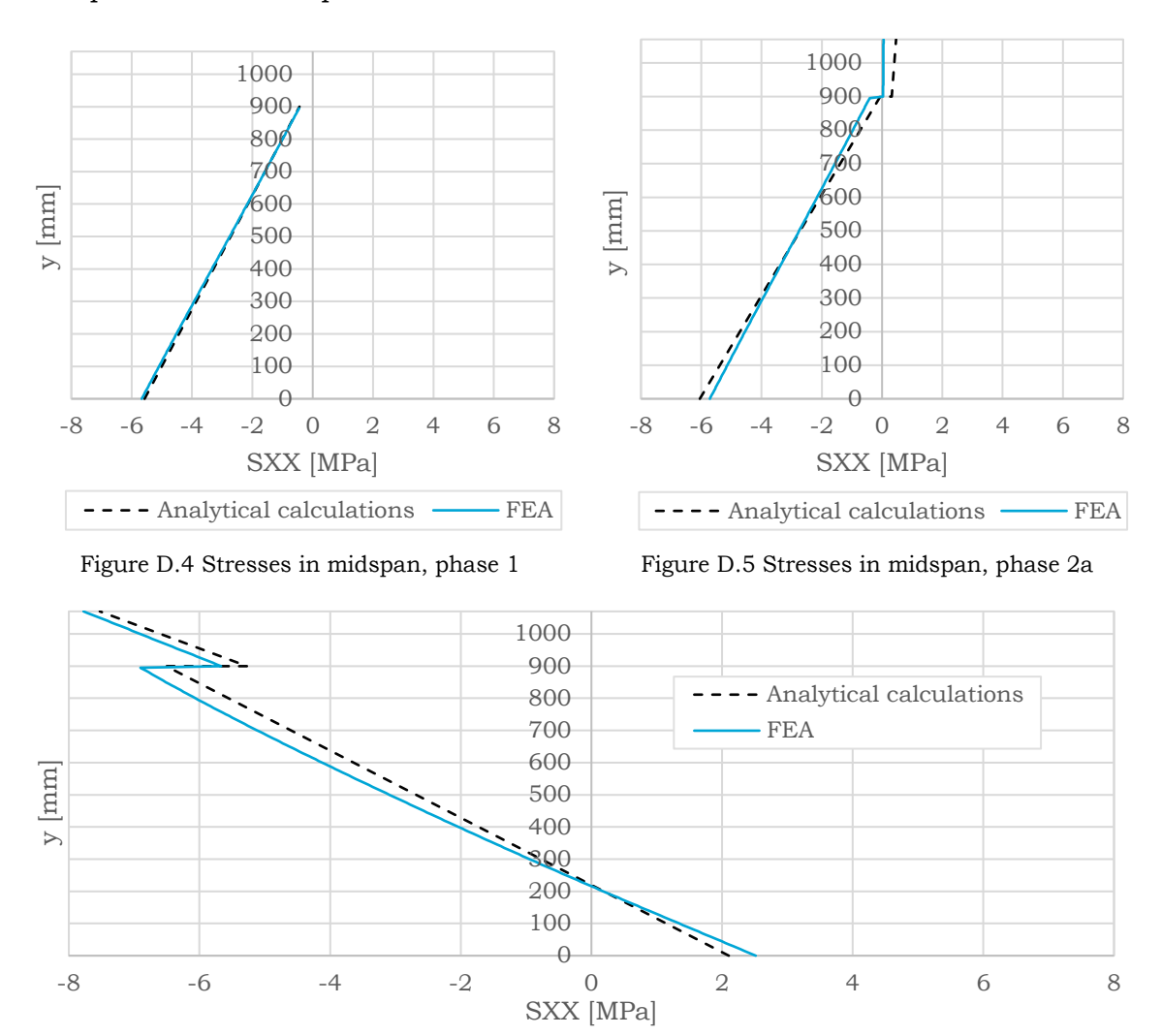


Figure D.6 Stresses in midspan, phase 2b

Point of load application – section DD

As the load is applied in relatively close vicinity to the midspan, the stresses in phases 1 and 2a are expected to be similar as in section CC, therefore only the phase 2b is evaluated.

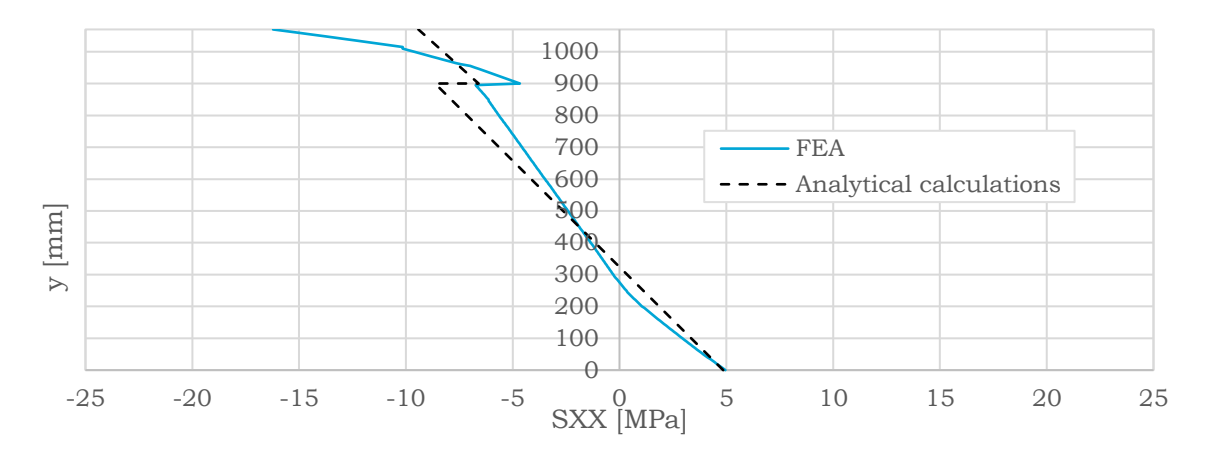


Figure D.7 Stresses at the cross-section below the point of load application, phase 2b

122 Annex D

D.2 Shear stresses

The comparison was also made between shear stresses at the aforementioned cross-sections. Shear stresses are significant after the live load application, hence only this stage is analysed. The graphs below were also shown in the main body of the report.

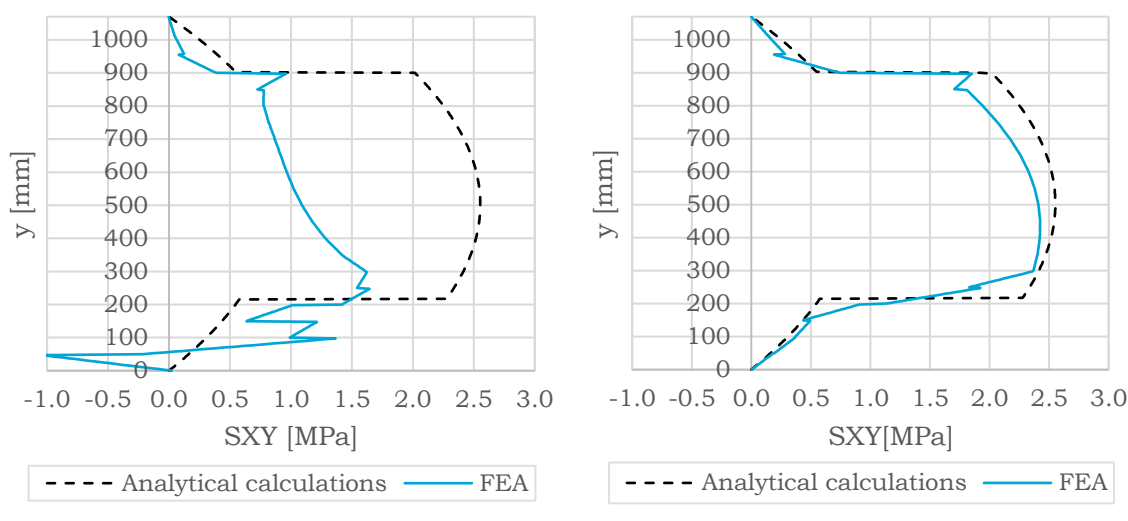


Figure D.8 Shear stresses above the support

Figure D.9 Shear stresses in midspan

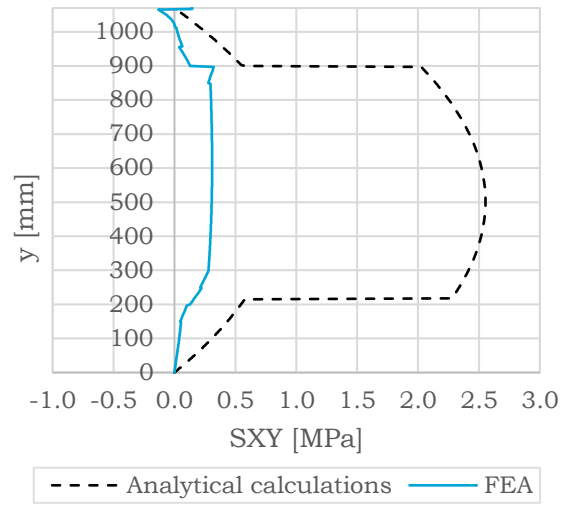


Figure D.10 Shear stresses below the point of load application

E.1 Additional results of the analysis of S-CCSC-RC

Additional results obtained from the analysis of S-CCSC-RC model under no external pressure. Deformation scaling factor for all presented results is equal to 10.

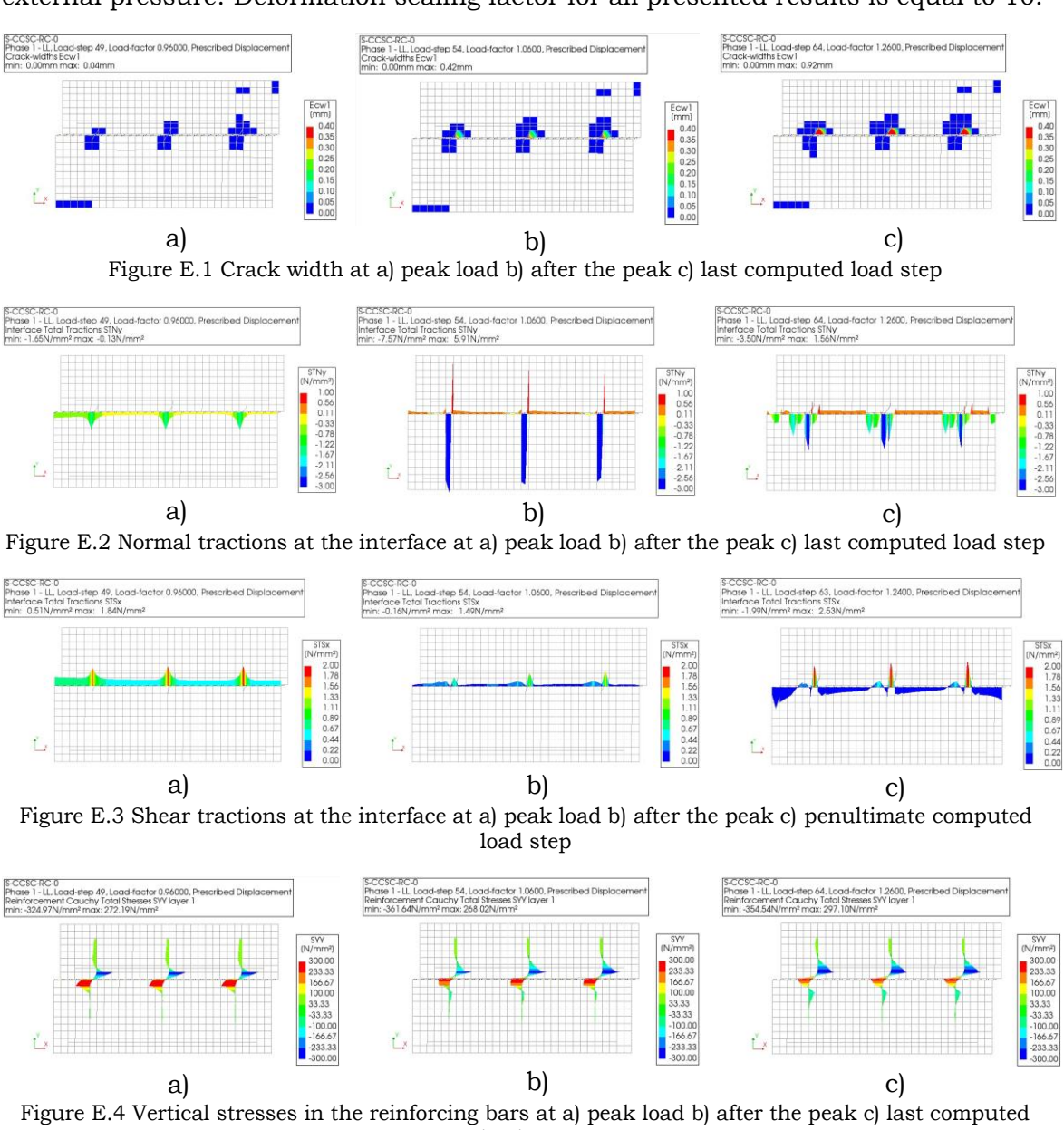


Figure E.4 Vertical stresses in the reinforcing bars at a) peak load b) after the peak c) last computed load step

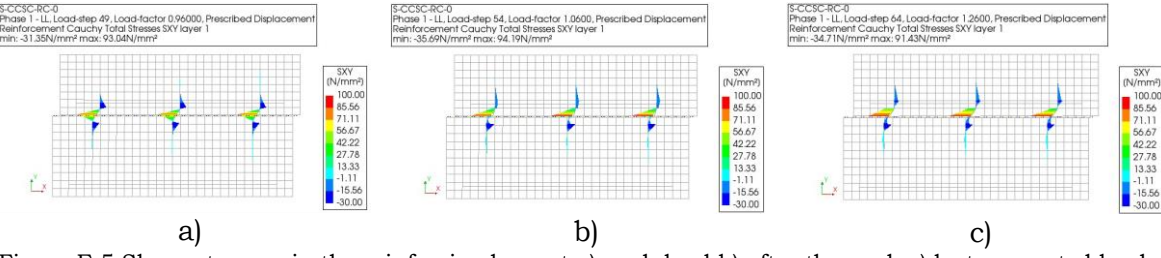
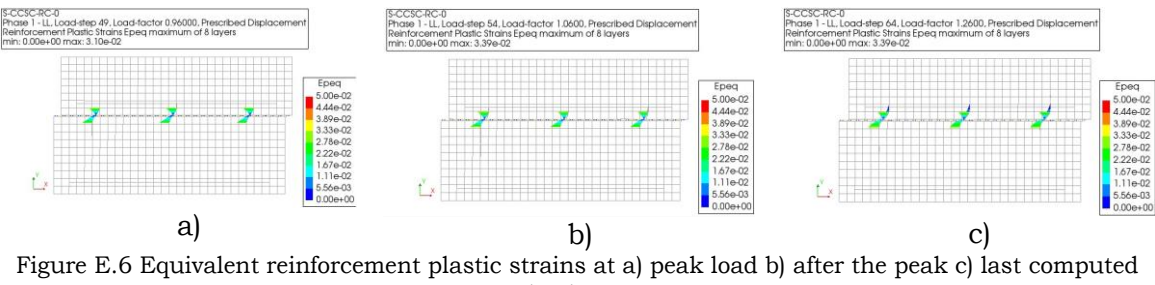


Figure E.5 Shear stresses in the reinforcing bars at a) peak load b) after the peak c) last computed load

124 Annex E



load step

